

**PETROGRAPHY AND MINERAL CHEMISTRY OF THE BASALTIC
ROCKS AND DYKES FROM THE BURUNKÖY (ÇORUM) REGION,
TURKEY**

**A THESIS SUBMITTED TO
THE GRADUATE SCHOOL OF NATURAL AND APPLIED SCIENCES
OF
THE MIDDLE EAST TECHNICAL UNIVERSITY**

BY

AYNUR (ATAK) KÜÇÜK

**IN PARTIAL FULFILLMENT OF THE REQUIREMENTS FOR THE
MASTER OF SCIENCE
IN
THE DEPARTMENT OF GEOLOGICAL ENGINEERING**

NOVEMBER 2014

Approval of the thesis:

PETROGRAPHY AND MINERAL CHEMISTRY OF THE BASALTIC ROCKS
AND DYKES FROM THE BURUNKÖY (ÇORUM) REGION, TURKEY

submitted by AYNUR (ATAK) KÜÇÜK in partial fulfillment of the requirements
for the degree of Master of Science in Geological Engineering Department, Middle
East Technical University by,

Prof. Dr. Gülbil Dural Ünver
Dean, Graduate School of Natural and Applied Sciences _____

Prof. Dr. Erdin Bozkurt
Head of Department, Geological Engineering _____

Assist. Prof. Dr. Fatma Toksoy Köksal
Supervisor, Geological Engineering Dept., METU _____

Examining Committee Members:

Prof. Dr. Cemal Göncüoğlu
Geological Engineering Dept., METU _____

Assist. Prof. Dr. Fatma Toksoy Köksal
Geological Engineering Dept., METU _____

Prof. Dr. Gültekin Topuz
Eurasia Institute of Earth Sciences, ITU, İstanbul _____

Doç. Dr. Kaan Sayıt
Geological Engineering Dept., METU _____

Assist. Prof. Dr. Ersin Koralay
Geological Engineering Dept., Dokuz Eylül University, İzmir _____

Date: _____

I hereby declare that all information in this document has been obtained and presented in accordance with academic rules and ethical conduct. I also declare that, as required by these rules and conduct, I have fully cited and referenced all material and results that are not original to this work.

Name, Last name: Aynur (Atak) Küçük

Signature:

ABSTRACT

PETROGRAPHY AND MINERAL CHEMISTRY OF THE BASALTIC ROCKS AND DYKES FROM THE BURUNKÖY (ÇORUM) REGION, TURKEY

(ATAK) KÜÇÜK, Aynur

M.Sc., Department of Geological Engineering

Supervisor: Assist.Prof.Dr.Fatma Toksoy Köksal

November 2014, 165 pages

Petrography and mineral chemistry of the basaltic rocks and dykes, which are outcropping in the Burunköy (Çorum) region, are discussed in the scope of this thesis. The studied rocks belong to the ophiolitic melange of İzmir-Ankara-Erzincan Suture Zone that were derived from the closure of northern branch of Neotethys. In the study area, the metamorphic rocks of Sakarya Composite Terrane tectonically overlies the ophiolitic melange units, and Upper Neocene sediments cover both units unconformably.

The rocks in the study area are divided into three categories; intensely foliated-sheared metabasalts, basalts and doleritic dykes. These rocks are mostly contain pyroxene and feldspar minerals with varying crystal sizes. The augite phenocrysts display reaction rims with reddish color, compositional zoning, corrosion and tailing properties which also observed for feldspars indicating more mafic hot magma impulse into magma chamber during crystallization.

The Electron Probe Microanalyser data from constituent minerals of the rock groups revealed that pyroxene and feldspar are augite and albite, respectively. Substitutional mechanism plots generally display more than one group inferring new melt influx(es) into magma that supports the petrographical observations. Mineral chemistry data indicate the rocks have a transitional character from subalkaline to alkaline that derived from a non-orogenic environment.

Whole rock geochemical data including isotopic once reveal that the rocks are alkaline in character and generated in a transitional environment between E-MORB and OIB. Furthermore, the data of studied rocks suggest that these rocks evolved from a melt formed by mixture of DMM and EM-I.

Keywords: Çorum, petrography, mineral chemistry.

ÖZ

TÜRKİYE BURUNKÖY (ÇORUM) BÖLGESİNDE YÜZEYLENEN BAZALTİK KAYAÇLARIN VE DAYKLARIN PETROGRAFİSİ VE MİNERAL KİMYASI

(ATAK) KÜÇÜK, Aynur

Yüksek Lisans, Jeoloji Mühendisliği Bölümü

Tez Yöneticisi: Yrd.Doç.Dr.Fatma Toksoy Köksal

Kasım 2014, 165 sayfa

Burunköy (Çorum) bölgesinde yüzeylenen bazaltik kayaçların ve daykların petrografisi ve mineral kimyası bu çalışma kapsamında değerlendirilmiştir. Üzerinde çalışılan kayaçlar Neotetis Okyanusu'nun kuzey kolumnun kapanmasıyla türeyen İzmir-Ankara-Erzincan Kenet Zonu'nun ofiyolitik melanjinine aittir. Çalışma alanında, Sakarya Kompozit'ine ait metamorfik kayaçlar tektonik olarak İzmir-Ankara-Erzincan Kenet Zonu'na ait ofiyolitik melanjin üzerinde yer almaktadır ve Üst Neojen yaşlı sedimanlar iki zona ait kayaçları da uyumsuz olarak örtmektedir.

Çalışma alanındaki kayalar üç kategoriye ayrılmıştır; yüksek derecede yapraklanmış-ezilmiş metabazaltlar, bazaltlar ve doleritik dayklar. Bu kayaçlar çeşitli kristal boyutlarında piroksen ve feldispat minerallerinden oluşmaktadır. Ojit fenokristalleri kristallenme sırasında magma odasına giren daha mafik sıcak magma impalsına işaret eden kırmızı renkli reaksiyon kenarı, kompozisyonal zonlanma, korozyon ve kuyruklanma özelliklerini göstermektedir. Benzer özellikler feldispat kristallerinde de gözlemlenmektedir.

Kayaç gruplarındaki ana minerallerin Elektron Prob Mikroanaliz verileri piroksenlerin ojit ve feldispatların albit bileşiminde olduğunu ortaya çıkarmıştır. Yer değişimli mekanizma çizimleri genellikle petrografik gözlemleri de destekleyen magmaya yeni magma inflakslarına işaret eden birden fazla gruplaşma sergilemektedir. Mineral kimyası verileri kayaçların sübalkalen ve alkalen arasında geçiş niteliği gösteren orojenik olmayan bir ortamdan türediklerini önermektedir.

İzotop verilerini de içeren tüm kaya jeokimyası verileri; kayaçların alkalen karakterde olup E-MORB ve OIB tipleri arasındaki bir geçiş ortamında oluştugu işaret etmektedir. Ayrıca veriler, yapılan kayaçların DMM ve EM-I karışımından oluşan bir eriyikten türediklerini önermektedir.

Anahtar kelimeler: Çorum, petrografi, mineral kimyası.

To my husband Cengiz Küçük & my family

ACKNOWLEDGMENTS

I am greatly indebted to my supervisor Assist. Prof. Dr. Fatma Toksoy KÖKSAL for her supervision and encouragement throughout the research, and for valuable criticisms and warm guidance.

I am greatly thankful to my colleague Dr. Serhat KÖKSAL from Central Laboratory, Middle East Technical University for his constructive suggestions, valuable criticisms and warm guidance like a brother. I also would like to express my sincere gratitude to him due to support in analysis made by TIMS (Thermal Ionisation Mass Spectrometer).

The financial support for field and preliminary studies was provided by Middle East Technical University, Research Fund Project (BAP) code: BAP-07.02.2012.101.

I would like to express my thanks to Management Board of Central Laboratory, Middle East Technical University for giving an opportunity to complete my thesis and to use facilities in the Laboratory.

Mr. Levent Yıldız from Central Laboratory, Middle East Technical University is acknowledged for his support in preparation of crushed and powdered rock samples for whole rock and isotope analyses.

I extend my gratitude to my mother and father for their patience and encouragement throughout my life.

Finally, I would like to express my sincere thanks to my husband Cengiz KÜÇÜK for his endless patience and encouragement throughout my study and during the preparation of this thesis.

TABLE OF CONTENTS

ABSTRACT	vii
ÖZ	ix
ACKNOWLEDGMENTS	xiii
TABLE OF CONTENTS	xv
LIST OF TABLES	xviii
LIST OF FIGURES	xix
CHAPTERS	
1. INTRODUCTION	1
1.1. Purpose and Scope.....	1
1.2. Geographic Setting	2
1.3. Methods of Study	2
1.3.1. Mineralogical Analyses.....	3
1.3.2. Whole Rock Element and Isotope Geochemistry Analyses.....	4
1.4. Review on Ophiolite Belts of Turkey.....	7
1.4.1. Intra-Pontide Ophiolite Belt.....	7
1.4.2. North Anatolian Ophiolite Belt.....	7
1.4.3. Southeast Anatolian Ophiolite Belt.....	8
2. GEOLOGY	11
2.1. Introduction	11
2.2. Regional Geological Setting.....	11
2.3. Geology of the Study Area	17
2.3.1. Basalts.....	18

2.3.2. Metabasalts	20
2.3.3. Dykes	21
3. PETROGRAPHY	29
3.1. Introduction	29
3.2. Basalts.....	29
3.3. Metabasalts	38
3.4. Dykes	46
4. MINERAL CHEMISTRY AND PETROGENETIC IMPLICATIONS	55
4.1. Introduction	55
4.2. Pyroxene	55
4.2.1. Compositional Variations	55
4.2.2. Nomenclature and Substitution Mechanisms.....	64
4.3.3. Implications for Petrology and Tectonic Setting	67
4.3. Feldspar	69
4.3.1. Compositional Variations	71
4.3.2. Nomenclature and Substitution Mechanisms.....	73
5. WHOLE-ROCK CHEMISTRY	77
5.1. Introduction	77
5.2. Effect of Alteration on Whole-Rock Composition.....	77
5.3. Compositional Variations	81
5.4. Chemical Classification and Implications for Tectonic Setting	84
5.5. Multi-Element and Rare Earth Element Diagrams.....	87
5.6. Isotope Geochemistry	88

6. DISCUSSION ON THE GENESIS OF THE STUDIED ROCKS	91
6.1. General Features	91
6.2. Mineralogical Constraints	91
6.3. Geochemical Constraints.....	93
6.4. Isotopic Constraints	99
7. CONCLUSIONS.....	103
8. REFERENCES.....	105
9. APPENDICES	115
A. MAJOR AND MINOR ELEMENT CHEMICAL ANALYSES FOR PYROXENE FROM METABASALTS	115
B. MAJOR AND MINOR ELEMENT CHEMICAL ANALYSES FOR PYROXENE FROM DYKES	117
C. MAJOR AND MINOR ELEMENT CHEMICAL ANALYSES FOR PYROXENE FROM BASALT PHENOCRYSTS	124
D. MAJOR AND MINOR ELEMENT CHEMICAL ANALYSES FOR PYROXENE FROM BASALT OVERGROWTHS	147
E. MAJOR AND MINOR ELEMENT CHEMICAL ANALYSES FOR PYROXENE FROM BASALT MATRIX	150
<u>F. MAJOR AND MINOR ELEMENT CHEMICAL ANALYSES FOR FELDSPAR FROM METABASALTS</u>	155
G. MAJOR AND MINOR ELEMENT CHEMICAL ANALYSES FOR FELDSPAR FROM DYKES	156
H. MAJOR AND MINOR ELEMENT CHEMICAL ANALYSES FOR FELDSPAR FROM BASALTS.....	161

LIST OF TABLES

Table 1. Minimum and maximum major oxide values of the pyroxenes for the studied rocks.....	56
Table 2. EPMA analyses results for the pyroxenes in Figure 32.	61
Table 3. Minimum and maximum major oxide values of the feldspars from the rock groups of studied rocks.	71
Table 4. Major oxide (wt%) compositions of the studied samples.	78
Table 5. Trace element (ppm) compositions of the studied samples.	79
Table 6. Sr-Nd isotope ratios for the studied samples.....	89
Table 7. Mg# ranges of the pyroxenes for the studied rocks.	91

LIST OF FIGURES

Figure 1. Location map of the study area.....	5
Figure 2. Main ophiolite belts of Turkey (Modified from 1:2 000 000 scaled geological map of Turkey, MTA).	9
Figure 3. Simplified geological map of the study area (modified from 1:100000 scale geology map of H33-Çorum) and (b) sample locations on the map. (c) Sketch of X-Y cross-section taken from the study area from N to S (not to scale).	18
Figure 4. Photograph showing the position of the marbles from the study area.....	19
Figure 5. Photograph showing pillow basalts from the study area.	20
Figure 6. Photograph showing a pillow basalts and talc in the matrix from the study area.	21
Figure 7. Metabasalts showing different degrees of schistosity and greenschist facies metamorphism (dark green chlorite spots) (a) weak, (b) moderate to strong, (c) strong.....	22
Figure 8. Photograph showing contact relationship between metabasalts and pillow basalts in the study area.....	24
Figure 9. Photographs showing parallel dyke system in the study area.....	25
Figure 10. Photograph showing general (a) and close-up view (b) of dykes from the study area.	26
Figure 11. Photograph showing doleritic dyke close to contact with marble from the study area.	27
Figure 12. Microphotograph showing (a) euhedral pyroxene phenocrysts with simple twinning in a basalt sample (b, c) corroded subhedral pyroxene crystals (pyx: pyroxene, cc:calcite, comp.zon.: compositional zoning).	31
Figure 13. Microphotograph of a basalt showing pyroxene aggregates (glomeroporphyritic texture) ((a) analyser out, (b) analyser in, pyx: pyroxene).	33

Figure 14. Microphotograph of a basalt showing pyroxene phenocrysts in a glassy groundmass with pyroxene microcrysts ((a) analyser out, (b) analyser in, pyx: pyroxene).....	34
Figure 15. Microphotograph of a basalt showing pinkish to reddish pyroxene phenocrysts with tailing property ((a) analyser in, (b) analyser out, pyx: pyroxene, felds: feldspar).....	35
Figure 16. Microphotograph of a basalt showing pyroxene crystals with reaction rim, compositional zoning and simple twinning((a) analyser out, (b) analyser in, pyx: pyroxene, chl: chlorite, rxn rim: reaction rim).....	36
Figure 17. Microphotograph of a basalt showing a corroded pyroxene crystal with compositional zoning (1) and reaction rim (formation of a new pyroxene, 2), corrosion (3) in (a) and (b) ((a) analyser out, (b) analyser in, pyx: pyroxene). (c) Back scattered image of a clinopyroxene crystal (1) showing overgrown by a new crystal material (2).	37
Figure 18. (a) Microphotograph of a basalt showing long-prismatic pyroxene microcrysts with tailing property in groundmass (analyser in, pyx: pyroxene, cc: calcite). (b) Back scattered image of a clinopyroxene crystal with tailing. (c) Back scattered image of a clinopyroxene crystal (1) showing overgrown by a new crystal material (2) and tailing (3).	39
Figure 19. Microphotograph of a basalt showing finely spongy cellular texture in the center and near the rim of feldspar crystals ((a) analyser out, (b) analyser in, pyx: pyroxene, felds: feldspar).....	41
Figure 20. Microphotograph of a metabasalt ((a) analyser out, (b) analyser in, ep: epidote, chl: chlorite, cc: calcite)	43
Figure 21. Microphotograph of a metabasalt showing a sheared vesicle resembling augen structure ((a) analyser out, (b) analyser in, ep: epidote, pyx: pyroxene, chl: chlorite, cc: calcite).	44

Figure 22. Microphotograph of a metabasalt showing simple twinning (a) and sector zoning (b & c) in clinopyroxene phenocrysts (pyx: pyroxene, comp.zon.: compositional zoning).....	45
Figure 23. Microphotograph of a metabasalt showing a pyroxene crystal displaying both simple twinning and compositional zoning. ((a) analyser out, (b) analyser in, pyx: pyroxene, cc: calcite, comp.zon.: compositional zoning).....	47
Figure 24. Microphotograph of a metabasalt showing a corroded pyroxene crystal. ((a) analyser out, (b) analyser in, pyx: pyroxene).	48
Figure 25. Microphotograph of a metabasalt showing growth of clinopyroxene microcrysts around a larger feldspar crystal. ((a) analyser out, (b) analyser in, felds: feldspar, pyx: pyroxene).....	49
Figure 26. Microphotograph of a dyke showing ophitic and intergranular textures (felds: feldspar, pyx: pyroxene).	50
Figure 27. Microphotograph of a dyke showing both compositional zoning and twinning in a pyroxene crystal and a feldspar crystal (felds: feldspar, pyx: pyroxene).	51
Figure 28. Microphotograph of a dyke showing a corroded pyroxene crystal with compositional zoning, and surrounding feldspars with sericitization ((a) analyser out, (b) analyser in, pyx: pyroxene, felds: feldspar).....	52
Figure 29. Microphotograph of a dyke showing twinned feldspars ((a) analyser out, (b) analyser in, pyx: pyroxene, felds: feldspar, chl: chlorite, cc: calcite).	53
Figure 30. Variation diagrams for major and minor element compositions for the studied rocks.	58
Figure 31. Sketch drawing showing three different crystallization stages for the pyroxenes of the basalts and their compositional constituents (not to scale).	59

Figure 32. (a) Microphotograph from a basalt sample in analyser out condition, (b) Back scattered image of the pyroxene crystal (1) (blue quadrangle) from (a) showing overgrown by two different crystal material (2) and (3). (c) Back scattered image of a pyroxene crystal (4) showing overgrowth of Fe-rich new crystal material (5).....	60
Figure 33. Covariation diagrams of $\text{Al}^{(\text{t})}$ and Ti (pfu) against $\text{Fe}^{(\text{t})} / (\text{Mg} + \text{Fe}^{(\text{t})})$ (the symbols are same as in Figure 30).	63
Figure 34. The relation between Ca# and Mg# for the studied rocks (the symbols are same as in Figure 30).	64
Figure 35. The place of pyroxene data on Q-J diagram adapted from Morimoto and Kitamura (1983) (a) and the plots of pyroxene on the Ca-Mg-Fe clinopyroxene classification diagram after Poldervaart & Hess (1951) (b) (the symbols are same as in Figure 30).	65
Figure 36. The substitution mechanisms and Ti-Al ^(t) ratio diagram (the symbols are same as in Figure 30).	67
Figure 37. The place of the pyroxene data on the Ti-Na-Al ^[4] triangle diagram proposed by Papike et al. (1974) (the symbols are as in Figure 30).	68
Figure 38. The place of the pyroxene data on the Ti+Cr-Ca diagram (Leterrier et al., 1982) (the symbols are as in Figure 30).	69
Figure 39. The place of pyroxene data on the diagrams of ; (a) $\text{SiO}_2 - \text{Al}_2\text{O}_3$ (wt%) (Le Bas, 1962), (b) Ti – (Ca+Na) (pfu) (Leterrier et al., 1982) and (c) Ti-Al ^(t) (pfu) (Liota et al., 1988) (the symbols are same as in Figure 30).	70
Figure 40. Variation diagrams of elements against Si (pfu) (symbols are same as in Figure 30).	72
Figure 41. The plots for the feldspars from studied rocks on feldspar ternary diagram (symbols are same as in Figure 30).	74
Figure 42. Plot showing coupled substitution mechanism for feldspars from the study area (symbols are same as in Figure 30).	75

Figure 43. Covariation diagrams of Ba, Sr, Rb, TiO ₂ , P ₂ O ₅ and K ₂ O againts Zr to show effect of alteration on the studied rocks.....	80
Figure 44. Major and trace element systematic against MgO (wt%) for the studied rocks	82
Figure 45. (a) Total alkalies vs. silica diagram and (b) Zr/TiO ₂ vs. Nb/Y diagram for the studied rocks (Irvine and Bragar, 1971; Winchester and Floyd, 1977).	85
Figure 46. Tectonomagmatic discrimination diagrams for the studied rocks: (a) Pearce (1982); (b) Pearce and Cann (1973); (c) Mullen (1983); (d) Wood (1980). ..	86
Figure 47. N-MORB, E-MORB and OIB normalized multi element diagrams and chondrite normalized rare earth element diagram and for studied rocks (Sun and McDonough. 1989)	88
Figure 48. N-MORB normalized multi element variation diagram comparing Group I rocks of the study belonging Çelik et al. (2013) with rocks from the study area (Sun & McDonough, 1989).	94
Figure 49. Chondrite normalized multi element variation diagram comparing Group I rocks of the study belonging Çelik et al. (2013) and average OIB and E-MORB values from Sun & McDonough (1989) with rocks from the study area.....	95
Figure 50. Ti-V discrimination diagram showing tectonic setting relationship of the studied rocks (Shervais, 1982).	96
Figure 51. Variation of Y/Nb against Zr/Nb for the studied samples. (Data sources for OIB, E-MORB, N-MORB and SSZ-type Tethyan basaltic rocks are belonging to Mahoe et al. (2004), Saccani and Photiades (2005) and Aldanmaz et al.(2008), Göncüoğlu et al. (2010)).	97
Figure 52. Variation of TiO ₂ (wt%) against Zr (ppm) for the studied samples. (Data sources for OIB, E-MORB, N-MORB and SSZ-type Tethyan basaltic rocks are same with Figure 51).....	98

Figure 53. Nd-Sr diagram of initial isotopic ratios for the studied rocks (closed diamonds). (DMM values are from Zindler and Hart (1986), MORB, HIMU and EM values are from Hart et al. (1999) and Workman and Hart (2005), and colored fields are data from Çelik et al. (2013)). The dashed DMMa, DMMb and MORB are values corrected to 150 Ma (from Çelik et al., 2013). Isotopic data for this thesis were corrected to 170 Ma..... 100

CHAPTER 1

INTRODUCTION

1.1.Purpose and Scope

Geology of Turkey stands for an important part in the Alpine-Himalayan orogenic system. Turkey is represented by a very complex geology. Although there are increasing amount of geological data, this complex geology results in different point of views on the geological evolution of Turkey (Okay, 2008). Geology of Turkey is closely related to the evolution of Neotethys. Subbranches of Neotethys Ocean once were surrounding the main tectonic units of Turkey. These tectonic units are now separated by sutures which were formed the closure of subbranches of Neotethys. Developed series of oceanic seaways and microcontinents during the fragmentation of the northern part of Gondwana were closed by convergence of Africa and Euroasia during the Late Cretaceous (Robertson, 2002). The complete closure of this ocean ended up with the İzmir-Ankara-Erzincan Suture. Study area of this thesis is on the İzmir-Ankara-Erzincan branch of the Alpine Neotethys.

Ophiolite occurrences in Earth history largely coincide with orogenic events causing the formation and break-up of supercontinents. Therefore, ophiolites and ophiolitic melanges are useful databanks in order to observe and examine ancient pieces of oceanic lithosphere and they keep significant evidence of some tectono-magmatic events such as opening of a rift or subducting of a continent or intra-plate magmatism (Göncüoğlu et al., 2010).

Today, it is possible to analyse rocks in terms of their mineral chemistry and geochemistry including isotopic once by using analytical methods such as electron microprobe and ion-probe techniques. Thus, this methods supply valuable information about petrologic history of rocks.

This thesis aims to provide contribution to the formation of the mafic magmatic rocks which are located around Çorum region by means of petrography, whole rock element and isotope geochemistry, and mineral chemistry. Firstly, a field study was conducted and rock samples were collected. After that, textural and mineralogical features of the studied rocks were examined by a petrographical study. Followingly, mineral chemistry study including nomenclature of minerals, substitutional mechanisms and their implications on petrology and tectonic settings were discussed. Additionally, geochemical interpretations were made based on major and trace elements, and isotopic characteristics of the studied rocks. Finally, in the light of the petrographical, mineralogical, whole rock geochemical characteristics, the comparison of the pyroxene occurrences in different rock samples and their crystallization processes were examined.

1.2.Geographic Setting

The study area is located between the city center of the Çorum and Alaca town of Çorum. It is located in H33 quadrangle of the 1:100 000 scaled topographic map of Turkey within latitudes 70-75 N and longitudes 55-60 E in the east of Central Anatolia (Figure 1).

1.3.Methods of Study

Geological features of volcanic rocks around Burunköy (Çorum) region are planned to be investigated in this thesis. The first part of the study includes the sampling from the field. Study area is located at southeast of Çorum, between city center of Çorum and Alaca (Figure 1). Rock outcrops were sampled from 10 different selected locations. Totally, 30 rock samples were collected for petrographical and geochemical studies. The petrographical study was performed in order to detect the main petrographical characteristics of the study area. 17 samples of total 30 samples were chosen from the rock samples in order to make petrographic interpretations and

mineral chemistry analyses (EPMA). Moreover, 6 of 17 samples were chosen for whole rock element analyses and isotope (TIMS) analysis.

1.3.1. Mineralogical Analyses

Major and minor element compositions of the minerals from the studied samples were performed by using Electron Probe Microanalyser (EPMA) which is an ideal method for non-destructive in-situ microanalysis. Coating and the analyses of the well-polished 46 mm x 25 mm thin-sections were carried out at Central Laboratory, Middle East Technical University. Non-conductive geological samples require a conductive coating in order to prevent charging under electron bombardement. Therefore, carbon coating is preferred using Electron Probe Microanalyser because it has a minimal effect on the X-ray spectrum. A carbon coater belonging to Quorum Technologies, Q150R ES, were used for this purpose. The optimum thickness of the carbon should be around 20 nm. The thickness of the carbon was controlled by the device by using a fixed current and evaporation time. The analyses on the minerals were performed by a fully automated JEOL-JXA-8230 electron microprobe at Central Laboratory, Middle East Technical University. The instrument has been operating in two ways. These are energy-dispersive and wavelength-dispersive modes. Energy-dispersive type spectrometer records X-rays of all energies and produces an output in the form of a plot of intensity versus X-ray photon energy. However, wavelength-dispersive type spectrometer uses crystals working according to Bragg reflection principle. Although spectral resolution is better in energy-dispersive spectrometer; however, wavelength-dispersive one is faster and more convenient. Both spectrometers were used according to purpose of the study. Energy-dispersive mode was generally used in order to determine what elements a mineral has, and wavelength-dispersive mode was used to measure major and minor oxides in percent. 15 kV acceleration voltage and 15 nA beam current were used during analyses. The applied beam size was 5 µm. A variety of natural and synthetic standards were used for calibration. The following elements were analysed using the

standards: Albite for Na, wollastonite for Ca and Si, Al_2O_3 for Al, MgO for Mg, hematite for Fe, rhodonite for Mn, Ni-metal for Ni, orthoclase for K, TiO_2 for Ti, Cr_2O_3 for Cr, SrTiO_3 for Sr and baryte for Ba. Matrix corrections were performed by the PRZ (XPP method metal/oxide) procedure in the JEOL software.

1.3.2. Whole Rock Element and Isotope Geochemistry Analyses

Whole rock samples for the chemical analyses were chosen after examining thin sections of the studied samples in terms of mineralogical compositions and degree of alteration. Six representative samples (2 basalt, 2 metabasalt, 2 dike) were selected for analyses. The rock samples were crushed to small chips, less than 1 cm size, in a jaw crusher. Then altered chips were eliminated by hand-picking. After that, the rest of the samples were ground in order to obtain sample powder. All these processes were carried at Central Laboratory, Middle East Technical University. For the whole rock analyses, powdered samples were sent to the Acme Laboratories, Canada. For major elements and the trace elements Ba, Nb, Ni, Sr, Sc, Y and Zr, an ICP emission spectrograph of Jarrel Ash AtomComb 975 model were used. An ICP mass spectrometer of Perkin-Elmer Elan 6000 model were used for the determination of other trace elements including rare earth elements. Accuracy for major elements and trace elements is better than 2% and 10%, respectively.

Isotope geochemistry experiments of Sr and Nd were performed at Middle East Technical University, Central Laboratory, R&D (Research and Development) Education and Measurement Center with methods of TLM-ARG-RIL-01 (Experiment instruction for isotope ratio analysis of Sr) and TLM-ARG-RIL-02 (Experiment instruction for isotope ratio analysis of Nd) which were adapted from methods in Köksal and Göncüoğlu (2008).

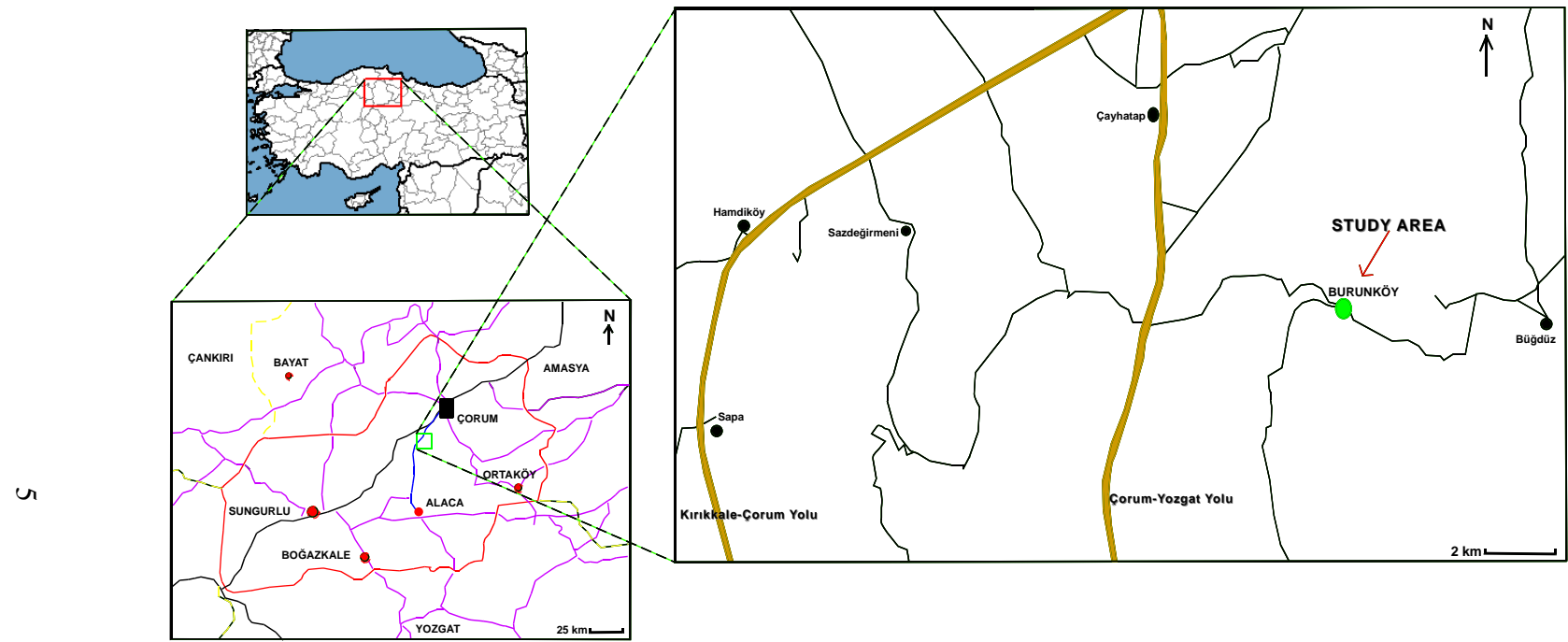


Figure 1. Location map of the study area.

Half of the sample powders of total whole rock analysis were used for this purpose. Weighing, chemical resolving and chromatography processes were performed at Clean Laboratory with 100 sanitation standard. About 80 mg rock powder were weighed from each specimen and they transferred into PFA (a kind of teflon) bottles. Samples were resolved completely in 4 mL 52% HF which were on a hot plate with the temperature of 160°C for 4 days. After that, dried samples were resolved for 1 day in 4 mL 6 N HCl solution. Then, these samples were evaporitized and dried on hot plate and they were placed in 1 mL 2.5 N HCl and prepared for chromatography. Sr element was separated in teflon columns by using 2.5 N HCl acid and 2 mL volume of Bio Rad AG 50 W-X8, 100-200 mesh resin. After collecting Sr, fraction of rare earth elements were collected with 6 N HCl. Sr was loaded on single Re-filament by using Ta-activator and measured on static mode. Data of $^{87}\text{Sr}/^{86}\text{Sr}$ were normalized to $^{86}\text{Sr}/^{88}\text{Sr}=0.1194$. During measurements, Sr standard NBS 987 was measured as 0.710261 ± 5 ($n=2$) and required bias corrections were done on measurement results. Nd element was separated in teflon columns by using 0.22 N HCl acid from other rare earth elements and run through 2 mL volume of Bio Rad (biobeads) resin which was surrounded by HDEHP (bis-ethyexyl phosphate). Separated Nd was located on Re-filament with 0.005 N H₃PO₄ and measured on static mode by using double filament technique. During analysis $^{143}\text{Nd}/^{144}\text{Nd}$ data were normalized with $^{146}\text{Nd}/^{144}\text{Nd}=0.7219$ and Nd LaJolla standard was measured as 0.511848 ± 5 ($n=2$). There was any bias collection done on Nd isotope ratio on measurement results. Measurements were performed as multi-collection by Triton Thermal Ionisation Mass Spectrometry (Thermo-Fisher). Analytical uncertainty is around 2 sigma. BCR-1 USGS rock standard which was measured by the same processes with experiment samples gives $^{87}\text{Sr}/^{86}\text{Sr}=0.705028\pm 9$ and $^{143}\text{Nd}/^{144}\text{Nd}=0.512626\pm 4$.

1.4. Review on Ophiolite Belts of Turkey

Ophiolitic remnants of the Paleotethys and Neotethys are observed as isolated outcrops throughout Turkey. There are three main ophiolite belts in Turkey. These are Intra-Pontide Ophiolite Belt, North Anatolian Ophiolite Belt and Southeast Anatolian Ophiolite Belt (Figure 2).

1.4.1. Intra-Pontide Ophiolite Belt

The Intra-Pontide Ophiolite Belt is composed of sequence of dismembered metaophiolites such as serpentized peridotite, layered cumulate gabbros, isotropic gabbros, diabase dikes, sheeted dikes and mafic lavas and overlying epi-ophiolitic deep-sea cover sediments (Bozkurt and Mittwede, 2001). It is located between Rhodope-Strandja and Istanbul-Zonguldak terranes in the north and Sakarya Composite Terrane in the south (Göncüoğlu et al., 1997). Since North Anatolian Transform Fault is still active, oblique and strike-slip movements within this fault have been affecting the main components of the Intra-Pontide Ophiolite Belt. Although the opening age of the Intra-Pontide oceanic branch has not been clearly revealed, according to literature, time passing from middle of Middle Jurassic to middle of Late Cretaceous is the ridge spreading age of the unit.

1.4.2. North Anatolian Ophiolite Belt

The North Anatolian Ophiolite Belt represents the northern Neotethyan ophiolite and seen as allochthonous fragments. The North Anatolian Ophiolite Belt is composed of huge bodies of ophiolitic sequences and tectonic melanges of the Izmir-Ankara accretionary complex (Göncüoğlu et al., 1997; Okay and Tüysüz, 1999). The North Anatolian Ophiolite Belt were positioned on the Tauride-Anatolide Platform in South during Late Cretaceous. Moreover, the units of Sakarya Composite Terrane overlie on the ophiolites in northwest Anatolia tectonically. However, the ophiolites are thrust onto Tertiary basins along steep basements in Central and East Anatolia (Göncüoğlu et al., 1997). The ophiolites display several characteristics geochemical

features of MORB, OIB and supra-subduction zone-type ophiolites and were transported towards south onto the Tauride-Anatolide Platform (Göncüoğlu et al., 2006 a,b; Yalınız et al., 2000). Since the geochemistry of the rocks within the melange displays several characteristics, it indicates a complex oceanic lithosphere formation. The earliest ages of MORB are Carnian indicating that the formation of Izmir-Ankara oceanic crust corresponded to Middle Triassic and lasted until Late Cretaceous (Göncüoğlu et al., 2000a; Tekin et al., 2002).

1.4.3. Southeast Anatolian Ophiolite Belt

The Southeast Anatolian Ophiolite Belt was located between Tauride platform in the north and Arabian platform in the south representing the southern part of the Neotethyan ophiolite and contains different imbricated structural units of oceanic and island-arc clusters. The Southern Neotethyan ocean was active during the period from Triassic to Eocene (Şengör and Yılmaz, 1981; Robertson et al., 2007; Parlak et al., 2009). According to studied paleontological data from the ophiolitic unit, its age is corresponding to Jurassic-Late Cretaceous (Göncüoğlu, 2010). The studied data about ophiolitic sequences of the Souteast Anatolian Ophiolite Belt indicate that a supra-subduction zone setting (Robertson, 2002; Parlak et al., 2002, 2004). Moreover, Kızıldağ Ophiolite in Hatay forms an ophiolitic succession and can be correlated with Zagros and Oman ophiolites and the Troodos Massif in Cyprus (Göncüoğlu, 2010).

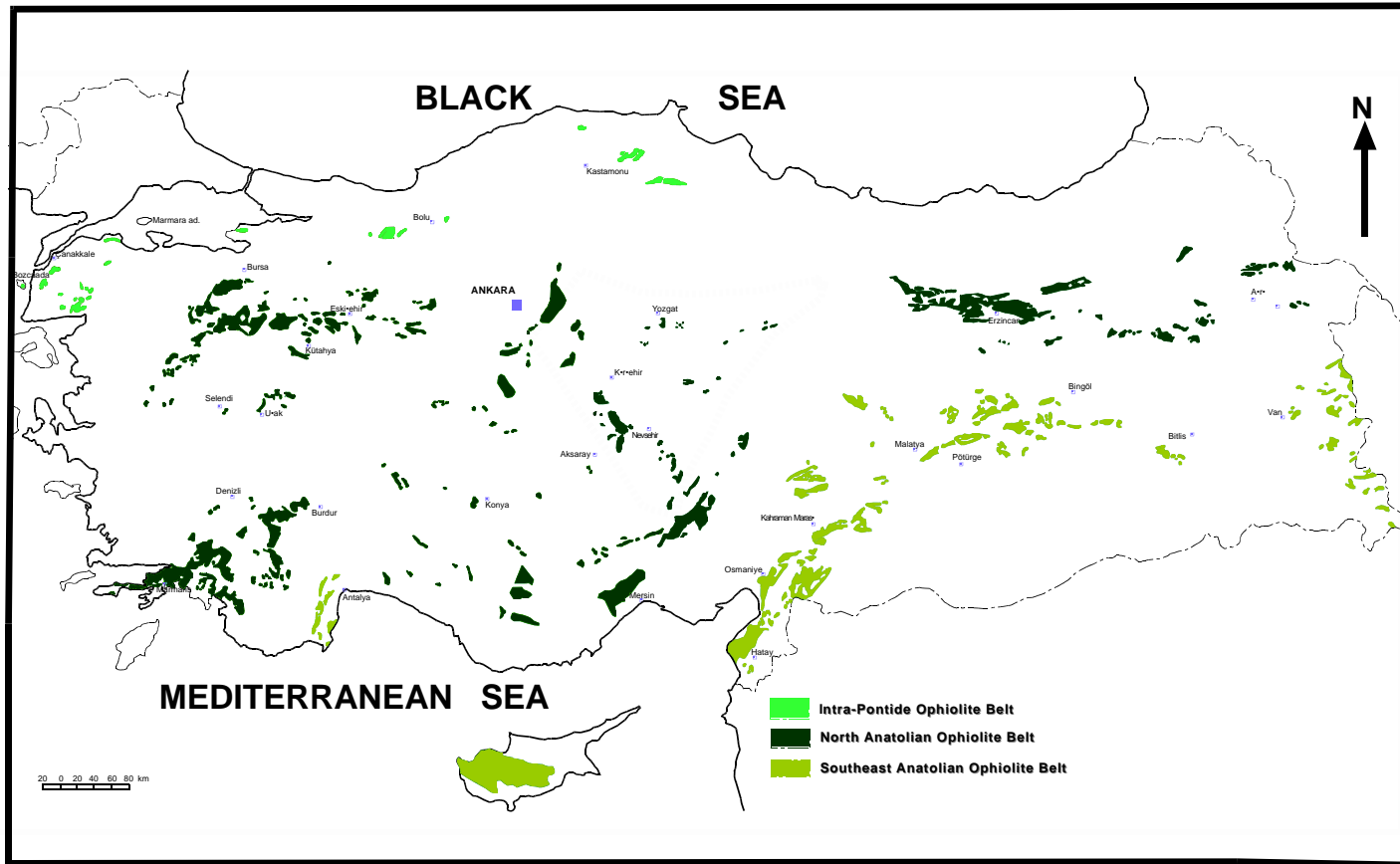


Figure 2. Main ophiolite belts of Turkey (Modified from 1:2 000 000 scaled geological map of Turkey, MTA).

CHAPTER 2

GEOLOGY

2.1. Introduction

Anatolia is grouped into 3 main continental zones (Okay, 2008). These continental zones are the Pontides, the Anatolide-Tauride Block and the Arabian Platform from north to south. These continental zones are separated from each other by suture zones: The Intra-Pontide Ophiolite Belt, the North-Anatolian Ophiolite Belt and the Southeast Anatolian Suture Belt from north to south, respectively. Among them, the North Anatolian Ophiolite Belt is composed of huge bodies of ophiolitic sequences and tectonic melanges of the Izmir-Ankara accretionary complex (Göncüoğlu et al., 1997; Okay and Tüysüz, 1999). The well known ophiolitic melange which is known as Ankara Melange of Bailey and Mc Callien (1953) is mainly composed of dismembered blocks of red to green, intensely folded-fractured, thin bedded radiolarites; fractured peridotites-serpentinites; fractured radiolaria bearing pelagic limestones; folded and fractured Jurassic-Cretaceous carbonates; Cenomanian-Turonian marl-argillaceous limestone sequences and rare fragments of low-grade metamorphic blocks. All of the units of the ophiolitic melange are found in an intensely tectonized, mylonitic-brecciated ophiolitic matrix. In the extent of this thesis, the mafic rocks (basaltic rocks and doleritic dykes) belonging to ophiolitic Ankara melange from the Burunköy area (Çorum) are studied.

2.2. Regional Geological Setting

Turkey is an important segment of the Alpine-Himalayan orogenic belt which lies between the cratons of Laurasia in the north and Gondwana in the south. Within this suture zone, remnants of oceanic basins of Tethys ocean, of which the Eastern Mediterranean sea is the last surviving remnant, can be found. Paleozoic ocean Paleotethys was followed by smaller Mesozoic ocean basins (Neotethys) (Pickett et

al., 1996). The Mediterranean ophiolites belonging to Tethys ocean were divided into two groups (Nicolas & Jackson, 1972; Rocci et al., 1975; Abbate et al., 1976): a) the western and central Mediterranean ophiolites (Alps-Apennines-Carpathians-Dinarides-Hellenides), b) the eastern Mediterranean ophiolites (Cyprus-Turkey-Syria-Oman). Another study was suggested that Tethyan ophiolites were grouped into as subduction related (eastern Tethyan region) and subduction unrelated (western Tethyan region) (Toksoy-Köksal, 2003 and references therein).

Ophiolites in the Mediterranean region show differences from each other in terms of age and tectonic setting. The Mid-Late Jurassic ophiolites in western region composed of different tectonic settings such as subduction related Eastern Albanian and Vourinas ophiolites in Greece, mid-ocean ridge (MORB) related Western Albanian ophiolites, transitional character related (from MORB to supra-subduction zone (SSZ)) South Albanian ophiolites, Pindos and Asproptamos ophiolites in Greece and intracontinental back-arc basin related Guevgueli ophiolite in northeast Greece (Robertson, 2002; Dilek and Thy, 2009; Topuz et al., 2013). However, the Late Cretaceous ophiolites in Turkey, Troodos in Cyprus and Baer-Bassit in Syria show supra-subduction zone (SSZ) character (Parlak et al., 2009 and references therein). According to studies conducted on the Anatolian ophiolites, the common lithological and isotopic features suggest that Anatolian ophiolites formed as a part of a very large ophiolite body comparable with the size of the Semail Ophiolite in Oman (Okay et al., 2001).

The Turkish branch of Neotethys is characterized by three major east-west trending belts (Figure 2). Each of belt records closure of a separate branch of Neotethys: a)Intra-Pontide Ophiolite Belt, b)İzmir-Ankara-Erzincan Ophiolite Belt, c)Southeast Anatolian Suture Belt. The İzmir-Ankara-Erzincan Suture Zone extends in an east-west direction for more than 2000 km from the Aegean coast to the Sevan-Akera suture in Armenia. Moreover, it continues across the Aegean Sea and links with the Vardar Suture in the Balkan region (Figure 2).

The İzmir-Ankara Suture Zone which is in the northern Turkey represents the remnants of the Neotethyan İzmir-Ankara-Erzincan Ocean, which is one of the most notable branches of the Neotethys in Turkey, dating back to Devonian that was consumed by northward subduction under the Pontides from Late Paleozoic to Late Mesozoic with continental collision during Paleocene to Early Eocene resulting in southwergent obduction of ophiolite (Okay & Tüysüz, 1999; Yalınız et al., 2000; Tekin et al., 2002; Toksoy-Köksal, 2003; Göncüoğlu et al., 2006; Topuz et al., 2013). It has a key importance to study the formation of ophiolites and related oceanic rocks. Ophiolite related rocks were integrated into the subduction accretion prisms and melange complexes and come through subduction.

Generally suture zones are composed of allochthonous assemblages which comprise of subduction-accretion units, ophiolites and metamorphic equivalents of the continental margin sequences. The presence of ophiolite-bearing melange complexes or accretionary prisms along IAESZ have been known since Bailey and McCallien (1950). According to Şengör and Yılmaz (1981), the Sakarya Composite Terrane in the north and the Kırşehir Massif and the Anatolide-Tauride block in the south were separated by İzmir-Ankara-Erzincan Ocean during the Jurassic time. Moreover, it is indicated by an association of alkali ocean island basalts (OIB) type metabasites and mid-ocean ridge basalts (MORB). The İzmir-Ankara Erzincan Suture Zone is formed by several segments (Okay & Tüysüz, 1999). The segment between İzmir and Balıkesir is around 180 km long. Along this segment, Sakarya Composite Terrane is in contact with Bornova Flysch Zone of Anatolide-Tauride block. The Sakarya Composite Terrane contains the Karakaya Complex, which is represented by the Nilüfer Unit that is characterized by low-grade greenschist facies metamorphism in this region, unconformably overlain by a Jurassic to Lower Cretaceous succession (Okay & Tüysüz, 1999; Sayit, 2005).

Another segment is between Balıkesir and Beypazarı is around 280 km long. Along this segment, the Sakarya Composite Terrane is in contact with Tavşanlı Zone of

Anatolide-Tauride block. Tavşanlı Zone represents a regional blueschist belt. Karakaya Complex units and the overlying Jurassic–Cretaceous succession of the Sakarya Composite Terrane are found in the north of the suture and for the Central Sakarya Basin in Mudurnu-Göynük area and Nallıhan area. In the south, there are Cretaceous blueschists, accretionary complex, ophiolite and Eocene granodiorites of the Tavşanlı Zone (Okay, 1984b, Okay & Tüysüz, 1999).

In the segment between Beypazarı and Ankara, the width of the Tavşanlı Zone getting increased. To the southeast of Beypazarı, there is a major turbidite dominated Late Cretaceous–Eocene basin called the Haymana Basin. The contact between the Haymana Basin and Tavşanlı blueschists are tectonically covered by Neogene sedimentary rocks. The basement of the Haymana Basin is formed by an accretionary complex and Jurassic – Lower Cretaceous carbonates of the Sakarya Composite Terrane (Görür et al., 1984; Koçyiğit, 1991).

The İzmir-Ankara-Erzincan Suture Zone has a contact of Sakarya Composite Terrane and Kırşehir Massif between the Haymana Basin and Sivas. In this region, the rocks of the Sakarya Composite Terrane was emplaced over the Tethyan subduction-accretion complexes forming a 5-10 km wide tectonic belt resulting in a large loop of the suture called Çankırı loop (Okay & Tüysüz, 1999). Sakarya Composite Terrane comes in direct contact with the Anatolide-Tauride block in the region of south of the Eastern Pontides and the length of this segment is 320 km. In the north of this segment, there is a well-developed Upper Cretaceous magmatic island arc. In the south, there is a Senonian fore-arc region represented by the Inner Eastern Pontides (Okay & Tüysüz, 1999).

During the convergence of İzmir-Ankara-Erzincan Ocean, Pontides stood for the upper plate and the Anatolide-Taurides for the lower plate. Between Late Turonian and Latest Campanian, the arc magmatism of the Pontides formed along which the Black Sea coast. Moreover, ophiolite obduction over the passive margin of

Anatolide-Tauride block started in the Santonian and took place after the origination of subduction in the Turonian (Okay et al., 2001).

Oceanic accretionary complexes cover wide areas below the İzmir-Ankara suture. They dominantly consist of mafic lava, pyroclastics, radiolarian chert and pelagic shale with small amounts of pelagic limestone, greywacke and serpentinite (Bozkurt and Mittwede, 2010). However, some accretionary complexes also contain continental margin sequences such as Lycian melange most probably because of the incorporation with the continental crust during their emplacement.

Moreover, these accretionary complexes differ from their Pacific counterparts in terms of insufficiency of the siliciclastic sediments. The accretionary prism units of the İzmir-Ankara Ocean, that is Central Sakarya Ophiolite Complex according to Göncüoğlu et al. (2000, 2006a) were thrust onto the Anatolide unit along steep contacts. Basement rocks of the Sakarya Composite Terrane represented by the oceanic remnants of the İzmir-Ankara Ocean and they are overthrusted onto the upper tectonic unit.

The Sakarya Composite Terrane which is the active margin of the İzmir-Ankara Ocean contains several tectonic units. The basement of the unit is composed of high-grade metaclastic and metabasic rocks which are intruded by Variscan granitoids. The first overstep sequence is formed by platform type deposits and belong to Permian time. Extensional basin development was observed in the Early Triassic and it is followed by the emplacement of Paleotethys. The second overstep sequence is composed of Lower Jurassic to Mid-Cretaceous platform type deposits which were overlie on the Karakaya complex unconformably. Moreover, this second overstep is overlain by the oceanic assemblages of Intra-Pontide branch of Neotethys during its Alpine closure (Göncüoğlu et al., 2010 and references therein).

The basement of Anatolide unit, which represents the metamorphic northern margin of the Anatolide-Tauride Block, is composed of orthogneisses, quartzofeldspathic

schists and mica schists with garnet and greenschists (Bortolotti et al., 2013). Lithologic counterpart of this unit occur around Afyon area of Central Turkey and represents the Cadomian basement of the Anatolide-Taurides (Gürsu and Göncüoğlu, 2006). The overlying succession lies on disconformably and contains quartzites and quartzite-recrystallized limestone bands and it is thought to belong to Middle Permian. On top of them, the Mesozoic succession starts with red continental clastics of Early Triassic and grades into a package of platformal limestone which is belonging to Mid-Triassic to Late Jurassic-Early Cretaceous. Towards upward, the succession grades into turbidites and olistostromes with ophiolitic detritus. The fossil called “*Globotruncana* sp” was found in pelagic cherty limestones of this succession and it indicates that the emplacement of İzmir-Ankara Ocean took place in Late Cretaceous (Göncüoğlu and Türeli, 1993; Göncüoğlu, 2000a; Bortolotti et al., 2013).

The ages obtained from accretionary complex, which represent the cover sediments of the subducted Tethyan oceanic crust, would be the best evidence for the age span of İzmir-Ankara-Erzincan Ocean (Okay & Tuysuz, 1999). According to Bragin and Tekin (1996) radiolarian ages from various outcrops located at northwest of Ankara have given age of Late Norian, Early Jurassic, Kimmeridgian-Tithonian, Early Cretaceous and Albian-Turonian. Moreover, other studies of radiolarian ages from different locations on west of İzmir-Ankara suture have yielded that Early Cretaceous from Biga Peninsula (Beccaletto and Stampfli, 2000) and from north of Eskişehir (Göncüoğlu et al., 2000). According to these data, it is concluded that İzmir-Ankara Neotethyan ocean had an age span of at least Late Norian to Albian.

The ages of the ophiolites which overlie the accretionary complex can be known as only the age of the preserved lower plutonic parts of the ophiolitic sequence (Okay & Tuysuz, 1999). According to several studies conducted on metamorphic soles of several ophiolite bodies such as Semail ophiolite (Oman) and Greek and Yugoslavian ophiolites (Lanphere, 1981; Spray et al., 1984; Okay & Tuysuz, 1999) reveal that age

of the metamorphic sole is very close to the age of the overlying ophiolite. In the light of this information, the isotopic ages of the metamorphic rocks of subophiolites suggest an age span of Late Jurassic to Campanian for the ophiolite of İzmir-Ankara-Erzincan Ocean (Özen & Hall, 1993; Harris et al., 1994; Okay & Tüysüz, 1999; Göncüoğlu et al., 2006).

2.3. Geology of the Study Area

The rocks from the study area to the southeast of Çorum are considered as a part of İzmir-Ankara-Erzincan suture zone. In the study area, the metamorphic rocks of the Sakarya Composite Terrane are tectonically overlying the ophiolitic melange of IAESZ (Bortolotti et al., 2013). Moreover, Upper Neogene rocks cover both units unconformably (Figure 3).

In this section, only description of lithological features of the rocks and their contact relations with cover units and underlying units are given. The geological map of the Burunköy (Çorum) area is given in Figure 3. In the study area, the oldest unit observed is the Silurian marbles belonging to Karakaya Complex that tectonically overlies the basaltic rocks in concern (Figure 4).

In the study area, the blocks belonging to the IAESZ melange is mainly composed of serpentinite, serpentinized peridotite, radiolarian chert, basalt, metabasalt and dyke. Serpentinite is the essential matrix material. The most extensive rock types are basalts and dykes. Basalts are metamorphosed up to greenschist facies place to place, especially at contacts with marble. Therefore, basalts are explained under two headings as basalts and metabasalts.

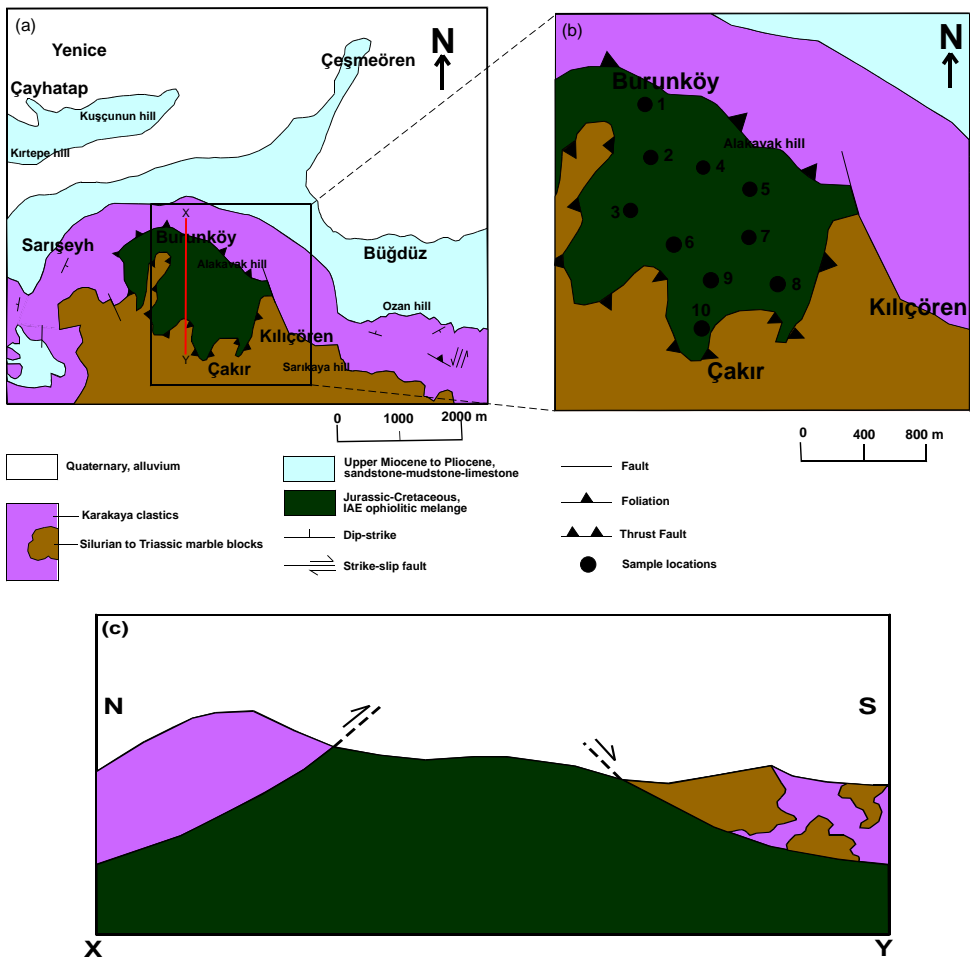


Figure 3. Simplified geological map of the study area (modified from 1:100000 scale geology map of H33-Çorum) and (b) sample locations on the map. (c) Sketch of X-Y cross-section taken from the study area from N to S (not to scale).

2.3.1. Basalts

The basalts away from the tectonic contact with Silurian marble are mostly free of shearing, foliation and metamorphism. They are dark brown to dark gray in color. They are pillow in shape. Pillow structures of the basalts are mostly preserved (Figure 5) even though they are highly fractured at some locations. At outer parts of the pillows, vesicles are widespread. The basalts are generally subjected to surface

alterations. The fractures and vesicles of the pillows are extensively filled by calcite and also epidote. It is rare to observe chert in the study area. In a fault zone, basalt pillows and chert fragments are observed as reworked in talc matrix due to hydrothermal alteration (Figure 6).

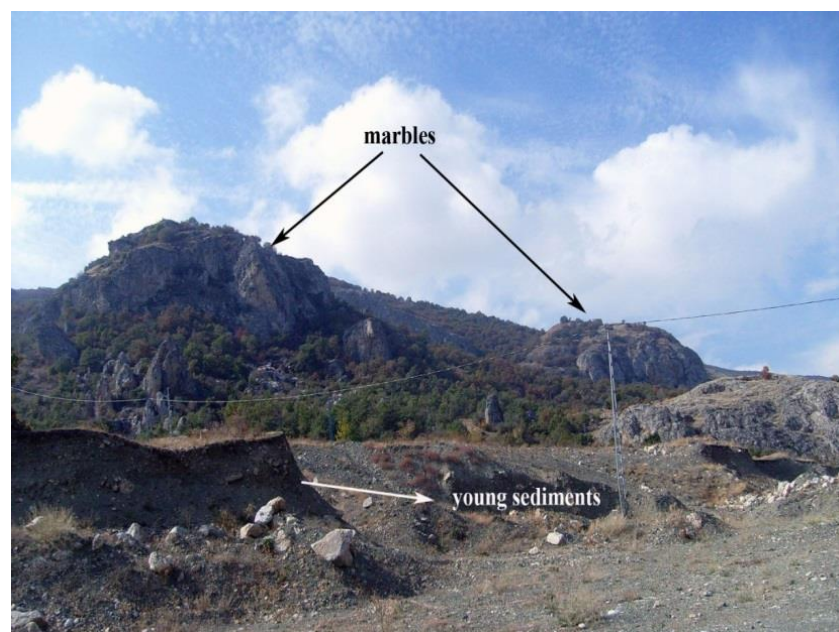


Figure 4. Photograph showing the position of the marbles from the study area.



Figure 5. Photograph showing pillow basalts from the study area.

2.3.2. Metabasalts

In the study area, the basaltic rocks in tectonic contact with and close to marble are highly dissected, sheared and foliated. Foliation varies with different degrees of schistosity (Figure 7). As a result of low-grade metamorphism, metabasalts show greenschist facies metamorphism including chlorite (Figure 7) that is characteristics both in hand specimen and supported with petrographical observations (see Chapter 3). Chlorite minerals are generally observed as elongated, parallel to sub-parallel spots. Boulders of metabasalts are in a olistostromal matrix in some places. Metabasalts display manganese enrichment according to the field observations. They are tectonically in contact with pillow basalts (Figure 8).



Figure 6. Photograph showing a pillow basalt and talc in the matrix from the study area.

2.3.3. Dykes

In the study area, parallel to sub-parallel dykes extensively outcrop (Figure 9). Intrusion direction of the dykes are roughly from north to south (Figure 9). They are dark greenish grey in color (Figure 10). They are fine to medium grained. They are doleritic in character. The dykes are fractured place to place, where they are filled by calcite and epidote. Close to the contact with Silurian marble shearing and fracturing in dykes increases (Figure 11).

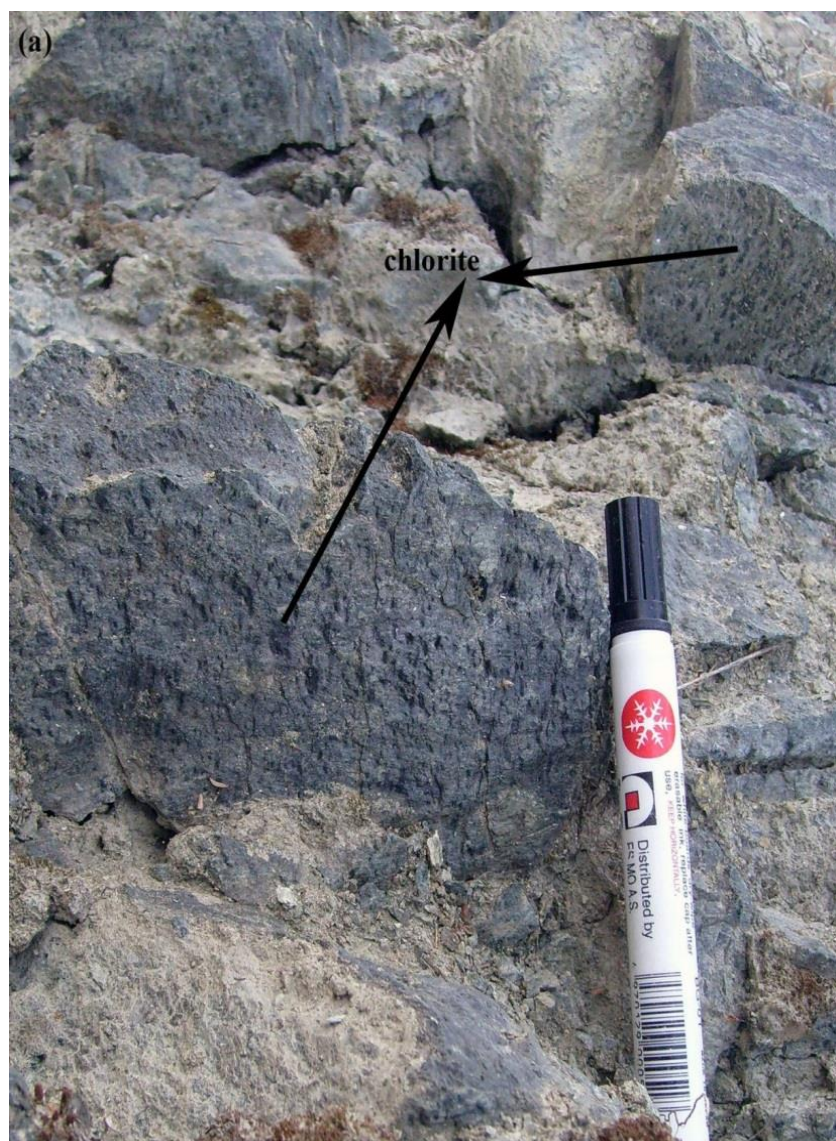


Figure 7. Metabasalts showing different degrees of schistosity and greenschist facies metamorphism (dark green chlorite spots) (a) weak, (b) moderate to strong, (c) strong.

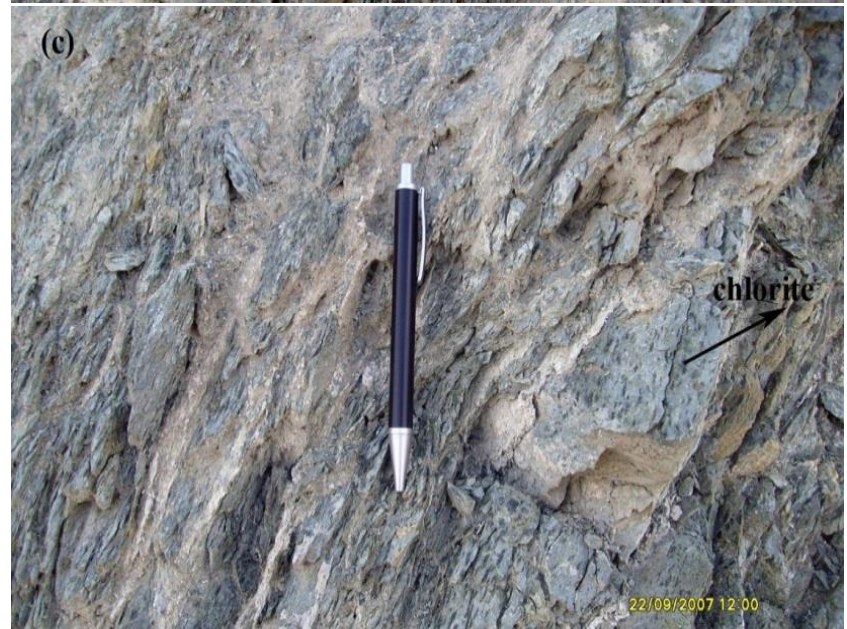
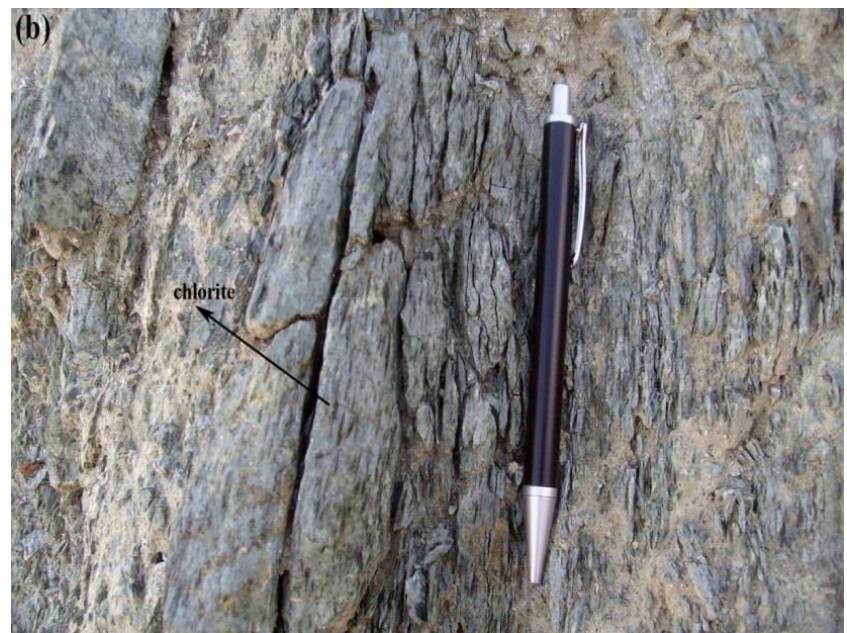


Figure 7. (continued).

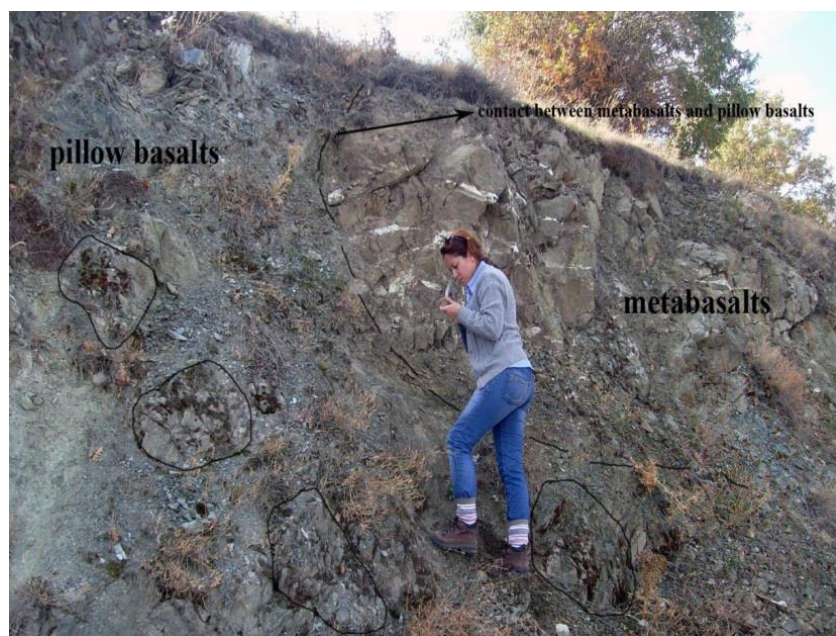


Figure 8. Photograph showing contact relationship between metabasalts and pillow basalts in the study area.

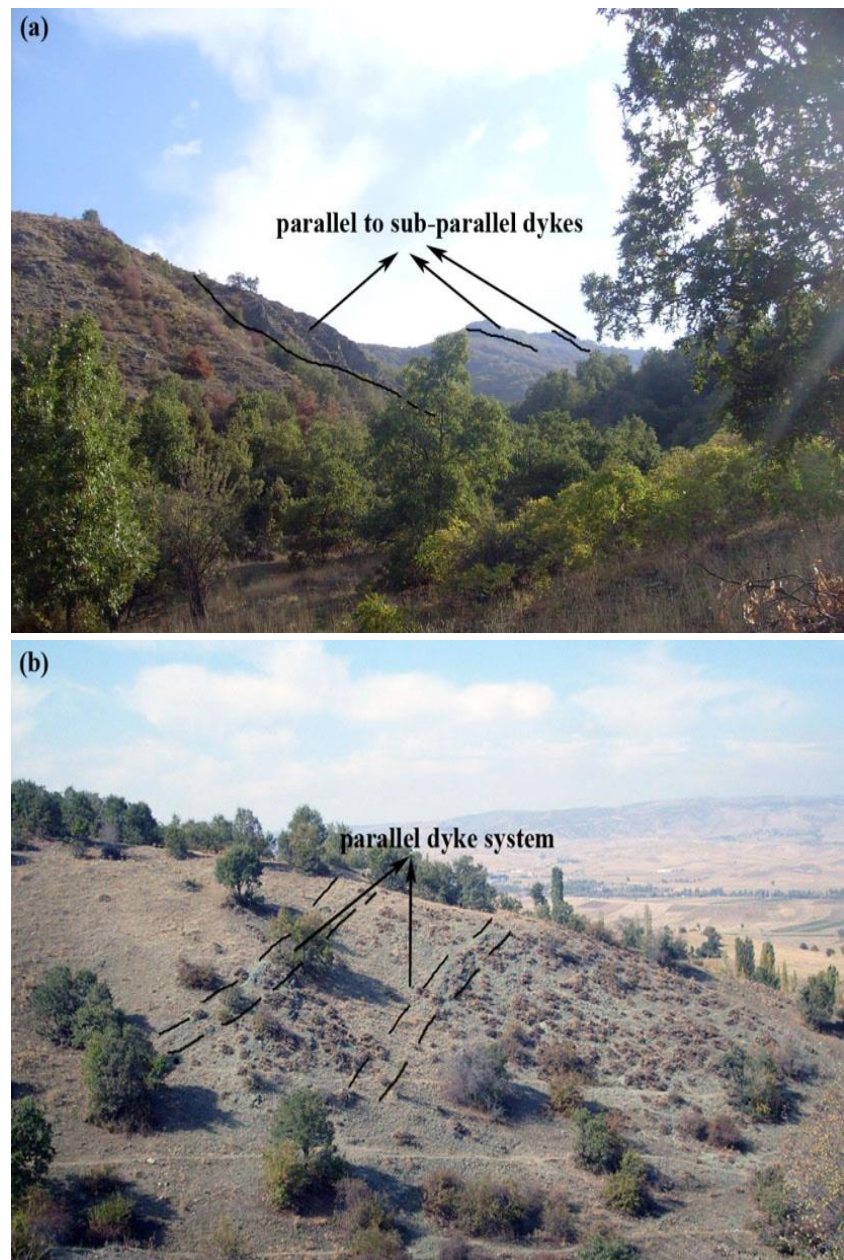


Figure 9. Photographs showing parallel dyke system in the study area.



Figure 10. Photograph showing general (a) and close-up view (b) of dykes from the study area.



Figure 11. Photograph showing doleritic dyke close to contact with marble from the study area.

CHAPTER 3

PETROGRAPHY

3.1. Introduction

Petrographical study of the rocks in concern was conducted on 23 thin sections. The studied thin sections were categorized into three main groups as basalts, metabasalts, and dykes based on field observations and petrographic studies. All the studied rocks essentially consist of pyroxenes and feldspars as phenocrysts, and as microcrysts in matrix. The studied rocks also consist of actinolite, chlorite and epidote, and calcite and sericite due to low-grade metamorphism and alteration, respectively. Moreover, limited amounts of opaque minerals are found as accessory minerals.

3.2. Basalts

Basaltic rocks are dark in hand specimen. They are characterized by aphanitic and porphyritic textures (Figure 12). Phenocrysts are rarely clustered into aggregates resulting in glomeroporphyritic texture (Figure 13). Vesicles of pillows are generally filled by calcite. In addition to phenocrysts of pyroxene and feldspar, groundmass of basalts is made up of glass and microcrysts of pyroxene and feldspar (Figure 12&14).

Petrographic examination of the basalts reveals that pyroxene is the most common phase with variable size from micro to 4-5 mm. More than 65% of the basalts are made up of pyroxene with moderate relief. Pyroxene crystals are colorless to pinkish reddish in color (Figure 15). The colored varieties show strong pleochroism. Extinction angle of pyroxene crystals varies between 40-45° that infer augitic composition. These pyroxenes have second order interference colors.

Not only the size of the pyroxene crystals but also the shape of them varies. It is possible to observe both euhedral and subhedral crystals (Figure 12a). Subhedral crystals are generally corroded, which are abundant (Figure 12b,c). Resorption observed in pyroxene giving a spongy cellular texture is abundant feature in the rocks (Figure 12a). Clinopyroxene crystals extensively display compositional zoning and twinning (Figures 12a, 16 & 17). Compositional zoning is predominantly observed at rims of pinkish to reddish Ti-rich clinopyroxene crystals. In addition to zoning, growth of fine grained clinopyroxene crystals both forming rims at earlier pyroxene and feldspar phenocrysts and in the groundmass is a common feature (Figure 16). In a single crystal of clinopyroxene, it is possible to identify compositional zoning, corrosion and also reaction rim (Figure 17). Moreover, tailing is a common property both in phenocrysts and microcrysts of pyroxenes (Figures 15 & 18).

Feldspars in the basalt samples are mostly found as microcrysts that are scattered into groundmass. Like pyroxenes, most of them generally display compositional zoning and twinning. The phenocrysts of feldspars commonly exhibit spongy cellular texture (Figure 19). Sericitization is a common property due to surface alteration.

The petrographical observations strongly infer open system magmatic behavior. All the textural features observed in the studied sections infer that there are chemical disequilibrium conditions during crystallization. Especially growth of pyroxene microcrysts at rim of feldspar and earlier pyroxene crystals, resorption and corrosion of pyroxene crystals strongly infer influx of higher temperature more mafic magma. The rocks could be products of multistage mixing during ascent. For instance; the properties observed in Figure 17 may infer at least three stages of growth of the crystal such as first stage of crystal growth, second stage of crystal growth and third stage of corrosion.

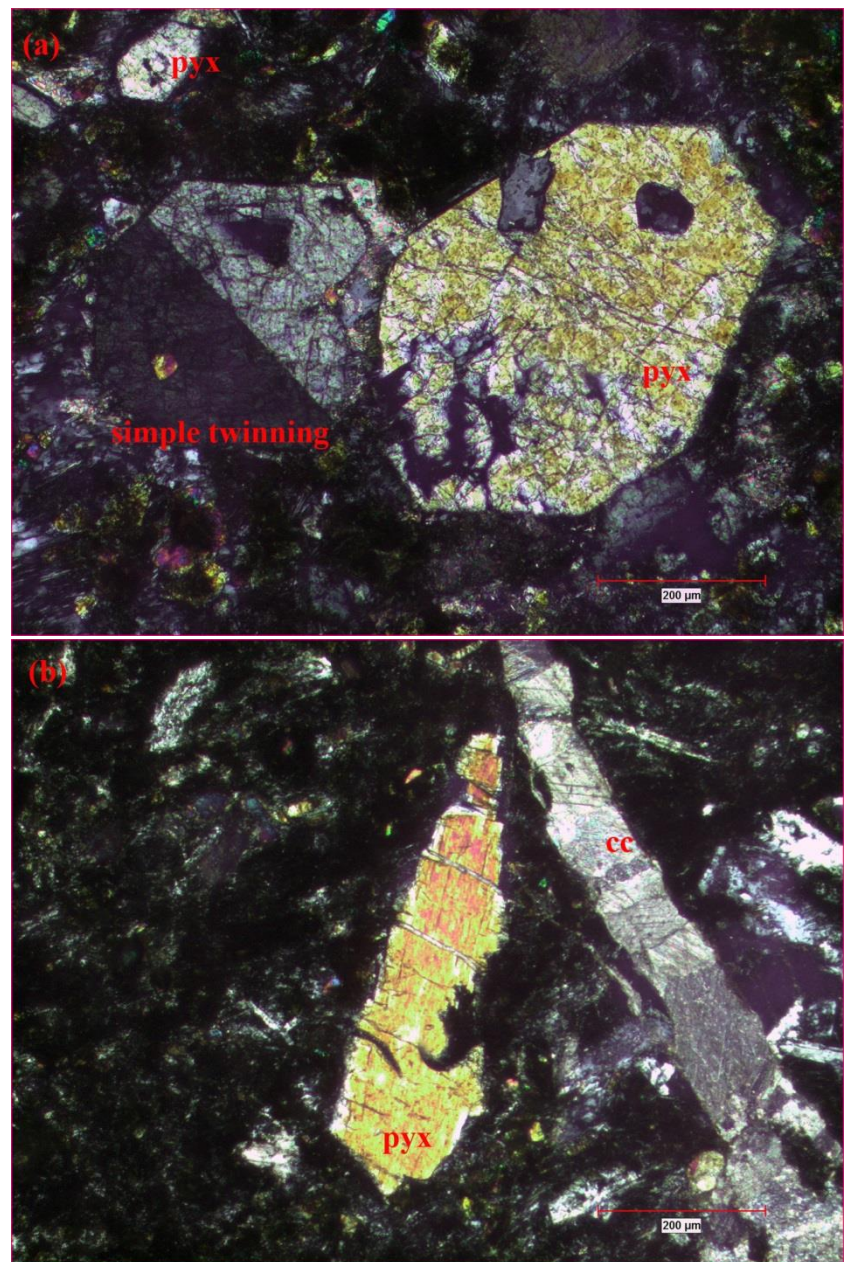


Figure 12. Microphotograph showing (a) euhedral pyroxene phenocrysts with simple twinning in a basalt sample (b, c) corroded subhedral pyroxene crystals (pyx: pyroxene, cc:calcite, comp.zon.: compositional zoning).

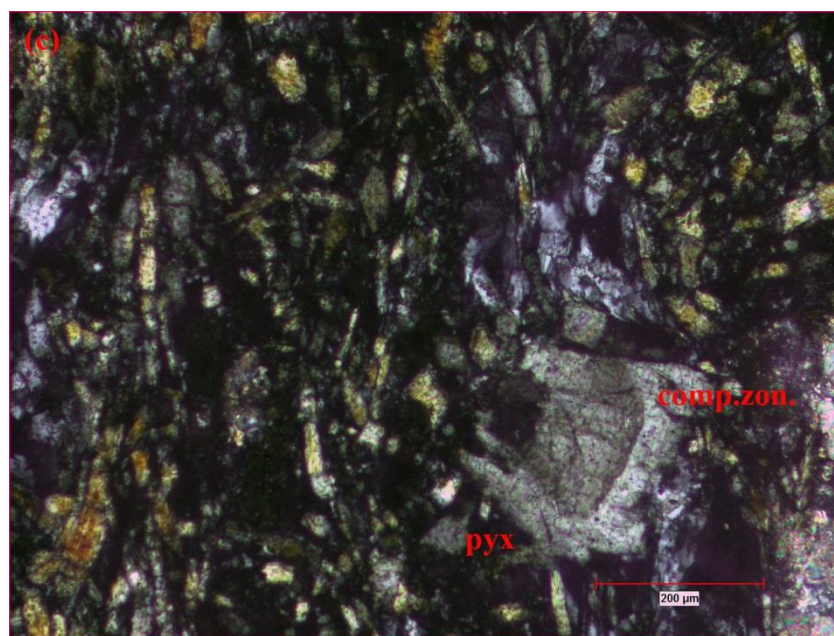


Figure 12 (continued).

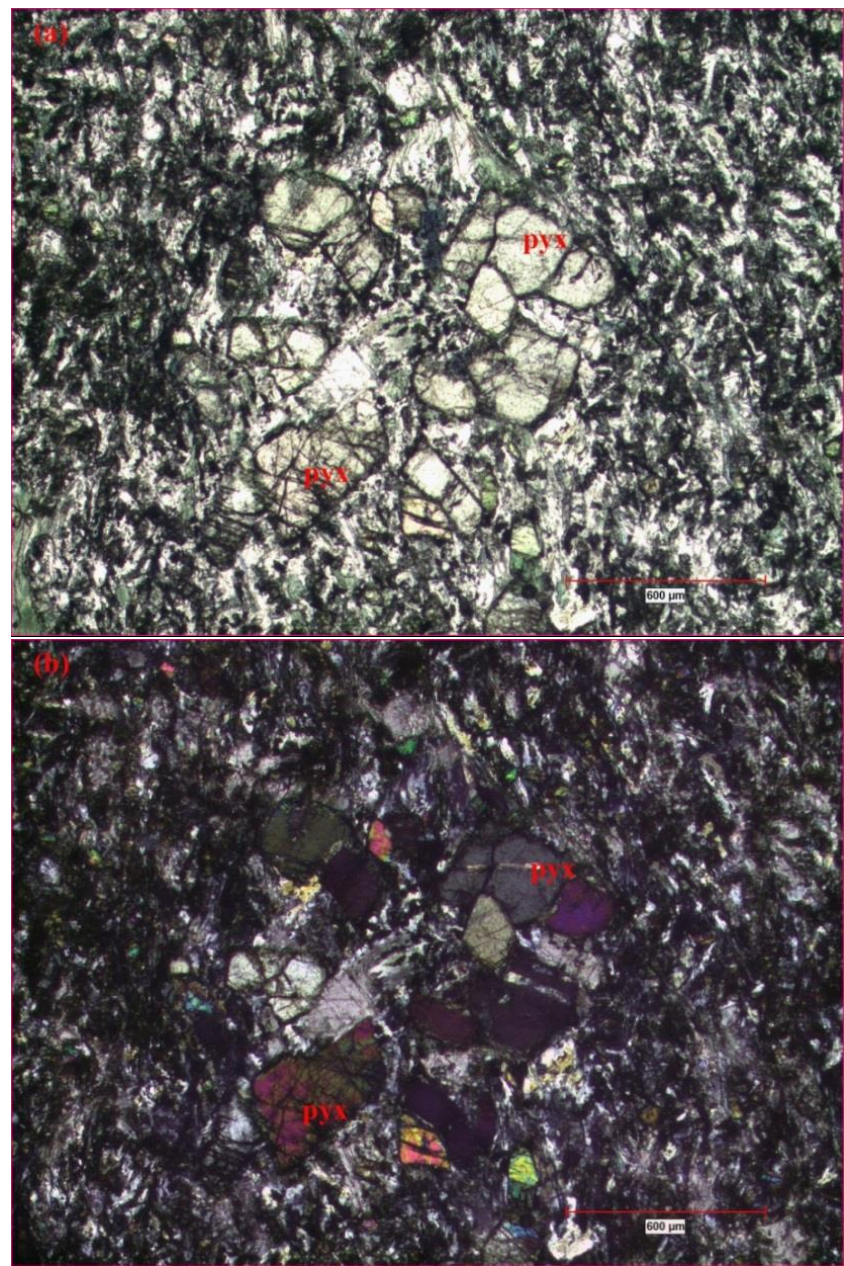


Figure 13. Microphotograph of a basalt showing pyroxene aggregates (glomeroporphritic texture) ((a) analyser out, (b) analyser in, pyx: pyroxene).

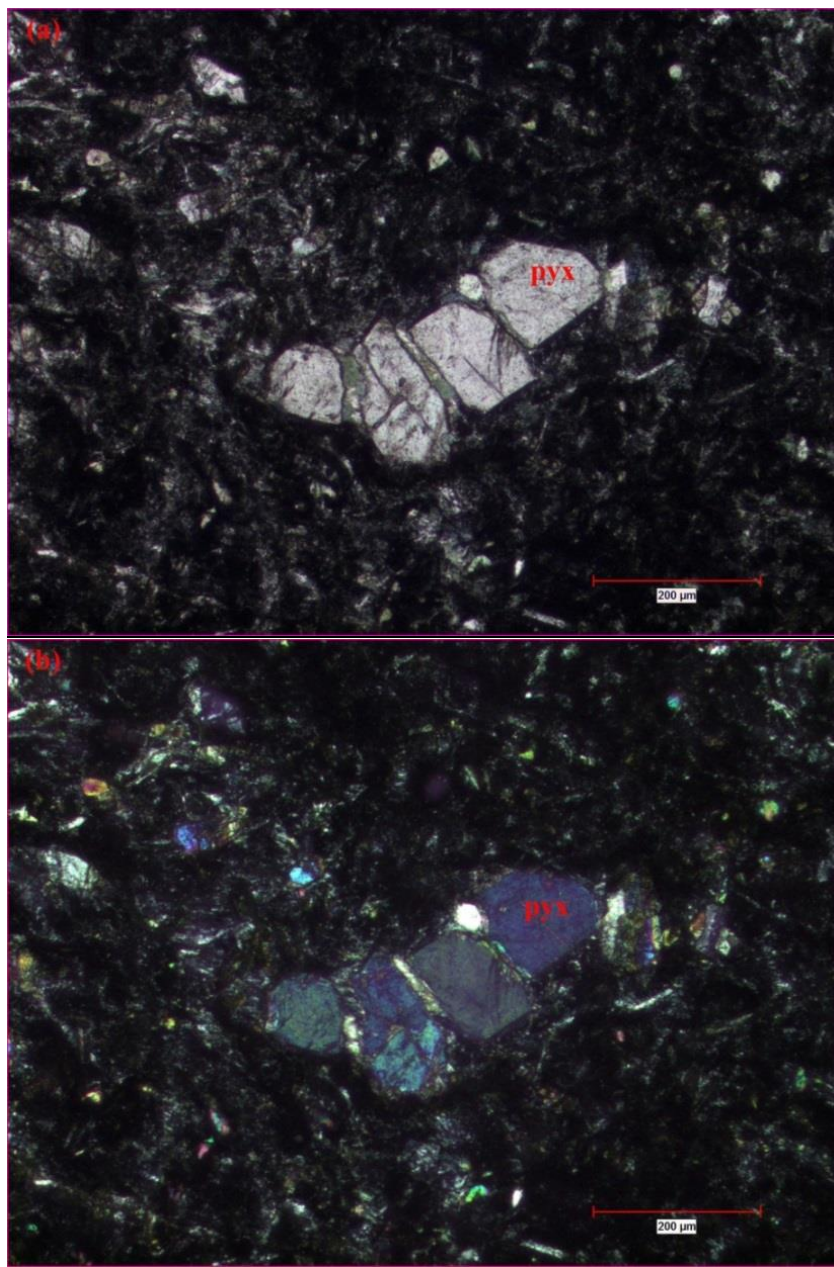


Figure 14. Microphotograph of a basalt showing pyroxene phenocrysts in a glassy groundmass with pyroxene microcrysts ((a) analyser out, (b) analyser in, pyx: pyroxene).

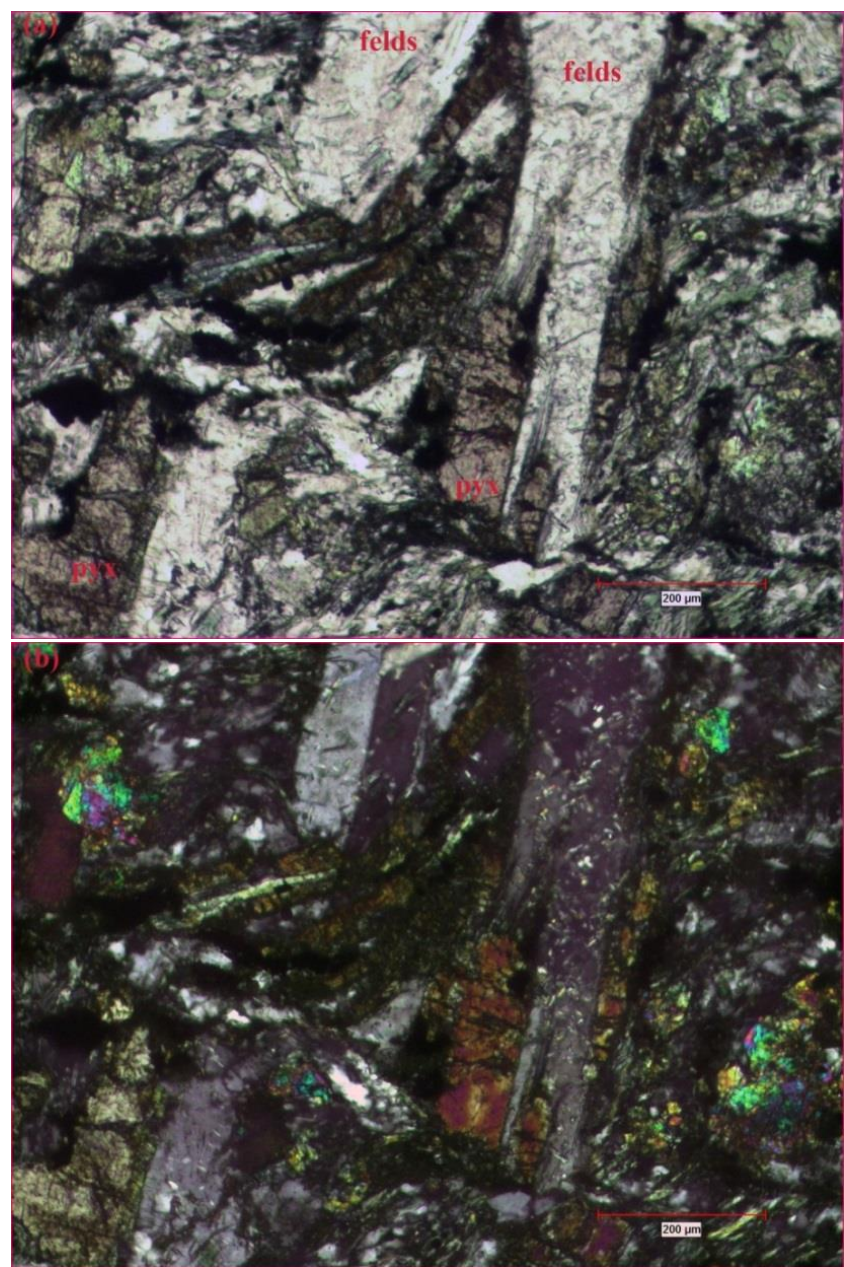


Figure 15. Microphotograph of a basalt showing pinkish to reddish pyroxene phenocrysts with tailing property ((a) analyser in, (b) analyser out, pyx: pyroxene, felds: feldspar).

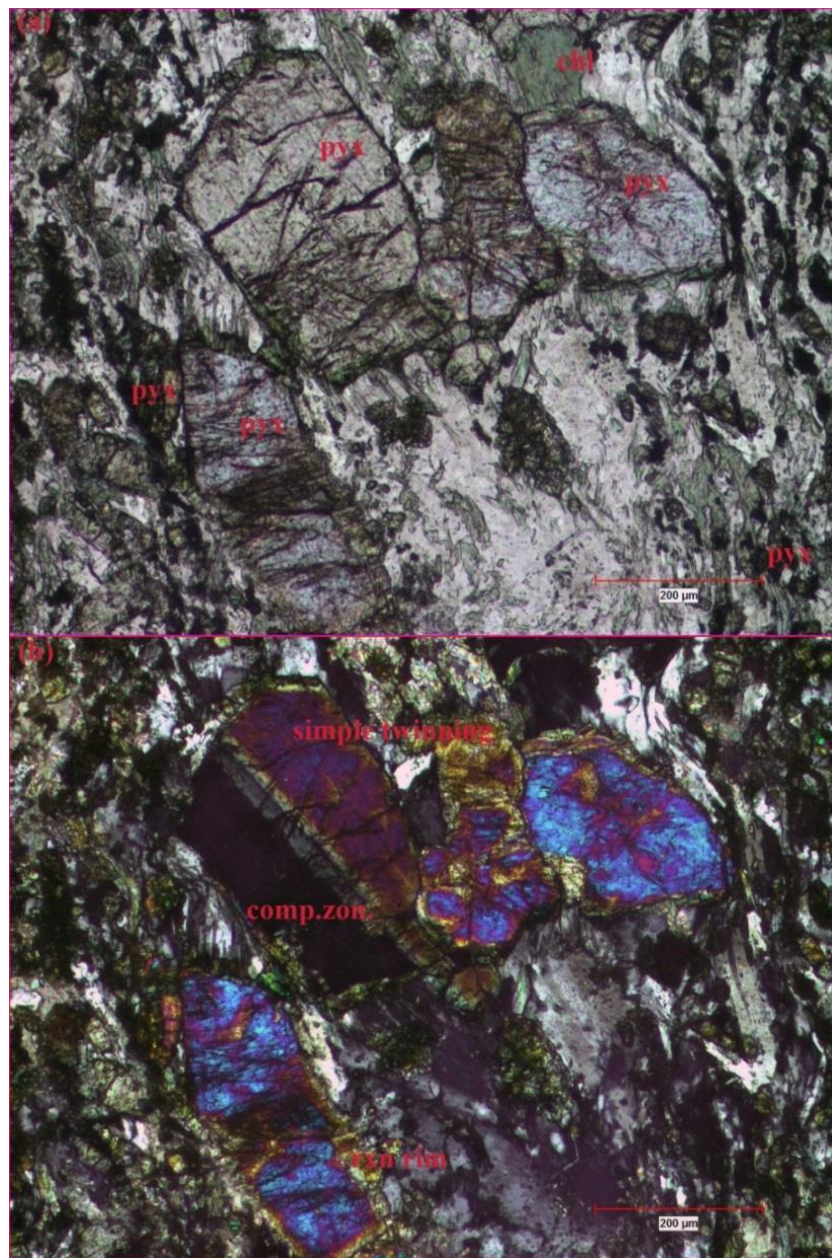


Figure 16. Microphotograph of a basalt showing pyroxene crystals with reaction rim, compositional zoning and simple twinning((a) analyser out, (b) analyser in, pyx: pyroxene, chl: chlorite, rxn rim: reaction rim).

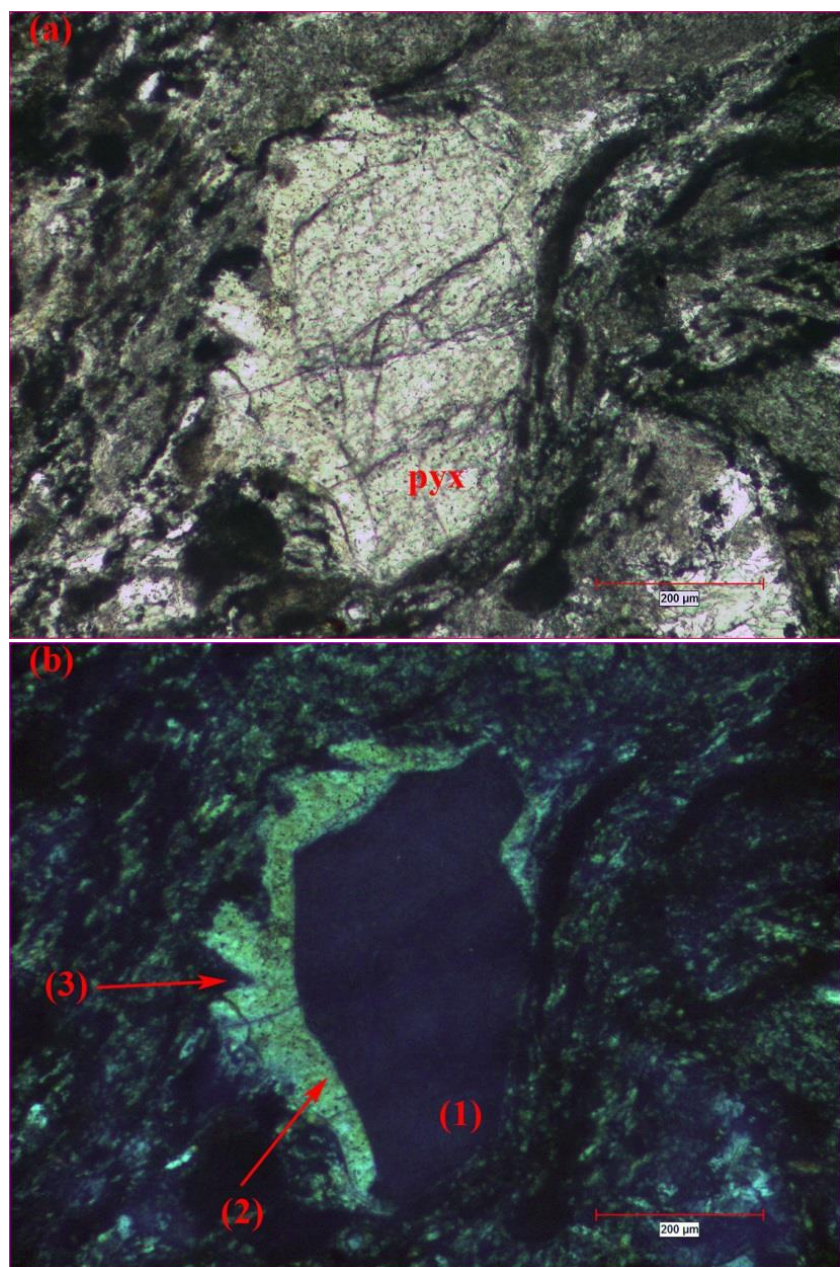


Figure 17. Microphotograph of a basalt showing a corroded pyroxene crystal with compositional zoning (1) and reaction rim (formation of a new pyroxene, 2), corrosion (3) in (a) and (b) ((a) analyser out, (b) analyser in, pyx: pyroxene). (c) Back scattered image of a clinopyroxene crystal (1) showing overgrown by a new crystal material (2).

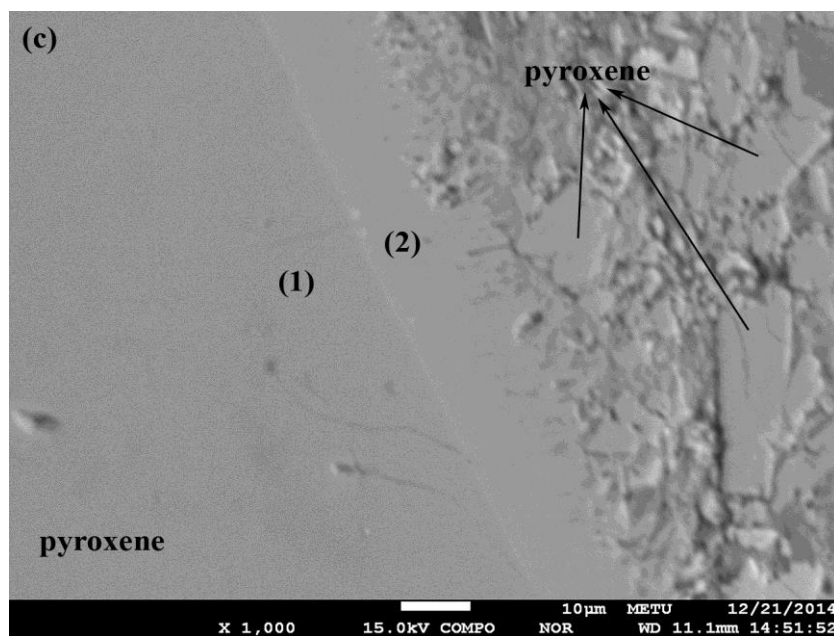


Figure 17. (continued).

3.3. Metabasalts

The basaltic rocks in tectonic contact with and close to marble display different degrees of foliation from weakly to strongly schistose. The metamorphosed basalts with varying degrees of foliation are called as metabasalt in this part. At the tectonic contact, especially strongly schistose ones are observed that are abundant in green minerals such as chlorite, actinolite and epidote (Figure 20). As the distance from the tectonic contact increases, schistosity and effect of metamorphism decreases. Due to shearing effect, vesicles in metabasalts are elongated resulting in augen-like structure (Figure 21).

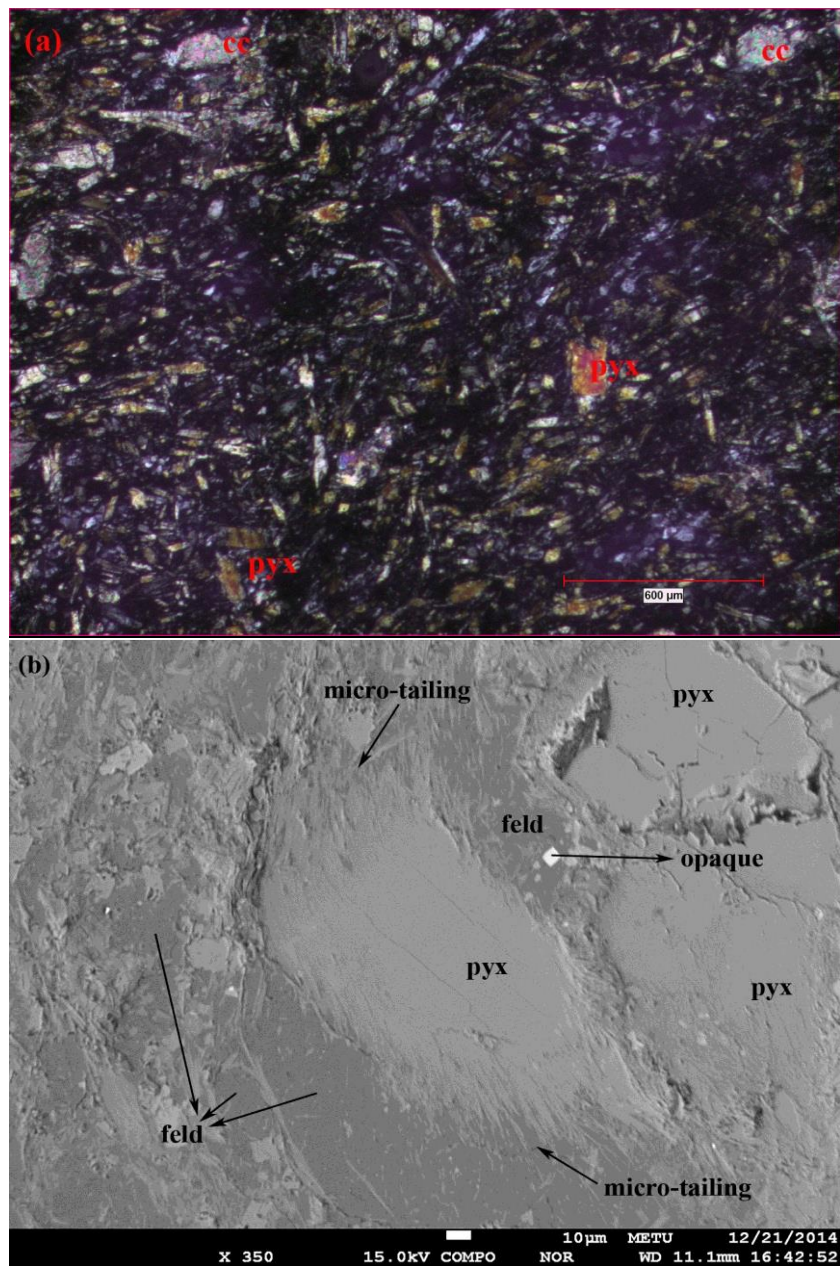


Figure 18. (a) Microphotograph of a basalt showing long-prismatic pyroxene microcrysts with tailing property in groundmass (analyser in, pyx: pyroxene, cc: calcite). (b) Back scattared image of a clinopyroxene crystal with tailing. (c) Back scattared image of a clinopyroxene crystal (1) showing overgrown by a new crystal material (2) and tailing (3).

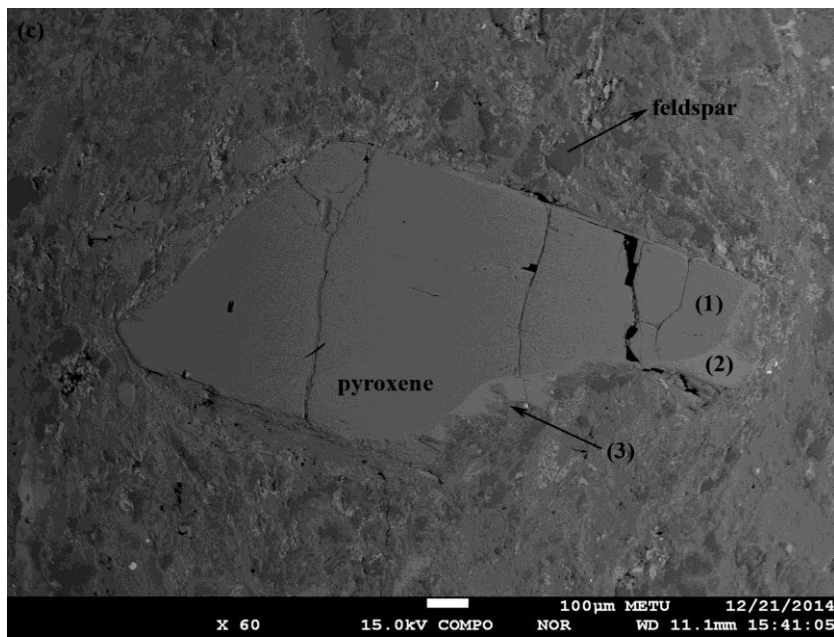


Figure 18. (continued).

Since the rocks undergone low-grade metamorphism, it is hard to observe well-preserved igneous textures. Where the igneous texture is preserved, aphanitic texture and porphyritic texture are identified with glassy groundmass and microcrysts of feldspar and pyroxene, and phenocrysts of pyroxene and feldspar. The rocks are dominated by phenocrysts of pyroxene ($\geq 65\%$). Pyroxene is colorless to pinkish-reddish in color with strong pleochroism that infer Ti-enrichment. Moreover, its extinction angle varies between $42\text{--}47^\circ$ indicating Ti-rich augitic composition. Clinopyroxene phenocrysts commonly display oscillatory and sector zoning, and twinning (Figures 22 & 23). Corrosion and resorption on clinopyroxene phenocrysts (Figures 22, 23 & 24) are extensive in the metabasalts similar to those observed in the basalts. In some of the sections similar to basalts, arrangement of clinopyroxene microcrysts around larger feldspar crystals are identified (Figure 25).

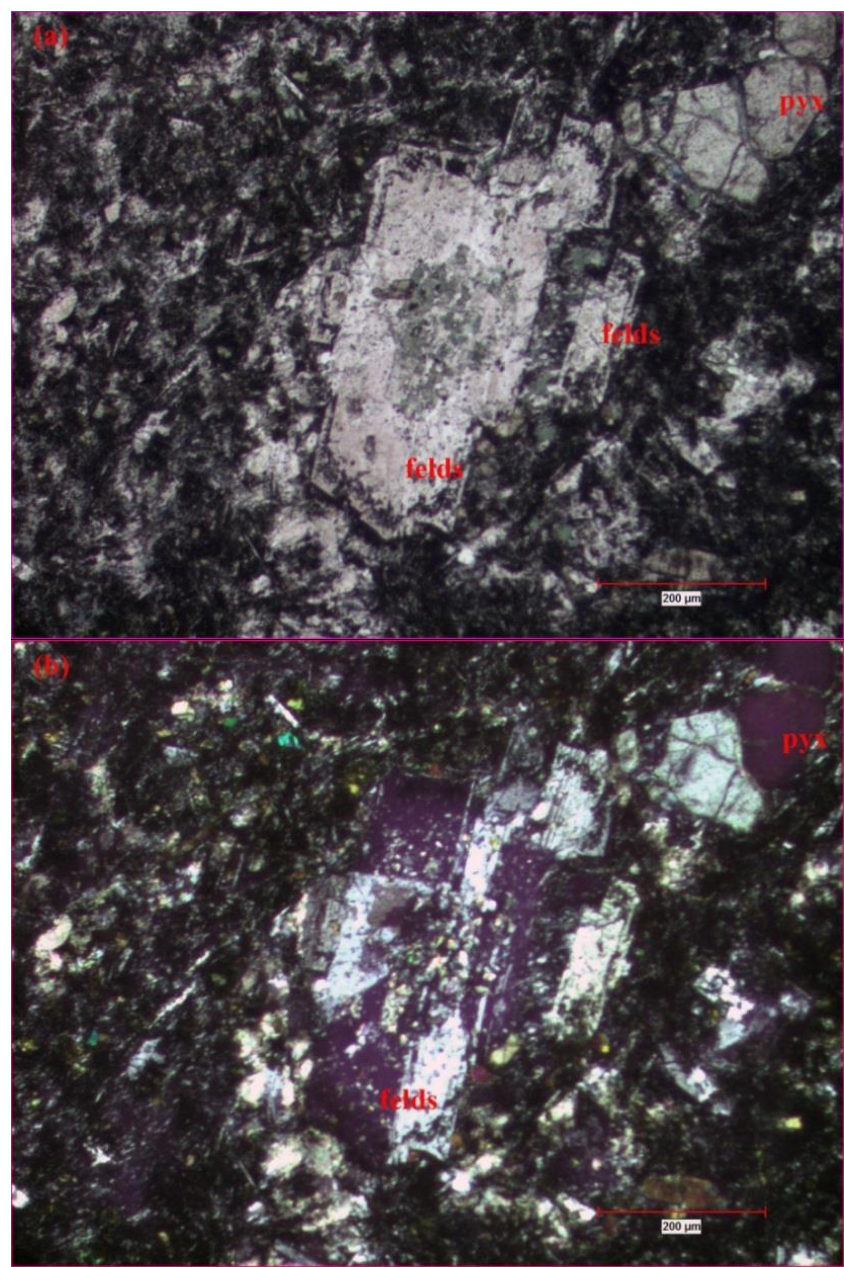


Figure 19. Microphotograph of a basalt showing finely spongy cellular texture in the center and near the rim of feldspar crystals ((a) analyser out, (b) analyser in, pyx: pyroxene, felds: feldspar).

Feldspars of metabasalts generally found as microliths scattered into groundmass. Phenocrysts of them are mostly subhedral. They display compositional zoning and twinning. Moreover, albitization is a common property due to low grade metamorphism.

Mineralogical and petrographical features of the metabasalts other than the metamorphic features are quite similar to those observed in the basalts that suggest derivation from the same magma. Moreover, petrographic features indicate open magmatic system, chemical dis-equilibrium conditions like reaction rims, overgrowth features on pyroxene, growth of pyroxene microcrysts around feldspars, tailing, resorption, corrosion. All are briefly explained to indicate as melt influx with higher temperature during magma ascent.

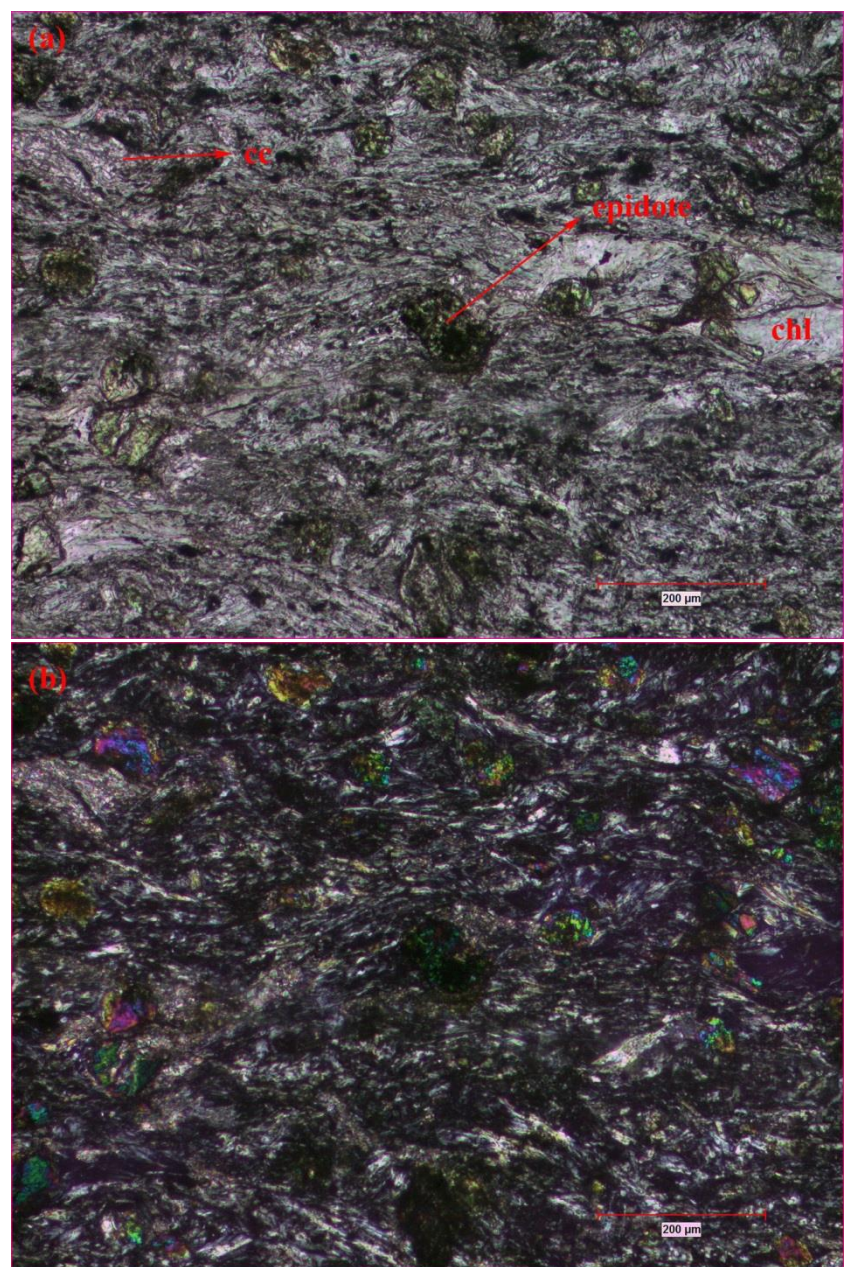


Figure 20. Microphotograph of a metabasalt ((a) analyser out, (b) analyser in, ep: epidote, chl: chlorite, cc: calcite)

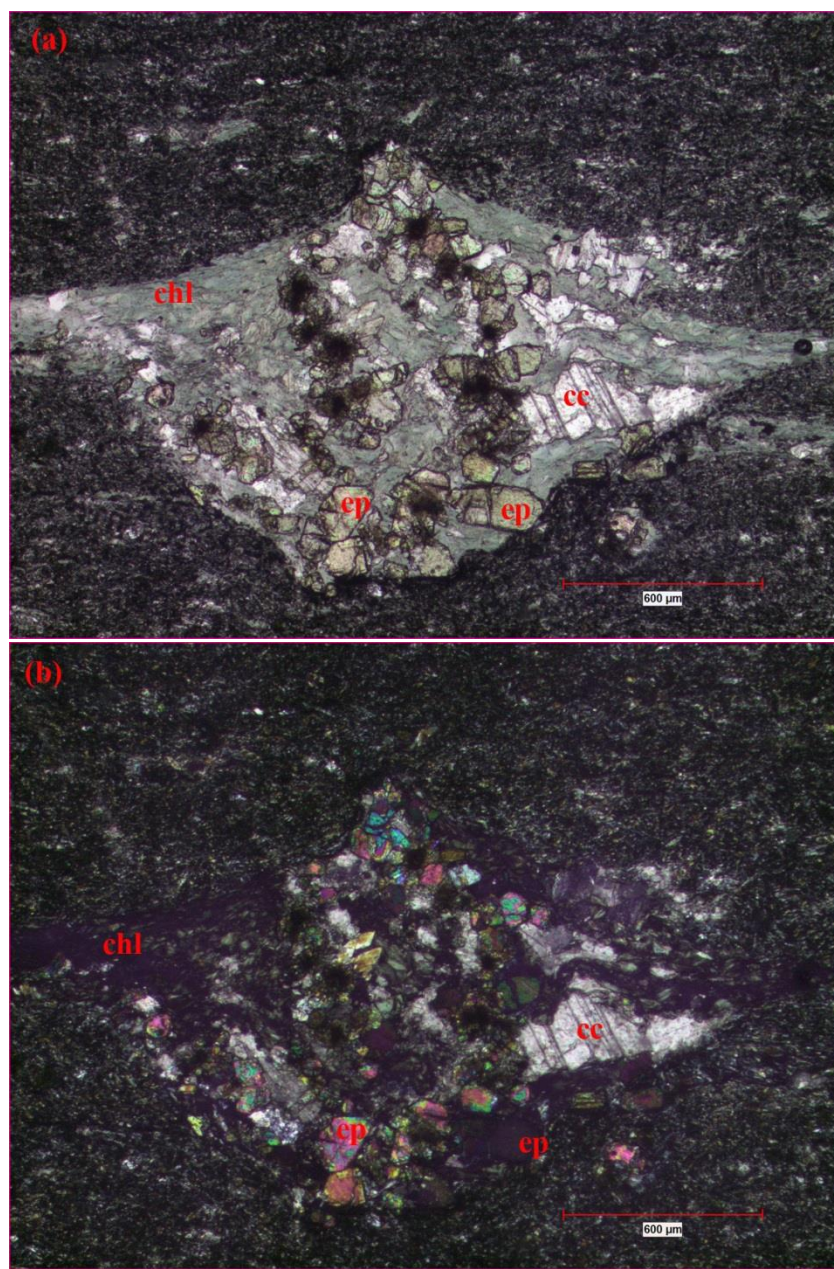


Figure 21. Microphotograph of a metabasalt showing a sheared vesicle resembling augen structure ((a) analyser out, (b) analyser in, ep: epidote, pyx: pyroxene, chl: chlorite, cc: calcite).

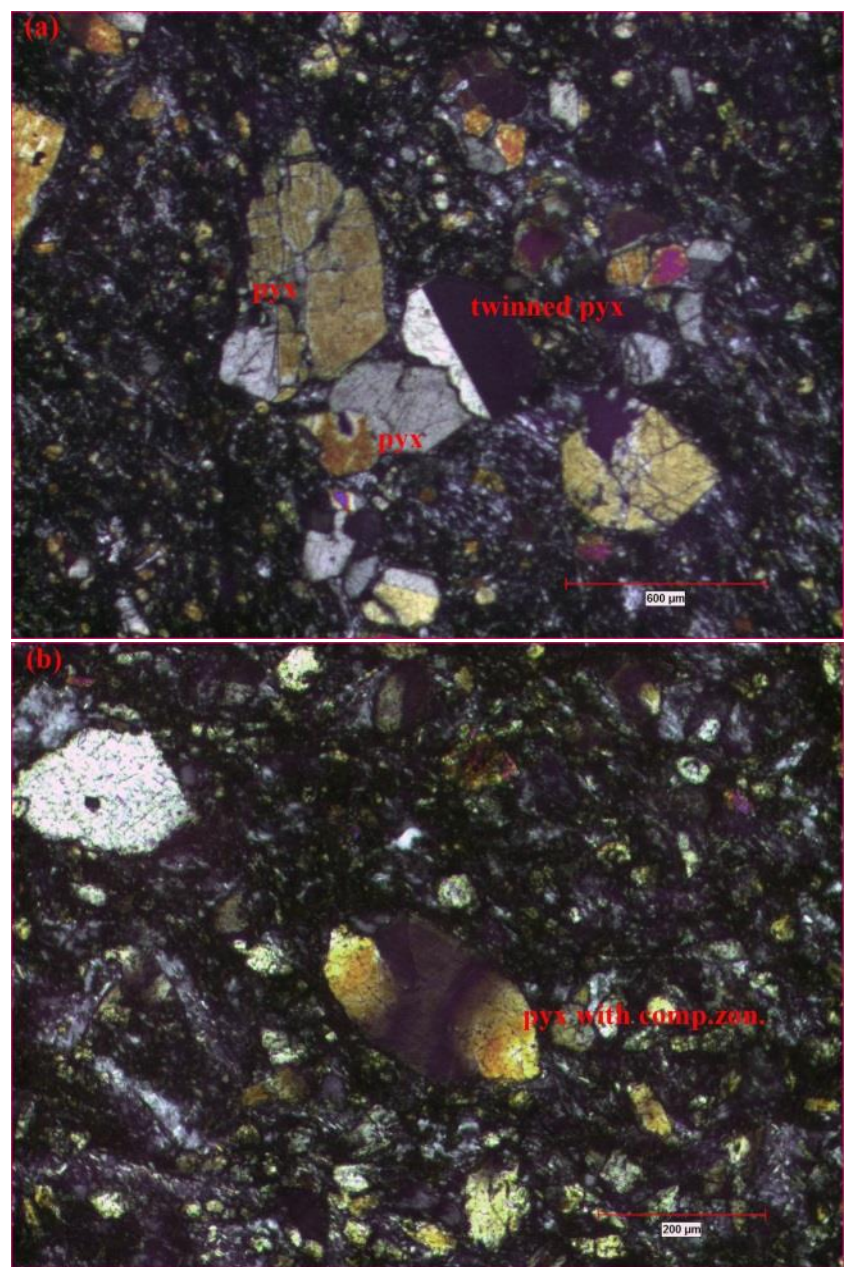


Figure 22. Microphotograph of a metabasalt showing simple twinning (a) and sector zoning (b & c) in clinopyroxene phenocrysts (pyx: pyroxene, comp.zon.: compositional zoning).

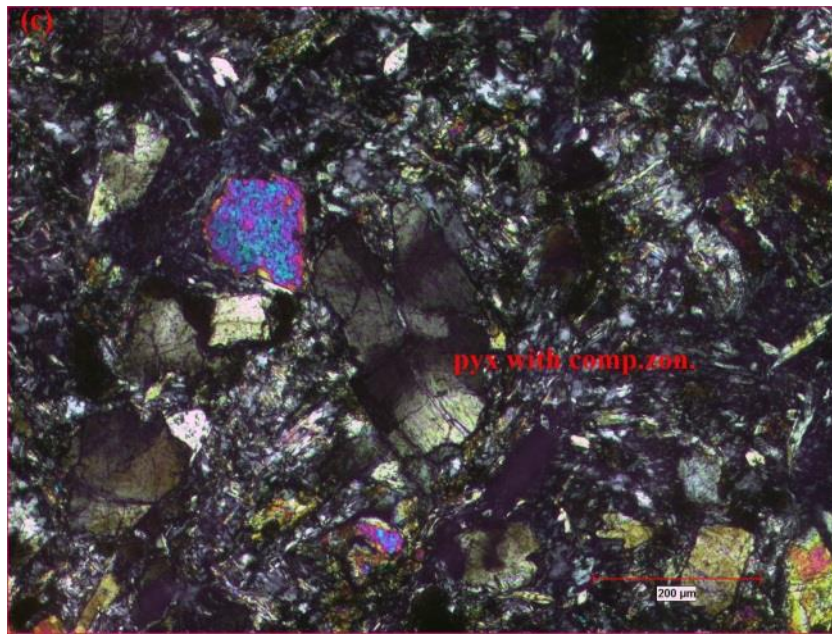


Figure 22. (continued).

3.4. Dykes

Dykes are dark-grey to black in color in hand specimen. The dykes are coarse-grained holocrystalline. Moreover, they display ophitic and intergranular textures (Figure 26). The rocks are dominated by 35-40% clinopyroxene and plagioclase (55-60%) with minor opaques.

The most of the pyroxenes have pinkish-reddish color indicating Ti-enrichment. In clinopyroxene crystals, compositional zoning and twinning properties (Figure 27) are common. Resorption and corrosion are extensively observed in the clinopyroxene crystals (Figures 26, 27 & 28).

Feldspars of the dykes found as coarse crystals in the dykes. They are generally subhedral crystals and display compositional zoning and twinning (Figure 29). Sericitization is common alteration type observed in feldspars.

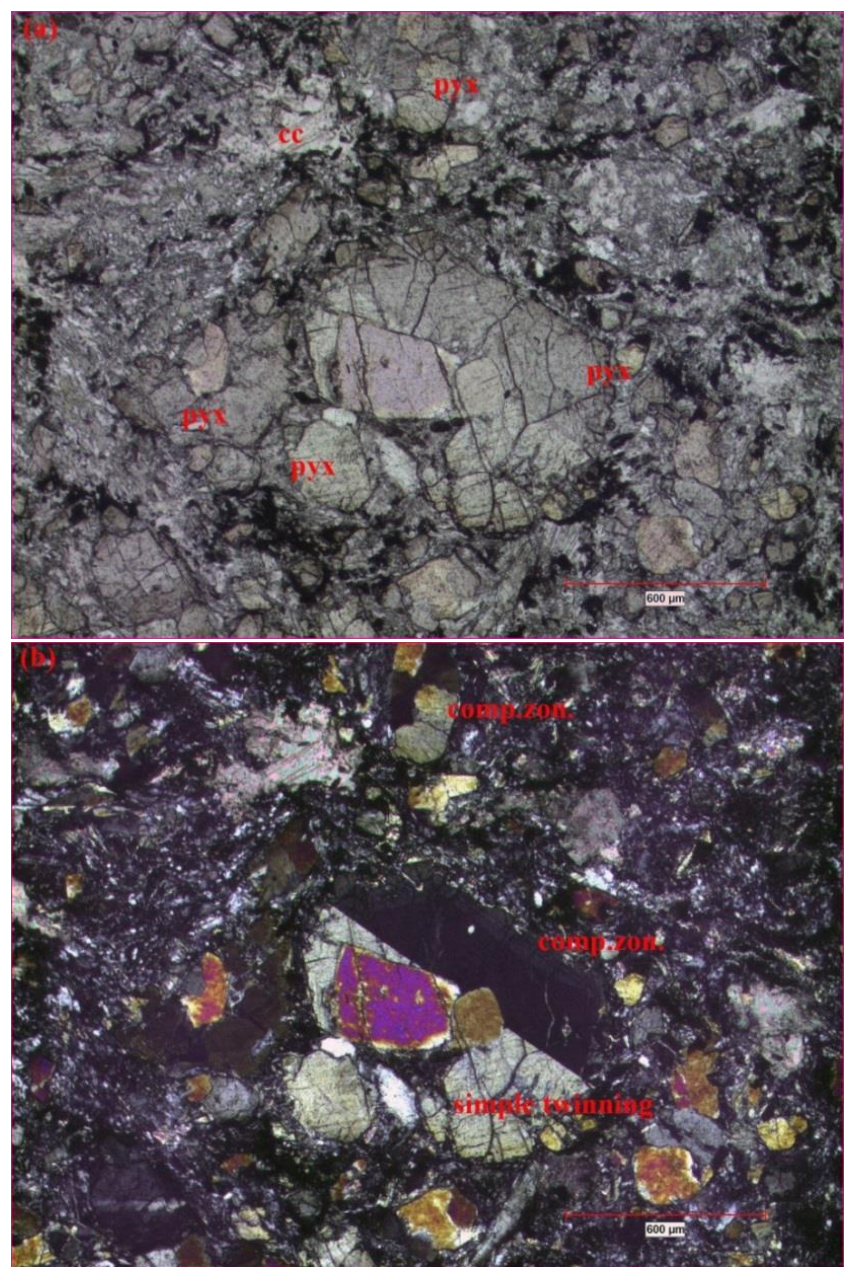


Figure 23. Microphotograph of a metabasalt showing a pyroxene crystal displaying both simple twinning and compositional zoning. ((a) analyser out, (b) analyser in, pyx: pyroxene, cc: calcite, comp.zon.: compositional zoning).

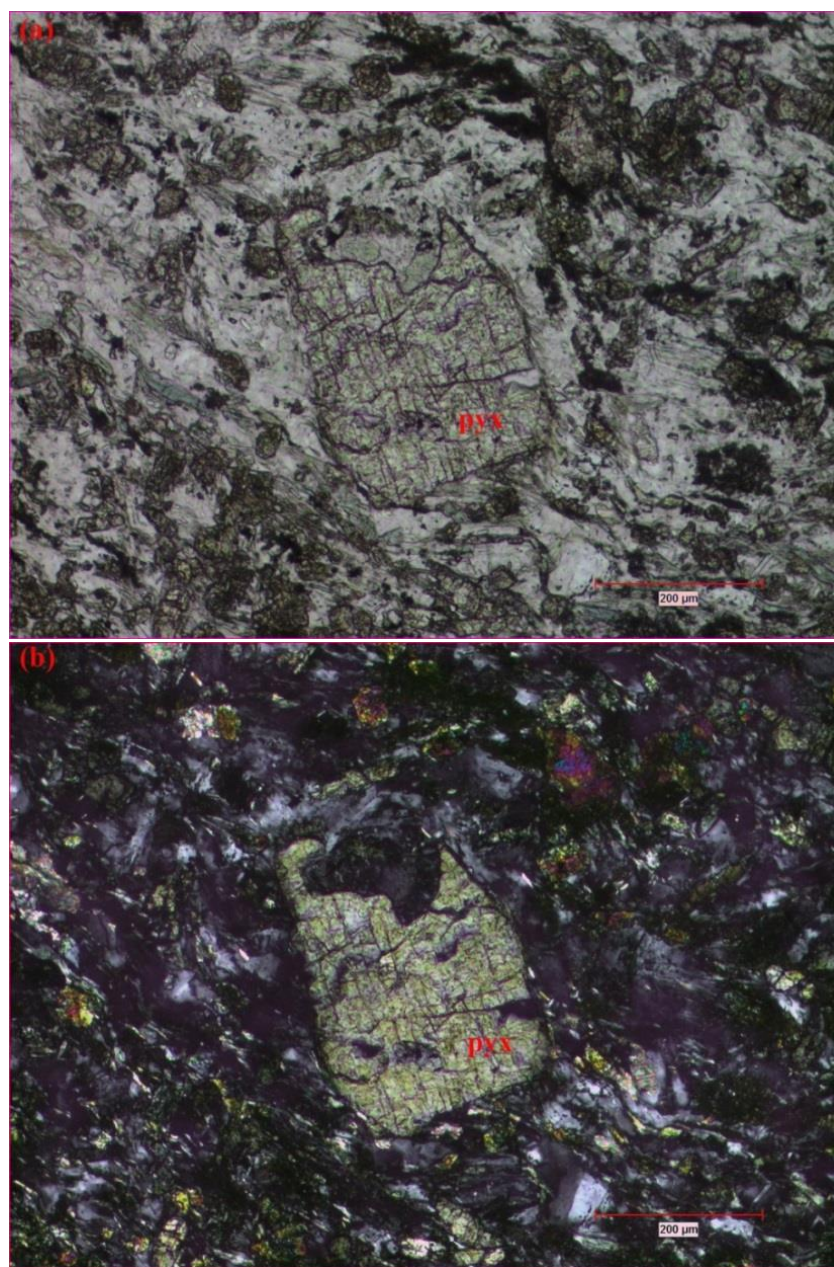


Figure 24. Microphotograph of a metabasalt showing a corroded pyroxene crystal.
((a) analyser out, (b) analyser in, pyx: pyroxene).

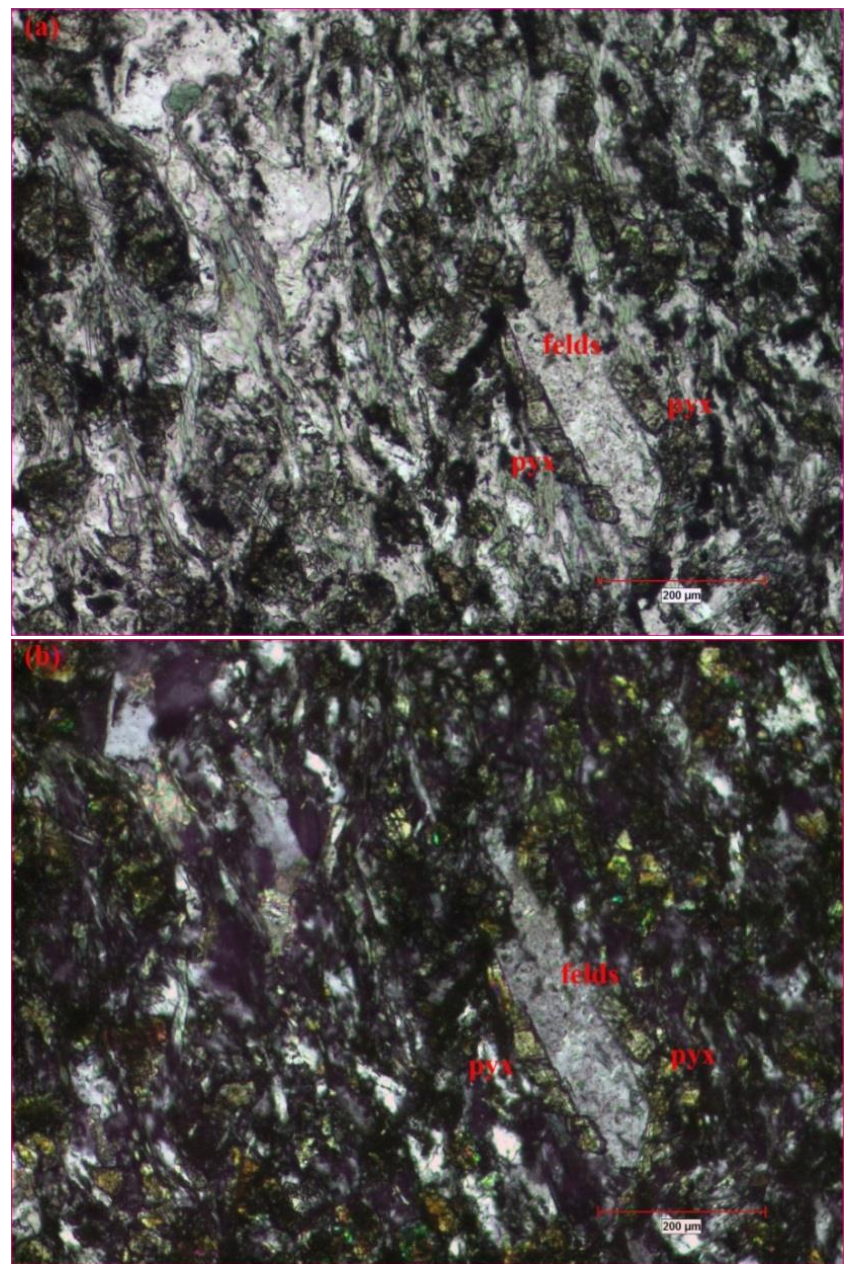


Figure 25. Microphotograph of a metabasalt showing growth of clinopyroxene microcrysts around a larger feldspar crystal. ((a) analyser out, (b) analyser in, felds: feldspar, pyx: pyroxene).

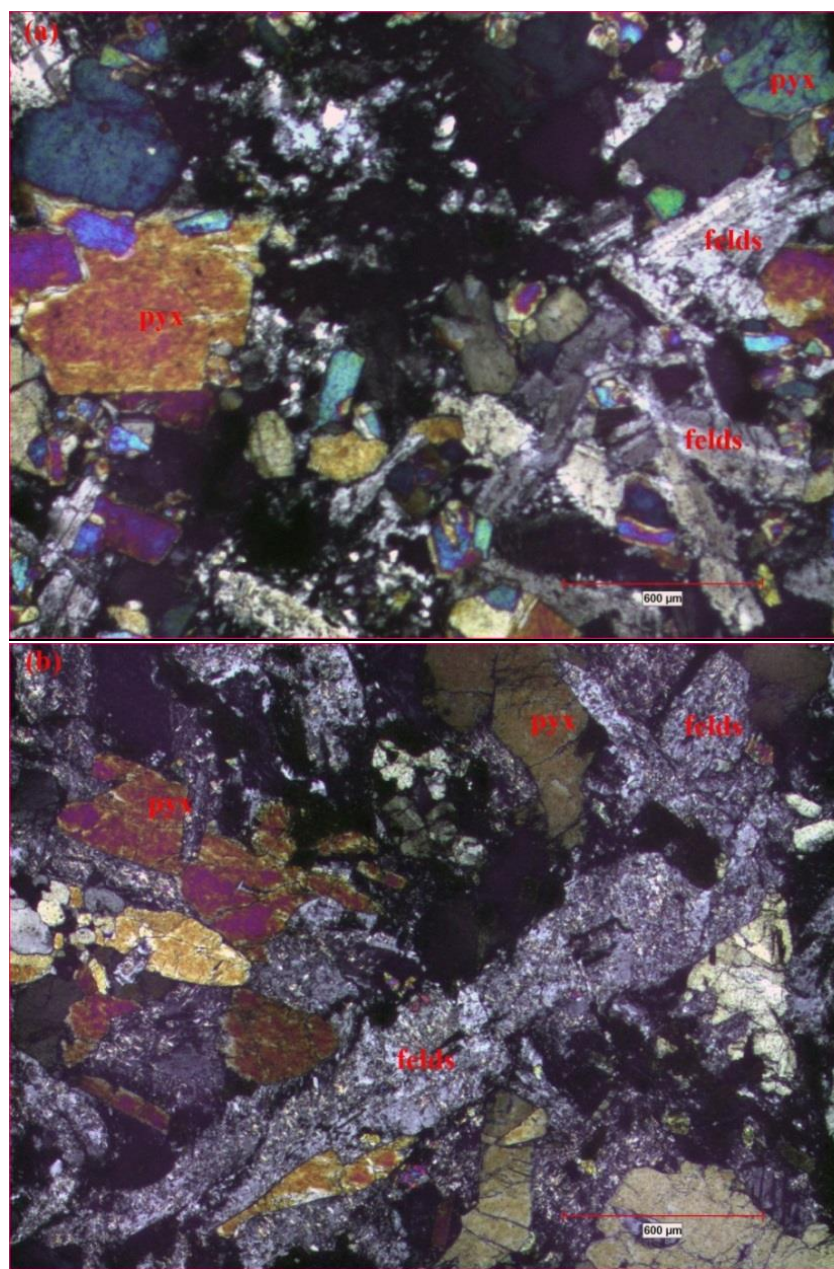


Figure 26. Microphotograph of a dyke showing ophitic and intergranular textures (felds: feldspar, pyx: pyroxene).

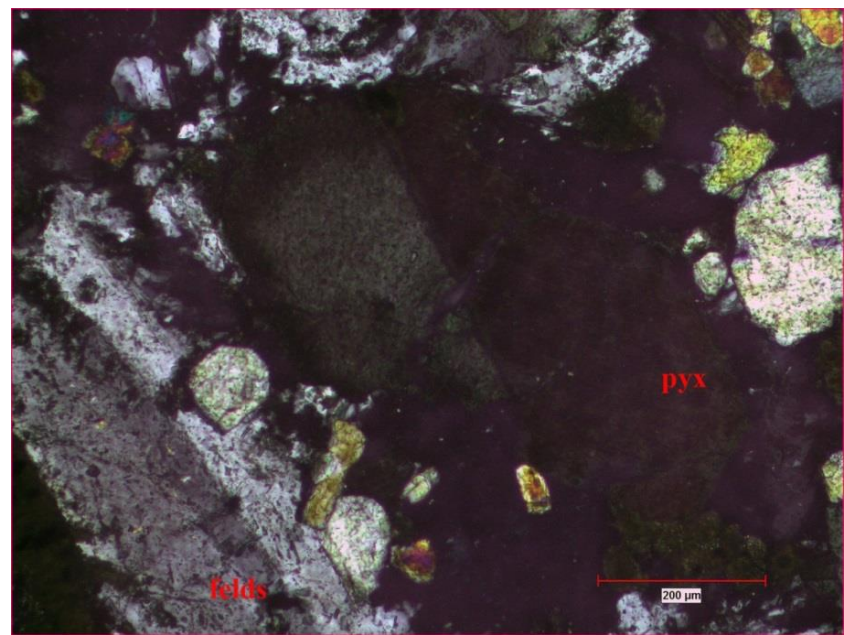


Figure 27. Microphotograph of a dyke showing both compositional zoning and twinning in a pyroxene crystal and a feldspar crystal (felds: feldspar, pyx: pyroxene).

In summary, all the rock types in concern (basalts, metabasalts and dykes) are mineralogically and petrographically similar to each other. Especially, all the rock types are dominated by chemical dis-equilibrium textures inferring open magma system as explained in detail in Section 3.1.

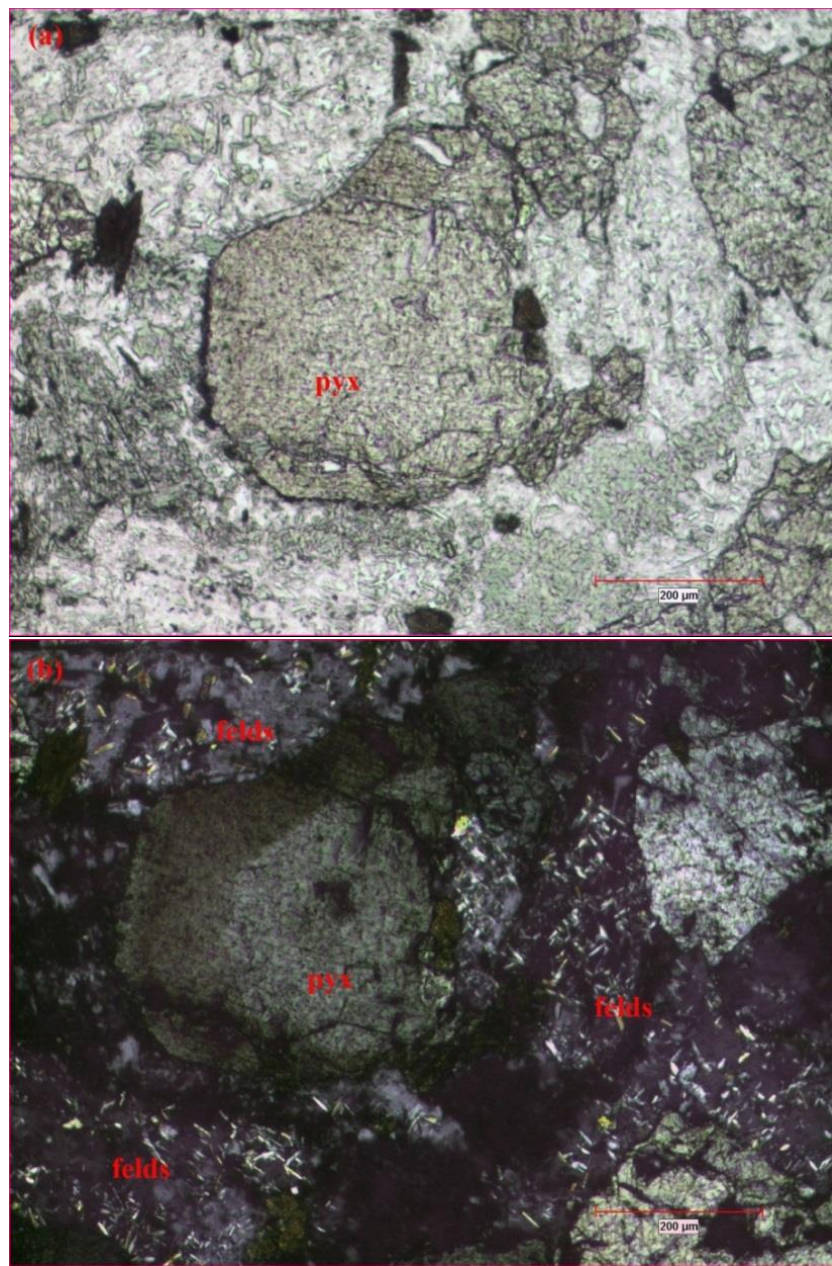


Figure 28. Microphotograph of a dyke showing a corroded pyroxene crystal with compositional zoning, and surrounding feldspars with sericitization ((a) analyser out, (b) analyser in, pyx: pyroxene, felds: feldspar).

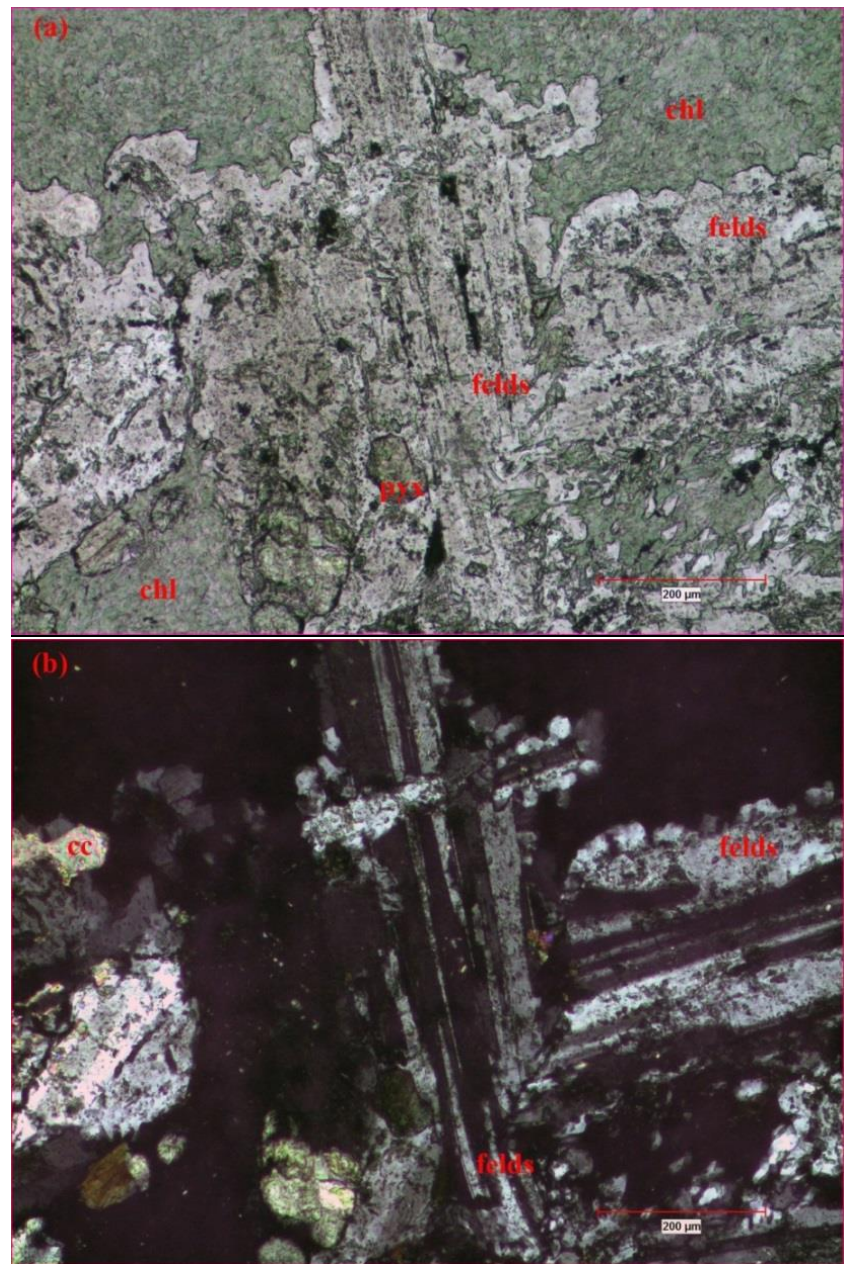


Figure 29. Microphotograph of a dyke showing twinned feldspars ((a) analyser out, (b) analyser in, pyx: pyroxene, felds: feldspar, chl: chlorite, cc: calcite).

CHAPTER 4

MINERAL CHEMISTRY AND PETROGENETIC IMPLICATIONS

4.1. Introduction

Mineral chemistry studies of the rocks were performed by using electron probe microanalyser (EPMA). The details about the analysis conditions are given in Section 1.3.1. Since EPMA gives the results as oxide values, the results were converted to cations per formula unit (pfu) for each mineral in terms of their crystal chemistry. Recalculations for oxide values into pfu were carried out using the formulations prepared by Assist. Prof. Dr. Fatma Toksoy Köksal under Microsoft Excel program.

4.2. Pyroxene

Pyroxene is the first crystallizing phase according to petrographical observations in the studied rocks. Major and minor element contents of pyroxene were obtained in oxide form from EPMA (Appendices A,B,C,D and E) and then these values were converted to cations pfu values discussed in Section 4.1. Pyroxene calculations were based on 6 oxygen atoms and 4 cations. Cation totals were normalized to stoichiometric values of Vieten and Hamm (1978). Moreover, Fe^{2+} and Fe^{3+} used in stoichiometric calculations were derived by Droop Equation (1987) from $\text{FeO}^{(t)}$.

4.2.1. Compositional Variations

The compositional ranges for the rock groups of the studied samples show similarities inferring that they are derived from the similar magma source (Table 1). Pyroxenes in basalts of the studied samples display texturally different occurrences. Some of the pyroxenes are found in a glassy groundmass and they have phenocrysts and new crystal overgrowths around these phenocrysts. The other group of basalts have smaller pyroxene microcrysts in their groundmass. The final group of basalts

have small pyroxenes which grow around grain boundaries of pyroxene and feldspar phenocrysts (Figure 5). Considering this petrographical groups, Mg# of the basalt samples show wide ranges. Phenocrysts of all basalts have Mg# ranging between 0.42-0.91, while new crystal overgrowths have Mg# as 0.50-0.69. Pyroxenes of basalts which are found in matrix as microcrysts display Mg# ranging between 0.70-0.83. Pyroxenes of the metabasalts have high Mg# (0.82-0.88) while Mg# of pyroxenes in dykes changes between 0.66-0.86. Major oxide ranges of the pyroxenes from the rock groups are shown in Table 1.

Table 1. Minimum and maximum major oxide values of the pyroxenes for the studied rocks.

(wt%)	metabasalt		dyke		basalt					
	phenocryst		crystal		phenocryst		phenocryst overgrowth		matrix	
	min.	max.	min.	max.	min.	max.	min.	max.	min.	max.
SiO ₂	48.74	51.99	48.93	52.97	45.72	53.16	50.82	54.20	47.48	48.69
TiO ₂	0.12	0.50	0.43	0.57	0.00	1.68	0.01	0.60	0.87	2.69
Al ₂ O ₃	1.75	4.30	1.33	4.36	1.27	5.58	0.74	1.46	2.76	6.92
Fe ₂ O ₃	4.83	8.00	4.69	6.88	3.63	19.98	12.05	18.10	5.67	7.28
MnO	0.09	0.22	0.07	0.12	0.01	0.32	0.22	1.09	0.08	0.13
MgO	19.14	23.05	12.69	19.10	7.16	19.36	10.53	13.81	12.60	13.77
CaO	15.71	20.18	19.64	21.53	12.09	21.75	11.57	14.28	20.15	21.57
Na ₂ O	0.20	0.60	0.18	0.33	0.16	5.27	0.26	0.42	0.18	0.38
K ₂ O	0.00	0.02	0.00	0.03	0.00	0.01	0.07	0.11	0.00	0.03
Cr ₂ O ₃	0.19	0.61	0.00	0.96	0.00	1.37	0.00	0.08	0.00	0.22
NiO	0.00	0.07	0.00	0.09	0.00	0.07	0.00	0.07	0.00	0.06

In order to see compositional changes for pyroxene through different rock groups, cation pfu vs. Mg# were plotted (Figure 30). Pyroxenes of metabasalts have high Mg contents and low Ni, Fe^(t), Mn, Ti and K contents (Appendix A, Figure 30e, c, d, f, h and k).

Pyroxenes of dykes have high Ca and Cr contents but their Mn and K contents are low (Appendix B, Figure 30g, i, f and k). Mineral chemistry values for the analyses taken from different occurrences in basalts display wide ranges. Si, Fe^(t), Mn and K contents of basalt overgrowths (Appendix D) are higher than those of basalt matrix (Appendix E) and basalt phenocrysts (Appendix C, Figure 30a, d, f and k). Moreover, pyroxene overgrowths have low Al^(t), Ni, Ca, Ti and Cr contents (Figure 30b, c, g, h and i). Pyroxenes of basalt matrix have low Si, Fe^(t) and Mn contents while high Al^(t), Ca and Ti contents (Figure 30a, d, f, b, g and h). Pyroxenes of basalt phenocrysts generally display medium values from those of overgrowths and basalt matrix. When Al^(t), Ti, Ca and Na contents are taken into consideration, for pyroxenes of all studied rocks each element shows a decreasing pattern for each rock type (Figure 30b, h, g and j). This may be caused by albitic nature of plagioclase in studied rocks where Al^(t) slightly partitioned into pyroxene. Furthermore, when Cr plot (Figure 30i) is examined in detail, there is a decrease in Cr with decreasing Mg# due to compatibility of Cr with clinopyroxene. Ti contents (Figure 30h) of basalt phenocrysts and basalt matrix display a fractionation pattern indicating Ti enrichment which is supported by petrographical observations.

When all variation diagrams are considered, three different groups are clearly observed. Especially these groups are more distinctive in the plots of Si, Al^(t), Fe^(t), Mg, Mn, Ca, Ti and K. In petrographical observations, three different occurrences are realized for basalts (Figure 31). These occurrences are simply pyroxene phenocrysts, a new crystal material overgrowth around these phenocrysts and small pyroxenes in matrix of the basalts. When petrographical observations and mineral chemistry analyses are taken into account together, these three occurrences correspond to three groupings in the variation diagrams. That is, this may infer there are at least three crystallization stages for the pyroxenes of basalts.

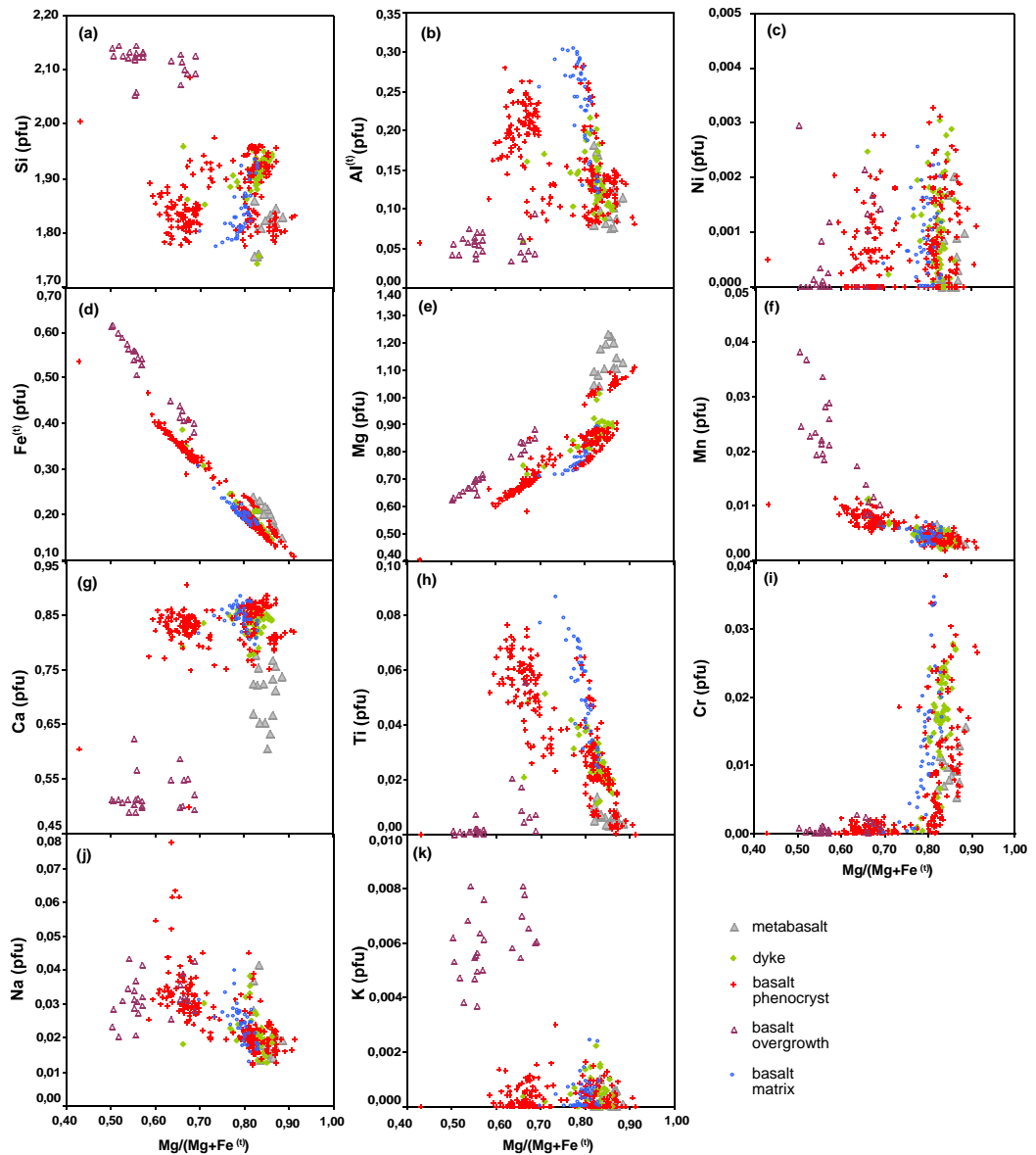


Figure 30. Variation diagrams for major and minor element compositions for the studied rocks.

In the first stage coarse pyroxene phenocrysts, which were rich in Ca and Mg contents but depleted in Ti and Fe^(t) contents, were formed. Then there was an influx of melt to the magma that was rich in Fe^(t) and Mn contents but its Ti, Ca and Mg

contents are low inferring that this new influx made the system subalkaline (see Section 4.3.3). Finally, there was a second influx which was rich in Al^(t), Ti, Ca, Cr and Mg contents, but depleted in Fe^(t) and Mn contents which affected the system and made it alkaline (see Section 4.3.3). Table 2 and Figure 32 clearly exemplify the compositional differences phenocryst and overgrowth zones during the crystallization stages of a pyroxene phenocrysts in basalt samples.

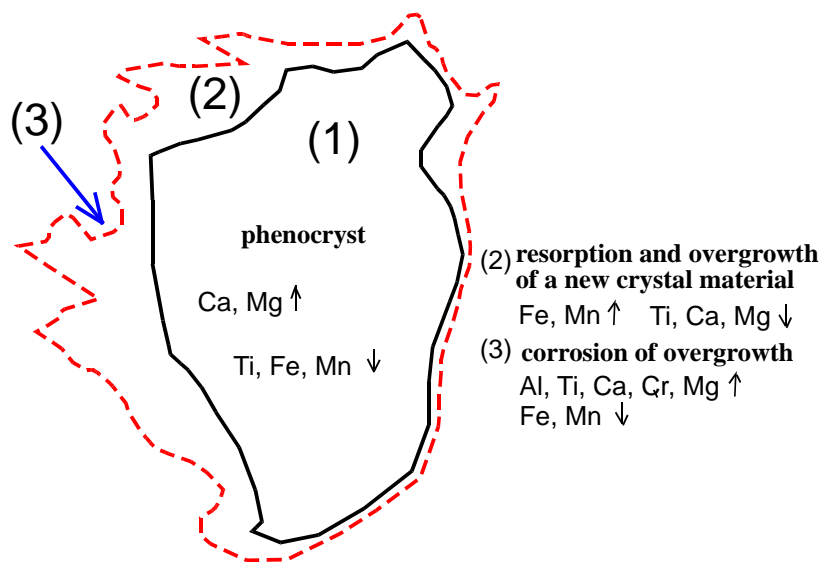


Figure 31. Sketch drawing showing three different crystallization stages for the pyroxenes of the basalts and their compositional constituents (not to scale).

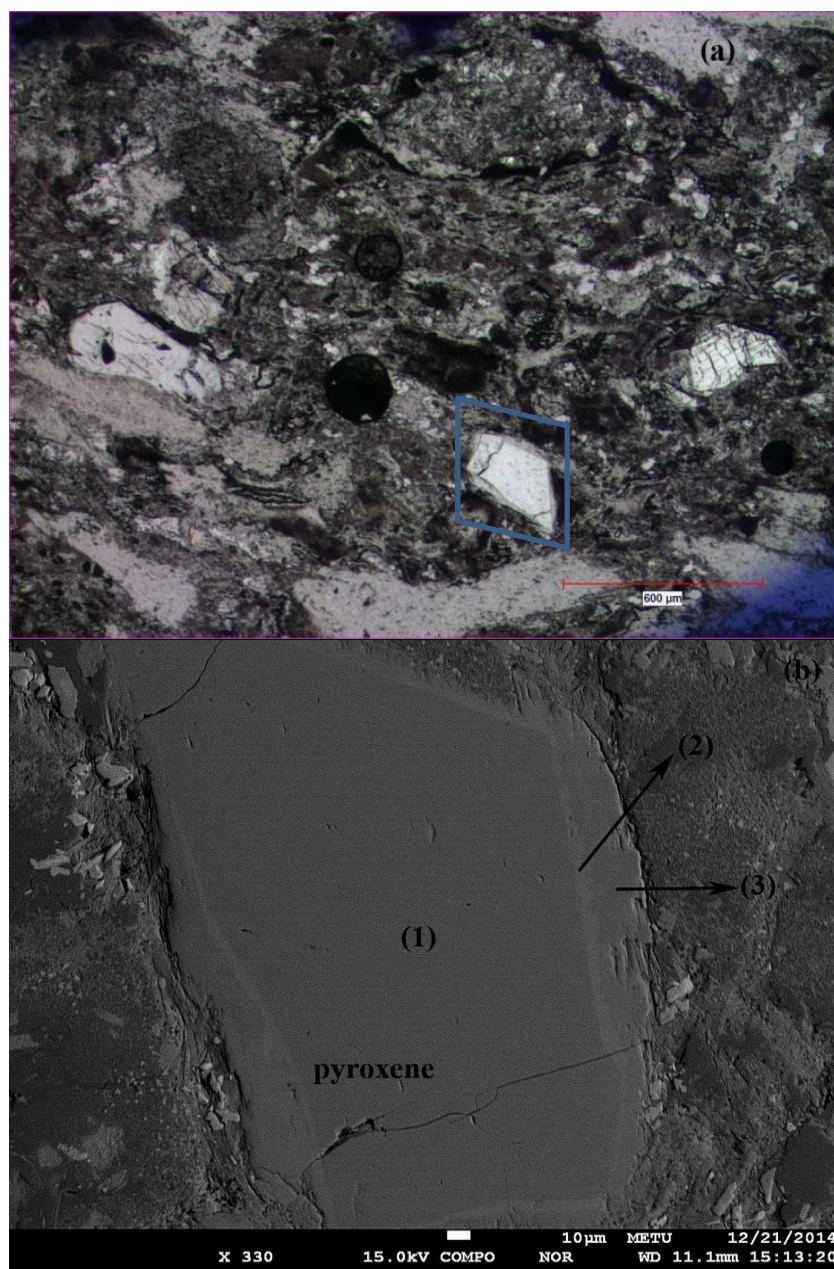


Figure 32. (a) Microphotograph from a basalt sample in analyser out condition, (b) Back scattered image of the pyroxene crystal (1) (blue quadrangle) from (a) showing overgrown by two different crystal material (2) and (3). (c) Back scattered image of a pyroxene crystal (4) showing overgrowth of Fe-rich new crystal material (5).

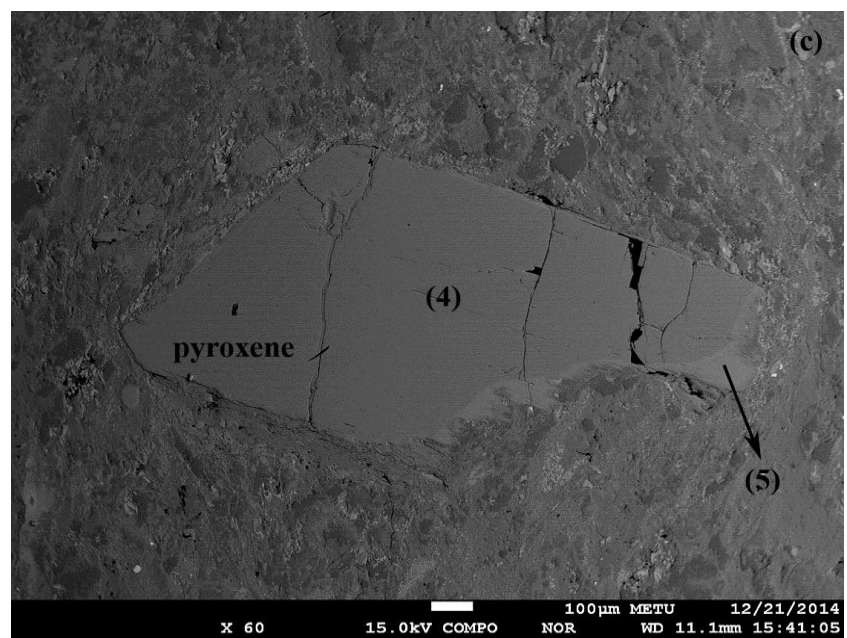


Figure 32. (continued).

Table 2. EPMA analyses results for the pyroxenes in Figure 32.

	1	2	3	4	5
SiO ₂	53.10	54.58	55.22	52.76	53.93
TiO ₂	0.77	0.06	0.05	0.77	0.04
Al ₂ O ₃	1.94	1.31	2.11	2.01	0.87
Fe ₂ O ₃	6.15	16.16	12.05	5.99	18.50
MnO	0.15	0.78	0.22	0.14	1.13
MgO	15.98	12.09	15.02	15.92	10.53
CaO	21.58	12.16	12.83	21.62	12.04
Na ₂ O	0.22	0.39	0.58	0.23	0.30
K ₂ O	0.00	0.12	0.12	0.00	0.12
Cr ₂ O ₃	0.14	0.02	0.03	0.12	0.02
NiO	0.00	0.04	0.05	0.00	0.09
Total	100.03	97.70	98.28	99.56	97.59

According to obtained chemical composition data of pyroxenes from different rock groups, it seems that pyroxenes crystallize from a system having high Ca content. After that, there is another crystallization stage which makes the system subalkaline due to high Fe content (see Section 4.3.3). The final crystallization stage is rich in Mg and Al which affects the system and make the system alkaline (see Section 4.3.3).

Except for basalt pyroxene overgrowths, the other rock groups give a positive correlation of $\text{Al}^{(t)}$ and Ti with $\text{Fe}^{(t)} / (\text{Fe}^{(t)} + \text{Mg})$ which is known as fractionation index according to Figure 33a,b (Toksoy-Köksal, 2003). Since basalt pyroxene overgrowths are rich in Fe contents, they do not give a positive pattern. Index of fractionation must give negative correlation with iron oxide minerals; therefore, minor amounts of iron oxide minerals in the other rock groups may one of the reasons for their positive correlation.

Pyroxenes in basalt phenocrysts have the highest Ca# and pyroxenes in basalt matrix and dykes have moderate Ca# (Figure 34). Pyroxenes of the basalt overgrowths have the lowest Ca# and Mg#. Pyroxenes of metabasalts show moderately low Ca# and high Mg#. Furthermore, three different groups of pyroxenes for the studied rocks also can be observed clearly from the relation between Ca# and Mg#.

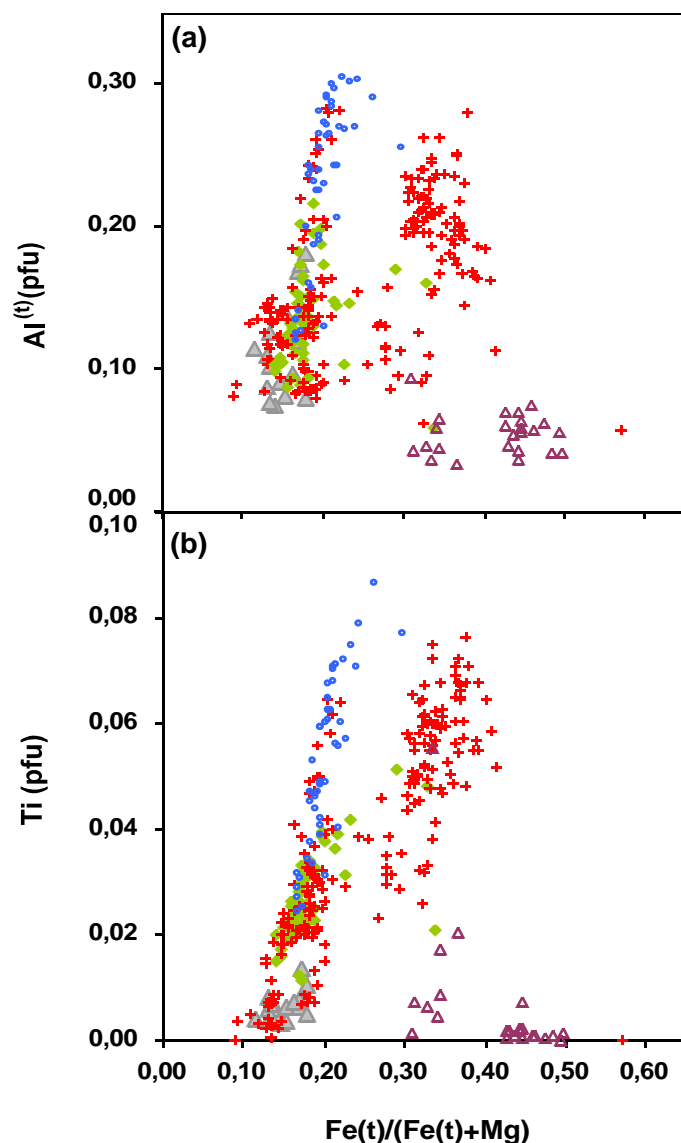


Figure 33. Covariation diagrams of $\text{Al}^{(t)}$ and Ti (pfu) against $\text{Fe}^{(t)} / (\text{Mg} + \text{Fe}^{(t)})$ (the symbols are same as in Figure 30).

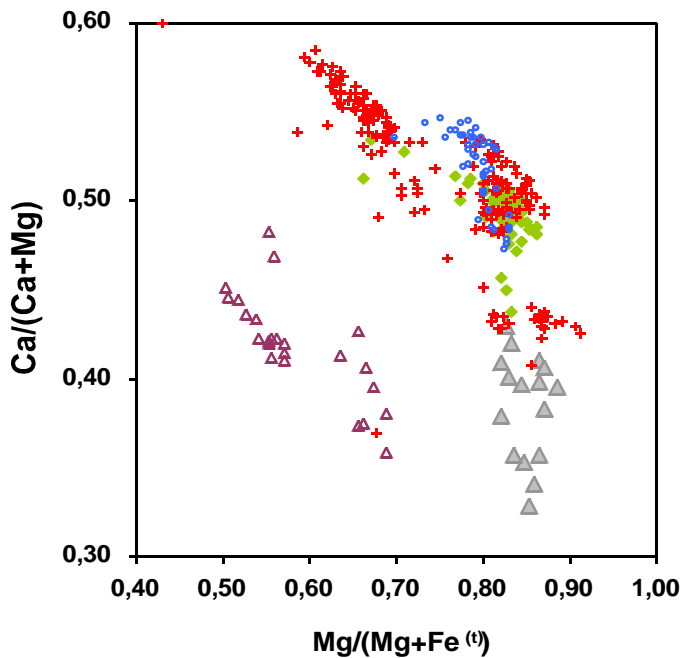


Figure 34. The relation between Ca# and Mg# for the studied rocks (the symbols are same as in Figure 30).

4.2.2. Nomenclature and Substitution Mechanisms

Formula calculation and nomenclature for pyroxene were made according to Morimoto (1989). Morimoto (1989) was suggested that $M_2M_1T_2O_6$ as chemical formula for pyroxene where both M1 and M2 stand for octahedral site cations (M1 for regular coordinations and M2 for distorted coordinations) and T for tetrahedral site cations. According to the Morimoto (1989), Si, Al, then Fe^{3+} (their sum to 2); Al, Fe^{3+} (excess after that used in T site) and then Ti, Cr, Mg, Fe^{2+} and Mn (their sum to 1); Mg, Fe^{2+} , Mn (excess after that used in M1 site) and then Ca and Na (their sum to 1).

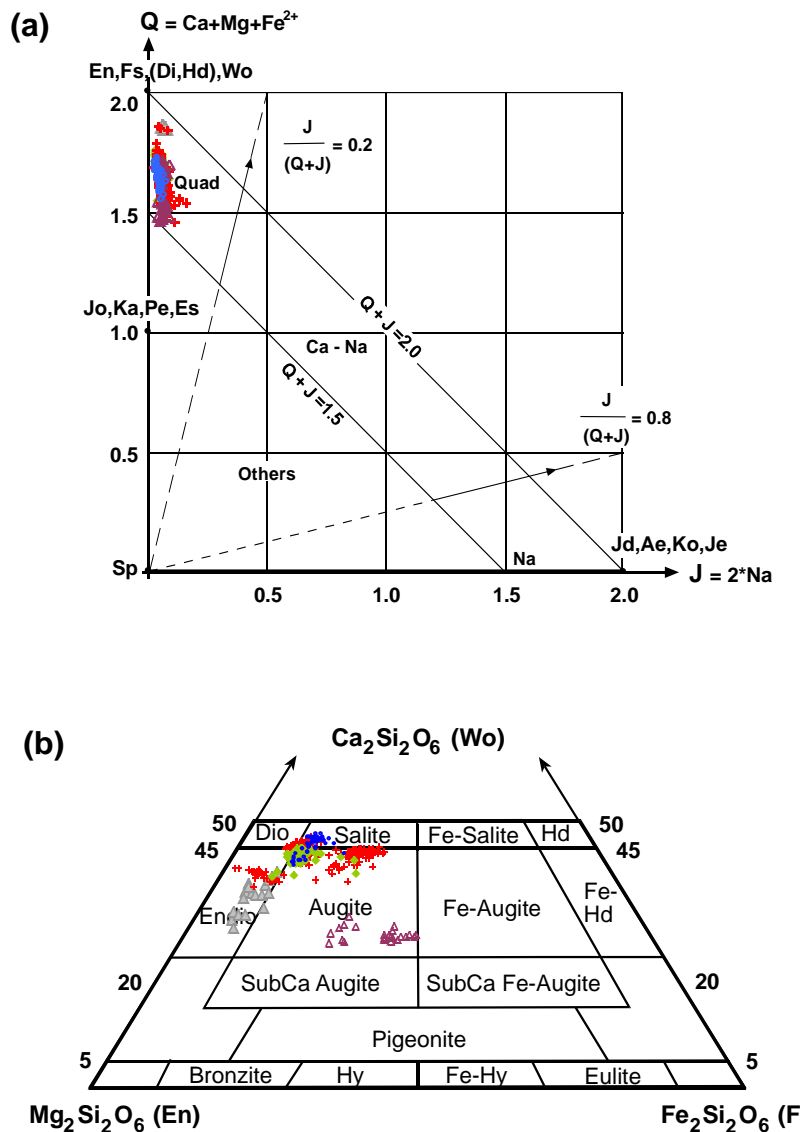
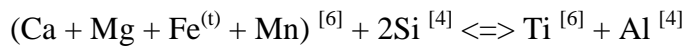
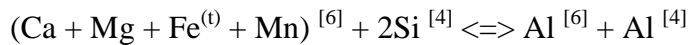
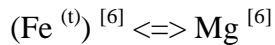


Figure 35. The place of pyroxene data on Q-J diagram adapted from Morimoto and Kitamura (1983) (a) and the plots of pyroxene on the Ca-Mg-Fe clinopyroxene classification diagram after Poldervaart & Hess (1951) (b) (the symbols are same as in Figure 30).

On the Q-J diagram adapted from Morimoto and Kitamura (1983) chemical compositions of pyroxenes fall to Ca-Mg-Fe group (Wollastonite ($\text{Ca}_2\text{Si}_2\text{O}_6$), Enstatite ($\text{Mg}_2\text{Si}_2\text{O}_6$) and Ferrosillite ($\text{Fe}_2\text{Si}_2\text{O}_6$)) as shown in Figure 35a. Moreover, most of the pyroxene phenocrysts and overgrowths of basalts and dykes are in augite field in the ternary Wo-En-Fs system (Figure 35b). Pyroxenes in matrix of basalts lie on both salite and augite field. Chemical composition for metabasalts is in endiopside field. As a result, the studied pyroxenes are augitic in composition generally. The compositional ranges for pyroxenes are $\text{Wo}_{30.72-46.71} - \text{En}_{26.01-57.58} - \text{Fs}_{1.05-34.94}$ based on calculations after Morimoto (1989).

Pyroxene shows the following substitution mechanisms:



and Ti/Al ratio mostly between 1:5 – 1:20 (Figure 36). These features indicate that Al entered pyroxene structure as Ca-Ti- tschermak (Tal) and Ca-tschermak (Cal) molecules (Figure 37). The substitution mechanism $(\text{Fe}^{(t)})^{[6]} \rightleftharpoons \text{Mg}^{[6]}$ (Figure 36a) shows a scattered plot with three trends; however, coupled substitution mechanisms show less scattered correlations with two trends (Figure 36c,d). This indicates that coupled substitution mechanisms are the controlling factor for pyroxenes of the studied rocks.

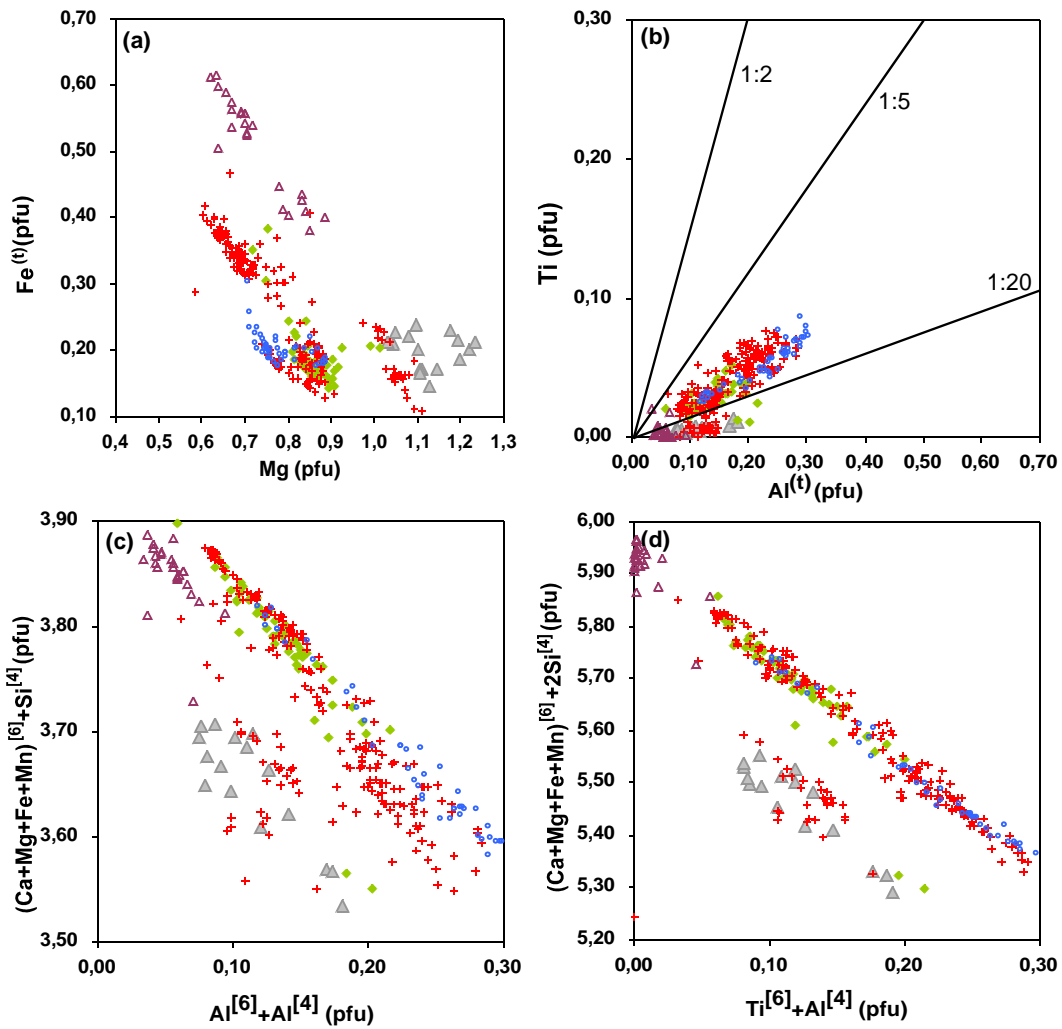


Figure 36. The substitution mechanisms and Ti-Al^(t) ratio diagram (the symbols are same as in Figure 30).

4.3.3. Implications for Petrology and Tectonic Setting

The chemical data of pyroxenes were plotted on SiO₂ – Al₂O₃ (wt%) and Ti – (Ca+Na) (pfu) covariation diagrams (Figure 39a, b). Pyroxenes from the studied rocks display a transitional character between subalkaline and alkaline (Figure 39a). Pyroxene phenocrysts with Mg and Al contents, and pyroxene microcrysts with high Mg and Al that is abundant in groundmass from basalts strongly infer alkaline

chemistry (Figure 39). Moreover, in Ti – (Ca+Na) diagram, pyroxene data plot in both fields inferring transitional character (Figure 39b). The rocks showing subalkaline affinities (Figure 39a,b) display tholeiitic character in Ti-Al^(t) diagram (Figure 39c) due to Fe-enrichment at second stage of crystallization in the studied rocks. According to the plots of Ti+Cr – Ca (pfu) (Figure 38), pyroxene data mostly plot in non-orogenic basalt field.

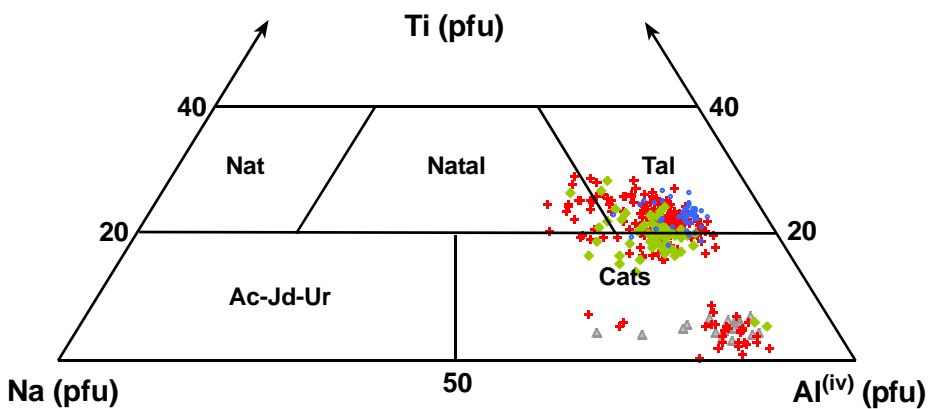


Figure 37. The place of the pyroxene data on the Ti-Na-Al^[4] triangle diagram proposed by Papike et al. (1974) (the symbols are as in Figure 30).

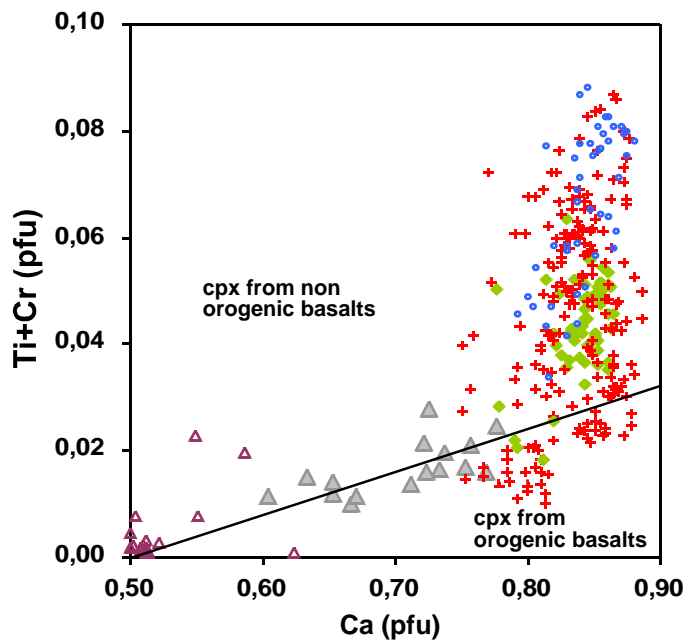


Figure 38. The place of the pyroxene data on the Ti+Cr-Ca diagram (Leterrier et al., 1982) (the symbols are as in Figure 30).

4.3. Feldspar

Major and minor elements of feldspar were obtained in oxide form from EPMA (Appendices F,G, and H) and then these values were converted to cations pfu values. For the feldspar, the calculations were based on 8 oxygen atoms and 5 cations and cation totals were normalized to stoichiometric values of Deer et al. (1980).

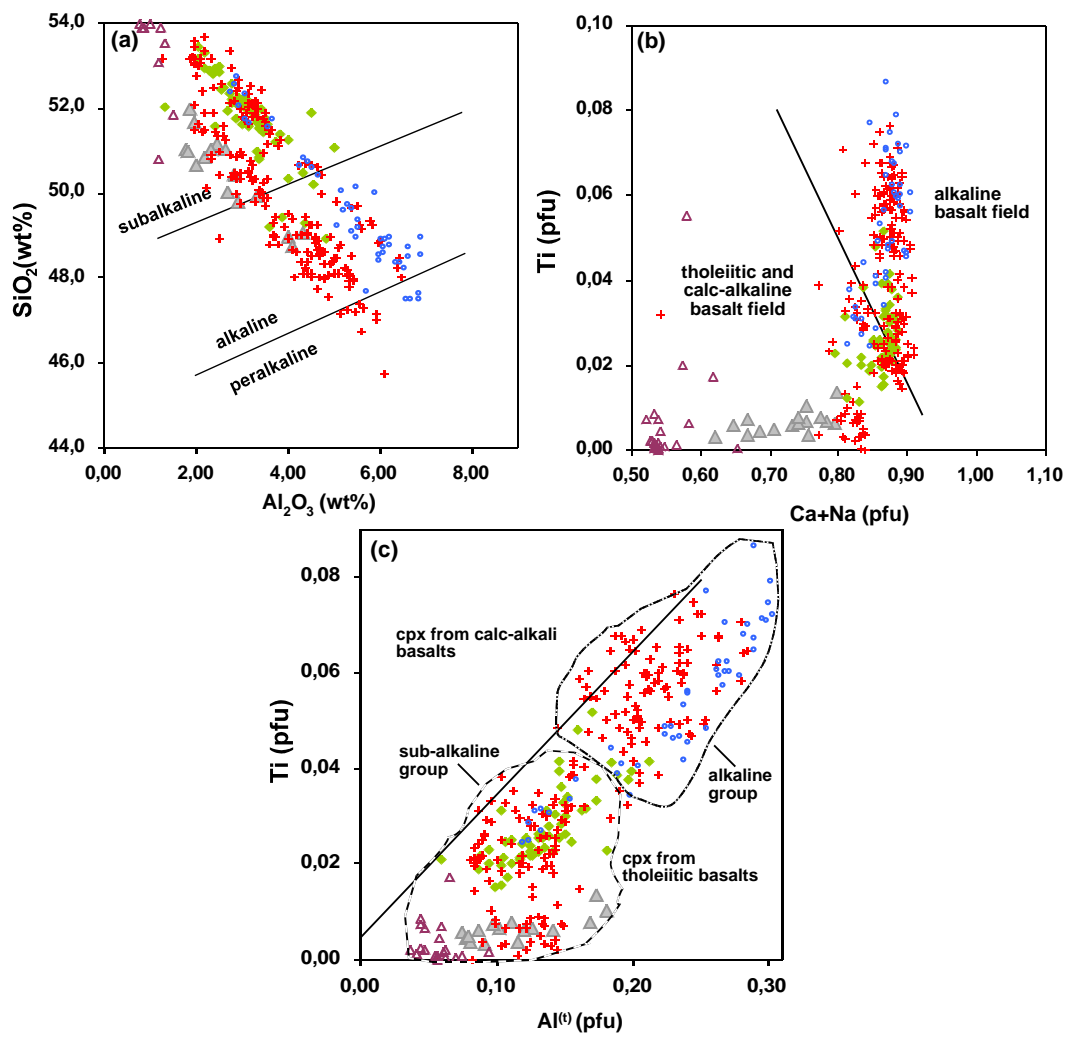


Figure 39. The place of pyroxene data on the diagrams of ; (a) $\text{SiO}_2 - \text{Al}_2\text{O}_3$ (wt%) (Le Bas, 1962), (b) $\text{Ti} - (\text{Ca}+\text{Na})$ (pfu) (Leterrier et al., 1982) and (c) $\text{Ti}-\text{Al}^{(\text{t})}$ (pfu) (Liotaud et al., 1988) (the symbols are same as in Figure 30).

4.3.1. Compositional Variations

Chemical compositions of the feldspars from the studied rocks were examined. The feldspars from all studied rock types have similar compositional ranges which are tabulated as Table 3. Chemical compositions for Fe and Ba are in negligible amounts.

In order to determine elemental relations for feldspar, Al (pfu), Ca (pfu), Na (pfu) and K (pfu) against Si (pfu) were plotted (Figure 40). Al and Ca contents show reverse relationship with Si content. That is, while Si content is increasing, Al and Ca contents are decreasing (Figure 40a, b). However, Na and K contents show weak positive trend with increasing Si content (Figure 40c, d).

Table 3. Minimum and maximum major oxide values of the feldspars from the rock groups of studied rocks.

	metabasalt		dyke		basalt	
	min.	max.	min.	max.	min.	max.
SiO ₂	66.10	67.98	66.10	69.90	67.49	70.35
Al ₂ O ₃	18.49	18.88	18.75	19.84	17.50	19.84
CaO	0.01	0.20	0.00	1.35	0.01	1.16
FeO	0.15	0.61	0.05	0.41	0.01	1.33
BaO	0.00	0.18	0.00	0.24	0.00	0.12
Na ₂ O	9.36	11.57	10.90	11.92	10.82	12.07
K ₂ O	0.04	2.64	0.02	0.71	0.01	0.59

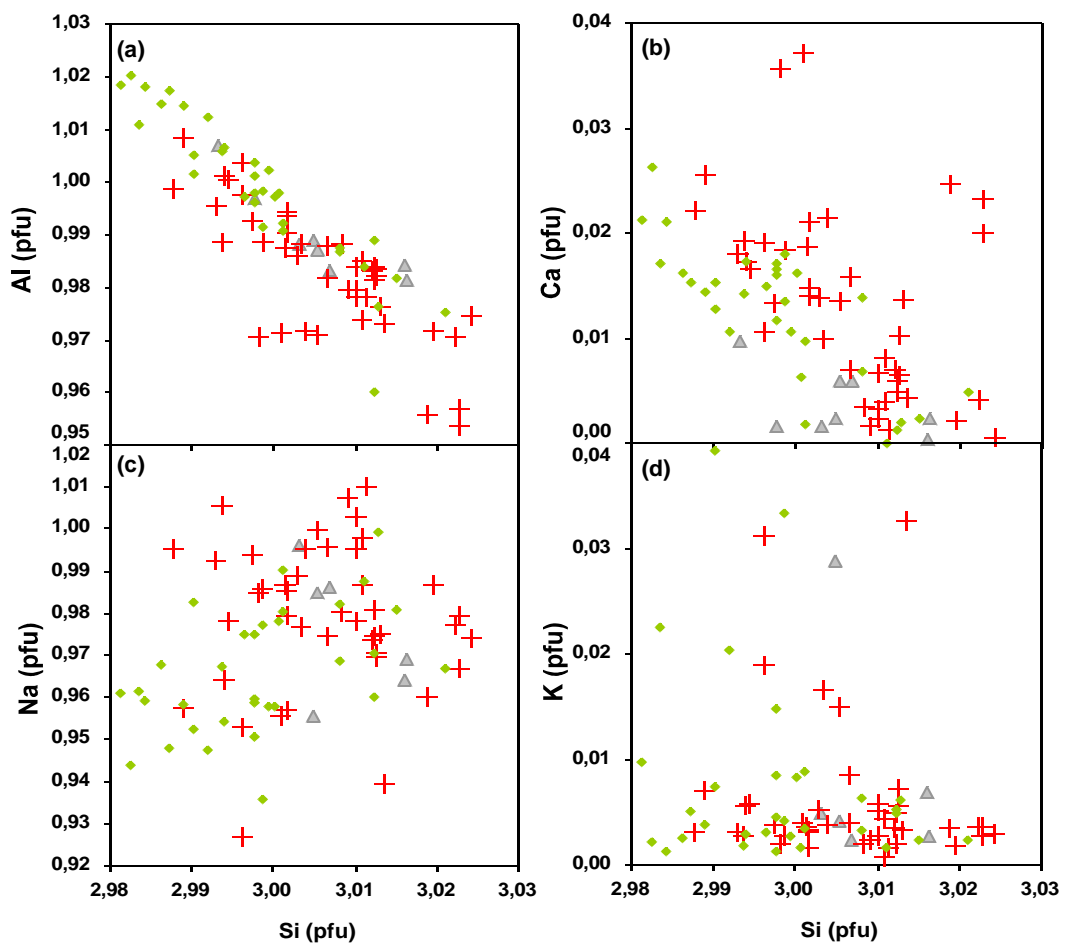


Figure 40. Variation diagrams of elements against Si (pfu) (symbols are same as in Figure 30).

4.3.2. Nomenclature and Substitution Mechanisms

Since feldspar structure is formed by a three-dimensional tetrahedra framework, the formula for feldspars was calculated on the basis of five cations. Tetrahedral site is filled by Si, Al (their sum to 4) and large cation site is filled by Na, Ca, K and Ba (their sum to 1). By using the relations among the $\text{NaAlSi}_3\text{O}_8$ (albite), $\text{CaAl}_2\text{Si}_2\text{O}_8$ (anorthite) and KAlSi_3O_8 (K-feldspar), which are three end-members, the albite-anorthite and orthoclase contents for the studied feldspars were calculated from $100*\text{Ca}/(\text{Ca}+\text{Na}+\text{K})$, $100*\text{Na}/(\text{Ca}+\text{Na}+\text{K})$, $100*\text{K}/(\text{Ca}+\text{Na}+\text{K})$, respectively. Then the calculated values were plotted on ternary diagram of orthoclase-albite-anorthite (Figure 41). According to Figure 41, feldspars of studied rocks are Na-rich and most of them fall into the albite zone. The compositional ranges for feldspar type are K-feldspar_{0,08-2,92}–Albite_{84,21-97,05}–Anorthite_{0,00-2,50}.

Although the albitic composition of the feldspars from the study area seems to be albitization alteration according to petrographical observations, the feldspars preserve their twinnings. As a result, the main reason for the albitic composition of the studied feldspars is that the final alkaline influx which is rich in Na and K to the magma chamber.

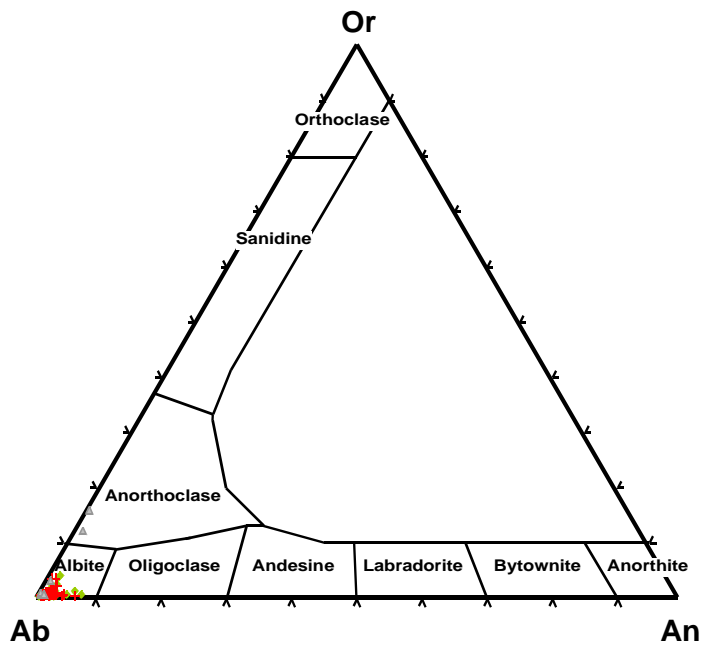


Figure 41. The plots for the feldspars from studied rocks on feldspar ternary diagram (symbols are same as in Figure 30).

According to Figure 42, while $\text{Al} + \text{Ca}$ (pfu) is increasing, $\text{Si} + \text{Na}$ (pfu) is decreasing. There is a reverse relation. This is explained as besides substitution of Na and Ca in the large sites, there exist substitution between Al and Si in the tetrahedral site. Therefore, a coupled (charge-balanced) substitution $\text{Ca}+\text{Al} \leftrightarrow \text{Na}+\text{Si}$ is effective in controlling the solid solution between albite and anorthite.

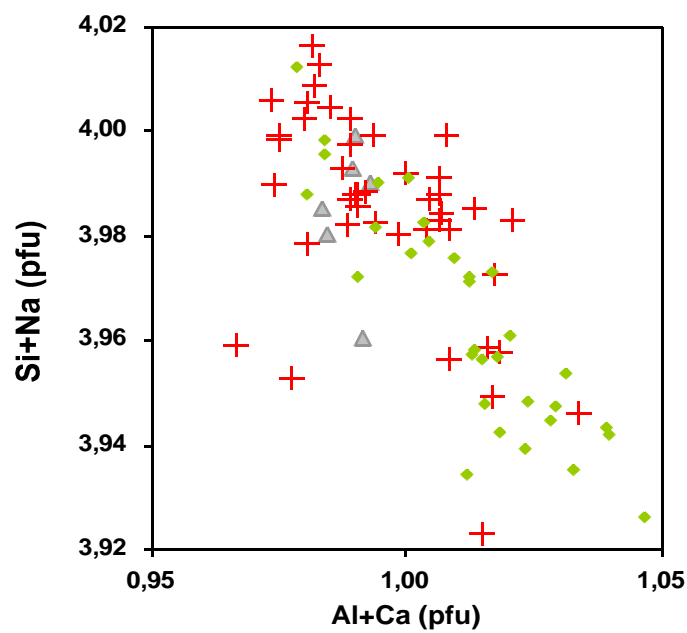


Figure 42. Plot showing coupled substitution mechanism for feldspars from the study area (symbols are same as in Figure 30).

CHAPTER 5

WHOLE-ROCK CHEMISTRY

5.1. Introduction

After detailed examinations of petrographical and mineral chemical data, six samples were selected for major oxide and trace element geochemical interpretations. These samples are AA-11c and AA-12 from basalts, AA-6 and AA-7 from metabasalts, AA-10a and AA-10d from doleritic dikes. Since petrographical and mineral chemistry data strongly infer that these rock groups are originated from the same magma, the same symbol is used for all rock groups to interpret geochemically in this chapter. Concentrations of major oxides and trace elements of the studied rocks are given in Table 4 and Table 5, respectively.

All analyses were performed by ACME Analytical Laboratories Ltd. (Vancouver, CANADA). Major oxides including Ba, Ni and Sc were measured by inductively-coupled plasma atomic emission spectrograph (ICP-AES) and rest of the elements including rare earth elements were measured by inductively-coupled plasma mass spectrometer (ICP-MS).

Data obtained from the measurements are used to identify the geochemical character and original tectonic environment of the area.

5.2. Effect of Alteration on Whole-Rock Composition

Petrographical and mineralogical studies revealed that the studied samples appear to have been influenced by low-grade hydrothermal alteration and surface alterations in varying degrees.

Varying degrees of hydrothermal alteration on basalts and dykes in ophiolites in intra-oceanic conditions is common feature. Therefore, relatively stable elements should be used to determine geochemical compositions of them (Dilek and Furnes, 2011). In literature, studies show that alteration causes loss or gain of most of alkali earth elements and large ion lithophile elements (LILE) such as Rb, Sr, Pb, Ba, Cs and U. Moreover, some minor and trace elements tend to have been remobilized under low-grade hydrothermal metamorphism (e.g. Pearce and Norry, 1979).

To identify degree of alteration for the studied samples, covariation diagrams of Ba, Sr, Rb, TiO₂, P₂O₅ and K₂O against Zr were plotted, since Zr is an immobile element (Figure 43). The elements mostly show good correlation with Zr. It is resulted that alteration is unlikely to affect on chemical composition of the studied rocks.

Table 4. Major oxide (wt%) compositions of the studied samples.

Sample	AA-6	AA-7	AA-10a	AA-10d	AA-11c	AA-12
Rock	metabasalt	metabasalt	dike	dike	basalt	basalt
SiO ₂	47.45	48.72	48.95	48.14	47.72	47.26
Al ₂ O ₃	11.77	13.46	12.87	14.82	11.49	14.36
Fe ₂ O ₃	10.85	11.49	10.19	10.36	9.07	14.08
MgO	11.16	6.30	9.04	6.70	4.36	5.55
CaO	8.54	8.52	9.31	9.44	14.31	7.88
Na ₂ O	3.25	3.87	3.99	3.93	3.92	4.54
K ₂ O	0.49	1.49	0.18	0.79	0.52	0.40
TiO ₂	1.98	2.49	2.12	2.36	1.37	2.43
P ₂ O ₅	0.25	0.30	0.27	0.29	0.19	0.34
MnO	0.14	0.16	0.14	0.14	0.13	0.16
Cr ₂ O ₃	0.11	0.03	0.13	0.03	0.02	n.d.*
LOI	3.70	2.90	2.50	2.60	6.70	2.70
Total	99.70	99.72	99.68	99.58	99.82	99.75

*: not detectable

Table 5. Trace element (ppm) compositions of the studied samples.

Sample	AA-6	AA-7	AA-10a	AA-10d	AA-11c	AA-12
Rock	metabasalt	metabasalt	dike	dike	basalt	basalt
Ni	373	94	189	95	97	30
Co	49.8	37.0	38.7	33.3	30.6	38.5
Sc	26	28	34	30	24	23
Ba	99	251	169	285	85	149
Pb	1.4	0.9	0.2	0.3	0.3	0.6
Hf	3.9	4.5	3.8	4.3	2.4	4.4
Nb	18.6	21.9	22.2	25.2	16.6	33.6
Rb	8.6	28.0	3.6	11.3	8.4	6.0
Sr	106.6	356.5	507.1	1392.2	151.9	224.9
Ta	1.2	1.4	1.3	1.7	1.1	2.1
Th	2.1	2.2	2.3	2.6	2.1	4.0
U	0.4	0.4	0.3	0.4	0.5	0.8
V	211	255	239	267	205	314
Zr	153.1	184.1	152.5	170.9	94.1	172.5
Y	19.9	24.0	21.8	22.8	18.1	30.6
La	18.0	20.0	20.8	23.5	17.2	31.0
Ce	37.4	46.3	44.3	49.5	31.8	60.0
Pr	4.83	5.73	5.25	5.79	3.77	6.89
Nd	21.1	26.2	22.5	24.9	15.5	26.5
Sm	4.88	6.11	5.05	5.62	3.28	5.92
Eu	1.70	2.00	1.76	1.93	1.15	1.94
Gd	5.06	6.02	5.24	5.88	3.86	6.42
Tb	0.77	0.88	0.80	0.87	0.61	1.01
Dy	4.22	4.93	4.17	4.70	3.50	5.96
Ho	0.77	0.93	0.83	0.92	0.67	1.14
Er	1.98	2.17	2.06	2.22	1.90	3.12
Tm	0.25	0.33	0.29	0.30	0.26	0.46
Yb	1.56	1.87	1.71	1.91	1.62	2.74
Lu	0.23	0.27	0.25	0.28	0.26	0.41

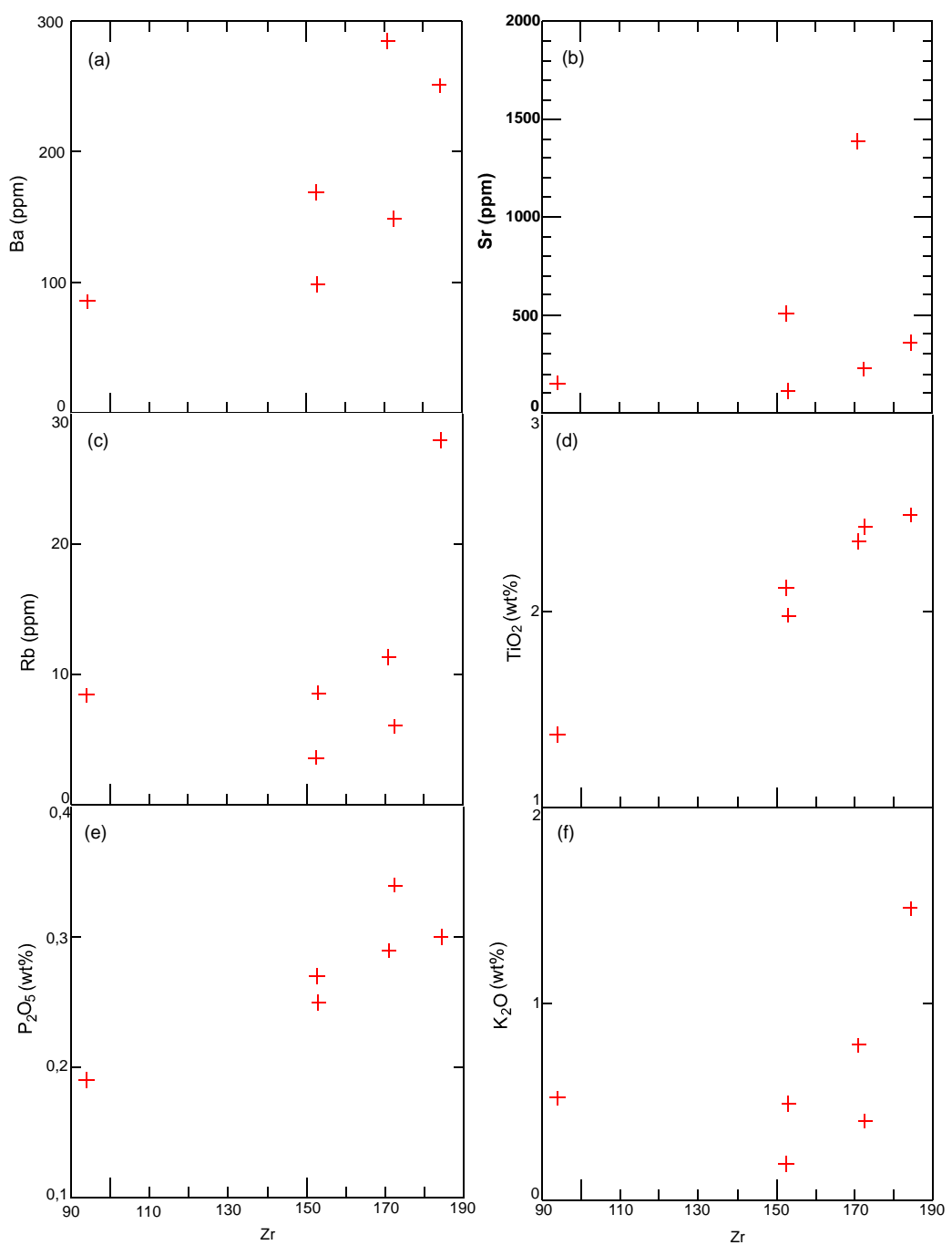


Figure 43. Covariation diagrams of Ba, Sr, Rb, TiO₂, P₂O₅ and K₂O against Zr to show effect of alteration on the studied rocks.

5.3. Compositional Variations

Chemistry of the rocks are generally controlled by modal mineralogy; therefore, studied samples show slight different ranges of compositions: 47.26-48.95 (wt% SiO₂), 11.49-14.82 (wt% Al₂O₃), 7.88-14.31 (wt% CaO), 1.37-2.49 (wt% TiO₂), 9.07-14.08 (wt% Fe₂O₃), 4.36-11.16 (wt% MgO), 0.18-1.49 (wt% K₂O), 3.25-4.54 (wt% Na₂O), 0.13-0.16 (wt% MnO), 0.19-0.34 (wt% P₂O₅), <0.002-0.130 (Cr₂O₃). Moreover, the whole-rock compositions indicate the relative proportions of the minerals.

Al₂O₃ percentage is decreasing while CaO percentage is increasing firstly, then it is decreasing again with increasing MgO percentage (Figure 44a,d). This may be caused by the varying modal ratios of plagioclase/clinopyroxene (Toksoy-Köksal, 2003). Na₂O/K₂O ratio and Sr (ppm) are increasing with the increasing MgO percentage as a common feature of alkaline rocks (Figure 44g, k). The decreasing trend of TiO₂ (wt%), Fe₂O₃ (wt%), Y (ppm), Nb (ppm) and V (ppm) are due to having low distribution coefficients of these elements contained by minerals such as pyroxenes (Figure 44c,e,i,k,l). The enrichment in SiO₂ (wt%) and depletion in P₂O₅ (wt%) with respect to MgO (wt%) indicates fractionation of pyroxene. Moreover, P₂O₅ (wt%) fractionation indicates apatite crystallization supporting alkaline affinity of the rocks (Figure 44f). Decreasing patterns of the Zr (ppm) and, V (ppm) and Y (ppm) against MgO (wt%) infers fractionation of zircon and opaque minerals (Figure 44l,j,k).

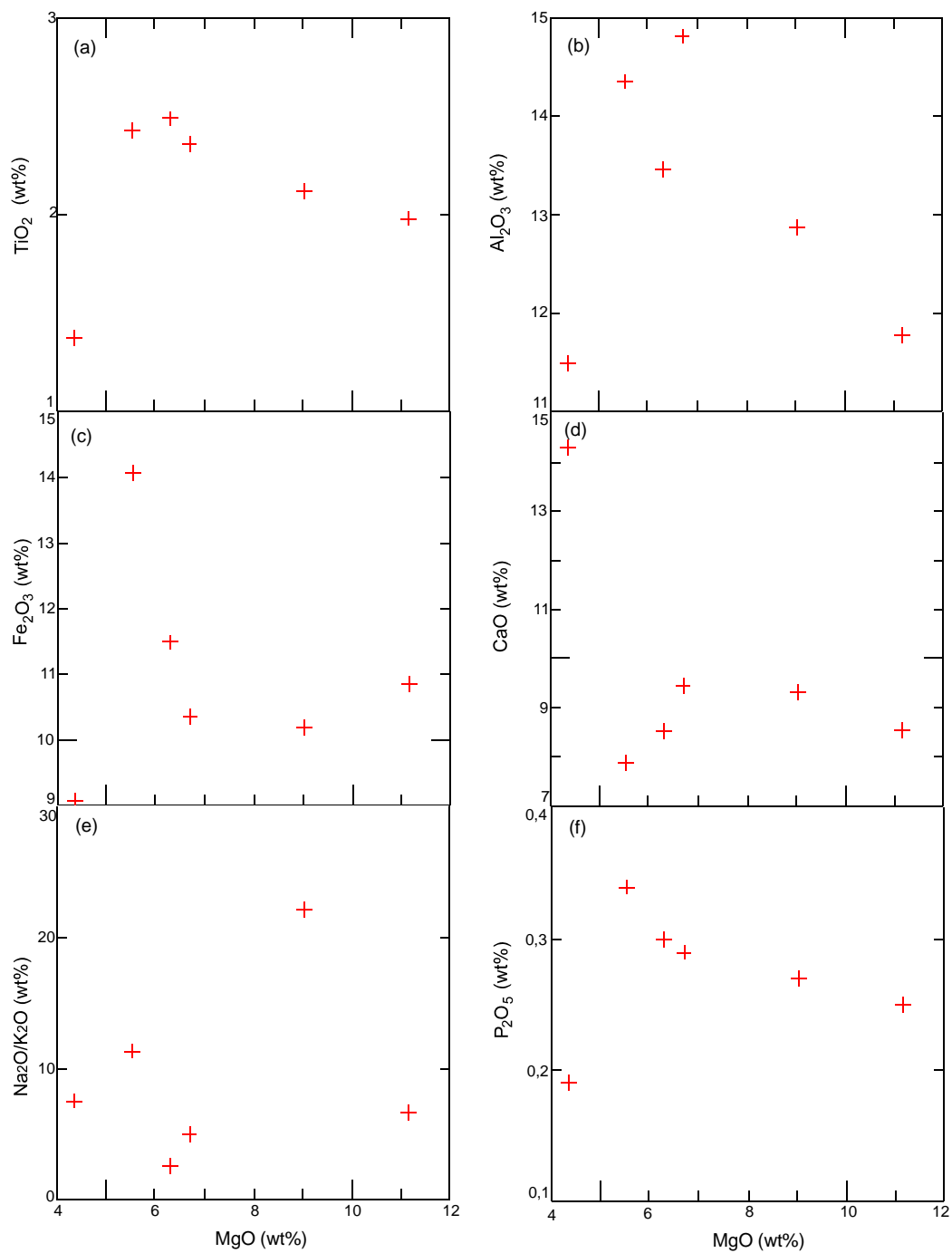


Figure 44. Major and trace element systematic against MgO (wt%) for the studied rocks.

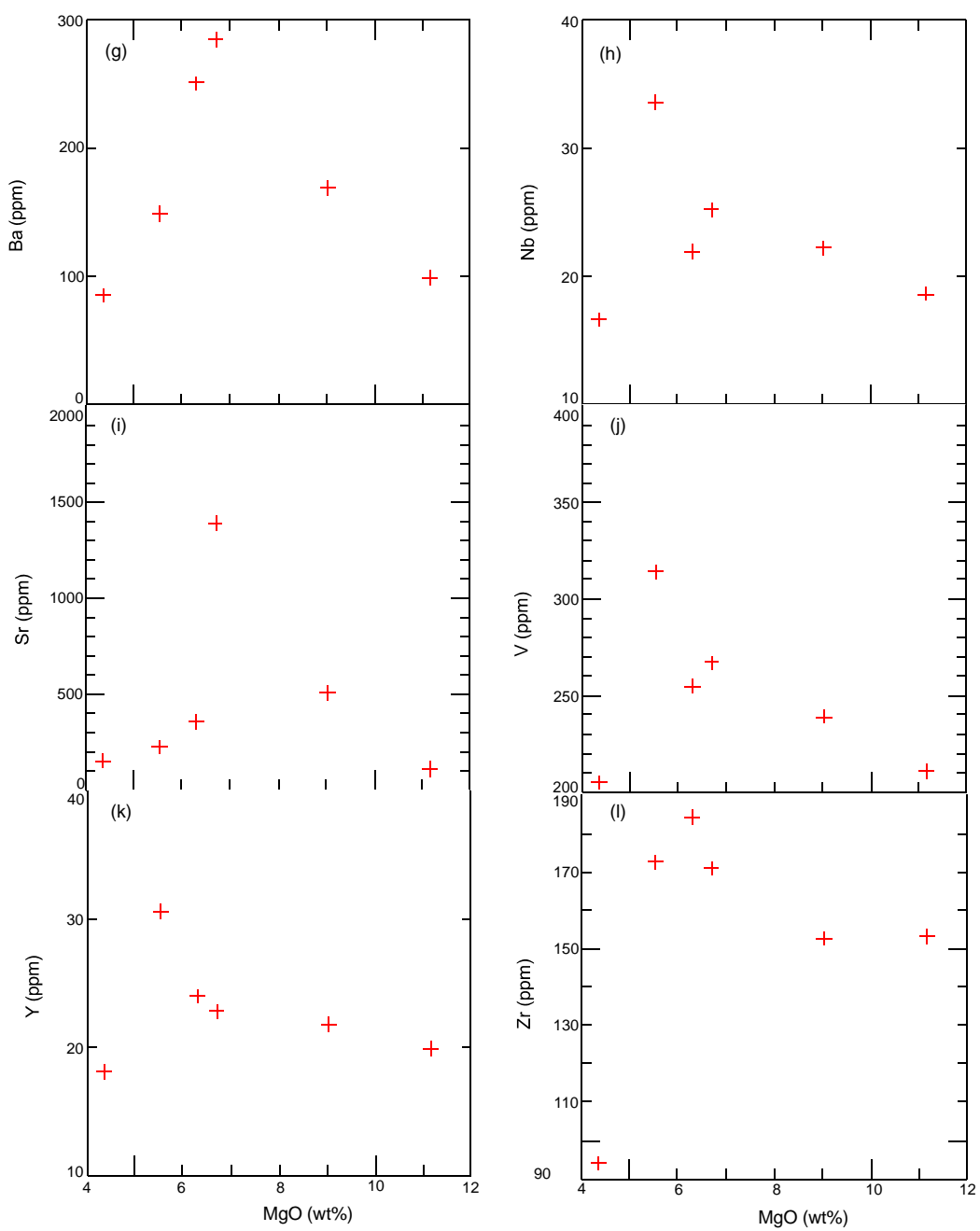


Figure 44 (continued).

5.4. Chemical Classification and Implications for Tectonic Setting

The studied rocks are alkaline (Figure 45a) in character and placed in alkali basalt field (Figure 45b). High Nb/Y values suggest that transitional character and within plate tectonic setting for the studied rocks (Figure 46a). Pearce and Cann (1973) also supports a within plate tectonic setting for the generation of the magma(s) of the studied rocks (Figure 46b). In addition, according to Mullen (1983) and Wood (1980) the studied rocks have transitional affinity between OIT-OIA (Figure 46c) and E-MORB-OIB (Figure 46d), respectively.

The studied rocks show a large range of TiO_2 contents changing between 1.37 and 2.49 wt% compared to TiO_2 contents (0.36-1.55 wt%) of Göncüoğlu et al. (2010). Moreover, low Y/Nb values (0.90-1.1) of the studied samples resembles to enriched basaltic rocks such as E-MORB and OIB-type from other Tethyan ophiolites such as $(\text{Y/Nb})_{\text{OIB}} = 1.12$, $(\text{Y/Nb})_{\text{E-MORB}} = 4.49$ and $(\text{Y/Nb})_{\text{OIB}} = 0.47$ from Saccani and Photiades (2005), Aldanmaz et al. (2008) and Çelik et al. (2013). These may infer that involvement of different mantle sources and/or a heterogeneous source and/or different degrees of partial melting (Göncüoğlu et al., 2010). These can be indicators for generation of the studied samples.

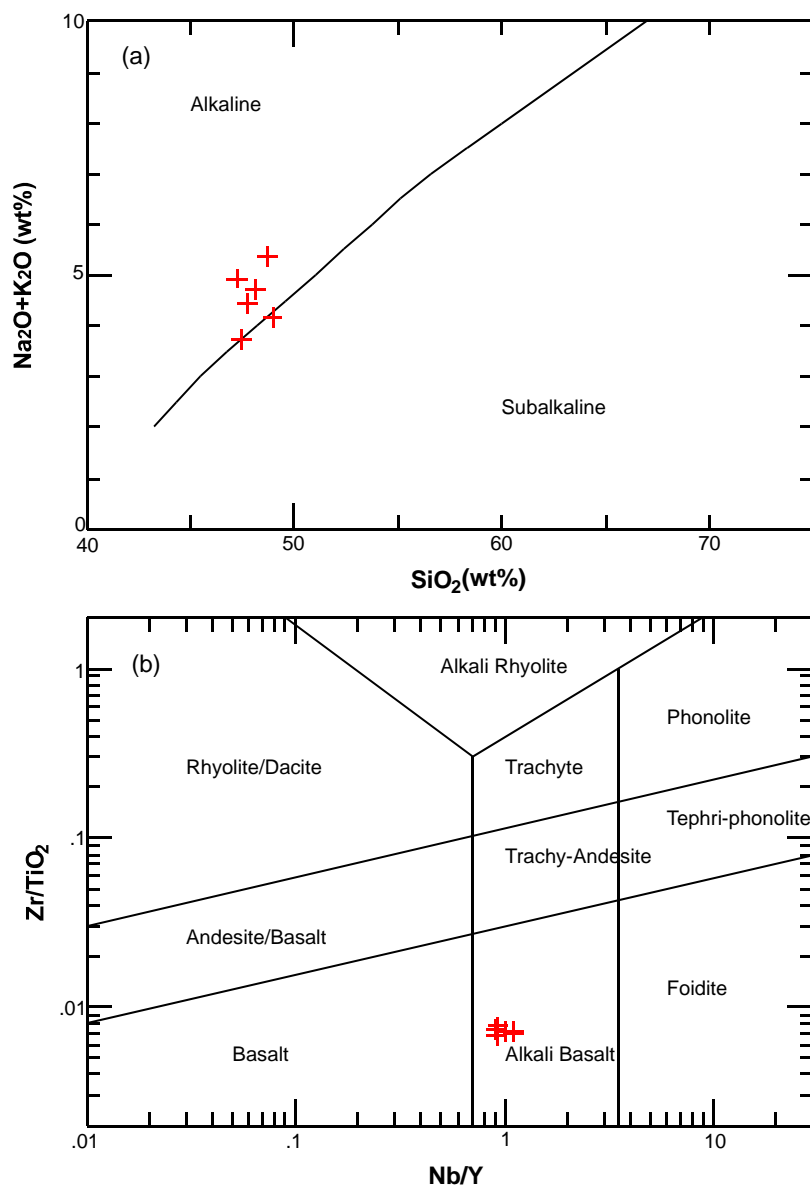


Figure 45. (a) Total alkalies vs. silica diagram and (b) Zr/TiO_2 vs. Nb/Y diagram for the studied rocks (Irvine and Bragard, 1971; Winchester and Floyd, 1977).

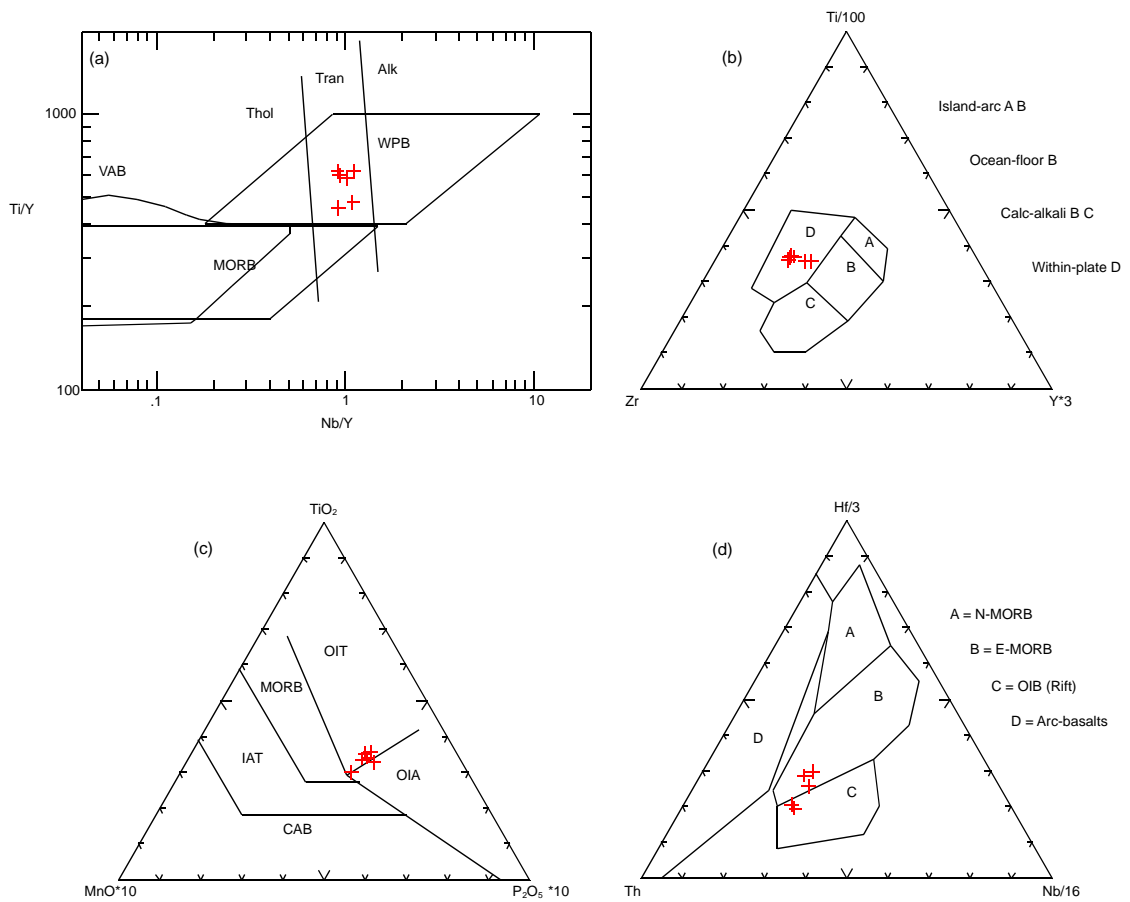


Figure 46. Tectonomagmatic discrimination diagrams for the studied rocks: (a) Pearce (1982); (b) Pearce and Cann (1973); (c) Mullen (1983); (d) Wood (1980).

5.5. Multi-Element and Rare Earth Element Diagrams

Multi-element and rare earth element patterns of the studied rocks are examined by normalizing the data to E-MORB and OIB of Sun and McDonough (1989). There is enrichment relative to N-MORB (Figure 47a) and similarities and sub-parallelism relative to E-MORB (Figure 47b) and OIB-type (Figure 47c) basalts. In N-MORB normalized diagram large ion lithophile elements (LILE) show relatively decreasing pattern. These patterns are common in environments which are influenced by mantle plumes with low degree of partial melting.

Moreover, in N-MORB normalized diagrams of subduction unrelated ophiolites, an increase towards the most incompatible elements such as Ba, Rb, Cs and a flat pattern between V and Zr are generally observed (Dilek and Furnes, 2011). The sub-parallelism with E-MORB and OIB-type basalts multi-element diagrams with the studied samples may infer that a transitional environment between E-MORB environment and OIB environment.

The chondrite normalized rare earth diagram (Figure 47d) is shown by a steady decrease from light rare earth elements to heavy rare earth elements. This is explained by the alkaline affinity and within plate basalt characteristics of the studied samples (Çelik et al., 2013).

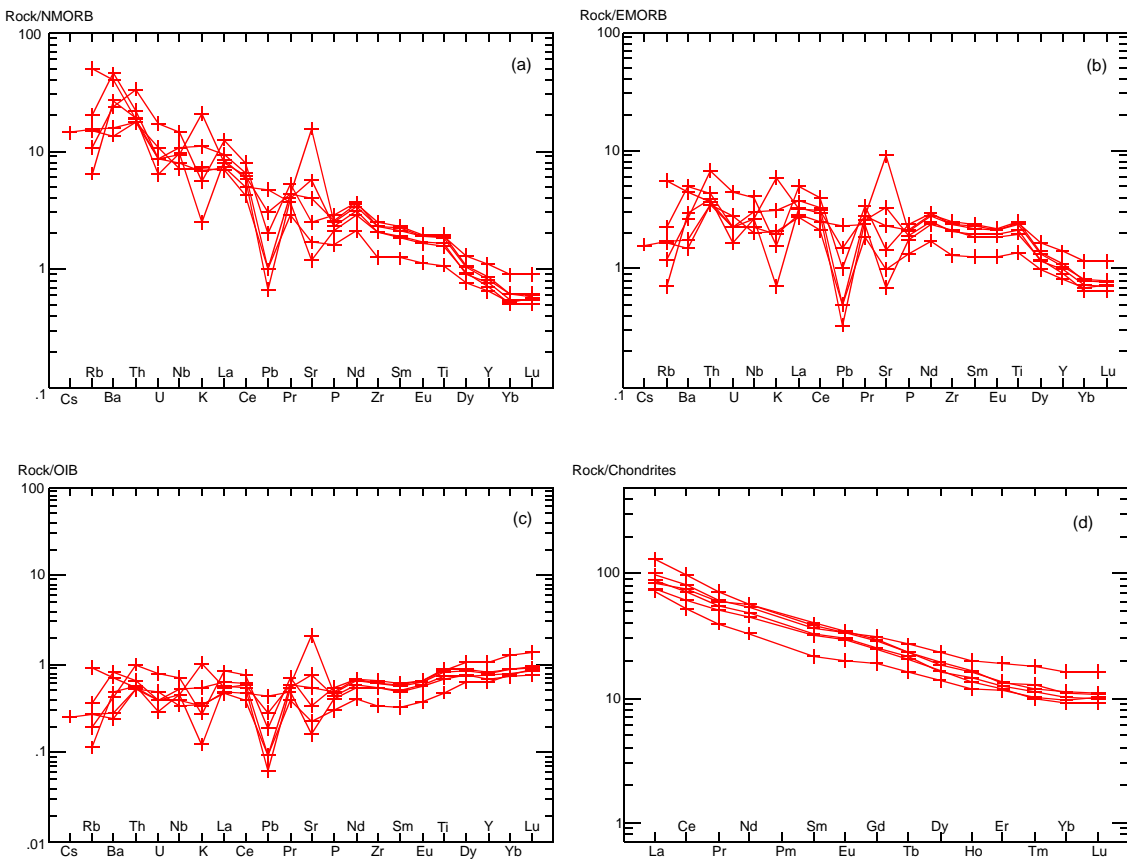


Figure 47. N-MORB, E-MORB and OIB normalized multi element diagrams and chondrite normalized rare earth element diagram and for studied rocks (Sun and McDonough. 1989).

5.6. Isotope Geochemistry

In the scope of this thesis, Sr and Nd isotope analyses of six samples were performed. The analyses results are tabulated briefly in Table 6. For the initial isotope ratio determination, formation age was estimated as 170 Ma by using the data from the literature (e.g. Bortolotti et al., 2013; Tekin et al., 2002, Topuz et al., 2013).

Table 6. Sr-Nd isotope ratios for the studied samples

Sample Code	$^{87}\text{Sr}/^{86}\text{Sr}_{(\text{m})}$	Rb (ppm)	Sr(ppm)	$^{87}\text{Sr}/^{86}\text{Sr}_{(\text{T})}$	$^{143}\text{Nd}/^{144}\text{Nd}_{(\text{m})}$	Nd (ppm)	Sm(ppm)	$^{143}\text{Nd}/^{144}\text{Nd}_{(\text{T})}$	$\epsilon\text{Nd}_{(\text{T})}$
AA-6	0.705425	8.6	106.6	0.704861	0.512593	21.1	4.88	0.512437	0.4
AA-7	0.705325	28	356.5	0.704775	0.512603	26.2	6.11	0.512446	0.5
AA-10a	0.70473	3.6	507.1	0.70468	0.512607	22.5	5.05	0.512456	0.7
AA-10d	0.704722	11.3	1392.2	0.704665	0.51261	24.9	5.62	0.512458	0.8
AA-11c	0.705591	8.4	151.9	0.705204	0.512588	15.5	3.28	0.512446	0.5
AA-12a	0.704866	6	224.9	0.704679	0.512588	26.5	5.92	0.512438	0.4

CHAPTER 6

DISCUSSION ON THE GENESIS OF THE STUDIED ROCKS

6.1. General Features

The rocks from the study area are found as allochthonous isolated bodies below the units belonging to Sakarya Composite Terrane. The studied rocks are assumed to be parts of İzmir-Ankara-Erzincan Suture Zone (IAESZ). Tectonism and metamorphism are two effective mechanisms dominant in the study area. Although some pillow basalts preserve their pillow structure, much of them are highly dissected and undergone low-grade metamorphism. The rocks in concern from the study area mainly contain pyroxene and feldspar as phenocrysts and as microcrysts in matrix in varying modes and crystal sizes. Some of the basalts have glassy matrix indicating rapid cooling. Some volcanic rocks are mainly composed of metamorphic phases including chlorite, actinolite and epidote due to low-grade metamorphism.

6.2. Mineralogical Constraints

Pyroxene is the first crystallizing phase in the studied rocks. It is in augitic composition with a wide range of Mg# (Table 7).

Table 7. Mg# ranges of the pyroxenes for the studied rocks.

	metabasalt		dyke		basalt					
					phenocryst		overgrowth		matrix	
	min.	max.	min.	max.	min.	max.	min.	max.	min.	max.
Mg#	0.82	0.88	0.66	0.86	0.42	0.91	0.50	0.69	0.70	0.83

The petrographical examination reveals that pyroxenes of the studied rocks generally have reddish colors indicating Ti-enrichment. Moreover, especially in the basalt samples, compositional zoning, resorption and corrosion are common features. In some thin sections, it is possible to distinguish compositional zoning, resorption, overgrowth of new crystal material and corrosion within a single crystal of pyroxene. The petrographical observations strongly indicate an open system magmatic behavior inferring there are chemical dis-equilibrium conditions during crystallization of the studied rocks. The rocks from the study area may be the products of multistage mixing during magma ascent. The petrographic observations also revealed that there is occurrence of secondary mineral phases which are the result of hydrothermal alteration and low-grade metamorphism of the primordial rocks. Chloritization is common in both the glassy part of the rocks and on the minerals. This is common in greenschist facies metamorphism of oceanic basalts during hydrothermal circulation (Humpris and Thompson, 1978).

Although pyroxene compositions show similarities among different rock types, different pyroxene occurrences in the basalts show differences in elemental plots compared to metabasalts and dykes. There are three different groups in elemental plots of the pyroxenes (Figure 30) which correspond to three different occurrences. These explain stages during growth of pyroxenes as phenocryst, overgrowth and corrosion observed from petrographical observations. This may infer that there are at least three stages during the growth of pyroxenes in the studied rocks. This petrographical and mineral chemistry evidences are explained by multistage mixing phenomenon. First of all, Ca-rich pyroxene phenocrysts are formed. After that, there was an influx which was rich in Fe affecting the affinity of the system as subalkaline and forming overgrowths around resorbed pyroxene phenocrysts. Finally, there was a second influx, which was rich in Mg and Al, made the system alkaline forming small pyroxene crystals arranged around coarse pyroxene and feldspar crystals in matrix.

Chemistry of the pyroxenes indicates a transitional character between subalkaline to alkaline compositions according to Figure 35a and tholeiitic affinity for the subalkaline rocks from the study area according to Figure 35b as discussed in Section 4.3.3. For the rocks which show tholeiitic affinity, the tetrahedral site of pyroxene is almost filled by Si indicating an important feature of pyroxene crystallized from a subalkaline magma (Conticelli, 1998).

Feldspar mainly characterized by high albite content display a wide range of composition (albite%: 84.21-99.84) with negligible K-feldspar content for all rock types. The feldspar crystals scattered to matrix in both metamorphosed and basalt and found as sericitized large crystals in dykes.

6.3. Geochemical Constraints

The studied rocks are composed of large range of TiO_2 contents (1.37-2.49 wt%) indicating involvement of several mantle sources – a heterogeneous source and/or different degrees of partial melting for their genesis. Besides high TiO_2 contents, high Nb (16.6-33.6 ppm) and Zr (94.1-184.1 ppm) concentrations of the studied rocks pointing at a more enriched source or small degree of partial melting (Göncüoğlu et al., 2010). Moreover, low Mg# between 0.34-0.57 indicates that studied samples have undergone fractional crystallization, which is they do not reflect their primary magma compositions.

All the rock samples from the study area show a relative enrichment in LREE relative to N-MORB and display regularly decreasing N-MORB normalized patterns. During hydrothermal alteration of basaltic pillow lavas, Ba shows variable alteration trends and Pb shows a depleted pattern as easily seen from Figure 47.

In N-MORB normalized multi-element diagrams, the continental margin, mid-ocean ridge and plume related ophiolites display flat patterns between V and Zr and there is generally an increase towards the most incompatible elements such as Ba, Rb and Cs.

This immobility usually affects mafic and ultramafic rocks in the oceanic environment (Dilek and Furnes, 2011). When N-MORB normalized rare earth element diagram of the studied samples was compared with those of an another study conducted by Çelik et al. (2011), both data sets mostly show consistency with each other (Figure 48).

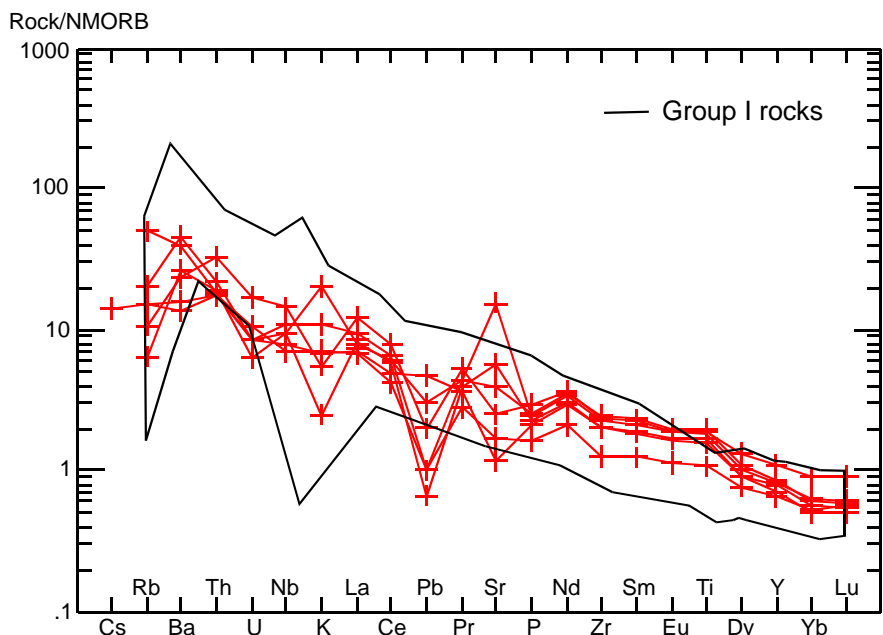


Figure 48. N-MORB normalized multi element variation diagram comparing Group I rocks of the study belonging Çelik et al. (2013) with rocks from the study area (Sun & McDonough, 1989).

According to Zr/TiO_2 vs Nb/Y diagram (Figure 45) the studied rocks are completely in alkali basalt field. Their chondrite normalized pattern is characterized by a steady decrease from LREE to HREE. When chondrite normalized spectra is compared with another set of samples belonging to central IAESZ, a study of Çelik et al. (2013), there is a high consistency between both set of data (Figure 49). Moreover, chondrite

normalized data of the studied samples show parallelism with average OIB of Sun & McDonough (1989). HFSE's of average E-MORB of Sun & McDonough (1989) display similarities with those of the studied samples. This may be caused by the transitional character of the studied samples.

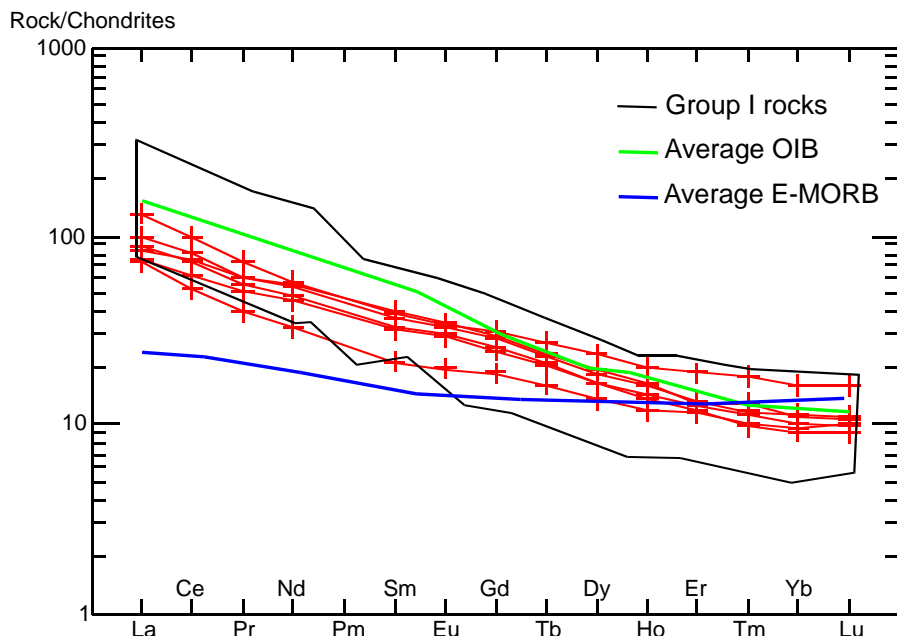


Figure 49. Chondrite normalized multi element variation diagram comparing Group I rocks of the study belonging Çelik et al. (2013) and average OIB and E-MORB values from Sun & McDonough (1989) with rocks from the study area.

In a Ti-V discrimination diagram, subduction unrelated ophiolites stand in the field where Ti/V ratios between 20 and 50; however, subduction related ophiolites display a wider Ti/V ratios which are smaller than 10 to higher than 50 (Shervais, 1982; Dilek and Furnes, 2011). The Ti/V ratio of the studied rocks mostly lies on the 50 ratio line indicating a P-MORB affinity which is a transitional character between MORB and OIB (Figure 50) (Bortolotti et al., 2013).

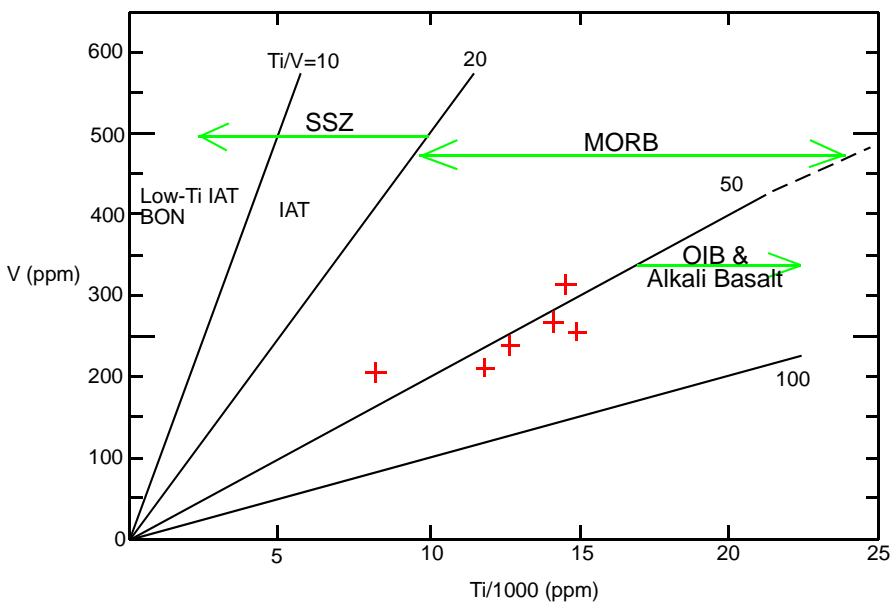


Figure 50. Ti-V discrimination diagram showing tectonic setting relationship of the studied rocks (Shervais, 1982).

Although, there is a little influence by the fractional crystallization of clinopyroxene and feldspar on highly incompatible element ratios such as Zr/Nb, Ce/Y, Zr/Y and Nb/Y; these elemental ratios are believed to represent the elemental ratios of the source because they are competent elements (Bortolotti et al., 2013 and references therein).

According to Y/Nb vs Zr/Nb diagram, studied rocks fall into both OIB and E-MORB type fields (Figure 51). Moreover, this overlap is also observed in TiO_2 vs Zr diagram (Figure 52). From these diagrams, transitional character of the studied rocks can be concluded.

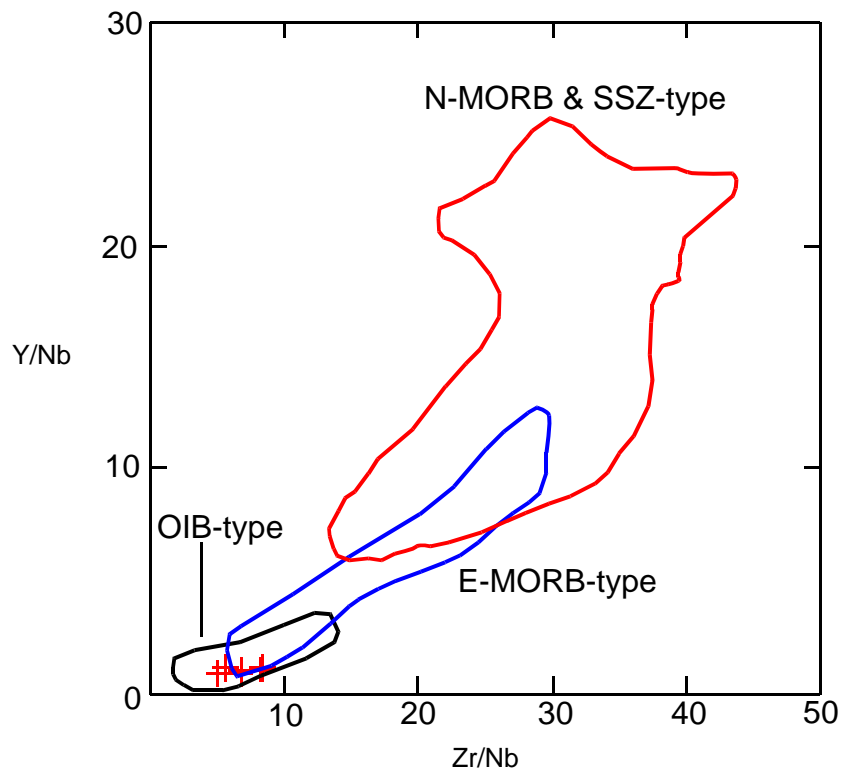


Figure 51. Variation of Y/Nb against Zr/Nb for the studied samples. (Data sources for OIB, E-MORB, N-MORB and SSZ-type Tethyan basaltic rocks are belonging to Mahoe et al. (2004), Saccani and Photiades (2005) and Aldanmaz et al.(2008), Göncüoğlu et al. (2010)).

High TiO_2/Yb ratios change between 0.84-1.33 may indicate negligible crustal contamination according to Göncüoğlu et al. (2010). Besides TiO_2/Yb ratio, La/Ta and La/Nb ratios may be helpful in order to make more precise estimations. Basalts with La/Ta ratios smaller than 22 and La/Nb ratios smaller than 1.5 are accepted as affected by minimal crustal contamination (Hart et al., 1989). La/Ta and La/Nb ratios of the studied rocks which are ranging between 13.8-16 and 0.91-1.03, respectively indicates they have examined minimal or no crustal contamination.

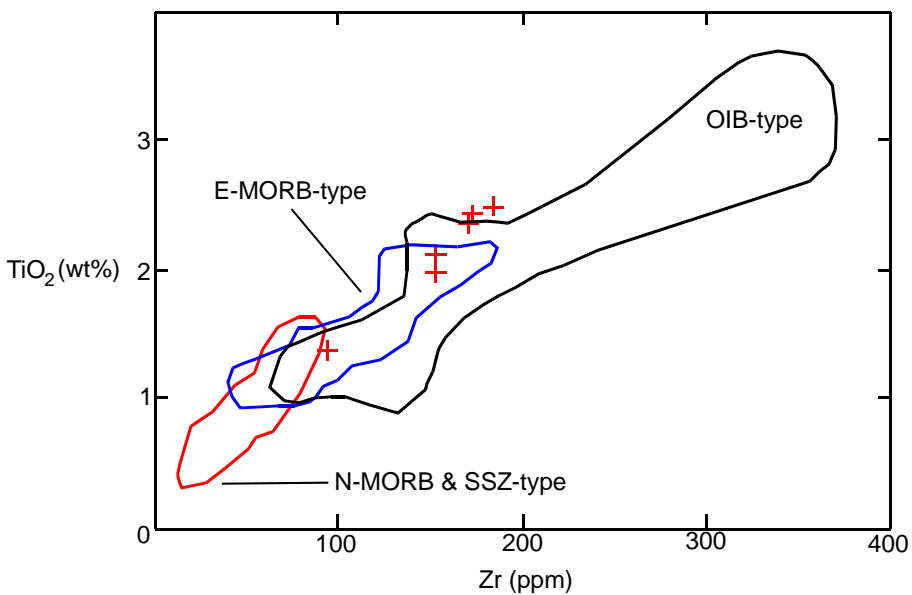


Figure 52. Variation of TiO_2 (wt%) against Zr (ppm) for the studied samples. (Data sources for OIB, E-MORB, N-MORB and SSZ-type Tethyan basaltic rocks are same with Figure 51).

In summary, whole-rock data strongly infer alkaline character with a P-MORB affinity that is transitional between MORB and OIB without crustal contamination. On other hand, mineral chemistry of the rocks in concern suggests that the rocks originate in non-orogenic system with a transitional character between subalkaline and alkaline affinities. Mineral chemistry data strongly supports the textural features of the rocks that infer chemical dis-equilibrium conditions (open magmatic conditions). Pyroxene phenocrysts are mostly sub-alkaline but show transition to alkaline also. New growth pyroxene material inferring new melt influx is essentially rich in Fe, K contents increasing subalkalinity, following a new growth of pyroxene material around phenocrysts that is alkaline in character with high Mg and Al contents. Moreover, microcrysts of pyroxene with high Mg and Al contents growing around phenocrysts of both pyroxene and feldspar are alkaline in character.

It can be concluded that although phenocrysts of the rocks indicate subalkaline affinity, the last melt influx with high Mg and Al contents make the whole magma composition alkaline.

The last influx with alkaline affinity is mainly observed as groundmass material in the studied rocks. According to petrographical observations, glassy parts of the groundmass are intensely chloritized. Mg-rich final influx is the reason for the chloritization of volcanic glass of the studied rocks because Mg is generally taken to use in chlorite formation during hydrothermal circulation (Humpris and Thompson, 1978).

6.4. Isotopic Constraints

Figure 53 shows $^{143}\text{Nd}/^{144}\text{Nd}_{(i)}$ vs $^{87}\text{Sr}/^{86}\text{Sr}_{(i)}$ values. DMMa and DMMb are standing for two different end members of “Depleted MORB Mantle” from Zindler and Hart (1986). DMM is defined by the most depleted MORB samples with the highest $^{143}\text{Nd}/^{144}\text{Nd}$ and the lowest $^{87}\text{Sr}/^{86}\text{Sr}$ ratios. HIMU is standing for “High μ ” where μ represents $^{238}\text{U}/^{204}\text{Pb}$ ratio. HIMU has the lowest $^{87}\text{Sr}/^{86}\text{Sr}$ of any OIB that is its Sr isotopic ratio is almost as low as MORB. St Helena and Austral Islands are the examples for HIMU basalts. EM-I is standing for “Enriched Mantle I” having low $^{143}\text{Nd}/^{144}\text{Nd}$ and moderate $^{87}\text{Sr}/^{86}\text{Sr}$ isotopic ratios than DMM and HIMU. The Pitcairn and Tristan hotspots are the representatives of EM-I. EM-II (Enriched Mantle II) has the highest $^{87}\text{Sr}/^{86}\text{Sr}$ ratios among the others. Societies and Samoa hotspots are the examples for EM II (Hofmann, 1997). MORB, HIMU and EM reservoirs in the figure are taken from Hart et al. (1999) and Workman and Hart (2005).

The studied rocks have Sr and Nd isotopic compositions that are more evolved than those of both DMM and MORB reservoirs. It is suggested that, all studied rocks have an enriched component with respect to DMM source. Purple, light blue, light green and pink areas are for the isotopic ratios of the studied rocks in the central IAESZ belonging to Çelik et al. (2013). According to Nd isotope point of view, the studied

samples have lower values of $^{143}\text{Nd}/^{144}\text{Nd}$ than the data of Çelik et al. (2013). According to Gökten and Floyd (2007), Nd-Sr isotope data of OIB in IAESZ shows a mixture of EM I with a minor DMM component. According to Workman and Hart (2005), OIBs are compatible with the partial melting of EM-type sources.

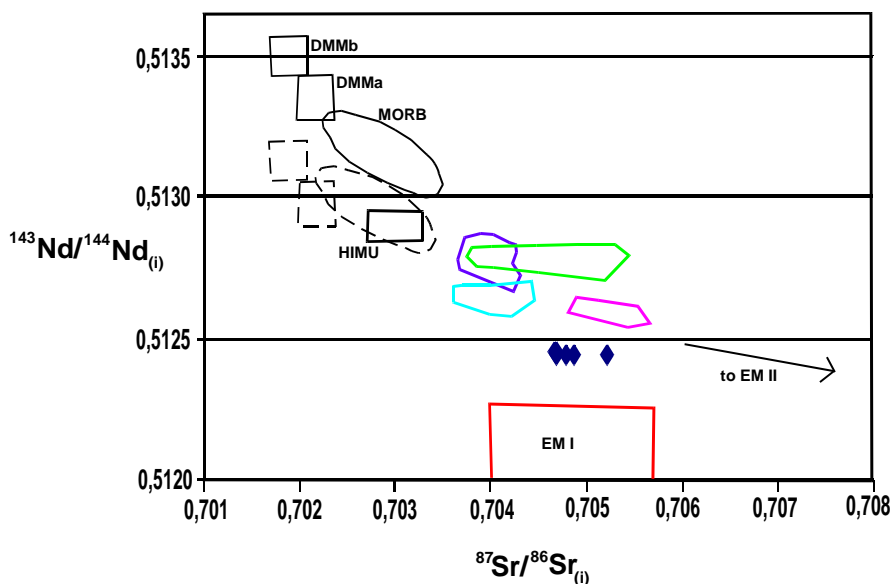


Figure 53. Nd-Sr diagram of initial isotopic ratios for the studied rocks (closed diamonds). (DMM values are from Zindler and Hart (1986), MORB, HIMU and EM values are from Hart et al. (1999) and Workman and Hart (2005), and colored fields are data from Çelik et al. (2013)). The dashed DMMa, DMMb and MORB are values corrected to 150 Ma (from Çelik et al., 2013). Isotopic data for this thesis were corrected to 170 Ma.

Moreover, E-MORBs may be derived from a mantle source which is slightly enriched when compared to DMM source. However, P-MORBs can be generated from a mantle source which is significantly enriched with respect to DMM (Workman and Hart, 2005). These two approaches prove that the studied rocks have an enriched component with respect to DMM source indicating a P-MORB affinity.

Hellenic and Dinaric ophiolites in the Balkans are Jurassic-Early Cretaceous (Robertson, 2002). According to the studies conducted on Vourinos ophiolite from Greece, the crystallization age was found as 172.9 ± 3.1 Ma based on U/Pb geochronology.

Moreover, the volcanic rocks from the Sevan ophiolite from Armenia and the Khoy ophiolite from Iran were dated by using $^{40}\text{Ar}/^{39}\text{Ar}$ geochronology and their ages were reported as 165-170 Ma and 156-159 Ma, respectively (Çelik et al., 2013 and references therein).

In this thesis, formation age was estimated as 170 Ma for the initial isotopic ratio determination according to the information in literature (e.g. Topuz et al., 2013, Bortolotti et al., 2013; Tekin et al., 2002,). As a result, it is suggested that the studied rocks belonging to IAESZ represent a link between Neotethyan Jurassic ophiolite which resting from Balkans through Turkey and Armenia to Iran.

CHAPTER 7

CONCLUSIONS

The volcanic rocks from the study area (Burunköy, Çorum) are found as isolated units within İzmir-Ankara-Erzincan Suture Zone. In the study area, the metamorphic rocks of Sakarya Composite Terrane are tectonically overlying on the ophiolitic mélange of IAESZ. Upper Neocene rocks cover both units unconformably.

The rocks in the study area are divided into three main categories as basalts, metabasalts and dykes. The basalts which are away from the tectonic contact with Silurian marble preserve their pillow structure. However, metabasalts which are in tectonic contact with the marble are highly dissected and undergone low-grade metamorphism. The basalts and metabasalts are the same rocks other than low grade metamorphism.

Petrographical study reveals that all rock types are mainly composed of augitic pyroxene and plagioclase. As a result of surface alteration and low-grade metamorphism, calcite, sericite, actinolite, chlorite, epidote and albite are also observed. Moreover, petrographical observations on the rocks strongly infer chemical dis-equilibrium textures like resorption, corrosion, reaction rims, compositional zoning, and tailing properties that indicate influx(s) of more mafic melt into magma during crystallization/ascent.

Electron probe microanalyser (EPMA) analyses were carried out for the constituents of the studied rocks. It was observed that pyroxenes and feldspars are augite and albite in composition, respectively. Minerals show similar compositions among the rock types. However, micro probe analyses from different occurrences of the basalts give slight chemical differences according to elemental plots. That is, phenocrysts of the basalts are rich in Ca and Mg and depleted in Ti, Fe and Mn.

However, basalt overgrowths show Fe and Mn enrichment indicating subalkaline affinity. The basalt microcrysts are rich in Al and Mg inferring alkalinity of magma. Chemistry of pyroxene indicates a transitional character between subalkaline to alkaline compositions with more than one influx during ascent of magma in non-orogenic environment. It can be concluded that although phenocrysts of the rocks indicate subalkaline affinity, the last melt influx with high Mg and Al contents make the whole magma composition alkaline. Mineral chemistry data strongly supports the textural features of the rocks that infer chemical dis-equilibrium conditions (open magmatic conditions).

Whole-rock data strongly infer alkaline character with a P-MORB affinity that is transitional between MORB and OIB without crustal contamination. Whole-rock geochemical data showed that the rocks of concern are characterized by high TiO₂, Nd and Zr contents indicating partial melting of an enriched source for the formation of the studied rocks. Moreover, isotopic values (¹⁴³Nd/¹⁴⁴Nd and ⁸⁷Sr/⁸⁶Sr) of the studied rocks gives that they are derived from a mantle source which is significantly enriched with respect to MORB.

Evaluation of all the petrographical, mineral chemistry and whole rock geochemistry evidences infer that all the studied rocks belonging to Ankara melange are derived from similar enriched source. Moreover, the detailed mineral chemistry studies strongly suggest that pyroxenes are crystallized by at least three melt influxes into the magma chamber. It is chemically identified that the last melt influx is Mg-rich with alkaline affinity. This last influx, mainly observed as groundmass of the studied rock, is suggested to control the whole-rock chemistry.

REFERENCES

- Abbate, E., Bortolotti, V., and Paserini, P., 1976. Major structural events related to ophiolites of the Tethyan Belt. *Ophioliti*, 1, 5-32.
- Aldanmaz, E., Yalınız, M.K., Güctekin, A., and Göncüoğlu, M.C., 2008. Geochemical characteristics of mafic lavas from the Neotethyan ophiolites in western Turkey: implications for heterogeneous source contribution during variable stages of ocean crust generation. *Geological Magazine*, 145, 37-54.
- Bailey, E.B., and McCallien, W.J., 1950. The Ankara Melange and the Anatolian Thrust. *M.T.A. magazine*, 40, 12-22.
- Bailey, E.B., and McCallien, W.J., 1953. Serpentine lavas, the Ankara Melange and the Anatolian Thrust. *MTA Bull.*, 40, 17-21. In: Rojay, B., and Süzen, M.L., 1997. Tectonostratigraphic evolution of the Cretaceous dynamic basins on accretionary ophiolitic mélange prism, SW of Ankara region. *TPJD Bull.*, 9, 1-12.
- Beccaletto, L., and Stampfli, G., 2000. New data on the Çetmi Melange (Biga peninsula, NW Turkey). International Earth Sciences Colloquium on the Aegean region. Abstracts, p. 242.
- Beccaluva, L., Macciotta, G., Piccardo, G.B. and Zeda, O., 1989. Clinopyroxene composition of ophiolite basalts as petrogenetic indicator. *Chemical Geology*, 77, 165-182.
- Bortolotti, V., Chiari, M., Göncüoğlu, M.C., Marcucci, M., Principi, G., Tekin, U.K., Saccani, E., and Tassinari, R., 2013. Age and geochemistry of basalt-chert associations in the ophiolites of Izmir-Ankara mélange east of Ankara, Turkey: Preliminary data. *Ophioliti*, 38, 157-173.
- Bozkurt, E., and Mittwede, S.K., 2001. Introduction to the Geology of Turkey- A synthesis. *International Geology Review*, 43:7, 578-594.
- Bragin, N.Y., and Tekin, U.K., 1996. Age of Radiolarian-chert blocks from the Senonian Ophiolitic Melange (Ankara, Turkey). *Island arc*, 5, 114-122.
- Cabanis, B., and Lecolle, M., 1989. Le diagramme La/10-Y/15-Nb/8: un outil pour la discrimination des séries volcaniques et la mise en évidence des processus de mélange et/ou de contamination crustale. *Comptes Rendus de l'Academie des Sciences –Séries II* 309, 2023-2029.

- Conticelli, S., 1998. The effect of crustal contamination on ultrapotassic magmas with lamproitic affinity: mineralogical, geochemical and isotope data from the Torre Alfina lavas and xenoliths, Central Italy. *Chemical Geology*, 149, 51-81.
- Çelik, Ö.F., Chiaradia, M., Marzoli, A., Billor, Z., and Marschik, R., 2013. The Eldivan ophiolite and volcanic rocks in the Izmir-Ankara-Erzincan suture zone Northern Turkey: Geochronology, whole-rock geochemical and Nd-Sr-Pb isotope characteristics. *Lithos*, 172, 31-46.
- Deer, W.A., Howie, R.A., and Zussman, J., 1980. An Introduction to the Rock Forming Minerals. 1st Edition (20th Impression), Longman, London, 528 p.
- Dilek, Y., Thy, P., Hacker, B., and Grundvig, S., 1999. Structure and petrology of Tauride ophiolites and mafic dyke intrusions (Turkey): Implications for the Neo-Tethyan Ocean. *Geol.Soc.Am.Bull.*, 111, 1192-1216.
- Dilek, Y., 2003. Ophiolite pulses, mantle plumes and orogeny. In: Dilek, Y. and Robinson, P.T. (eds.), 2003. Ophiolites in Earth History. Geological Society, London, Special Publications, 218, 9-19.
- Dilek, Y., and Thy, P., 2009. Island arc tholeiite to boninitic melt evolution of the Cretaceous Kızıldağ (Turkey) ophiolite: model for multi-stage early arc-forearc magmatism in Tethyan subduction factories. *Lithos*, 113, 68-87.
- Dilek, Y., and Furnes, H., 2011. Ophiolite genesis and global tectonics: Geochemical and tectonic fingerprinting of ancient oceanic lithosphere. *Geological Society of America Bulletin*, 123, 387-411.
- Droop, G.T.R., 1987. A general equation for estimating Fe³⁺ concentrations in ferromagnesian silicates and oxides from microprobe analyses, using stoichiometric criteria. *Mineralogical Magazine*, 51, 431-437.
- Floyd, P.A., Yalınız, M.K., and Göncüoğlu, M.C., 1998. Geochemistry and petrogenesis of intrusive and extrusive ophiolite plagiogranites, Central Anatolian Crystalline Complex, Turkey. *Lithos*, 42, 225-241.
- Gökten, E., and Floyd, P.A., 2007. Stratigraphy and geochemistry of pillow basalts within the ophiolitic mélange of the Izmir-Ankara-Erzincan suture zone: implications for the geotectonic character of the northern branch of Neotethys. *Int. J. Earth Sci.*, 96, 725-741.

Göncüoğlu, M.C., and Türeli, T.K., 1993. Petrology and geodynamic interpretation of plagiogranites from Central Anatolian ophiolites (Aksaray-Turkey). *Ophioliti*, 18, 187.

Göncüoğlu, M.C., Dirik, K., and Kozlu, H., 1997. General characteristics of pre-Alpine and Alpine Terranes in Turkey: Exploratory notes to the terrane map of Turkey. *Annales Geologique de Pays Hellenique*, 37, 515-536.

Göncüoğlu, M.C., Turhan, N., Şentürk, K., Özcan, A., Uysal, Ş., and Yalınız, K., 2000a. A geotraverse across NW Turkey: tectonic units of the Central Sakarya region and their tectonic evolution. In: Bozkurt, E., Winchester, J., and Piper, J.A. (eds.) *Tectonics and magmatism in Turkey and the surrounding area*. Geol.Soc.London Spec.Publ., 173, 139-161.

Göncüoğlu, M.C., Yalınız, K., and Tekin, U.K., 2006a. Geochemical features and radiolarian ages of volcanic rocks from the Izmir-Ankara Suture Belt, Western Turkey. Proceed. Int symp. Mesozoic Ophiolite Belts of the N Balkan Peninsula (Belgrade- Banja Luka, 11 May- 6 June, 2006) 41-44.

Göncüoğlu, M.C., Yalınız, K., and Tekin, U.K., 2006b. Geochemistry, tectono-magmatic discrimination and radiolarian ages of basic extrusives within the Izmir-Ankara Suture Belt (NW Turkey): Time constraints for the Neotethyan Evolution. *Ophioliti*, 31, 25-38.

Göncüoğlu, M.C., Sayit, K., and Tekin, U.K., 2010. Oceanization of the northern Neotethys: Geochemical evidence from ophiolitic mélange basalts within the Izmir-Ankara suture belt, NW Turkey. *Lithos*, 116, 175-187.

Göncüoğlu, M.C., 2010. Introduction to the Geology of Turkey: Geodynamic evolution of the pre-Alpine and Alpine Terranes. General Directorate of Mineral and Research, Monography Series, 5, 69 pages.

Görür, N., Şengör, A.M.C., Akkök, R., and Yılmaz, Y., 1983. Pontidler'de Neo-Tetis'in kuzey kolunun açılmasına ilişkin sedimentolojik veriler. *Geological Bulletin of Turkey*, 26, 11-20.

Görür, N., Oktay, F.Y., Seymen, I., and Şengör, A.M.C., 1984. Paleotectonic evolution of Tüz Gölü Basin complex, central Turkey. In: Okay, A.I., and Tüysüz, O., 1999. Tethyan sutures of northern Turkey. Geological Society, London, Special Publications, 156, 475-515.

- Gürsu, S., and Göncüoğlu, M.C., 2006. Petrogenesis and tectonic setting of Cadomian felsic igneous rocks, Sandıklı area of the western Taurides, Turkey. *Int.Journ. Earth Sci.*, 95, 741-757.
- Harris, N.B.W., Kelley, S.P., and Okay, A.I., 1994. Post-collision magmatism and tectonics in northwest Turkey. *Contributions to Mineralogy and Petrology*, 117, 241-252. In: Okay, A.I., and Tüysüz, O., 1999. Tethyan sutures of northern Turkey. *Geol.Soc.London, Spec. Publ.*, 156, 475-515.
- Hart, W.K., Wolde, G.G., Walter, R.C., and Mertzman, S.A., 1989. Basaltic volcanism in Ethiopia: constraints on continental rifting and mantle interactions. *Journal of Geophysical Research*, 94, 7731-7748.
- Hart, S.R., Blusztajn, J., Dick, H.J.B., Meyer, P.S., and Muehlenbachs, K., 1999. The fingerprint of seawater circulation in a 500-meter section of ocean crust gabbros. *Geochimica et Cosmochimica Acta*, 63, 4059-4080.
- Hoffman, A.W., 1997. Mantle geochemistry: the message from oceanic volcanism. *Nature*, 385.
- Humpris, S.E., and Thompson, G., 1978. Hydrothermal alteration of oceanic basalts by seawater. *Geochimica et Cosmochimica Acta*, 42, 107-125.
- Irvine, T.N., and Baragar, W.R.A., 1971. A guide to the geochemical classification of the common volcanic rocks. *Canadian Journal of Earth Sciences*, 8, 523-548.
- Koçyigit, A., 1991. An example of an accretionary forearc basin from northern Central Anatolia and its implications for the history of subduction of Neo-Tethys in Turkey. *Geol. Soc. Am. Bull.*, 103, 22-36.
- Köksal, S., and Göncüoğlu, M.C., 2008. Sr and Nd isotopic characteristics of some S-, I-, and A-type granitoids from Central Anatolia. *Turkish Journal of Earth Sciences*, 17, 111-127.
- Lanphere, M.A., 1981. K-Ar ages of metamorphic rocks at the base of the Semail Ophiolite, Oman. *Journal of Geophysical Research*, 86, 2777-2782. In: Okay, A.I., and Tüysüz, O., 1999. Tethyan sutures of northern Turkey. *Geol.Soc.London, Spec. Publ.*, 156, 475-515.
- Le Bas, M.J., 1962. The role of alumina in igneous clinopyroxenes with relation to their percentage. *American Jornal off Science*, 260, 267-288.

- Leterrier, J., Maury, R.C., Thonon, P., Ginard, D., and Marchal, M., 1982. Clinopyroxene composition as a method of identification of the magmatic affinities of paleo-volcanic series. *Earth and Planetary Science Letters*, 59, 139-154.
- Liotard, J.M., Dupuy, C., Dostal, J., and Cornen, G., 1982. Geochemistry of the island of Annobon, Gulf of Guinea. *Chemical Geology*, 35, 115-128.
- Loucks, R.R., 1990. Discrimination of ophiolitic from nonophiolitic ultramafic allochthons in orogenic belts by the Al/Ti ratio in clinopyroxene. *Geology*, 18, 346-349.
- Mahoe, G., Bertrand, H., Guillot, S., Villa, I.M., Keller, F., and Capiez, P., 2004. The South Ladakh ophiolites (NW Himalaya, India): an intra-oceanic tholeiitic arc origin with implication for the closure of the Neo-Tethys. *Chemical Geology*, 203, 273-303.
- Moix, P., Beccaletto, L., Kozur, H.W., Hochard, C., Rosselet, F., and Stampfli, G.M., 2008. A new classification of the Turkish terranes and sutures and its implication for the paleotectonic history of the region. *Tectonophysics*, 451, 7-39.
- Morimoto, N., and Kitamura, M., 1983. Q-J diagram for classification of pyroxenes. *Journal of Japanese Association, Mineralogy, Petrology and Economic Geology*, 78, p. 141 (in Japanese).
- Morimoto, N., 1989. Nomenclature of pyroxenes. *Canadian Mineralogist*, 27, 143-156.
- Mullen, E.D., 1983. MnO/TiO₂/P₂O₅: a minor element discriminant for basaltic rocks of oceanic environments and its implications for petrogenesis. *Earth and Planetary Science Letters*, 62, 53-62.
- Nicolas, A., and Jackson, E.D., 1972. Repartition en deux provinces des peridotites des chaînes alpines longeant la Méditerranée: implications tectoniques. *Suisse Min. Pet. Bull.*, 52, 479-495. In: Nicolas, A., Boudier, F., and Bouchez, J.L., 1980. Interpretation of peridotite structures from ophiolitic and oceanic environments. *American Journal of Science*, 280, 192-210.
- Okay, A.I., 1984b. Kuzeybatı Anadolu'da yer alan metamorfik kuşaklar, in Proceedings Ketin Symposium, Ankara, February 1984, 83-92.
- Okay, A.I., and Tüysüz, O., 1999. Tethyan sutures of northern Turkey. *Geol.Soc.London, Spec. Publ.*, 156, 475-515.

Okay, A.I., Tansel, I., and Tüysüz, O., 2001. Obduction, subduction and collision as reflected in the Upper Cretaceous- Lower Eocene sedimentary record of western Turkey. Geological Magazine, 138, 117-142.

Okay, A.I., 2008. Geology of Turkey: A synopsis. Anschmitt, 21, 19-42.

Önen, A.P., and Hall, R., 1993. Ophiolites and related metamorphic rocks from the Kütahya region, north-west Turkey. Geological Journal, 28, 399-412. In: Okay, A.I., and Tüysüz, O., 1999. Tethyan sutures of northern Turkey. Geol.Soc.London, Spec. Publ., 156, 475-515.

Parlak, O., Önal, A., Höck, V., Kürüm, S., Delaloye, M., Bağcı, U., and Rızaoğlu, T., 2002. Inverted metamorphic zonation beneath the Yüksekova ophiolite in SE Anatolia. 1st International Symposium of the Faculty of Mines (ITU) on Earth Sciences and Engineering, 16-18 May 2002, Istanbul-Turkey, 133.

Parlak, O., Höck, V., Kozlu, H., and Delaloye, M., 2004. Oceanic crust generation in an island arc tectonic setting, SE Anatolian orogenic belt (Turkey). Min. Mag., 141, 583-603.

Parlak, O., Rızaoğlu, T., Bağcı, U., Karaoğlan, F., and Höck, V., 2009. Tectonic significance of the geochemistry and petrology of ophiolites in southeast Anatolia, Turkey. Tectonophysics, 473, 173-187.

Pearce, J.A., and Cann, J.R., 1973. Tectonic setting of basic volcanic rocks determined using trace element analyses. Earth and Planetary Science Letters, 19, 290-300.

Pearce, J.A., and Norry, M.J., 1979. Petrogenetic implications of Ti, Zr, Y and Nb variations in volcanic rocks. Contributions to Mineralogy and Petrology, 69, 33-47.

Pearce, J.A., 1982. Trace element characteristics of lavas from destructive plate boundaries. In: Bortolotti, V., Chiari, M., Göncüoğlu, M.C., Marcucci, M., Principi, G., Tekin, U.K., Saccani, E. and Tassinari, R., (eds.), 2013. Age and geochemistry of basalt-chert associations in the ophiolites of Izmir-Ankara mélange east of Ankara, Turkey: Preleminary data. Ofioliti, 38, 157-173.

Pickett, E., and Robertson, A.H.F., 1996. Formation of the Late Paleozoic-Early Mesozoic Karakaya Complex and related ophiolites in NW Turkey by Paleotethyan subduction-accretion. Journal of Geological Society of London, 153, 995-1009.

- Poldervaart, A., and Hess, H.H., 1951. Pyroxenes in crystallization of basaltic magmas. *J.Geol.*, 59, 472-489. In: Seaman, S.J., 2000. Crystal clusters, feldspar glomerocrysts, and magma envelopes in the Atascosa Lookout Lava Flow, southern Arizona, USA. *Recorders of magmatic events*, 41, 693-716.
- Robertson, A.H.F., Dixon, J.E., Brown, S., Collins, A., Morris, A., Pickett, E.A., Sharp, I., and Ustaömer, T., 1996. Alternative tectonic models for the Late Paleozoic-Early Tertiary development of Tethys in the Eastern Mediterranean region. In: Bortolotti, V., Chiari, M., Göncüoğlu, M.C., Marcucci, M., Principi, G., Tekin, U.K., Saccani, E., and Tassinari, R., (eds.), 2013. Age and geochemistry of basalt-chert associations in the ophiolites of Izmir-Ankara mélange east of Ankara, Turkey: Preliminary data. *Ophioliti*, 38, 157-173.
- Robertson, A.H.F., 2002. Overview of the genesis and emplacement of Mesozoic ophiolites in the Eastern Mediterranean Tethyan region. *Lithos*, 65, 1-67.
- Robertson, A.H.F., Parlak, O. Rızaoglu, T., Ünlügenç, Ü., İnan, N., Taslı, K., and Ustaömer, T., 2007. Tectonic evolution of the south Tethyan ocean: evidence from the eastern Taurus Mountains (Elazığ region, SE Turkey). In: Ries, A.C., Butler, R.W.H., and Graham, R.H., (eds) Deformation of continental crust. Geological Society, London, Special Publications, 272, 231-270.
- Rocci, G., Ohnenstetter, D., and Ohnenstetter, M., 1975. Duality of Tethyan ophiolites. *Petrologie*, 1, 172-174.
- Rojay, B., Altiner, D., Özkan-Altiner, S., Önen, P., James, S., and Thirlwall, M.F., 2004. Geodynamic significance of the Cretaceous pillow basalts from North Anatolian Ophiolitic Melange Belt (Central Anatolia, Turkey): geochemical and paleontological constraints. *Geodinamica Acta*, 17:5, 349-361.
- Saccani, E., and Photiades, A., 2005. Petrogenesis and tectonomagmatic significance of volcanic and subvolcanic rocks in the Albanide-Hellenide ophiolitic melanges. *The Island Arc*, 14, 494-516.
- Sayıt, K., 2005. Geology and petrology of the mafic volcanic rocks within the Karakaya Complex from Central (Ankara) and NW (Geyve and Edremit) Anatolia. 173 pages.
- Shervais, M., 1982. Ti-V plots and the petrogenesis of modern and ophiolitic lavas. *Earth and Planetary Science Letters*, 59, 101-118.

- Spray, J.G., Bebien, J., Rex, D.C., and Roddick, J.C., 1984. Age constraints on the igneous and metamorphic evolution of magmatism in the Hellenic-Dinaric ophiolites. In: Okay, A.I., and Tüysüz, O., 1999. Tethyan sutures of northern Turkey. *Geol.Soc.London, Spec. Publ.*, 156, 475-515.
- Sun, S.S., and McDonough, W.F., 1989. Chemical and isotopic systematics of oceanic basalts: implications for mantle composition and processes. In: Çelik, Ö.F., Chiaradia, M., Marzoli, A., Billor, Z., and Marschik, R., (eds.), 2013. The Eldivan ophiolite and volcanic rocks in the Izmir-Ankara-Erzincan suture zone Northern Turkey: Geochronology, whole-rock geochemical and Nd-Sr-Pb isotope characteristics. *Lithos*, 172, 31-46.
- Şengör, A.M.C., and Yılmaz, Y., 1981. Tethyan evolution of Turkey: a plate tectonic approach. *Tectonophysics*, 75, 81-241.
- Tekin, U.K., Göncüoğlu, M.C., and Turhan, N., 2002. First evidence of Late Carnian radiolarians from the Izmir-Ankara suture complex, central Sakarya, Turkey: implications for the opening age of the Izmir-Ankara branch of Neo-Tethys. *Geobios*, 35, 127-135.
- Toksoy-Köksal, F., Göncüoğlu, M.C., and Yalınız, M.K., 2001. Petrology of the Kurancalı Phlogopitic Metagabbro: An island arc-type ophiolitic sliver in the Central Anatolian Crystalline Complex, Turkey. *International Geological Review*, 43(7), 624-639.
- Toksoy-Köksal, F., 2003. Petrology of the phlogopite-bearing ultramafic-mafic plutonic rocks within Central Anatolian Crystalline Complex, Turkey. 274 pages.
- Topuz, G., Çelik, Ö.F., Şengör, A.M.C., Altıntaş, İ. E., Zack, T., Rolland, Y., and Barth, M., 2013. Jurassic ophiolite formation and emplacement as backstop to a subduction-accretion complex in northeast Turkey, the Refahiye Ophiolite, and relation to the Balkan ophiolites. *American Journal of Science*, 313, 1054-1087.
- Vieten, K., and Hamm, H.M., 1978. Additional notes on the calculation of the crystal chemical formula of clinopyroxenes and their contents of Fe³⁺ from microprobe analyses. *Neues Jahrbuch für Mineralogie, Monatshefte*, 71-88.
- Winchester, J.A., and Floyd, P.A., 1977. Geochemical discrimination of different magma series and their differentiation products using immobile elements. *Chemical Geology*, 20, 325-343.
- Wood, C.A., 1980. Morphometric evolution of cinder cones. *J. Volcanol. Geotherm.*, 7, 387-413.

- Workman, R.K., and Hart, S.R., 2005. Major and trace element composition of the depleted MORB mantle (DMM). *Earth and Planetary Science Letters*, 231, 53-72.
- Yalınız, M.K., Göncüoğlu, M.C., Özkan-Altiner, S., and Parlak, O., 2000. Formation and emplacement ages of the SSZ-type Neotethyan ophiolites in Central Anatolia, Turkey: Paleotectonic implications. *Geol.Journ.*, 35, 53-68.
- Zeyen, H., Volker, F., Wehrle, V., Fuchs, K., Sobolev, S.V., and Altherr, R., 1997. Styles of continental rifting: crust-mantle detachment and mantle plumes. *Tectonophysics*, 278, 329-352.
- Zindler, A.E., and Hart, S.R., 1986. Chemical geodynamics. *Annual Review of Earth and Planetary Sciences*, 14, 493-571.

APPENDIX A
MAJOR AND MINOR ELEMENT CHEMICAL ANALYSES FOR
PYROXENE FROM METABASALTS

Sample No	AA-7-1	AA-7-1	AA-7-1	AA-7-1	AA-7-1	AA-7-1	AA-7-1	AA-7-1
Photo Area	A	A	A	A	A	A	C	C
Analysis No	2	3	5	6	7	8	16	17
SiO₂	50.0400	50.6500	51.0100	49.8100	50.9800	50.8600	49.9400	50.4500
TiO₂	0.1409	0.2210	0.2171	0.2454	0.1701	0.1191	0.2318	0.2310
Al₂O₃	2.6700	2.0200	1.7548	2.9200	1.8168	2.1600	3.3300	2.8400
Fe₂O₃	4.8300	5.6100	6.6500	5.6100	6.2100	7.0700	6.7300	7.0300
MnO	0.0968	0.1235	0.1592	0.0964	0.1498	0.1569	0.1673	0.1812
MgO	20.6700	21.0600	22.7700	20.3500	22.3900	23.0500	20.6600	19.5100
CaO	18.8100	18.2300	16.4200	18.7100	17.3200	15.7100	18.8600	19.6300
Na₂O	0.2706	0.2909	0.2025	0.3027	0.2763	0.2386	0.2572	0.5984
K₂O	0.0015	0.0126	0.0000	0.0139	0.0116	0.0011	0.0094	0.0223
Cr₂O₃	0.5400	0.2587	0.3254	0.3280	0.1850	0.2964	0.3405	0.3770
NiO	0.0334	0.0099	0.0697	0.0183	0.0307	0.0000	0.0584	0.0000
TOTAL	98.1032	98.4866	99.5787	98.4047	99.5403	99.6621	100.5846	100.8699
Si	1.8302	1.8466	1.8352	1.8200	1.8334	1.8257	1.7893	1.8081
Al^[4]	0.1151	0.0868	0.0744	0.1257	0.0770	0.0914	0.1406	0.1200
Al^[6]	0.0000	0.0000	0.0000	0.0000	0.0000	0.0000	0.0000	0.0000
Ti	0.0039	0.0061	0.0059	0.0067	0.0046	0.0032	0.0062	0.0062
Fe³⁺	0.1477	0.1711	0.2001	0.1714	0.1868	0.2122	0.2017	0.2107
Fe²⁺	0.0000	0.0000	0.0000	0.0000	0.0000	0.0000	0.0000	0.0000
Mn	0.0030	0.0038	0.0049	0.0030	0.0046	0.0048	0.0051	0.0055
Mg	1.1270	1.1446	1.2212	1.1085	1.2004	1.2335	1.1035	1.0424
Cr	0.0156	0.0075	0.0093	0.0095	0.0053	0.0084	0.0096	0.0107
Ni	0.0010	0.0003	0.0020	0.0005	0.0009	0.0000	0.0017	0.0000
Ca	0.7371	0.7121	0.6330	0.7325	0.6674	0.6042	0.7240	0.7538
Na	0.0192	0.0206	0.0141	0.0214	0.0193	0.0166	0.0179	0.0416
K	0.0001	0.0006	0.0000	0.0006	0.0005	0.0001	0.0004	0.0010
TOTAL	4.0000	4.0000	4.0000	4.0000	4.0000	4.0000	4.0000	4.0000
Mg/(Fe(t)+Mg)	0.8841	0.8700	0.8592	0.8661	0.8654	0.8532	0.8455	0.8318

Sample No	AA-7-1	AA-7-1	AA-7-1	AA-7-1	AA-7-1	AA-7-1	AA-7-1	AA-7-1
Photo Area	C	C	C	C	D	D	D	D
Analysis No	18	19	21	22	23	24	25	26
SiO₂	51.1700	51.6600	48.9600	51.0100	48.7400	49.0900	51.0200	51.9900
TiO₂	0.2528	0.1449	0.2928	0.2766	0.4970	0.3845	0.2979	0.1824
Al₂O₃	2.4400	1.9400	3.9800	2.3400	4.0800	4.3000	2.6300	1.8842
Fe₂O₃	5.8200	7.3200	7.3500	7.7400	7.1100	7.5900	5.5800	8.0000
MnO	0.1449	0.1849	0.1398	0.1690	0.1286	0.1523	0.1271	0.2168
MgO	20.8900	22.6900	20.1200	22.2500	19.1400	19.6100	20.8200	20.5900
CaO	20.1800	17.2400	18.7200	17.1800	20.1000	18.8900	19.8100	17.4900
Na₂O	0.2060	0.2235	0.2730	0.1981	0.2829	0.4029	0.2498	0.5278
K₂O	0.0048	0.0077	0.0000	0.0044	0.0109	0.0000	0.0000	0.0010
Cr₂O₃	0.3234	0.2806	0.4823	0.2452	0.3938	0.6129	0.4551	0.2260
NiO	0.0000	0.0051	0.0045	0.0299	0.0259	0.0392	0.0042	0.0059
TOTAL	101.4319	101.6967	100.3224	101.4432	100.5091	101.0718	100.9941	101.1141
Si	1.8169	1.8238	1.7627	1.8092	1.7573	1.7580	1.8184	1.8590
Al^[4]	0.1021	0.0807	0.1689	0.0978	0.1734	0.1815	0.1105	0.0794
Al^[6]	0.0000	0.0000	0.0000	0.0000	0.0000	0.0000	0.0000	0.0000
Ti	0.0068	0.0038	0.0079	0.0074	0.0135	0.0104	0.0080	0.0049
Fe³⁺	0.1728	0.2161	0.2213	0.2296	0.2144	0.2273	0.1663	0.2230
Fe²⁺	0.0000	0.0000	0.0000	0.0000	0.0000	0.0000	0.0000	0.0163
Mn	0.0044	0.0055	0.0043	0.0051	0.0039	0.0046	0.0038	0.0066
Mg	1.1058	1.1942	1.0799	1.1765	1.0288	1.0469	1.1062	1.0976
Cr	0.0091	0.0078	0.0137	0.0069	0.0112	0.0174	0.0128	0.0064
Ni	0.0000	0.0001	0.0001	0.0009	0.0008	0.0011	0.0001	0.0002
Ca	0.7677	0.6521	0.7221	0.6529	0.7765	0.7248	0.7565	0.6701
Na	0.0142	0.0153	0.0191	0.0136	0.0198	0.0280	0.0173	0.0366
K	0.0002	0.0003	0.0000	0.0002	0.0005	0.0000	0.0000	0.0000
TOTAL	4.0000	4.0000	4.0000	4.0000	4.0000	4.0000	4.0000	4.0000
Mg/(Fe(t)+Mg)	0.8648	0.8468	0.8299	0.8367	0.8275	0.8216	0.8693	0.8210

APPENDIX B
MAJOR AND MINOR ELEMENT CHEMICAL ANALYSES FOR
PYROXENE FROM DYKES

Sample No	AA-10a	AA-10a	AA-10a	AA-10a	AA-10a	AA-10a	AA-10a	AA-10a	AA-10a
Photo Area	General	General	A	A	A	A	A	A	A
Analysis No	32	39	1	2	3	4	5	6	7
SiO₂	49.30	48.93	50.33	51.43	52.90	50.47	51.40	52.01	51.09
TiO₂	0.45	0.43	1.35	0.94	0.77	1.39	1.15	0.94	0.91
Al₂O₃	4.36	4.82	3.98	3.47	2.44	4.32	3.82	3.18	4.99
Fe₂O₃	6.88	6.97	6.62	5.80	5.18	6.70	5.84	6.13	6.12
MnO	0.12	0.13	0.14	0.15	0.11	0.15	0.15	0.15	0.14
MgO	19.10	18.65	14.86	15.65	16.35	15.34	15.34	15.85	14.85
CaO	20.69	21.23	21.55	21.36	21.71	20.57	21.44	21.19	20.85
Na₂O	0.30	0.28	0.27	0.23	0.18	0.30	0.29	0.24	0.54
K₂O	0.03	0.00	0.03	0.01	0.01	0.01	0.00	0.00	0.00
Cr₂O₃	0.34	0.24	0.48	0.76	0.50	0.46	0.58	0.60	0.50
NiO	0.07	0.01	0.08	0.10	0.00	0.04	0.02	0.00	0.06
TOTAL	101.65	101.69	99.68	99.90	100.15	99.75	100.03	100.28	100.04
Si	1.7572	1.7450	1.8653	1.8949	1.9340	1.8651	1.8906	1.9077	1.8774
Al^[4]	0.1832	0.2026	0.1347	0.1051	0.0619	0.1349	0.1079	0.0912	0.1226
Al^[6]	0.0000	0.0000	0.0391	0.0456	0.0435	0.0533	0.0578	0.0464	0.0935
Ti	0.0121	0.0115	0.0377	0.0261	0.0212	0.0386	0.0318	0.0258	0.0251
Fe³⁺	0.2051	0.2079	0.0270	0.0021	0.0000	0.0134	0.0000	0.0000	0.0025
Fe²⁺	0.0000	0.0000	0.1782	0.1766	0.1587	0.1937	0.1798	0.1882	0.1856
Mn	0.0036	0.0039	0.0044	0.0045	0.0033	0.0046	0.0047	0.0046	0.0043
Mg	1.0149	0.9915	0.8210	0.8596	0.8930	0.8451	0.8418	0.8672	0.8135
Cr	0.0097	0.0066	0.0139	0.0222	0.0146	0.0135	0.0170	0.0173	0.0146
Ni	0.0021	0.0003	0.0023	0.0031	0.0000	0.0011	0.0005	0.0000	0.0018
Ca	0.7901	0.8112	0.8557	0.8432	0.8522	0.8145	0.8456	0.8333	0.8209
Na	0.0206	0.0194	0.0193	0.0165	0.0128	0.0217	0.0209	0.0172	0.0382
K	0.0015	0.0000	0.0014	0.0005	0.0006	0.0006	0.0000	0.0000	0.0000
TOTAL	4.0000	4.0000	4.0000	4.0000	3.9959	4.0000	3.9985	3.9989	4.0000
Mg/(Fe^(t)+Mg)	0.8319	0.8267	0.8001	0.8279	0.8491	0.8032	0.8240	0.8217	0.8122

Sample No	AA-10a	AA-10a	AA-10a	AA-10a	AA-10a	AA-10a	AA-10a	AA-10a	AA-10a
Photo Area	A	A	A	A	A	A	A	A	A
Analysis No	8	9	10	11	12	13	14	15	16
SiO₂	52.36	51.94	51.62	52.06	52.20	52.13	52.14	51.59	52.90
TiO₂	0.76	0.77	0.81	0.79	0.82	0.81	0.92	1.13	0.55
Al₂O₃	2.71	2.68	2.99	2.89	2.99	2.85	2.79	3.15	2.29
Fe₂O₃	5.37	5.85	6.28	5.61	5.55	5.16	5.71	6.02	4.77
MnO	0.14	0.11	0.14	0.13	0.09	0.09	0.12	0.10	0.11
MgO	15.92	15.48	15.15	15.91	16.11	15.81	15.96	15.31	16.56
CaO	21.84	21.09	21.01	21.65	21.78	21.44	21.22	21.64	21.39
Na₂O	0.22	0.37	0.49	0.25	0.30	0.27	0.28	0.30	0.28
K₂O	0.00	0.05	0.03	0.00	0.01	0.01	0.01	0.00	0.01
Cr₂O₃	0.48	0.55	0.60	0.59	0.63	0.62	0.57	0.60	0.93
NiO	0.07	0.04	0.00	0.02	0.02	0.08	0.00	0.03	0.05
TOTAL	99.88	98.92	99.13	99.91	100.49	99.28	99.71	99.87	99.84
Si	1.9245	1.9297	1.9173	1.9149	1.9065	1.9246	1.9198	1.9036	1.9378
Al^[4]	0.0738	0.0688	0.0827	0.0851	0.0935	0.0715	0.0784	0.0957	0.0595
Al^[6]	0.0436	0.0486	0.0481	0.0402	0.0352	0.0528	0.0428	0.0413	0.0395
Ti	0.0211	0.0214	0.0227	0.0218	0.0226	0.0224	0.0254	0.0314	0.0152
Fe³⁺	0.0000	0.0000	0.0082	0.0024	0.0168	0.0000	0.0000	0.0000	0.0000
Fe²⁺	0.1652	0.1819	0.1869	0.1701	0.1527	0.1596	0.1760	0.1858	0.1463
Mn	0.0044	0.0033	0.0045	0.0041	0.0027	0.0027	0.0037	0.0031	0.0035
Mg	0.8731	0.8580	0.8389	0.8724	0.8771	0.8719	0.8769	0.8425	0.9056
Cr	0.0140	0.0160	0.0177	0.0170	0.0181	0.0182	0.0166	0.0174	0.0270
Ni	0.0021	0.0012	0.0001	0.0007	0.0007	0.0024	0.0000	0.0009	0.0016
Ca	0.8608	0.8402	0.8361	0.8532	0.8523	0.8498	0.8379	0.8558	0.8407
Na	0.0157	0.0270	0.0353	0.0180	0.0213	0.0195	0.0201	0.0218	0.0202
K	0.0000	0.0022	0.0014	0.0000	0.0004	0.0005	0.0006	0.0000	0.0004
TOTAL	3.9984	3.9985	4.0000	4.0000	4.0000	3.9961	3.9982	3.9994	3.9973
Mg/(Fe^(t)+Mg)	0.8409	0.8251	0.8113	0.8349	0.8380	0.8452	0.8328	0.8193	0.8609

Sample No	AA-10a	AA-10a	AA-10a	AA-10a	AA-10a	AA-10a	AA-10a	AA-10a	AA-10a
Photo Area	A	A	A	B	B	B	B	B	B
Analysis No	17	19	20	37	38	39	40	41	42
SiO₂	51.74	52.49	53.20	50.99	53.47	52.94	52.03	50.22	53.01
TiO₂	0.85	0.73	0.79	1.41	0.69	0.73	0.73	1.41	0.91
Al₂O₃	2.87	2.57	2.04	3.32	2.03	2.19	1.33	4.54	2.48
Fe₂O₃	5.68	5.79	6.10	7.31	5.52	5.75	12.24	6.40	6.14
MnO	0.14	0.11	0.14	0.14	0.17	0.15	0.35	0.13	0.16
MgO	15.54	16.25	16.47	14.74	16.69	16.80	13.38	14.64	16.19
CaO	21.76	20.94	20.81	21.39	21.21	20.90	19.64	20.90	21.28
Na₂O	0.32	0.30	0.19	0.27	0.20	0.18	0.25	0.44	0.30
K₂O	0.00	0.03	0.00	0.00	0.01	0.01	0.01	0.00	0.00
Cr₂O₃	0.75	0.61	0.13	0.08	0.58	0.76	0.00	0.82	0.42
NiO	0.04	0.06	0.03	0.03	0.06	0.00	0.08	0.06	0.04
TOTAL	99.69	99.88	99.91	99.68	100.63	100.42	100.05	99.58	100.92
Si	1.9101	1.9285	1.9506	1.8939	1.9459	1.9332	1.9590	1.8620	1.9300
Al^[4]	0.0899	0.0707	0.0436	0.1061	0.0496	0.0646	0.0410	0.1380	0.0682
Al^[6]	0.0350	0.0407	0.0448	0.0392	0.0377	0.0297	0.0182	0.0604	0.0383
Ti	0.0237	0.0203	0.0219	0.0393	0.0189	0.0200	0.0208	0.0394	0.0248
Fe³⁺	0.0081	0.0000	0.0000	0.0055	0.0000	0.0000	0.0000	0.0067	0.0000
Fe²⁺	0.1673	0.1780	0.1876	0.2216	0.1684	0.1758	0.3854	0.1918	0.1871
Mn	0.0043	0.0036	0.0044	0.0045	0.0052	0.0048	0.0112	0.0042	0.0051
Mg	0.8552	0.8904	0.9029	0.8162	0.9076	0.9156	0.7510	0.8092	0.8795
Cr	0.0220	0.0178	0.0038	0.0023	0.0167	0.0219	0.0000	0.0242	0.0121
Ni	0.0011	0.0017	0.0009	0.0008	0.0017	0.0000	0.0025	0.0018	0.0012
Ca	0.8607	0.8247	0.8199	0.8512	0.8289	0.8187	0.7923	0.8303	0.8309
Na	0.0226	0.0214	0.0136	0.0194	0.0143	0.0130	0.0182	0.0318	0.0209
K	0.0000	0.0016	0.0000	0.0000	0.0007	0.0005	0.0004	0.0002	0.0000
TOTAL	4.0000	3.9992	3.9943	4.0000	3.9955	3.9978	4.0000	4.0000	3.9982
Mg/(Fe^(t)+Mg)	0.8298	0.8334	0.8280	0.7823	0.8435	0.8389	0.6609	0.8031	0.8246

Sample No	AA-10a	AA-10a	AA-10a	AA-10a	AA-10a	AA-10a	AA-10a	AA-10a	AA-10a
Photo Area	B	B	B	B	D	D	D	D	D
Analysis No	43	44	45	46	47	48	49	50	51
SiO₂	52.12	51.62	52.83	52.23	52.03	51.98	53.33	52.28	50.83
TiO₂	0.92	0.88	0.72	0.95	0.94	1.03	0.83	0.79	1.30
Al₂O₃	3.11	3.56	2.38	3.09	3.03	3.41	2.17	2.91	3.38
Fe₂O₃	5.38	5.50	4.69	5.40	5.24	5.61	6.65	5.66	7.17
MnO	0.10	0.12	0.12	0.12	0.08	0.13	0.14	0.10	0.12
MgO	15.75	15.42	16.26	15.65	15.57	15.44	16.92	16.00	14.77
CaO	21.82	21.67	21.36	21.83	21.85	22.02	19.84	21.48	21.65
Na₂O	0.32	0.28	0.26	0.27	0.30	0.29	0.23	0.24	0.33
K₂O	0.00	0.00	0.00	0.00	0.00	0.00	0.01	0.01	0.00
Cr₂O₃	0.82	0.79	0.92	0.83	0.87	0.60	0.18	0.62	0.01
NiO	0.00	0.03	0.02	0.04	0.09	0.05	0.01	0.04	0.04
TOTAL	100.35	99.88	99.55	100.41	100.01	100.56	100.31	100.12	99.61
Si	1.9086	1.9001	1.9393	1.9112	1.9116	1.9019	1.9469	1.9176	1.8862
Al^[4]	0.0907	0.0984	0.0535	0.0857	0.0860	0.0970	0.0479	0.0812	0.1138
Al^[6]	0.0435	0.0561	0.0499	0.0477	0.0454	0.0501	0.0457	0.0446	0.0340
Ti	0.0254	0.0245	0.0198	0.0263	0.0261	0.0283	0.0228	0.0217	0.0362
Fe³⁺	0.0000	0.0000	0.0000	0.0000	0.0000	0.0000	0.0000	0.0000	0.0307
Fe²⁺	0.1648	0.1694	0.1445	0.1655	0.1612	0.1718	0.2036	0.1737	0.1918
Mn	0.0032	0.0037	0.0037	0.0037	0.0026	0.0041	0.0043	0.0030	0.0038
Mg	0.8601	0.8468	0.8931	0.8551	0.8539	0.8427	0.9233	0.8754	0.8171
Cr	0.0237	0.0231	0.0268	0.0239	0.0252	0.0173	0.0053	0.0181	0.0004
Ni	0.0000	0.0008	0.0005	0.0010	0.0028	0.0015	0.0004	0.0012	0.0013
Ca	0.8564	0.8553	0.8432	0.8573	0.8612	0.8637	0.7781	0.8447	0.8608
Na	0.0228	0.0203	0.0184	0.0195	0.0215	0.0204	0.0161	0.0173	0.0238
K	0.0000	0.0000	0.0000	0.0000	0.0000	0.0000	0.0005	0.0002	0.0000
TOTAL	3.9993	3.9985	3.9928	3.9970	3.9975	3.9990	3.9948	3.9988	4.0000
Mg/(Fe^(t)+Mg)	0.8392	0.8333	0.8607	0.8378	0.8412	0.8307	0.8193	0.8344	0.7860

Sample No	AA-10a	AA-10a	AA-10a	AA-10a	AA-10a	AA-10a	AA-10a	AA-10a	AA-10a
Photo Area	D	D	D	D	D	D	D	D	D
Analysis No	52	53	54	55	56	57	58	59	60
SiO₂	49.43	51.28	52.60	51.95	52.20	51.56	51.74	51.68	51.63
TiO₂	1.83	1.20	0.79	1.02	0.88	1.23	1.09	1.10	1.18
Al₂O₃	3.86	4.00	2.77	3.19	2.75	3.49	3.49	3.30	3.43
Fe₂O₃	9.77	5.69	5.33	5.80	5.51	5.96	5.69	5.78	6.22
MnO	0.21	0.13	0.10	0.13	0.17	0.12	0.07	0.18	0.13
MgO	13.37	15.44	16.26	15.70	15.78	15.07	15.42	15.31	15.22
CaO	20.79	21.57	21.57	21.68	21.91	21.56	21.79	21.89	21.36
Na₂O	0.42	0.30	0.26	0.27	0.26	0.31	0.24	0.29	0.35
K₂O	0.00	0.00	0.00	0.00	0.00	0.00	0.00	0.01	0.00
Cr₂O₃	0.01	0.78	0.80	0.73	0.65	0.56	0.83	0.69	0.64
NiO	0.01	0.02	0.08	0.02	0.00	0.05	0.06	0.04	0.02
TOTAL	99.70	100.42	100.57	100.49	100.10	99.91	100.44	100.28	100.18
Si	1.8523	1.8799	1.9192	1.9028	1.9173	1.9003	1.8962	1.8993	1.8993
Al^[4]	0.1477	0.1200	0.0795	0.0970	0.0822	0.0961	0.1014	0.1004	0.0992
Al^[6]	0.0227	0.0528	0.0397	0.0407	0.0369	0.0557	0.0495	0.0425	0.0496
Ti	0.0516	0.0332	0.0216	0.0280	0.0243	0.0341	0.0302	0.0305	0.0328
Fe³⁺	0.0520	0.0000	0.0000	0.0000	0.0000	0.0000	0.0000	0.0000	0.0000
Fe²⁺	0.2542	0.1745	0.1628	0.1777	0.1693	0.1840	0.1746	0.1777	0.1915
Mn	0.0068	0.0042	0.0032	0.0041	0.0053	0.0038	0.0022	0.0056	0.0042
Mg	0.7469	0.8438	0.8850	0.8574	0.8643	0.8296	0.8435	0.8389	0.8353
Cr	0.0004	0.0226	0.0230	0.0212	0.0187	0.0165	0.0241	0.0201	0.0185
Ni	0.0002	0.0006	0.0023	0.0005	0.0000	0.0015	0.0018	0.0012	0.0005
Ca	0.8347	0.8473	0.8438	0.8509	0.8625	0.8530	0.8567	0.8621	0.8426
Na	0.0303	0.0210	0.0186	0.0195	0.0188	0.0218	0.0173	0.0209	0.0251
K	0.0002	0.0000	0.0000	0.0000	0.0000	0.0000	0.0000	0.0006	0.0000
TOTAL	4.0000	3.9999	3.9987	3.9998	3.9995	3.9965	3.9976	3.9997	3.9985
Mg/(Fe^(t)+Mg)	0.7092	0.8287	0.8447	0.8283	0.8362	0.8184	0.8285	0.8252	0.8135

Sample No	AA-10a	AA-10a	AA-10a	AA-10a	AA-10a	AA-10a	AA-10a	AA-10a	AA-10a
Photo Area	D	D	D	D	D	E	E	E	E
Analysis No	61	62	63	64	65	71	72	73	74
SiO₂	50.81	52.87	51.23	52.44	49.19	52.15	51.85	52.10	51.53
TiO₂	1.49	0.63	1.13	0.90	1.69	0.92	0.82	0.86	0.92
Al₂O₃	3.35	2.51	3.73	2.55	3.59	3.03	3.27	3.14	3.37
Fe₂O₃	7.86	5.14	5.73	5.91	11.08	6.01	5.95	5.56	5.75
MnO	0.15	0.13	0.10	0.16	0.23	0.10	0.14	0.16	0.13
MgO	14.53	16.62	15.23	15.65	12.69	15.88	15.49	15.73	15.72
CaO	21.40	21.75	21.83	21.31	20.30	21.10	21.49	21.77	21.58
Na₂O	0.32	0.22	0.25	0.27	0.42	0.26	0.39	0.30	0.29
K₂O	0.01	0.00	0.00	0.01	0.00	0.00	0.00	0.00	0.00
Cr₂O₃	0.02	0.74	0.76	0.39	0.04	0.57	0.76	0.84	0.80
NiO	0.04	0.01	0.05	0.06	0.00	0.03	0.01	0.00	0.01
TOTAL	99.98	100.62	100.05	99.66	99.24	100.05	100.17	100.46	100.09
Si	1.8845	1.9260	1.8867	1.9331	1.8620	1.9151	1.9046	1.9073	1.8932
Al^[4]	0.1155	0.0740	0.1128	0.0625	0.1380	0.0824	0.0954	0.0927	0.1068
Al^[6]	0.0310	0.0338	0.0491	0.0486	0.0222	0.0489	0.0462	0.0428	0.0391
Ti	0.0417	0.0173	0.0313	0.0250	0.0481	0.0254	0.0226	0.0236	0.0254
Fe³⁺	0.0239	0.0000	0.0000	0.0000	0.0490	0.0000	0.0096	0.0000	0.0140
Fe²⁺	0.2199	0.1566	0.1765	0.1826	0.3018	0.1848	0.1732	0.1702	0.1627
Mn	0.0048	0.0040	0.0031	0.0050	0.0075	0.0031	0.0042	0.0050	0.0041
Mg	0.8034	0.9026	0.8364	0.8620	0.7161	0.8705	0.8483	0.8585	0.8610
Cr	0.0004	0.0213	0.0223	0.0115	0.0012	0.0166	0.0221	0.0244	0.0233
Ni	0.0013	0.0002	0.0014	0.0017	0.0000	0.0010	0.0003	0.0001	0.0004
Ca	0.8504	0.8490	0.8616	0.8436	0.8233	0.8313	0.8458	0.8539	0.8495
Na	0.0227	0.0152	0.0181	0.0195	0.0307	0.0185	0.0276	0.0213	0.0205
K	0.0004	0.0002	0.0001	0.0005	0.0000	0.0000	0.0001	0.0000	0.0000
TOTAL	4.0000	4.0000	3.9995	3.9956	4.0000	3.9976	4.0000	3.9999	4.0000
Mg/(Fe^(t)+Mg)	0.7672	0.8522	0.8257	0.8252	0.6712	0.8249	0.8227	0.8345	0.8297

Sample No	AA-10a	AA-10a	AA-10a
Photo Area	E	E	E
Analysis No	75	76	77
SiO₂	51.57	51.88	52.97
TiO₂	1.13	1.13	0.57
Al₂O₃	2.39	4.51	2.39
Fe₂O₃	7.91	6.24	4.99
MnO	0.19	0.14	0.09
MgO	15.27	15.18	16.47
CaO	21.29	19.67	21.53
Na₂O	0.31	0.46	0.33
K₂O	0.01	0.02	0.02
Cr₂O₃	0.03	0.65	0.97
NiO	0.07	0.03	0.10
TOTAL	100.17	99.90	100.44
Si	1.9050	1.9013	1.9325
Al^[4]	0.0950	0.0881	0.0668
Al^[6]	0.0091	0.1078	0.0360
Ti	0.0314	0.0313	0.0157
Fe³⁺	0.0448	0.0000	0.0000
Fe²⁺	0.1996	0.1923	0.1523
Mn	0.0060	0.0043	0.0029
Mg	0.8409	0.8340	0.8961
Cr	0.0010	0.0189	0.0279
Ni	0.0020	0.0007	0.0029
Ca	0.8427	0.7767	0.8419
Na	0.0220	0.0329	0.0234
K	0.0007	0.0010	0.0010
TOTAL	4.0000	3.9893	3.9994
Mg/(Fe^(t)+Mg)	0.7748	0.8126	0.8547

APPENDIX C
MAJOR AND MINOR ELEMENT CHEMICAL ANALYSES FOR
PYROXENE FROM BASALT PHENOCRYSTS

Sample No	AA-11c	AA-11c	AA-11c	AA-11c	AA-11c	AA-11c	AA-11c	AA-11c	AA-11c
Photo Area	B	B	B	B	B	C	C	C	C
Analysis No	17	18	19	20	21	23	24	25	28
SiO₂	50.35	50.13	49.74	49.98	50.79	49.87	49.97	50.06	51.36
TiO₂	0.25	0.37	0.49	0.27	0.30	0.27	0.15	0.08	0.11
Al₂O₃	2.87	2.23	2.97	2.85	2.33	3.53	3.38	3.38	2.44
Fe₂O₃	7.15	7.78	7.76	7.60	7.55	5.49	5.22	5.05	5.48
MnO	0.15	0.21	0.21	0.16	0.16	0.14	0.11	0.09	0.10
MgO	19.36	18.54	18.87	18.60	19.04	19.54	19.58	19.51	20.23
CaO	20.43	19.66	20.37	19.94	19.89	21.00	21.19	20.90	20.65
Na₂O	0.30	0.64	0.32	0.28	0.54	0.31	0.26	0.23	0.21
K₂O	0.00	0.01	0.00	0.01	0.02	0.01	0.00	0.02	0.01
Cr₂O₃	0.48	0.17	0.03	0.19	0.31	0.49	0.41	0.63	0.19
NiO	0.00	0.05	0.03	0.00	0.04	0.09	0.07	0.05	0.00
TOTAL	101.34	99.80	100.79	99.89	100.97	100.72	100.34	100.00	100.79
Si	1.8025	1.8253	1.7941	1.8201	1.8261	1.7870	1.7958	1.8058	1.8367
Al^[4]	0.1211	0.0957	0.1263	0.1223	0.0987	0.1491	0.1432	0.1437	0.1028
Al^[6]	0.0000	0.0000	0.0000	0.0000	0.0000	0.0000	0.0000	0.0000	0.0000
Ti	0.0066	0.0102	0.0132	0.0075	0.0081	0.0071	0.0040	0.0021	0.0031
Fe³⁺	0.2141	0.2369	0.2341	0.2315	0.2270	0.1645	0.1569	0.1523	0.1639
Fe²⁺	0.0000	0.0000	0.0000	0.0000	0.0000	0.0000	0.0000	0.0000	0.0000
Mn	0.0046	0.0066	0.0064	0.0048	0.0048	0.0041	0.0035	0.0029	0.0032
Mg	1.0332	1.0064	1.0146	1.0098	1.0205	1.0438	1.0490	1.0492	1.0785
Cr	0.0136	0.0049	0.0009	0.0056	0.0089	0.0139	0.0116	0.0179	0.0054
Ni	0.0000	0.0015	0.0009	0.0000	0.0011	0.0025	0.0019	0.0015	0.0000
Ca	0.7836	0.7670	0.7872	0.7780	0.7662	0.8063	0.8160	0.8078	0.7912
Na	0.0207	0.0450	0.0224	0.0201	0.0375	0.0215	0.0182	0.0159	0.0148
K	0.0000	0.0004	0.0000	0.0003	0.0010	0.0003	0.0000	0.0009	0.0004
TOTAL	4.0000	4.0000	4.0000	4.0000	4.0000	4.0000	4.0000	4.0000	4.0000
Mg/(Fe^(t)+Mg)	0.8284	0.8094	0.8125	0.8135	0.8180	0.8638	0.8699	0.8732	0.8681

Sample No	AA-11c	AA-11c	AA-11c	AA-11c	AA-11c	AA-11c	AA-11c	AA-11c	AA-11c
Photo Area	C	C	E	E	E	E	E	E	E
Analysis No	29	30	33	36	40	41	43	44	45
SiO₂	50.39	48.78	50.90	50.02	50.99	50.74	50.46	50.31	50.43
TiO₂	0.24	0.54	0.02	0.43	0.24	0.28	0.12	0.25	0.08
Al₂O₃	2.77	3.76	2.73	3.42	2.52	3.19	2.51	3.23	2.86
Fe₂O₃	5.32	7.96	5.43	5.49	5.30	5.40	5.48	5.49	5.73
MnO	0.10	0.16	0.10	0.14	0.14	0.13	0.13	0.10	0.19
MgO	19.73	17.91	19.98	20.00	19.89	19.74	19.98	19.85	19.37
CaO	20.98	20.45	21.29	20.92	20.78	21.13	21.14	21.18	20.65
Na₂O	0.23	0.40	0.26	0.29	0.31	0.32	0.28	0.27	0.34
K₂O	0.00	0.04	0.00	0.00	0.00	0.01	0.01	0.01	0.00
Cr₂O₃	0.25	0.04	0.25	0.31	0.24	0.33	0.21	0.32	0.28
NiO	0.05	0.00	0.00	0.01	0.05	0.07	0.00	0.01	0.01
TOTAL	100.06	100.04	100.96	101.04	100.46	101.34	100.32	101.03	99.94
Si	1.8167	1.7758	1.8168	1.7842	1.8301	1.8064	1.8125	1.7956	1.8220
Al^[4]	0.1177	0.1613	0.1148	0.1438	0.1066	0.1338	0.1063	0.1359	0.1218
Al^[6]	0.0000	0.0000	0.0000	0.0000	0.0000	0.0000	0.0000	0.0000	0.0000
Ti	0.0066	0.0149	0.0006	0.0115	0.0066	0.0076	0.0033	0.0068	0.0021
Fe³⁺	0.1604	0.2423	0.1621	0.1638	0.1591	0.1608	0.1646	0.1639	0.1731
Fe²⁺	0.0000	0.0000	0.0000	0.0000	0.0000	0.0000	0.0000	0.0000	0.0000
Mn	0.0029	0.0051	0.0029	0.0043	0.0042	0.0040	0.0040	0.0030	0.0059
Mg	1.0604	0.9720	1.0632	1.0635	1.0642	1.0477	1.0699	1.0562	1.0433
Cr	0.0070	0.0011	0.0070	0.0089	0.0068	0.0093	0.0061	0.0090	0.0079
Ni	0.0015	0.0000	0.0000	0.0004	0.0013	0.0020	0.0000	0.0003	0.0003
Ca	0.8104	0.7977	0.8142	0.7995	0.7991	0.8060	0.8136	0.8099	0.7994
Na	0.0163	0.0282	0.0183	0.0201	0.0219	0.0222	0.0196	0.0189	0.0241
K	0.0000	0.0016	0.0000	0.0000	0.0000	0.0003	0.0003	0.0005	0.0001
TOTAL	4.0000	4.0000	4.0000	4.0000	4.0000	4.0000	4.0000	4.0000	4.0000
Mg/(Fe^(t)+Mg)	0.8686	0.8004	0.8677	0.8666	0.8700	0.8670	0.8667	0.8657	0.8577

Sample No	AA-11c	AA-11c	AA-11c	AA-11c	AA-11c	AA-11c	AA-11c	AA-11c	AA-11c
Photo Area	General	General	General	General	General	General	General	General	General
Analysis No	81	82	83	85	89	91	93	96	97
SiO₂	51.46	51.47	50.36	50.36	50.91	50.26	50.48	50.41	50.49
TiO₂	0.13	0.00	0.10	0.31	0.27	0.28	0.14	0.32	0.33
Al₂O₃	2.13	1.94	3.28	2.95	2.32	3.47	2.96	3.18	3.12
Fe₂O₃	3.79	3.63	5.29	7.18	7.28	5.26	6.20	5.75	5.54
MnO	0.11	0.08	0.12	0.12	0.16	0.09	0.16	0.12	0.11
MgO	20.66	20.93	19.35	18.97	18.75	19.43	20.51	19.16	19.69
CaO	21.60	21.51	20.23	20.32	19.58	20.87	19.65	21.02	21.19
Na₂O	0.24	0.28	0.32	0.34	0.56	0.30	0.28	0.36	0.23
K₂O	0.01	0.00	0.00	0.02	0.01	0.00	0.02	0.00	0.00
Cr₂O₃	0.97	0.94	0.55	0.26	0.85	0.45	0.38	0.33	0.33
NiO	0.01	0.04	0.03	0.03	0.04	0.05	0.06	0.02	0.01
TOTAL	101.12	100.82	99.62	100.86	100.72	100.46	100.85	100.67	101.04
Si	1.8293	1.8311	1.8243	1.8124	1.8380	1.8056	1.8035	1.8106	1.8045
Al^[4]	0.0892	0.0813	0.1400	0.1251	0.0987	0.1469	0.1246	0.1346	0.1314
Al^[6]	0.0000	0.0000	0.0000	0.0000	0.0000	0.0000	0.0000	0.0000	0.0000
Ti	0.0035	0.0000	0.0027	0.0085	0.0073	0.0075	0.0038	0.0088	0.0089
Fe³⁺	0.1127	0.1080	0.1603	0.2161	0.2198	0.1580	0.1853	0.1727	0.1656
Fe²⁺	0.0000	0.0000	0.0000	0.0000	0.0000	0.0000	0.0000	0.0000	0.0000
Mn	0.0034	0.0023	0.0036	0.0038	0.0050	0.0026	0.0050	0.0036	0.0034
Mg	1.0948	1.1100	1.0450	1.0177	1.0091	1.0406	1.0924	1.0259	1.0491
Cr	0.0274	0.0265	0.0157	0.0075	0.0241	0.0129	0.0108	0.0095	0.0092
Ni	0.0004	0.0011	0.0009	0.0008	0.0012	0.0013	0.0017	0.0005	0.0003
Ca	0.8227	0.8199	0.7852	0.7835	0.7574	0.8033	0.7522	0.8089	0.8114
Na	0.0163	0.0196	0.0224	0.0239	0.0389	0.0210	0.0197	0.0248	0.0162
K	0.0003	0.0000	0.0000	0.0008	0.0004	0.0002	0.0010	0.0000	0.0000
TOTAL	4.0000	4.0000	4.0000	4.0000	4.0000	4.0000	4.0000	4.0000	4.0000
Mg/(Fe^(t)+Mg)	0.9067	0.9113	0.8670	0.8249	0.8211	0.8682	0.8550	0.8559	0.8637

Sample No	AA-11c	AA-11c	AA-12a	AA-12a	AA-12a	AA-12a	AA-12a	AA-12a	AA-12a
Photo Area	General	General	A	A	A	A	A	A	A
Analysis No	98	99	2	3	4	5	7	8	9
SiO₂	50.66	50.53	47.76	48.98	50.33	48.51	48.34	50.97	48.59
TiO₂	0.12	0.19	2.42	1.79	1.37	1.76	2.11	1.25	1.94
Al₂O₃	3.21	3.13	4.63	4.59	3.56	4.50	4.93	2.96	4.41
Fe₂O₃	4.76	4.36	11.88	10.43	9.65	10.34	10.67	9.67	10.42
MnO	0.08	0.12	0.21	0.25	0.18	0.20	0.20	0.21	0.22
MgO	20.17	20.17	11.63	12.78	13.87	12.59	12.34	14.20	12.83
CaO	21.26	21.41	20.67	20.49	20.17	20.38	20.55	20.29	20.39
Na₂O	0.29	0.23	0.45	0.33	0.36	0.42	0.39	0.30	0.39
K₂O	0.00	0.00	0.00	0.00	0.00	0.02	0.02	0.03	0.00
Cr₂O₃	0.53	0.60	0.00	0.03	0.04	0.01	0.00	0.01	0.00
NiO	0.00	0.05	0.01	0.00	0.02	0.05	0.04	0.06	0.04
TOTAL	101.07	100.79	99.68	99.67	99.55	98.77	99.61	99.94	99.22
Si	1.8029	1.8033	1.8103	1.8424	1.8849	1.8401	1.8231	1.9012	1.8353
Al^[4]	0.1346	0.1317	0.1897	0.1576	0.1151	0.1599	0.1769	0.0988	0.1647
Al^[6]	0.0000	0.0000	0.0171	0.0459	0.0420	0.0413	0.0422	0.0313	0.0317
Ti	0.0032	0.0051	0.0690	0.0507	0.0387	0.0502	0.0599	0.0349	0.0551
Fe³⁺	0.1417	0.1301	0.0678	0.0335	0.0202	0.0499	0.0447	0.0204	0.0512
Fe²⁺	0.0000	0.0000	0.3088	0.2946	0.2820	0.2781	0.2918	0.2812	0.2780
Mn	0.0023	0.0036	0.0068	0.0080	0.0057	0.0064	0.0064	0.0066	0.0069
Mg	1.0701	1.0731	0.6572	0.7166	0.7744	0.7119	0.6938	0.7896	0.7224
Cr	0.0149	0.0169	0.0001	0.0010	0.0012	0.0004	0.0000	0.0002	0.0000
Ni	0.0000	0.0014	0.0004	0.0000	0.0006	0.0014	0.0012	0.0018	0.0011
Ca	0.8107	0.8187	0.8395	0.8258	0.8094	0.8283	0.8304	0.8109	0.8252
Na	0.0197	0.0161	0.0332	0.0240	0.0258	0.0310	0.0287	0.0214	0.0284
K	0.0000	0.0000	0.0001	0.0000	0.0000	0.0010	0.0010	0.0016	0.0000
TOTAL	4.0000	4.0000	4.0000	4.0000	4.0000	4.0000	4.0000	4.0000	4.0000
Mg/(Fe^(t)+Mg)	0.8831	0.8918	0.6357	0.6859	0.7193	0.6846	0.6734	0.7236	0.6870

Sample No	AA-12a	AA-12a	AA-12a	AA-12a	AA-12a	AA-12a	AA-12a	AA-12a	AA-12a
Photo Area	A	A	A	A	A	B	B	B	B
Analysis No	11	12	13	14	15	21	22	26	27
SiO₂	48.04	48.97	47.16	48.48	48.81	48.70	48.32	48.13	46.75
TiO₂	2.09	2.10	2.37	2.17	2.04	1.59	1.99	1.93	2.52
Al₂O₃	4.68	3.69	5.89	5.02	3.58	4.70	4.78	5.07	5.58
Fe₂O₃	11.06	11.93	10.65	10.69	13.05	10.13	10.50	10.93	11.94
MnO	0.19	0.28	0.23	0.25	0.26	0.20	0.22	0.22	0.25
MgO	12.13	11.27	12.43	12.57	10.66	12.21	12.31	12.39	11.57
CaO	20.30	20.35	20.02	20.32	20.56	20.89	20.99	20.16	20.03
Na₂O	0.41	0.40	0.36	0.49	0.42	0.40	0.35	0.41	0.44
K₂O	0.00	0.01	0.01	0.00	0.00	0.00	0.00	0.02	0.00
Cr₂O₃	0.04	0.01	0.05	0.02	0.00	0.05	0.04	0.01	0.00
NiO	0.00	0.02	0.00	0.09	0.04	0.01	0.04	0.04	0.02
TOTAL	98.94	99.03	99.17	100.10	99.41	98.90	99.54	99.32	99.09
Si	1.8265	1.8730	1.7843	1.8168	1.8689	1.8465	1.8234	1.8191	1.7811
Al^[4]	0.1735	0.1262	0.2157	0.1832	0.1311	0.1535	0.1766	0.1809	0.2189
Al^[6]	0.0363	0.0402	0.0470	0.0385	0.0304	0.0565	0.0359	0.0450	0.0316
Ti	0.0598	0.0605	0.0675	0.0612	0.0588	0.0455	0.0565	0.0549	0.0722
Fe³⁺	0.0472	0.0000	0.0593	0.0574	0.0147	0.0342	0.0523	0.0569	0.0751
Fe²⁺	0.3045	0.3818	0.2777	0.2777	0.4031	0.2870	0.2790	0.2886	0.3053
Mn	0.0060	0.0091	0.0074	0.0078	0.0083	0.0063	0.0071	0.0072	0.0082
Mg	0.6875	0.6429	0.7011	0.7023	0.6085	0.6902	0.6925	0.6981	0.6571
Cr	0.0011	0.0004	0.0015	0.0007	0.0000	0.0015	0.0011	0.0004	0.0000
Ni	0.0000	0.0006	0.0000	0.0028	0.0012	0.0005	0.0012	0.0013	0.0005
Ca	0.8270	0.8343	0.8116	0.8159	0.8435	0.8487	0.8487	0.8164	0.8176
Na	0.0305	0.0295	0.0266	0.0358	0.0314	0.0296	0.0255	0.0302	0.0323
K	0.0002	0.0007	0.0004	0.0000	0.0002	0.0001	0.0001	0.0010	0.0000
TOTAL	4.0000	3.9992	4.0000	4.0000	4.0000	4.0000	4.0000	4.0000	4.0000
Mg/(Fe^(t)+Mg)	0.6616	0.6274	0.6754	0.6770	0.5928	0.6824	0.6764	0.6689	0.6333

Sample No	AA-12a	AA-12a	AA-12a	AA-12a	AA-12a	AA-12a	AA-12a	AA-12a	AA-12a
Photo Area	B	B	B	B	B	C	C	C	C
Analysis No	28	29	30	32	33	39	40	44	45
SiO₂	48.07	48.51	47.15	48.13	48.67	49.69	49.91	48.39	51.43
TiO₂	2.04	1.86	2.66	2.32	1.74	1.45	1.35	2.06	1.17
Al₂O₃	4.85	4.52	5.13	4.34	4.64	3.48	3.44	4.95	2.43
Fe₂O₃	10.86	11.47	11.89	11.88	10.62	10.83	11.05	10.23	10.04
MnO	0.21	0.26	0.26	0.26	0.24	0.27	0.25	0.24	0.23
MgO	12.26	11.73	11.07	11.32	12.23	11.87	12.25	12.33	14.61
CaO	20.75	20.76	20.52	20.69	20.43	21.11	20.94	21.00	19.79
Na₂O	0.40	0.47	0.48	0.44	0.47	0.39	0.42	0.45	0.27
K₂O	0.01	0.01	0.01	0.00	0.00	0.00	0.01	0.00	0.00
Cr₂O₃	0.07	0.00	0.07	0.00	0.00	0.06	0.02	0.00	0.02
NiO	0.07	0.01	0.00	0.03	0.00	0.03	0.00	0.07	0.04
TOTAL	99.58	99.60	99.23	99.40	99.05	99.16	99.63	99.71	100.04
Si	1.8144	1.8356	1.7989	1.8324	1.8443	1.8876	1.8840	1.8203	1.9168
Al^[4]	0.1856	0.1644	0.2011	0.1676	0.1557	0.1124	0.1160	0.1797	0.0832
Al^[6]	0.0302	0.0371	0.0296	0.0272	0.0515	0.0434	0.0371	0.0398	0.0235
Ti	0.0579	0.0529	0.0764	0.0664	0.0496	0.0414	0.0384	0.0583	0.0327
Fe³⁺	0.0669	0.0562	0.0524	0.0400	0.0394	0.0130	0.0326	0.0560	0.0136
Fe²⁺	0.2759	0.3068	0.3270	0.3383	0.2972	0.3311	0.3162	0.2658	0.2994
Mn	0.0066	0.0085	0.0084	0.0083	0.0077	0.0085	0.0079	0.0076	0.0074
Mg	0.6899	0.6617	0.6296	0.6425	0.6909	0.6722	0.6894	0.6915	0.8117
Cr	0.0021	0.0000	0.0021	0.0000	0.0000	0.0017	0.0005	0.0000	0.0006
Ni	0.0020	0.0004	0.0000	0.0009	0.0000	0.0010	0.0000	0.0020	0.0010
Ca	0.8392	0.8417	0.8389	0.8440	0.8295	0.8592	0.8469	0.8464	0.7903
Na	0.0291	0.0345	0.0353	0.0325	0.0343	0.0284	0.0305	0.0327	0.0198
K	0.0003	0.0002	0.0004	0.0000	0.0000	0.0001	0.0005	0.0000	0.0000
TOTAL	4.0000	4.0000	4.0000	4.0000	4.0000	4.0000	4.0000	4.0000	4.0000
Mg/(Fe^(t)+Mg)	0.6680	0.6458	0.6240	0.6294	0.6724	0.6614	0.6640	0.6824	0.7218

Sample No	AA-12a	AA-12a	AA-12a	AA-12a	AA-12a	AA-12a	AA-12a	AA-12a	AA-12a
Photo Area	C	C	C	C	C	D	D	D	D
Analysis No	46	47	48	49	50	51	52	53	54
SiO₂	49.24	51.27	48.07	48.79	49.42	47.54	47.00	51.33	48.92
TiO₂	1.72	1.06	2.26	1.76	1.68	2.29	2.38	1.11	1.81
Al₂O₃	4.65	2.65	5.25	5.12	3.74	4.87	5.90	2.57	4.60
Fe₂O₃	10.37	9.64	10.15	10.00	11.23	11.90	11.27	9.64	10.13
MnO	0.20	0.21	0.24	0.20	0.27	0.20	0.29	0.20	0.23
MgO	12.85	14.20	12.10	12.46	12.02	11.36	12.13	14.11	12.64
CaO	20.41	20.31	20.55	20.67	20.99	20.89	19.73	20.02	20.91
Na₂O	0.41	0.28	0.51	0.38	0.41	0.59	0.52	0.27	0.52
K₂O	0.00	0.00	0.01	0.00	0.00	0.01	0.00	0.00	0.01
Cr₂O₃	0.02	0.01	0.03	0.01	0.02	0.02	0.00	0.01	0.00
NiO	0.01	0.00	0.02	0.07	0.00	0.03	0.02	0.06	0.03
TOTAL	99.88	99.62	99.19	99.46	99.78	99.71	99.24	99.31	99.81
Si	1.8460	1.9183	1.8183	1.8377	1.8661	1.7999	1.7794	1.9261	1.8345
Al^[4]	0.1540	0.0817	0.1817	0.1623	0.1339	0.2001	0.2206	0.0718	0.1655
Al^[6]	0.0515	0.0352	0.0524	0.0650	0.0325	0.0172	0.0426	0.0419	0.0379
Ti	0.0485	0.0297	0.0643	0.0499	0.0477	0.0652	0.0678	0.0313	0.0511
Fe³⁺	0.0346	0.0067	0.0375	0.0249	0.0353	0.0958	0.0804	0.0000	0.0636
Fe²⁺	0.2906	0.2950	0.2836	0.2901	0.3193	0.2810	0.2764	0.3028	0.2541
Mn	0.0065	0.0068	0.0076	0.0065	0.0086	0.0064	0.0092	0.0063	0.0074
Mg	0.7182	0.7921	0.6823	0.6996	0.6766	0.6412	0.6846	0.7902	0.7066
Cr	0.0005	0.0003	0.0009	0.0002	0.0006	0.0007	0.0000	0.0002	0.0001
Ni	0.0002	0.0000	0.0007	0.0021	0.0000	0.0009	0.0006	0.0018	0.0010
Ca	0.8199	0.8142	0.8329	0.8342	0.8492	0.8474	0.8003	0.8058	0.8402
Na	0.0296	0.0200	0.0374	0.0275	0.0299	0.0436	0.0380	0.0197	0.0378
K	0.0000	0.0000	0.0004	0.0000	0.0002	0.0005	0.0000	0.0000	0.0004
TOTAL	4.0000	4.0000	4.0000	4.0000	4.0000	4.0000	4.0000	3.9979	4.0000
Mg/(Fe^(t)+Mg)	0.6884	0.7242	0.6800	0.6895	0.6561	0.6299	0.6574	0.7229	0.6898

Sample No	AA-12a	AA-12a	AA-12a	AA-12a	AA-12a	AA-12a	AA-12a	AA-12a	AA-12a
Photo Area	D	D	D	D	D	E	E	E	E
Analysis No	55	56	57	58	59	66	67	68	69
SiO₂	47.95	47.92	48.63	51.58	47.23	48.40	48.26	48.26	48.10
TiO₂	2.29	2.12	2.08	1.27	2.49	2.37	2.15	2.14	2.32
Al₂O₃	5.43	5.34	4.73	2.58	5.25	4.27	4.35	5.23	5.31
Fe₂O₃	10.35	11.40	11.07	10.53	11.55	12.14	11.17	10.78	10.12
MnO	0.22	0.28	0.20	0.26	0.19	0.26	0.24	0.17	0.22
MgO	12.15	12.44	11.87	14.13	11.37	11.33	11.78	12.16	12.64
CaO	20.95	19.55	20.58	19.89	21.00	20.42	20.86	20.69	20.75
Na₂O	0.48	0.45	0.56	0.31	0.44	0.43	0.38	0.42	0.40
K₂O	0.00	0.00	0.02	0.01	0.00	0.00	0.00	0.00	0.03
Cr₂O₃	0.02	0.01	0.03	0.01	0.02	0.06	0.00	0.00	0.06
NiO	0.05	0.03	0.00	0.01	0.03	0.00	0.05	0.02	0.00
TOTAL	99.90	99.54	99.76	100.58	99.58	99.68	99.24	99.86	99.95
Si	1.8015	1.8086	1.8337	1.9174	1.7913	1.8397	1.8343	1.8157	1.8033
Al^[4]	0.1985	0.1914	0.1663	0.0826	0.2087	0.1603	0.1657	0.1843	0.1967
Al^[6]	0.0420	0.0462	0.0439	0.0304	0.0260	0.0309	0.0292	0.0476	0.0380
Ti	0.0647	0.0602	0.0590	0.0355	0.0710	0.0678	0.0615	0.0606	0.0654
Fe³⁺	0.0613	0.0577	0.0456	0.0035	0.0728	0.0236	0.0414	0.0462	0.0569
Fe²⁺	0.2639	0.3022	0.3035	0.3239	0.2936	0.3623	0.3136	0.2930	0.2604
Mn	0.0071	0.0088	0.0063	0.0082	0.0061	0.0085	0.0077	0.0053	0.0069
Mg	0.6805	0.6999	0.6673	0.7830	0.6429	0.6420	0.6675	0.6820	0.7065
Cr	0.0007	0.0003	0.0009	0.0003	0.0005	0.0018	0.0000	0.0000	0.0016
Ni	0.0015	0.0010	0.0000	0.0003	0.0010	0.0000	0.0015	0.0005	0.0000
Ca	0.8433	0.7906	0.8315	0.7922	0.8534	0.8316	0.8495	0.8341	0.8335
Na	0.0347	0.0331	0.0413	0.0223	0.0327	0.0315	0.0280	0.0307	0.0292
K	0.0002	0.0000	0.0009	0.0003	0.0000	0.0000	0.0000	0.0000	0.0015
TOTAL	4.0000	4.0000	4.0000	4.0000	4.0000	4.0000	4.0000	4.0000	4.0000
Mg/(Fe^(t)+Mg)	0.6766	0.6605	0.6565	0.7052	0.6370	0.6246	0.6528	0.6679	0.6901

Sample No	AA-12a	AA-12a	AA-12a	AA-12a	AA-12a	AA-12a	AA-12a	AA-12a	AA-12a
Photo Area	E	E	E	E	E	E	E	F	F
Analysis No	70	71	72	73	74	75	76	85	86
SiO₂	48.53	47.38	48.65	49.04	51.61	48.18	47.79	48.61	48.10
TiO₂	2.06	2.54	2.11	1.69	0.91	2.20	2.09	2.11	2.25
Al₂O₃	5.35	5.56	4.70	4.43	2.05	5.29	5.30	4.18	4.50
Fe₂O₃	9.83	10.88	10.81	10.80	11.76	10.91	11.30	11.52	11.96
MnO	0.20	0.21	0.19	0.18	0.31	0.21	0.27	0.24	0.24
MgO	12.70	12.21	11.86	12.31	13.91	12.05	11.79	11.38	11.39
CaO	20.86	20.27	20.81	20.98	18.69	20.84	20.24	21.03	20.21
Na₂O	0.38	0.41	0.53	0.43	0.59	0.40	0.50	0.41	0.53
K₂O	0.00	0.00	0.00	0.01	0.00	0.01	0.00	0.00	0.00
Cr₂O₃	0.08	0.00	0.05	0.00	0.06	0.00	0.00	0.03	0.00
NiO	0.00	0.02	0.04	0.01	0.03	0.02	0.01	0.00	0.00
TOTAL	100.00	99.47	99.74	99.90	99.92	100.13	99.30	99.53	99.19
Si	1.8165	1.7905	1.8350	1.8435	1.9333	1.8099	1.8114	1.8467	1.8329
Al^[4]	0.1835	0.2095	0.1650	0.1565	0.0667	0.1901	0.1886	0.1533	0.1671
Al^[6]	0.0525	0.0381	0.0440	0.0398	0.0238	0.0441	0.0481	0.0338	0.0350
Ti	0.0580	0.0722	0.0599	0.0478	0.0257	0.0622	0.0596	0.0603	0.0645
Fe³⁺	0.0403	0.0568	0.0384	0.0529	0.0322	0.0517	0.0583	0.0285	0.0424
Fe²⁺	0.2674	0.2871	0.3026	0.2866	0.3362	0.2911	0.2999	0.3375	0.3387
Mn	0.0063	0.0069	0.0062	0.0057	0.0099	0.0068	0.0087	0.0079	0.0079
Mg	0.7087	0.6879	0.6669	0.6899	0.7768	0.6748	0.6662	0.6445	0.6470
Cr	0.0024	0.0000	0.0014	0.0000	0.0019	0.0000	0.0000	0.0010	0.0000
Ni	0.0000	0.0005	0.0011	0.0005	0.0009	0.0007	0.0003	0.0000	0.0000
Ca	0.8366	0.8207	0.8410	0.8450	0.7501	0.8388	0.8220	0.8560	0.8251
Na	0.0278	0.0297	0.0386	0.0312	0.0425	0.0294	0.0368	0.0305	0.0393
K	0.0000	0.0001	0.0000	0.0006	0.0000	0.0005	0.0001	0.0000	0.0000
TOTAL	4.0000	4.0000	4.0000	4.0000	4.0000	4.0000	4.0000	4.0000	4.0000
Mg/(Fe^(t)+Mg)	0.6972	0.6667	0.6617	0.6702	0.6783	0.6632	0.6503	0.6378	0.6293

Sample No	AA-12a	AA-12a	AA-12a	AA-12a	AA-12a	AA-12a	AA-12a	AA-12a	AA-12a
Photo Area	F	F	F	F	F	F	F	F	G
Analysis No	87	88	89	90	91	92	93	94	102
SiO₂	48.01	48.39	48.04	48.67	48.85	48.58	48.01	47.99	45.72
TiO₂	2.36	2.00	2.35	2.25	1.84	1.98	2.10	2.20	2.41
Al₂O₃	4.14	4.39	4.48	4.10	4.57	4.68	4.75	4.75	6.09
Fe₂O₃	12.59	11.94	11.92	12.65	10.47	11.02	10.46	11.02	12.24
MnO	0.30	0.28	0.24	0.31	0.19	0.26	0.22	0.19	0.22
MgO	11.02	11.23	11.35	10.59	12.22	12.27	12.37	11.56	11.19
CaO	20.51	20.31	20.75	20.14	20.98	20.47	20.90	20.90	18.44
Na₂O	0.46	0.47	0.46	0.74	0.37	0.50	0.39	0.52	0.45
K₂O	0.00	0.00	0.01	0.00	0.00	0.00	0.01	0.02	0.03
Cr₂O₃	0.00	0.02	0.04	0.07	0.02	0.00	0.04	0.02	0.04
NiO	0.00	0.01	0.00	0.01	0.00	0.02	0.04	0.00	0.02
TOTAL	99.40	99.05	99.64	99.52	99.51	99.78	99.30	99.16	96.85
Si	1.8333	1.8481	1.8241	1.8560	1.8439	1.8292	1.8152	1.8231	1.7838
Al^[4]	0.1667	0.1519	0.1759	0.1440	0.1561	0.1708	0.1848	0.1769	0.2162
Al^[6]	0.0196	0.0457	0.0246	0.0403	0.0472	0.0369	0.0269	0.0358	0.0638
Ti	0.0678	0.0575	0.0671	0.0645	0.0523	0.0561	0.0597	0.0629	0.0707
Fe³⁺	0.0459	0.0254	0.0501	0.0270	0.0311	0.0584	0.0665	0.0542	0.0447
Fe²⁺	0.3562	0.3559	0.3284	0.3765	0.2994	0.2886	0.2642	0.2960	0.3547
Mn	0.0097	0.0092	0.0077	0.0101	0.0061	0.0081	0.0069	0.0062	0.0072
Mg	0.6273	0.6394	0.6425	0.6020	0.6876	0.6887	0.6972	0.6547	0.6509
Cr	0.0000	0.0007	0.0011	0.0021	0.0006	0.0000	0.0013	0.0005	0.0014
Ni	0.0000	0.0003	0.0000	0.0002	0.0000	0.0006	0.0011	0.0000	0.0007
Ca	0.8391	0.8311	0.8442	0.8229	0.8485	0.8258	0.8467	0.8507	0.7709
Na	0.0342	0.0348	0.0338	0.0544	0.0272	0.0367	0.0289	0.0385	0.0338
K	0.0001	0.0001	0.0004	0.0000	0.0000	0.0000	0.0005	0.0008	0.0013
TOTAL	4.0000	4.0000	4.0000	4.0000	4.0000	4.0000	4.0000	4.0000	4.0000
Mg/(Fe^(t)+Mg)	0.6094	0.6264	0.6293	0.5988	0.6754	0.6650	0.6783	0.6516	0.6197

Sample No	AA-12a	AA-12a	AA-12a	AA-12a	AA-12a	AA-12a	AA-12a	AA-12a	AA-12a
Photo Area	G	G	G	G	G	G	G	G	G
Analysis No	103	104	105	106	107	108	109	110	111
SiO₂	48.09	49.20	49.28	49.82	48.94	49.01	47.91	48.63	47.18
TiO₂	2.27	1.92	1.92	1.70	1.99	1.80	2.17	2.01	2.63
Al₂O₃	4.42	3.89	3.66	3.25	4.02	4.19	5.39	4.76	5.47
Fe₂O₃	11.76	11.66	12.46	11.96	11.68	10.74	10.27	11.12	10.76
MnO	0.24	0.36	0.29	0.26	0.29	0.21	0.20	0.20	0.27
MgO	11.50	11.35	10.80	11.20	11.44	11.96	11.95	12.25	12.09
CaO	20.84	20.25	21.14	21.17	21.32	21.24	20.64	20.58	20.29
Na₂O	0.44	1.06	0.45	0.60	0.46	0.39	0.46	0.51	0.48
K₂O	0.00	0.00	0.03	0.00	0.00	0.00	0.02	0.00	0.02
Cr₂O₃	0.01	0.00	0.01	0.00	0.06	0.00	0.04	0.05	0.04
NiO	0.06	0.00	0.03	0.00	0.00	0.00	0.00	0.00	0.00
TOTAL	99.63	99.68	100.06	99.96	100.20	99.55	99.06	100.11	99.22
Si	1.8246	1.8574	1.8703	1.8855	1.8464	1.8527	1.8160	1.8255	1.7876
Al^[4]	0.1754	0.1426	0.1297	0.1145	0.1536	0.1473	0.1840	0.1745	0.2124
Al^[6]	0.0222	0.0305	0.0340	0.0305	0.0252	0.0394	0.0567	0.0361	0.0319
Ti	0.0648	0.0545	0.0548	0.0484	0.0565	0.0512	0.0619	0.0568	0.0750
Fe³⁺	0.0556	0.0805	0.0201	0.0309	0.0472	0.0344	0.0373	0.0602	0.0654
Fe²⁺	0.3175	0.2877	0.3754	0.3476	0.3213	0.3052	0.2882	0.2889	0.2755
Mn	0.0077	0.0114	0.0094	0.0084	0.0094	0.0068	0.0063	0.0063	0.0085
Mg	0.6505	0.6388	0.6110	0.6319	0.6434	0.6740	0.6752	0.6855	0.6829
Cr	0.0004	0.0000	0.0003	0.0000	0.0017	0.0000	0.0011	0.0015	0.0012
Ni	0.0018	0.0000	0.0010	0.0000	0.0000	0.0000	0.0000	0.0000	0.0000
Ca	0.8472	0.8191	0.8596	0.8585	0.8618	0.8603	0.8382	0.8278	0.8237
Na	0.0324	0.0775	0.0329	0.0438	0.0335	0.0287	0.0340	0.0369	0.0349
K	0.0000	0.0000	0.0014	0.0000	0.0000	0.0001	0.0009	0.0000	0.0011
TOTAL	4.0000	4.0000	4.0000	4.0000	4.0000	4.0000	4.0000	4.0000	4.0000
Mg/(Fe^(t)+Mg)	0.6355	0.6344	0.6071	0.6254	0.6358	0.6650	0.6747	0.6626	0.6670

Sample No	AA-12a	AA-12a	AA-12a	AA-12a	AA-12a	AA-12a	AA-12a	AA-12a	AA-12a
Photo Area	G	G	G	G	G	G	G	G	G
Analysis No	112	113	114	115	116	117	118	119	120
SiO₂	49.03	48.97	51.50	50.87	48.98	46.35	49.54	51.91	49.24
TiO₂	1.99	1.91	1.19	1.15	1.72	9.32	1.65	1.02	1.59
Al₂O₃	3.68	3.74	2.16	2.85	4.93	2.38	4.00	2.18	4.47
Fe₂O₃	12.55	12.17	11.53	10.82	10.00	8.85	11.27	10.20	10.23
MnO	0.27	0.29	0.32	0.25	0.19	0.25	0.28	0.26	0.21
MgO	11.09	10.91	13.21	13.06	12.65	10.06	11.94	13.76	12.68
CaO	20.71	20.72	20.42	20.36	20.69	21.75	20.33	19.74	20.50
Na₂O	0.40	0.43	0.34	0.49	0.40	0.33	0.84	0.62	0.45
K₂O	0.01	0.00	0.00	0.02	0.02	0.00	0.00	0.00	0.01
Cr₂O₃	0.00	0.00	0.05	0.00	0.00	0.00	0.04	0.00	0.00
NiO	0.00	0.00	0.02	0.00	0.02	0.00	0.02	0.02	0.00
TOTAL	99.73	99.14	100.73	99.86	99.61	99.29	99.92	99.71	99.38
Si	1.8659	1.8737	1.9228	1.9088	1.8405	1.7695	1.8619	1.9428	1.8550
Al^[4]	0.1341	0.1263	0.0772	0.0912	0.1595	0.1092	0.1381	0.0572	0.1450
Al^[6]	0.0310	0.0424	0.0179	0.0348	0.0588	0.0000	0.0391	0.0389	0.0534
Ti	0.0570	0.0550	0.0334	0.0323	0.0486	0.2730	0.0466	0.0287	0.0451
Fe³⁺	0.0195	0.0060	0.0156	0.0279	0.0334	0.0000	0.0659	0.0060	0.0344
Fe²⁺	0.3799	0.3835	0.3444	0.3117	0.2808	0.2882	0.2884	0.3132	0.2879
Mn	0.0086	0.0095	0.0100	0.0079	0.0060	0.0081	0.0090	0.0082	0.0066
Mg	0.6292	0.6223	0.7353	0.7306	0.7086	0.5840	0.6690	0.7677	0.7121
Cr	0.0000	0.0000	0.0014	0.0000	0.0001	0.0000	0.0013	0.0000	0.0000
Ni	0.0000	0.0000	0.0007	0.0000	0.0005	0.0000	0.0007	0.0005	0.0000
Ca	0.8445	0.8494	0.8169	0.8186	0.8330	0.9075	0.8187	0.7916	0.8275
Na	0.0298	0.0320	0.0245	0.0355	0.0290	0.0248	0.0614	0.0451	0.0327
K	0.0005	0.0000	0.0000	0.0007	0.0011	0.0002	0.0000	0.0000	0.0003
TOTAL	4.0000	4.0000	4.0000	4.0000	4.0000	3.9646	4.0000	4.0000	4.0000
Mg/(Fe^(t)+Mg)	0.6117	0.6151	0.6713	0.6827	0.6928	0.6696	0.6538	0.7063	0.6884

Sample No	AA-12a	AA-12a	AA-12a	AA-12a	AA-12a	AA-12a	AA-12a	AA-12a	AA-12a
Photo Area	H	H	H	H	H	H	H	H	H
Analysis No	126	127	128	129	130	131	132	133	134
SiO₂	47.31	48.90	49.25	48.09	49.45	48.72	48.48	49.38	49.04
TiO₂	2.37	1.76	1.64	2.16	1.54	2.03	2.00	1.78	1.71
Al₂O₃	5.62	4.65	4.50	5.00	4.38	5.09	5.05	4.09	4.29
Fe₂O₃	11.74	10.35	10.02	10.57	10.41	10.20	10.11	11.54	11.77
MnO	0.26	0.22	0.21	0.18	0.27	0.25	0.19	0.33	0.26
MgO	11.41	12.84	12.99	12.31	13.39	12.89	12.46	11.73	11.72
CaO	19.81	20.72	20.68	20.84	19.79	20.61	20.97	20.42	20.07
Na₂O	0.71	0.42	0.39	0.45	0.42	0.37	0.45	0.87	0.84
K₂O	0.00	0.00	0.01	0.02	0.00	0.00	0.01	0.01	0.00
Cr₂O₃	0.00	0.02	0.04	0.02	0.00	0.02	0.00	0.02	0.02
NiO	0.01	0.00	0.00	0.05	0.09	0.00	0.02	0.02	0.00
TOTAL	99.24	99.88	99.74	99.69	99.74	100.16	99.74	100.18	99.73
Si	1.7959	1.8330	1.8466	1.8107	1.8529	1.8210	1.8209	1.8535	1.8493
Al^[4]	0.2041	0.1670	0.1534	0.1893	0.1471	0.1790	0.1791	0.1465	0.1507
Al^[6]	0.0473	0.0384	0.0455	0.0326	0.0463	0.0452	0.0445	0.0345	0.0400
Ti	0.0677	0.0496	0.0463	0.0612	0.0435	0.0571	0.0565	0.0503	0.0485
Fe³⁺	0.0738	0.0588	0.0431	0.0674	0.0441	0.0460	0.0546	0.0748	0.0745
Fe²⁺	0.2989	0.2656	0.2711	0.2655	0.2821	0.2728	0.2629	0.2875	0.2967
Mn	0.0082	0.0069	0.0068	0.0056	0.0085	0.0078	0.0061	0.0104	0.0083
Mg	0.6457	0.7175	0.7261	0.6910	0.7480	0.7182	0.6977	0.6564	0.6589
Cr	0.0000	0.0007	0.0012	0.0006	0.0000	0.0005	0.0000	0.0005	0.0007
Ni	0.0003	0.0000	0.0000	0.0017	0.0028	0.0000	0.0007	0.0006	0.0000
Ca	0.8057	0.8322	0.8308	0.8408	0.7945	0.8254	0.8439	0.8213	0.8109
Na	0.0522	0.0302	0.0287	0.0326	0.0302	0.0269	0.0325	0.0632	0.0615
K	0.0002	0.0000	0.0004	0.0012	0.0000	0.0000	0.0006	0.0006	0.0000
TOTAL	4.0000	4.0000	4.0000	4.0000	4.0000	4.0000	4.0000	4.0000	4.0000
Mg/(Fe^(t)+Mg)	0.6340	0.6886	0.6980	0.6749	0.6963	0.6926	0.6872	0.6444	0.6396

Sample No	AA-12a	AA-12a	AA-12a	AA-14	AA-14	AA-14	AA-14	AA-14	AA-14
Photo Area	H	H	I	A	A	A	A	A	A
Analysis No	135	136	143	1	2	3	4	6	7
SiO₂	49.09	48.54	53.16	51.16	50.46	51.12	48.94	52.40	50.49
TiO₂	1.84	2.10	0.01	1.38	1.41	1.16	1.78	0.70	0.79
Al₂O₃	4.41	4.68	1.27	3.54	4.73	3.75	2.49	2.86	2.82
Fe₂O₃	10.64	10.77	16.98	8.80	6.87	6.74	14.48	5.53	8.65
MnO	0.26	0.20	0.32	0.19	0.10	0.12	0.34	0.09	0.20
MgO	12.39	12.04	7.16	15.44	15.40	15.30	11.51	15.62	13.28
CaO	20.93	20.37	14.96	18.89	20.26	20.67	18.67	21.95	18.09
Na₂O	0.41	0.37	5.27	0.27	0.28	0.29	0.34	0.31	0.35
K₂O	0.01	0.00	0.00	0.01	0.00	0.01	0.01	0.00	0.06
Cr₂O₃	0.01	0.02	0.00	0.04	0.74	0.29	0.00	0.81	0.60
NiO	0.02	0.04	0.02	0.02	0.04	0.10	0.07	0.05	0.02
TOTAL	100.01	99.12	99.15	99.72	100.3	99.54	98.62	100.32	95.36
Si	1.8433	1.8430	2.0000	1.8975	1.8559	1.8931	1.8914	1.9203	1.9565
Al^[4]	0.1567	0.1570	0.0000	0.1005	0.1441	0.1065	0.1086	0.0787	0.0245
Al^[6]	0.0385	0.0524	0.0565	0.0544	0.0609	0.0572	0.0048	0.0449	0.1055
Ti	0.0520	0.0600	0.0002	0.0386	0.0391	0.0322	0.0518	0.0194	0.0232
Fe³⁺	0.0443	0.0112	0.3191	0.0000	0.0037	0.0000	0.0263	0.0000	0.0000
Fe²⁺	0.2898	0.3307	0.2165	0.2733	0.2076	0.2088	0.4417	0.1696	0.2830
Mn	0.0083	0.0065	0.0103	0.0060	0.0033	0.0039	0.0113	0.0027	0.0067
Mg	0.6936	0.6815	0.4025	0.8546	0.8444	0.8448	0.6631	0.8538	0.7746
Cr	0.0004	0.0006	0.0000	0.0013	0.0214	0.0085	0.0000	0.0236	0.0185
Ni	0.0006	0.0013	0.0005	0.0005	0.0010	0.0030	0.0021	0.0014	0.0008
Ca	0.8421	0.8287	0.6045	0.7515	0.7984	0.8203	0.7731	0.8623	0.7584
Na	0.0301	0.0272	0.3853	0.0196	0.0200	0.0206	0.0255	0.0223	0.0263
K	0.0004	0.0000	0.0000	0.0002	0.0001	0.0006	0.0004	0.0000	0.0030
TOTAL	4.0000	4.0000	3.9953	3.9980	4.0000	3.9996	4.0000	3.9990	3.9810
Mg/(Fe^(t)+Mg)	0.6749	0.6659	0.4291	0.7577	0.7998	0.8018	0.5863	0.8343	0.7324

Sample No	AA-14	AA-14	AA-14	AA-14	AA-14	AA-14	AA-14	AA-14	AA-14
Photo Area	A	A	A	A	A	B	B	B	B
Analysis No	8	9	11	12	13	14	16	18	19
SiO₂	52.03	52.08	51.90	51.64	51.80	52.15	52.50	52.04	49.36
TiO₂	0.72	0.71	0.68	1.09	0.65	0.78	0.91	0.91	1.78
Al₂O₃	3.15	3.21	3.08	3.14	3.23	2.71	2.38	3.29	5.79
Fe₂O₃	5.84	4.67	4.48	7.32	4.87	5.13	6.05	5.55	6.02
MnO	0.10	0.14	0.08	0.16	0.10	0.12	0.16	0.15	0.18
MgO	15.50	15.42	15.66	15.56	15.32	15.51	16.10	15.28	14.16
CaO	21.49	21.88	21.89	20.33	22.03	22.19	21.09	21.87	21.81
Na₂O	0.22	0.33	0.31	0.27	0.26	0.26	0.22	0.27	0.30
K₂O	0.02	0.00	0.02	0.01	0.03	0.01	0.02	0.02	0.00
Cr₂O₃	0.71	0.94	1.00	0.19	0.89	0.43	0.10	0.34	0.61
NiO	0.03	0.09	0.00	0.00	0.00	0.01	0.11	0.05	0.07
TOTAL	99.79	99.47	99.09	99.72	99.18	99.29	99.63	99.77	100.08
Si	1.9165	1.9185	1.9179	1.9102	1.9160	1.9277	1.9349	1.9159	1.8229
Al^[4]	0.0802	0.0768	0.0789	0.0890	0.0804	0.0698	0.0628	0.0804	0.1771
Al^[6]	0.0568	0.0629	0.0555	0.0480	0.0607	0.0484	0.0407	0.0626	0.0749
Ti	0.0199	0.0199	0.0188	0.0304	0.0181	0.0218	0.0252	0.0254	0.0495
Fe³⁺	0.0000	0.0000	0.0000	0.0000	0.0000	0.0000	0.0000	0.0000	0.0071
Fe²⁺	0.1802	0.1442	0.1387	0.2265	0.1509	0.1588	0.1867	0.1712	0.1788
Mn	0.0031	0.0042	0.0024	0.0049	0.0030	0.0036	0.0049	0.0046	0.0057
Mg	0.8526	0.8489	0.8641	0.8584	0.8464	0.8558	0.8856	0.8402	0.7796
Cr	0.0206	0.0276	0.0292	0.0055	0.0261	0.0125	0.0030	0.0101	0.0178
Ni	0.0008	0.0026	0.0000	0.0000	0.0001	0.0002	0.0031	0.0016	0.0022
Ca	0.8496	0.8657	0.8682	0.8061	0.8747	0.8800	0.8338	0.8644	0.8630
Na	0.0156	0.0239	0.0224	0.0196	0.0187	0.0185	0.0160	0.0191	0.0215
K	0.0008	0.0000	0.0008	0.0006	0.0013	0.0003	0.0010	0.0007	0.0000
TOTAL	3.9967	3.9953	3.9968	3.9992	3.9964	3.9974	3.9977	3.9963	4.0000
Mg/(Fe^(t)+Mg)	0.8255	0.8548	0.8617	0.7912	0.8487	0.8435	0.8259	0.8307	0.8074

Sample No	AA-14	AA-14	AA-14	AA-14	AA-14	AA-14	AA-14	AA-14	AA-14
Photo Area	B	B	C	C	C	C	C	C	C
Analysis No	20	21	24	25	26	27	29	32	34
SiO₂	52.13	52.51	51.60	51.78	51.83	53.17	53.10	53.59	50.95
TiO₂	0.80	0.66	1.12	1.17	0.98	0.75	0.77	0.71	1.13
Al₂O₃	3.21	2.36	3.49	3.47	3.31	2.32	1.94	1.94	3.46
Fe₂O₃	4.81	6.91	6.22	6.03	5.90	5.82	6.15	6.37	6.28
MnO	0.13	0.21	0.13	0.12	0.14	0.16	0.15	0.15	0.11
MgO	15.42	15.38	15.27	15.24	15.06	15.52	15.98	15.87	15.10
CaO	22.38	20.89	21.59	21.92	21.89	22.22	21.58	21.58	22.20
Na₂O	0.28	0.30	0.30	0.24	0.25	0.32	0.22	0.30	0.25
K₂O	0.00	0.02	0.00	0.00	0.00	0.00	0.00	0.00	0.02
Cr₂O₃	1.05	0.57	0.09	0.13	0.14	0.08	0.14	0.10	0.16
NiO	0.04	0.03	0.02	0.02	0.01	0.06	0.00	0.08	0.04
TOTAL	100.26	99.83	99.83	100.11	99.51	100.42	100.03	100.7	99.71
Si	1.9096	1.9395	1.9031	1.9036	1.9154	1.9455	1.9501	1.9559	1.8836
Al^[4]	0.0873	0.0573	0.0965	0.0943	0.0810	0.0516	0.0463	0.0403	0.1164
Al^[6]	0.0515	0.0456	0.0552	0.0562	0.0634	0.0486	0.0379	0.0434	0.0344
Ti	0.0222	0.0183	0.0312	0.0324	0.0273	0.0208	0.0212	0.0196	0.0314
Fe³⁺	0.0000	0.0000	0.0000	0.0000	0.0000	0.0000	0.0000	0.0000	0.0337
Fe²⁺	0.1476	0.2138	0.1919	0.1856	0.1827	0.1784	0.1892	0.1948	0.1605
Mn	0.0041	0.0064	0.0041	0.0038	0.0043	0.0051	0.0047	0.0047	0.0036
Mg	0.8434	0.8482	0.8397	0.8362	0.8312	0.8478	0.8765	0.8652	0.8322
Cr	0.0303	0.0166	0.0026	0.0038	0.0040	0.0022	0.0041	0.0029	0.0047
Ni	0.0012	0.0009	0.0006	0.0006	0.0004	0.0017	0.0000	0.0025	0.0011
Ca	0.8798	0.8281	0.8533	0.8644	0.8684	0.8724	0.8507	0.8456	0.8794
Na	0.0196	0.0213	0.0214	0.0170	0.0182	0.0230	0.0156	0.0213	0.0182
K	0.0002	0.0007	0.0000	0.0000	0.0002	0.0000	0.0000	0.0001	0.0009
TOTAL	3.9970	3.9968	3.9997	3.9979	3.9964	3.9971	3.9963	3.9961	4.0000
Mg/(Fe^(t)+Mg)	0.8511	0.7987	0.8140	0.8184	0.8198	0.8262	0.8224	0.8162	0.8108

Sample No	AA-14	AA-14	AA-14	AA-14	AA-14	AA-14	AA-14	AA-14	AA-14
Photo Area	C	C	D	D	D	D	D	E	E
Analysis No	37	38	40	41	42	43	46	52	53
SiO₂	53.47	52.68	51.83	52.01	52.76	53.21	51.68	53.03	53.02
TiO₂	0.52	0.56	0.91	1.01	0.77	0.75	1.04	0.78	0.87
Al₂O₃	1.94	2.91	3.02	2.95	2.01	1.92	3.48	2.00	1.98
Fe₂O₃	4.36	4.25	6.17	6.07	5.99	5.69	6.66	6.76	6.36
MnO	0.12	0.13	0.13	0.14	0.14	0.15	0.15	0.11	0.16
MgO	16.60	16.17	15.05	15.24	15.92	15.98	15.08	15.93	15.71
CaO	22.41	22.22	22.18	22.02	21.62	21.66	21.89	21.44	21.15
Na₂O	0.18	0.23	0.31	0.31	0.23	0.22	0.28	0.25	0.25
K₂O	0.02	0.00	0.00	0.00	0.00	0.00	0.01	0.00	0.00
Cr₂O₃	0.35	0.63	0.06	0.13	0.12	0.07	0.05	0.08	0.00
NiO	0.04	0.06	0.06	0.01	0.00	0.03	0.01	0.02	0.06
TOTAL	100.01	99.83	99.73	99.9	99.56	99.66	100.32	100.4	99.56
Si	1.9527	1.9281	1.9154	1.9177	1.9465	1.9565	1.9002	1.9451	1.9555
Al^[4]	0.0438	0.0686	0.0846	0.0821	0.0510	0.0374	0.0998	0.0540	0.0376
Al^[6]	0.0398	0.0572	0.0470	0.0461	0.0365	0.0460	0.0510	0.0325	0.0487
Ti	0.0144	0.0154	0.0253	0.0279	0.0215	0.0209	0.0288	0.0215	0.0243
Fe³⁺	0.0000	0.0000	0.0071	0.0000	0.0000	0.0000	0.0100	0.0000	0.0000
Fe²⁺	0.1334	0.1303	0.1836	0.1872	0.1851	0.1755	0.1948	0.2075	0.1969
Mn	0.0036	0.0039	0.0041	0.0043	0.0043	0.0046	0.0047	0.0035	0.0051
Mg	0.9054	0.8838	0.8291	0.8378	0.8767	0.8787	0.8266	0.8715	0.8668
Cr	0.0101	0.0181	0.0018	0.0039	0.0035	0.0019	0.0014	0.0022	0.0000
Ni	0.0012	0.0019	0.0018	0.0004	0.0000	0.0009	0.0002	0.0007	0.0016
Ca	0.8784	0.8729	0.8783	0.8700	0.8557	0.8560	0.8624	0.8430	0.8387
Na	0.0127	0.0164	0.0219	0.0223	0.0167	0.0155	0.0198	0.0177	0.0178
K	0.0009	0.0002	0.0000	0.0002	0.0000	0.0000	0.0004	0.0000	0.0000
TOTAL	3.9965	3.9966	4.0000	3.9998	3.9975	3.9940	4.0000	3.9990	3.9932
Mg/(Fe^(t)+Mg)	0.8716	0.8715	0.8130	0.8174	0.8257	0.8335	0.8014	0.8077	0.8149

Sample No	AA-14	AA-14	AA-14	AA-14	AA-14	AA-14	AA-14	AA-14	AA-14
Photo Area	E	E	E	E	F	F	F	F	G
Analysis No	54	62	63	64	68	69	70	73	75
SiO₂	53.04	52.44	50.63	52.53	51.91	51.41	53.17	48.88	52.37
TiO₂	0.73	1.07	1.50	0.95	1.12	1.16	0.76	2.21	0.77
Al₂O₃	1.97	3.42	4.63	3.16	3.49	3.57	1.96	5.98	3.12
Fe₂O₃	6.50	6.13	6.73	6.14	6.32	6.15	5.88	6.46	5.06
MnO	0.12	0.09	0.14	0.14	0.14	0.11	0.11	0.08	0.15
MgO	15.70	15.20	14.88	15.44	15.19	15.11	16.09	13.67	15.50
CaO	21.44	22.01	21.14	21.98	21.66	21.89	21.86	21.45	22.13
Na₂O	0.28	0.28	0.31	0.30	0.27	0.31	0.22	0.45	0.31
K₂O	0.00	0.00	0.00	0.00	0.02	0.00	0.00	0.01	0.00
Cr₂O₃	0.05	0.15	0.19	0.14	0.18	0.20	0.08	0.50	0.73
NiO	0.06	0.07	0.02	0.05	0.11	0.02	0.03	0.06	0.03
TOTAL	99.89	100.87	100.17	100.81	100.42	99.93	100.17	99.75	100.16
Si	1.9530	1.9129	1.8656	1.9173	1.9047	1.8956	1.9487	1.8145	1.9185
Al^[4]	0.0438	0.0833	0.1344	0.0814	0.0935	0.1044	0.0486	0.1855	0.0783
Al^[6]	0.0419	0.0640	0.0667	0.0547	0.0576	0.0507	0.0361	0.0761	0.0567
Ti	0.0203	0.0293	0.0417	0.0261	0.0311	0.0322	0.0211	0.0617	0.0212
Fe³⁺	0.0000	0.0000	0.0006	0.0000	0.0000	0.0057	0.0000	0.0042	0.0000
Fe²⁺	0.2005	0.1874	0.2068	0.1876	0.1941	0.1839	0.1805	0.1963	0.1553
Mn	0.0038	0.0029	0.0043	0.0044	0.0043	0.0036	0.0036	0.0026	0.0046
Mg	0.8632	0.8282	0.8174	0.8407	0.8317	0.8306	0.8803	0.7565	0.8479
Cr	0.0013	0.0045	0.0056	0.0040	0.0053	0.0058	0.0023	0.0147	0.0213
Ni	0.0018	0.0020	0.0005	0.0016	0.0033	0.0005	0.0010	0.0018	0.0010
Ca	0.8473	0.8620	0.8346	0.8602	0.8523	0.8648	0.8596	0.8531	0.8701
Na	0.0200	0.0198	0.0218	0.0209	0.0195	0.0222	0.0155	0.0326	0.0219
K	0.0000	0.0000	0.0000	0.0000	0.0008	0.0000	0.0000	0.0003	0.0000
TOTAL	3.9967	3.9962	4.0000	3.9986	3.9982	4.0000	3.9973	4.0000	3.9968
Mg/(Fe^(t)+Mg)	0.8115	0.8155	0.7976	0.8176	0.8108	0.8141	0.8299	0.7904	0.8452

Sample No	AA-14	AA-14	AA-14	AA-14	AA-14	AA-14	AA-14	AA-14	AA-14
Photo Area	G	G	G	G	G	G	G	H	H
Analysis No	76	77	78	80	81	82	83	84	85
SiO₂	53.66	53.35	53.36	54.32	52.11	53.35	52.97	50.88	53.00
TiO₂	0.68	0.66	0.73	1.10	0.83	0.59	0.74	1.64	0.91
Al₂O₃	2.16	2.74	2.72	1.37	3.32	2.18	2.77	3.00	2.06
Fe₂O₃	5.41	4.92	5.05	12.66	5.17	5.01	5.05	9.00	6.89
MnO	0.09	0.15	0.12	0.23	0.15	0.14	0.11	0.19	0.16
MgO	16.09	16.09	15.98	14.84	15.56	16.27	16.13	13.54	15.71
CaO	21.96	22.20	22.19	12.09	22.07	22.17	22.45	21.54	21.50
Na₂O	0.27	0.22	0.24	0.58	0.26	0.25	0.22	0.40	0.30
K₂O	0.02	0.00	0.01	0.22	0.00	0.00	0.00	0.02	0.01
Cr₂O₃	0.19	0.44	0.39	0.04	0.72	0.53	0.34	0.00	0.00
NiO	0.08	0.06	0.00	0.03	0.06	0.01	0.02	0.04	0.02
TOTAL	100.63	100.82	100.79	97.49	100.26	100.51	100.8	100.24	100.56
Si	1.9530	1.9360	1.9374	2.0000	1.9090	1.9441	1.9262	1.8944	1.9428
Al^[4]	0.0417	0.0586	0.0564	0.0000	0.0888	0.0529	0.0725	0.1056	0.0564
Al^[6]	0.0512	0.0589	0.0604	0.0619	0.0547	0.0409	0.0463	0.0260	0.0326
Ti	0.0187	0.0182	0.0200	0.0319	0.0230	0.0163	0.0202	0.0458	0.0250
Fe³⁺	0.0000	0.0000	0.0000	0.0000	0.0000	0.0000	0.0000	0.0179	0.0000
Fe²⁺	0.1651	0.1497	0.1538	0.4069	0.1586	0.1529	0.1537	0.2624	0.2113
Mn	0.0029	0.0046	0.0037	0.0076	0.0047	0.0043	0.0033	0.0061	0.0050
Mg	0.8754	0.8729	0.8677	0.8501	0.8508	0.8852	0.8750	0.7515	0.8588
Cr	0.0055	0.0126	0.0113	0.0013	0.0208	0.0154	0.0098	0.0000	0.0001
Ni	0.0023	0.0017	0.0000	0.0009	0.0016	0.0003	0.0005	0.0012	0.0007
Ca	0.8587	0.8656	0.8660	0.4978	0.8673	0.8669	0.8753	0.8593	0.8448
Na	0.0190	0.0158	0.0168	0.0436	0.0185	0.0175	0.0158	0.0291	0.0212
K	0.0011	0.0000	0.0003	0.0106	0.0000	0.0002	0.0001	0.0008	0.0005
TOTAL	3.9947	3.9946	3.9938	3.9126	3.9978	3.9970	3.9987	4.0000	3.9993
Mg/(Fe^(t)+Mg)	0.8413	0.8536	0.8494	0.6763	0.8429	0.8527	0.8506	0.7284	0.8025

Sample No	AA-14	AA-14	AA-14	AA-14	AA-14	AA-14	AA-14	AA-14	AA-14
Photo Area	H	H	H	H	H	I	I	I	J
Analysis No	86	87	88	90	91	100	101	102	105
SiO₂	51.27	52.10	53.07	51.92	52.42	52.16	51.99	51.50	53.47
TiO₂	1.46	1.12	0.96	1.37	1.05	0.81	0.87	1.47	0.74
Al₂O₃	3.80	1.97	2.10	2.38	2.14	3.27	3.30	3.62	1.95
Fe₂O₃	6.99	9.69	6.96	8.67	7.82	4.73	4.89	5.16	6.40
MnO	0.20	0.28	0.18	0.22	0.25	0.10	0.11	0.12	0.15
MgO	14.66	13.63	15.57	14.19	15.05	15.55	15.45	14.78	15.97
CaO	22.00	21.61	21.71	21.28	21.36	22.59	22.58	22.19	21.62
Na₂O	0.29	0.46	0.29	0.35	0.30	0.33	0.33	0.43	0.25
K₂O	0.02	0.02	0.00	0.01	0.00	0.01	0.00	0.02	0.00
Cr₂O₃	0.08	0.00	0.03	0.03	0.02	0.78	0.89	0.87	0.04
NiO	0.05	0.01	0.01	0.00	0.00	0.00	0.01	0.07	0.03
TOTAL	100.81	100.9	100.87	100.43	100.42	100.33	100.42	100.23	100.62
Si	1.8820	1.9296	1.9408	1.9242	1.9341	1.9084	1.9027	1.8916	1.9532
Al^[4]	0.1180	0.0704	0.0579	0.0747	0.0659	0.0914	0.0973	0.1050	0.0435
Al^[6]	0.0464	0.0156	0.0327	0.0293	0.0271	0.0496	0.0450	0.0520	0.0406
Ti	0.0402	0.0312	0.0265	0.0383	0.0291	0.0222	0.0240	0.0407	0.0202
Fe³⁺	0.0102	0.0261	0.0000	0.0000	0.0014	0.0000	0.0022	0.0000	0.0000
Fe²⁺	0.2043	0.2740	0.2130	0.2689	0.2399	0.1447	0.1475	0.1588	0.1958
Mn	0.0061	0.0089	0.0055	0.0071	0.0079	0.0032	0.0034	0.0037	0.0046
Mg	0.8022	0.7526	0.8494	0.7844	0.8278	0.8482	0.8429	0.8108	0.8711
Cr	0.0022	0.0000	0.0008	0.0010	0.0007	0.0225	0.0258	0.0254	0.0010
Ni	0.0016	0.0003	0.0004	0.0000	0.0001	0.0000	0.0002	0.0020	0.0008
Ca	0.8653	0.8576	0.8513	0.8455	0.8444	0.8857	0.8854	0.8749	0.8476
Na	0.0205	0.0330	0.0204	0.0254	0.0215	0.0235	0.0236	0.0308	0.0181
K	0.0008	0.0007	0.0000	0.0002	0.0000	0.0004	0.0000	0.0009	0.0000
TOTAL	4.0000	4.0000	3.9987	3.9990	4.0000	3.9998	4.0000	3.9965	3.9967
Mg/(Fe^(t)+Mg)	0.7890	0.7149	0.7995	0.7447	0.7743	0.8542	0.8492	0.8362	0.8164

Sample No	AA-14	AA-14	AA-14	AA-14	AA-15a	AA-15a	AA-15a	AA-15a	AA-15a
Photo Area	J	J	J	J	A	A	A	A	B
Analysis No	106	107	108	109	2	3	4	12	17
SiO₂	53.47	53.20	52.12	53.18	48.46	49.24	48.04	50.72	52.03
TiO₂	0.85	0.78	1.09	0.76	2.08	1.80	2.30	1.28	1.22
Al₂O₃	1.94	2.08	3.15	1.85	6.40	5.82	6.46	4.38	3.29
Fe₂O₃	6.33	5.93	6.45	6.69	6.33	5.97	6.21	5.66	6.33
MnO	0.12	0.11	0.10	0.18	0.11	0.18	0.11	0.13	0.15
MgO	15.95	15.79	15.05	15.94	13.65	13.88	13.57	15.01	15.85
CaO	21.72	21.69	21.94	21.26	21.71	21.51	21.74	21.79	20.58
Na₂O	0.22	0.24	0.27	0.26	0.35	0.31	0.31	0.32	0.17
K₂O	0.00	0.00	0.02	0.00	0.02	0.00	0.01	0.01	0.00
Cr₂O₃	0.01	0.05	0.06	0.08	0.43	1.16	0.73	0.43	0.29
NiO	0.08	0.05	0.02	0.03	0.01	0.07	0.03	0.01	0.03
TOTAL	100.7	99.91	100.27	100.23	99.56	99.94	99.51	99.75	99.94
Si	1.9515	1.9534	1.9159	1.9524	1.8012	1.8227	1.7890	1.8716	1.9112
Al^[4]	0.0441	0.0407	0.0818	0.0450	0.1988	0.1748	0.2110	0.1284	0.0819
Al^[6]	0.0395	0.0496	0.0549	0.0352	0.0815	0.0794	0.0725	0.0620	0.0610
Ti	0.0235	0.0216	0.0300	0.0209	0.0582	0.0502	0.0644	0.0355	0.0338
Fe³⁺	0.0000	0.0000	0.0000	0.0000	0.0144	0.0000	0.0113	0.0062	0.0000
Fe²⁺	0.1936	0.1826	0.1985	0.2057	0.1823	0.1851	0.1821	0.1685	0.1952
Mn	0.0036	0.0033	0.0031	0.0057	0.0034	0.0056	0.0036	0.0042	0.0048
Mg	0.8698	0.8669	0.8257	0.8736	0.7563	0.7670	0.7533	0.8257	0.8711
Cr	0.0002	0.0014	0.0018	0.0024	0.0128	0.0339	0.0214	0.0127	0.0086
Ni	0.0025	0.0015	0.0006	0.0008	0.0003	0.0020	0.0008	0.0002	0.0008
Ca	0.8513	0.8559	0.8652	0.8374	0.8646	0.8543	0.8674	0.8615	0.8129
Na	0.0159	0.0172	0.0192	0.0183	0.0251	0.0226	0.0225	0.0229	0.0118
K	0.0000	0.0000	0.0009	0.0000	0.0011	0.0000	0.0006	0.0006	0.0000
TOTAL	3.9956	3.9941	3.9976	3.9974	4.0000	3.9975	4.0000	4.0000	3.9931
Mg/(Fe^(t)+Mg)	0.8179	0.8260	0.8062	0.8094	0.7936	0.8056	0.7957	0.8254	0.8170

Sample No	AA-15a	AA-15a	AA-15a	AA-15a	AA-15a	AA-15a	AA-15a	AA-15a	AA-15a
Photo Area	D	D	D	D	D	D	D	D	F
Analysis No	48	49	53	54	55	56	57	58	64
SiO₂	52.17	49.99	48.23	48.84	49.27	50.67	49.73	51.89	52.57
TiO₂	1.05	1.33	2.27	2.01	1.70	1.17	1.80	1.18	0.88
Al₂O₃	2.84	4.72	6.38	5.97	5.53	4.52	5.52	3.27	2.55
Fe₂O₃	6.17	5.93	6.70	5.85	5.72	5.70	5.96	6.37	5.54
MnO	0.14	0.10	0.11	0.10	0.11	0.14	0.08	0.12	0.10
MgO	15.96	14.25	13.26	13.84	13.94	14.65	14.11	16.04	16.13
CaO	20.85	22.06	21.08	21.93	22.01	22.03	21.47	20.68	21.60
Na₂O	0.21	0.45	0.43	0.33	0.38	0.25	0.33	0.18	0.19
K₂O	0.01	0.00	0.01	0.01	0.02	0.00	0.00	0.03	0.00
Cr₂O₃	0.45	1.15	0.62	0.82	0.93	0.77	1.15	0.31	0.48
NiO	0.02	0.02	0.00	0.03	0.00	0.03	0.02	0.02	0.06
TOTAL	99.87	99.99	99.09	99.72	99.6	99.93	100.17	100.1	100.1
Si	1.9191	1.8469	1.8045	1.8121	1.8281	1.8696	1.8337	1.9052	1.9271
Al^[4]	0.0769	0.1531	0.1944	0.1879	0.1719	0.1290	0.1623	0.0919	0.0698
Al^[6]	0.0465	0.0524	0.0871	0.0731	0.0699	0.0677	0.0781	0.0498	0.0406
Ti	0.0290	0.0368	0.0639	0.0561	0.0475	0.0326	0.0500	0.0326	0.0243
Fe³⁺	0.0000	0.0253	0.0000	0.0028	0.0076	0.0000	0.0000	0.0000	0.0000
Fe²⁺	0.1902	0.1579	0.2098	0.1788	0.1699	0.1760	0.1842	0.1959	0.1701
Mn	0.0043	0.0033	0.0035	0.0032	0.0035	0.0044	0.0026	0.0038	0.0030
Mg	0.8771	0.7848	0.7400	0.7655	0.7711	0.8064	0.7773	0.8793	0.8829
Cr	0.0131	0.0337	0.0185	0.0239	0.0274	0.0226	0.0336	0.0090	0.0138
Ni	0.0007	0.0007	0.0000	0.0008	0.0001	0.0009	0.0006	0.0005	0.0018
Ca	0.8235	0.8732	0.8456	0.8718	0.8750	0.8716	0.8501	0.8148	0.8498
Na	0.0151	0.0319	0.0311	0.0236	0.0271	0.0177	0.0234	0.0129	0.0137
K	0.0004	0.0000	0.0005	0.0004	0.0008	0.0000	0.0001	0.0015	0.0000
TOTAL	3.9960	4.0000	3.9989	4.0000	4.0000	3.9986	3.9960	3.9972	3.9969
Mg/(Fe^(t)+Mg)	0.8218	0.8107	0.7791	0.8083	0.8129	0.8208	0.8084	0.8178	0.8384

Sample No	AA-15a	AA-15a	AA-15a	AA-15a	AA-15a	AA-15a
Photo Area	F	F	H	H	H	H
Analysis No	65	78	82	83	84	86
SiO₂	51.76	52.49	49.80	49.64	50.66	49.16
TiO₂	1.09	1.02	1.39	1.76	1.06	1.68
Al₂O₃	3.05	2.89	5.05	5.36	4.24	5.58
Fe₂O₃	6.68	6.16	5.43	5.58	5.15	5.65
MnO	0.12	0.14	0.13	0.15	0.06	0.11
MgO	15.76	16.03	14.57	14.11	15.00	14.17
CaO	20.41	20.80	22.18	21.95	22.16	21.75
Na₂O	0.24	0.22	0.27	0.28	0.26	0.27
K₂O	0.00	0.00	0.00	0.00	0.00	0.01
Cr₂O₃	0.29	0.46	1.38	0.81	1.29	1.37
NiO	0.01	0.00	0.01	0.00	0.07	0.07
TOTAL	99.42	100.2	100.21	99.63	99.96	99.82
Si	1.9148	1.9224	1.8351	1.8388	1.8676	1.8218
Al^[4]	0.0817	0.0720	0.1649	0.1582	0.1324	0.1779
Al^[6]	0.0515	0.0531	0.0544	0.0762	0.0518	0.0658
Ti	0.0305	0.0281	0.0386	0.0491	0.0295	0.0468
Fe³⁺	0.0000	0.0000	0.0125	0.0000	0.0025	0.0000
Fe²⁺	0.2070	0.1892	0.1548	0.1731	0.1563	0.1751
Mn	0.0038	0.0044	0.0041	0.0046	0.0018	0.0035
Mg	0.8707	0.8778	0.8004	0.7805	0.8244	0.7829
Cr	0.0085	0.0133	0.0402	0.0238	0.0377	0.0401
Ni	0.0004	0.0000	0.0002	0.0000	0.0020	0.0020
Ca	0.8105	0.8186	0.8757	0.8726	0.8753	0.8637
Na	0.0172	0.0155	0.0192	0.0201	0.0186	0.0195
K	0.0000	0.0000	0.0000	0.0000	0.0000	0.0004
TOTAL	3.9965	3.9944	4.0000	3.9970	4.0000	3.9997
Mg/(Fe^(t)+Mg)	0.8079	0.8227	0.8271	0.8184	0.8385	0.8172

APPENDIX D
MAJOR AND MINOR ELEMENT CHEMICAL ANALYSES FOR
PYROXENE FROM BASALT OVERGROWTHS

Sample No	AA-14	AA-14	AA-14	AA-14	AA-14	AA-14	AA-14	AA-14	AA-14	AA-14
Photo Area	A	A	B	B	C	C	C	C	C	C
Analysis No	5	10	15	17	28	30	31	33	35	
SiO₂	54.08	53.09	54.33	54.05	53.89	55.22	54.58	54.63	54.02	
TiO₂	0.60	0.01	0.69	0.02	1.89	0.05	0.06	0.01	0.06	
Al₂O₃	1.46	1.18	0.74	1.61	0.81	2.11	1.31	1.51	0.79	
Fe₂O₃	12.92	18.42	13.77	17.11	12.41	12.05	16.16	16.17	16.90	
MnO	0.42	0.73	0.52	0.58	0.25	0.22	0.78	0.64	1.01	
MgO	13.81	10.61	13.44	11.37	13.81	15.02	12.09	12.11	11.93	
CaO	14.28	11.85	13.15	11.57	13.13	12.83	12.16	11.90	12.13	
Na₂O	0.42	0.37	0.34	0.56	0.42	0.58	0.39	0.55	0.27	
K₂O	0.11	0.10	0.12	0.16	0.16	0.12	0.12	0.15	0.10	
Cr₂O₃	0.08	0.06	0.09	0.00	0.06	0.03	0.02	0.01	0.04	
NiO	0.07	0.00	0.00	0.00	0.03	0.05	0.04	0.00	0.00	
TOTAL	98.26	96.40	97.20	97.03	96.86	98.28	97.70	97.68	97.25	
Si	2.0000	2.0000	2.0000	2.0000	2.0000	2.0000	2.0000	2.0000	2.0000	
Al^[4]	0.0000	0.0000	0.0000	0.0000	0.0000	0.0000	0.0000	0.0000	0.0000	
Al^[6]	0.0660	0.0557	0.0342	0.0746	0.0371	0.0943	0.0605	0.0693	0.0366	
Ti	0.0174	0.0002	0.0202	0.0007	0.0554	0.0015	0.0017	0.0004	0.0019	
Fe³⁺	0.0000	0.0000	0.0000	0.0000	0.0000	0.0000	0.0000	0.0000	0.0000	
Fe²⁺	0.4141	0.6168	0.4486	0.5644	0.4046	0.3821	0.5282	0.5275	0.5573	
Mn	0.0138	0.0246	0.0172	0.0193	0.0084	0.0069	0.0259	0.0212	0.0337	
Mg	0.7889	0.6333	0.7805	0.6686	0.8026	0.8490	0.7044	0.7041	0.7012	
Cr	0.0024	0.0018	0.0028	0.0000	0.0018	0.0010	0.0005	0.0003	0.0012	
Ni	0.0021	0.0000	0.0000	0.0000	0.0010	0.0014	0.0012	0.0000	0.0001	
Ca	0.5863	0.5083	0.5488	0.4890	0.5484	0.5212	0.5092	0.4973	0.5124	
Na	0.0312	0.0285	0.0255	0.0432	0.0319	0.0426	0.0293	0.0416	0.0208	
K	0.0055	0.0053	0.0058	0.0081	0.0078	0.0060	0.0061	0.0076	0.0049	
TOTAL	3.9276	3.8745	3.8837	3.8679	3.8991	3.9062	3.8670	3.8692	3.8701	
Mg/(Fe^(t)+Mg)	0.6558	0.5066	0.6350	0.5422	0.6648	0.6896	0.5715	0.5717	0.5572	

Sample No	AA-14	AA-14	AA-14	AA-14	AA-14	AA-14	AA-14	AA-14	AA-14
Photo Area	C	D	D	D	E	E	E	E	F
Analysis No	36	39	44	45	51	55	61	65	66
SiO₂	54.23	53.93	53.53	50.82	53.90	54.61	54.24	51.87	55.63
TiO₂	0.03	0.04	0.02	0.02	0.03	0.07	0.07	3.50	0.30
Al₂O₃	1.18	0.87	1.34	1.16	1.22	1.01	1.36	1.50	0.98
Fe₂O₃	16.59	18.50	17.74	15.91	17.49	16.65	17.09	15.27	13.66
MnO	0.85	1.13	0.68	0.62	0.70	0.88	0.66	0.55	0.26
MgO	11.99	10.53	11.08	11.09	11.41	12.40	11.86	10.81	14.63
CaO	12.25	12.04	11.92	14.37	12.16	12.02	11.97	13.29	12.13
Na₂O	0.36	0.30	0.40	0.40	0.45	0.43	0.38	0.40	0.48
K₂O	0.13	0.12	0.08	0.11	0.14	0.10	0.11	0.07	0.14
Cr₂O₃	0.01	0.02	0.02	0.01	0.00	0.00	0.00	0.03	0.01
NiO	0.00	0.09	0.00	0.03	0.00	0.01	0.01	0.00	0.00
TOTAL	97.61	97.59	96.81	94.53	97.51	98.17	97.77	97.28	98.22
Si	2.0000	2.0000	2.0000	2.0000	2.0000	2.0000	2.0000	2.0000	2.0000
Al^[4]	0.0000	0.0000	0.0000	0.0000	0.0000	0.0000	0.0000	0.0000	0.0000
Al^[6]	0.0543	0.0406	0.0628	0.0555	0.0565	0.0465	0.0629	0.0704	0.0443
Ti	0.0009	0.0013	0.0005	0.0005	0.0009	0.0020	0.0022	0.1045	0.0085
Fe³⁺	0.0000	0.0000	0.0000	0.0000	0.0000	0.0000	0.0000	0.0000	0.0000
Fe²⁺	0.5436	0.6137	0.5892	0.5381	0.5754	0.5416	0.5597	0.5070	0.4369
Mn	0.0282	0.0381	0.0228	0.0213	0.0233	0.0288	0.0220	0.0184	0.0085
Mg	0.7003	0.6226	0.6560	0.6686	0.6692	0.7189	0.6924	0.6398	0.8342
Cr	0.0002	0.0007	0.0006	0.0003	0.0000	0.0000	0.0000	0.0008	0.0003
Ni	0.0000	0.0030	0.0000	0.0008	0.0001	0.0003	0.0003	0.0000	0.0000
Ca	0.5142	0.5117	0.5073	0.6227	0.5126	0.5009	0.5023	0.5654	0.4971
Na	0.0274	0.0233	0.0309	0.0312	0.0346	0.0321	0.0286	0.0305	0.0355
K	0.0064	0.0062	0.0038	0.0055	0.0068	0.0050	0.0054	0.0037	0.0070
TOTAL	3.8754	3.8610	3.8740	3.9447	3.8795	3.8761	3.8758	3.9406	3.8723
Mg/(Fe^(t)+Mg)	0.5630	0.5036	0.5268	0.5541	0.5377	0.5704	0.5530	0.5579	0.6563

Sample No	AA-14	AA-14	AA-14	AA-14	AA-14	AA-14
Photo Area	F	G	G	H	I	J
Analysis No	67	74	79	89	103	104
SiO₂	55.07	54.22	56.19	55.20	53.98	54.20
TiO₂	0.08	0.24	0.26	0.16	0.22	0.04
Al₂O₃	0.94	1.28	0.97	1.29	1.02	0.90
Fe₂O₃	17.13	17.08	12.65	13.37	12.62	18.10
MnO	0.59	0.66	0.32	0.33	0.35	1.10
MgO	12.06	11.85	15.66	14.58	14.55	10.86
CaO	11.74	12.02	12.17	12.20	13.24	12.10
Na₂O	0.49	0.45	0.38	0.52	0.41	0.26
K₂O	0.11	0.09	0.12	0.17	0.13	0.09
Cr₂O₃	0.01	0.03	0.01	0.00	0.05	0.01
NiO	0.00	0.00	0.00	0.04	0.05	0.00
TOTAL	98.22	97.92	98.74	97.87	96.62	97.66
Si	2.0000	2.0000	2.0000	2.0000	2.0000	2.0000
Al^[4]	0.0000	0.0000	0.0000	0.0000	0.0000	0.0000
Al^[6]	0.0433	0.0588	0.0434	0.0584	0.0465	0.0418
Ti	0.0024	0.0071	0.0074	0.0046	0.0064	0.0011
Fe³⁺	0.0000	0.0000	0.0000	0.0000	0.0000	0.0000
Fe²⁺	0.5578	0.5585	0.4005	0.4285	0.4094	0.5987
Mn	0.0195	0.0220	0.0102	0.0106	0.0115	0.0367
Mg	0.7001	0.6907	0.8837	0.8330	0.8414	0.6403
Cr	0.0002	0.0008	0.0004	0.0000	0.0015	0.0002
Ni	0.0000	0.0000	0.0000	0.0013	0.0017	0.0000
Ca	0.4898	0.5036	0.4936	0.5010	0.5503	0.5127
Na	0.0368	0.0338	0.0278	0.0389	0.0308	0.0202
K	0.0057	0.0047	0.0060	0.0081	0.0066	0.0047
TOTAL	3.8556	3.8800	3.8730	3.8845	3.9060	3.8564
Mg/(Fe^(t)+Mg)	0.5565	0.5529	0.6882	0.6603	0.6727	0.5168

APPENDIX E
MAJOR AND MINOR ELEMENT CHEMICAL ANALYSES FOR
PYROXENE FROM BASALT MATRIX

Sample No	AA-15a	AA-15a	AA-15a	AA-15a	AA-15a	AA-15a	AA-15a	AA-15a	AA-15a
Photo Area	A	A	A	A	A	A	A	B	B
Analysis No	5	6	7	8	9	10	11	18	19
SiO₂	48.53	50.80	50.73	48.20	51.55	48.50	51.72	52.02	48.72
TiO₂	2.69	1.40	1.47	2.51	1.20	2.16	0.96	1.11	2.03
Al₂O₃	6.92	4.38	4.44	6.54	3.58	5.99	3.07	2.96	6.08
Fe₂O₃	7.28	6.59	6.59	6.52	6.54	6.26	5.73	7.10	7.11
MnO	0.10	0.13	0.12	0.14	0.16	0.09	0.19	0.22	0.17
MgO	13.26	15.03	14.98	13.54	15.87	13.55	15.89	15.53	13.33
CaO	21.57	21.27	21.12	21.83	20.67	22.16	20.64	20.65	21.69
Na₂O	0.37	0.25	0.34	0.32	0.18	0.34	0.23	0.25	0.33
K₂O	0.01	0.02	0.01	0.00	0.02	0.01	0.05	0.00	0.00
Cr₂O₃	0.02	0.34	0.57	0.36	0.34	0.59	0.67	0.09	0.02
NiO	0.06	0.01	0.03	0.06	0.00	0.03	0.00	0.00	0.05
TOTAL	100.81	100.21	100.40	100.01	100.11	99.67	99.15	99.91	99.52
Si	1.7882	1.8707	1.8654	1.7871	1.8948	1.8031	1.9141	1.9186	1.8163
Al^[4]	0.2118	0.1293	0.1346	0.2129	0.1034	0.1969	0.0819	0.0785	0.1837
Al^[6]	0.0887	0.0608	0.0578	0.0728	0.0518	0.0656	0.0523	0.0504	0.0834
Ti	0.0746	0.0387	0.0405	0.0700	0.0331	0.0604	0.0269	0.0308	0.0569
Fe³⁺	0.0004	0.0000	0.0037	0.0124	0.0000	0.0180	0.0000	0.0000	0.0093
Fe²⁺	0.2239	0.2030	0.1990	0.1898	0.2012	0.1766	0.1777	0.2193	0.2124
Mn	0.0032	0.0040	0.0036	0.0043	0.0050	0.0028	0.0058	0.0068	0.0053
Mg	0.7284	0.8251	0.8212	0.7484	0.8704	0.7510	0.8785	0.8552	0.7408
Cr	0.0005	0.0100	0.0167	0.0104	0.0100	0.0172	0.0197	0.0026	0.0006
Ni	0.0018	0.0004	0.0008	0.0019	0.0000	0.0009	0.0001	0.0000	0.0014
Ca	0.8516	0.8392	0.8321	0.8672	0.8148	0.8827	0.8202	0.8173	0.8664
Na	0.0263	0.0179	0.0243	0.0227	0.0128	0.0242	0.0164	0.0176	0.0235
K	0.0007	0.0009	0.0003	0.0001	0.0008	0.0006	0.0024	0.0000	0.0000
TOTAL	4.0000	4.0000	4.0000	4.0000	3.9983	4.0000	3.9960	3.9970	4.0000
Mg/(Fe^(t)+Mg)	0.7645	0.8026	0.8021	0.7873	0.8122	0.7942	0.8317	0.7959	0.7697

Sample No	AA-15a	AA-15a	AA-15a	AA-15a	AA-15a	AA-15a	AA-15a	AA-15a	AA-15a
Photo Area	B	B	B	B	B	B	B	B	B
Analysis No	20	21	22	23	24	25	26	27	28
SiO₂	52.32	49.57	50.05	47.48	47.67	48.91	48.32	49.60	50.11
TiO₂	1.13	1.74	1.75	3.07	2.70	1.98	2.42	1.68	1.50
Al₂O₃	3.10	5.22	5.16	6.59	5.72	5.49	6.46	5.43	5.51
Fe₂O₃	5.93	6.45	6.36	8.16	9.62	6.77	6.62	5.67	6.33
MnO	0.14	0.08	0.12	0.18	0.19	0.10	0.14	0.09	0.09
MgO	16.29	14.04	14.51	12.79	12.60	13.48	13.58	14.18	14.53
CaO	20.51	21.51	21.21	21.13	20.15	21.71	21.32	22.08	21.44
Na₂O	0.23	0.33	0.28	0.36	0.42	0.49	0.42	0.34	0.34
K₂O	0.00	0.00	0.01	0.01	0.00	0.00	0.00	0.01	0.00
Cr₂O₃	0.53	0.53	0.61	0.05	0.00	0.17	0.33	1.15	0.29
NiO	0.07	0.05	0.02	0.04	0.01	0.01	0.02	0.04	0.01
TOTAL	100.26	99.52	100.09	99.86	99.09	99.14	99.64	100.29	100.16
Si	1.9134	1.8427	1.8463	1.7748	1.8014	1.8270	1.7966	1.8285	1.8451
Al^[4]	0.0815	0.1565	0.1510	0.2252	0.1986	0.1730	0.2034	0.1715	0.1549
Al^[6]	0.0525	0.0722	0.0736	0.0651	0.0561	0.0687	0.0796	0.0644	0.0842
Ti	0.0311	0.0487	0.0486	0.0863	0.0768	0.0556	0.0677	0.0466	0.0417
Fe³⁺	0.0000	0.0000	0.0000	0.0123	0.0201	0.0236	0.0088	0.0055	0.0030
Fe²⁺	0.1819	0.2006	0.1965	0.2428	0.2839	0.1879	0.1971	0.1693	0.1919
Mn	0.0044	0.0026	0.0037	0.0057	0.0060	0.0033	0.0045	0.0027	0.0030
Mg	0.8905	0.7784	0.7991	0.7127	0.7098	0.7507	0.7527	0.7793	0.7976
Cr	0.0152	0.0155	0.0177	0.0014	0.0000	0.0051	0.0096	0.0336	0.0085
Ni	0.0020	0.0014	0.0006	0.0012	0.0004	0.0004	0.0007	0.0012	0.0002
Ca	0.8058	0.8571	0.8395	0.8463	0.8158	0.8689	0.8493	0.8721	0.8458
Na	0.0165	0.0235	0.0199	0.0258	0.0311	0.0357	0.0300	0.0245	0.0241
K	0.0001	0.0000	0.0006	0.0004	0.0000	0.0000	0.0000	0.0007	0.0000
TOTAL	3.9949	3.9992	3.9974	4.0000	4.0000	4.0000	4.0000	4.0000	4.0000
Mg/(Fe^(t)+Mg)	0.8304	0.7951	0.8026	0.7364	0.7001	0.7802	0.7853	0.8168	0.8036

Sample No	AA-15a	AA-15a	AA-15a	AA-15a	AA-15a	AA-15a	AA-15a	AA-15a	AA-15a
Photo Area	B	B	B	C	C	C	C	C	C
Analysis No	29	30	31	36	37	38	39	40	41
SiO₂	49.15	48.93	48.89	48.73	50.63	48.89	48.38	49.22	47.48
TiO₂	1.62	2.23	2.23	2.15	1.58	2.15	2.10	1.66	2.54
Al₂O₃	5.54	6.21	6.06	6.21	4.28	6.15	5.98	5.08	6.87
Fe₂O₃	5.70	6.38	6.47	6.29	6.51	6.95	5.97	6.10	6.71
MnO	0.13	0.17	0.12	0.13	0.17	0.13	0.09	0.10	0.11
MgO	14.10	13.74	13.62	13.72	15.34	13.50	13.62	14.26	12.98
CaO	22.08	21.56	21.79	21.54	20.82	21.71	21.39	21.15	21.44
Na₂O	0.34	0.31	0.37	0.33	0.24	0.39	0.36	0.31	0.36
K₂O	0.00	0.02	0.00	0.01	0.01	0.00	0.00	0.01	0.02
Cr₂O₃	1.18	0.47	0.68	0.55	0.48	0.12	0.77	0.60	0.20
NiO	0.00	0.02	0.00	0.04	0.04	0.01	0.00	0.01	0.02
TOTAL	99.84	100.04	100.24	99.70	100.11	100.00	98.68	98.51	98.72
Si	1.8195	1.8106	1.8084	1.8095	1.8658	1.8119	1.8136	1.8449	1.7849
Al^[4]	0.1805	0.1879	0.1916	0.1898	0.1340	0.1881	0.1850	0.1544	0.2151
Al^[6]	0.0612	0.0832	0.0726	0.0821	0.0519	0.0805	0.0795	0.0701	0.0893
Ti	0.0451	0.0621	0.0621	0.0601	0.0439	0.0599	0.0593	0.0469	0.0718
Fe³⁺	0.0192	0.0000	0.0018	0.0000	0.0000	0.0124	0.0000	0.0000	0.0031
Fe²⁺	0.1573	0.1976	0.1983	0.1954	0.2007	0.2030	0.1873	0.1913	0.2079
Mn	0.0042	0.0053	0.0039	0.0040	0.0053	0.0041	0.0029	0.0033	0.0036
Mg	0.7781	0.7586	0.7510	0.7598	0.8428	0.7459	0.7617	0.7971	0.7274
Cr	0.0345	0.0136	0.0199	0.0163	0.0139	0.0036	0.0229	0.0179	0.0059
Ni	0.0000	0.0007	0.0000	0.0011	0.0012	0.0002	0.0000	0.0004	0.0006
Ca	0.8758	0.8555	0.8636	0.8573	0.8222	0.8621	0.8598	0.8497	0.8636
Na	0.0243	0.0226	0.0268	0.0236	0.0175	0.0283	0.0265	0.0227	0.0261
K	0.0002	0.0008	0.0001	0.0003	0.0006	0.0000	0.0000	0.0006	0.0008
TOTAL	4.0000	3.9985	4.0000	3.9993	3.9998	4.0000	3.9986	3.9994	4.0000
Mg/(Fe^(t)+Mg)	0.8151	0.7933	0.7896	0.7954	0.8077	0.7759	0.8026	0.8065	0.7752

Sample No	AA-15a	AA-15a	AA-15a	AA-15a	AA-15a	AA-15a	AA-15a	AA-15a	AA-15a
Photo Area	C	C	C	C	C	D	D	D	F
Analysis No	42	43	44	45	46	50	51	52	66
SiO₂	47.48	49.07	48.34	52.34	51.61	48.48	51.70	48.57	52.52
TiO₂	2.51	1.88	2.10	0.87	1.10	2.40	1.34	2.50	1.03
Al₂O₃	6.67	5.41	6.36	2.76	3.20	6.63	3.67	6.10	2.88
Fe₂O₃	6.40	5.87	6.01	5.81	5.91	6.29	6.35	7.43	5.71
MnO	0.18	0.09	0.13	0.13	0.17	0.11	0.20	0.18	0.17
MgO	13.05	14.14	13.58	16.18	16.03	13.41	15.64	13.09	15.90
CaO	21.67	20.99	21.70	21.13	20.38	21.47	20.30	20.91	21.34
Na₂O	0.35	0.29	0.26	0.24	0.25	0.38	0.22	0.46	0.25
K₂O	0.00	0.05	0.03	0.02	0.00	0.01	0.01	0.05	0.00
Cr₂O₃	0.26	1.13	0.39	0.58	0.80	0.45	0.38	0.14	0.51
NiO	0.00	0.03	0.05	0.04	0.07	0.05	0.07	0.02	0.01
TOTAL	98.57	98.95	98.95	100.11	99.53	99.70	99.88	99.46	100.31
Si	1.7869	1.8314	1.8072	1.9199	1.9044	1.8000	1.9010	1.8143	1.9212
Al^[4]	0.2131	0.1649	0.1919	0.0788	0.0923	0.1977	0.0917	0.1843	0.0739
Al^[6]	0.0828	0.0735	0.0884	0.0406	0.0471	0.0928	0.0679	0.0844	0.0506
Ti	0.0711	0.0529	0.0591	0.0240	0.0305	0.0671	0.0373	0.0703	0.0285
Fe³⁺	0.0059	0.0000	0.0000	0.0000	0.0000	0.0000	0.0000	0.0000	0.0000
Fe²⁺	0.1955	0.1836	0.1880	0.1784	0.1827	0.1956	0.1960	0.2323	0.1751
Mn	0.0056	0.0027	0.0040	0.0041	0.0052	0.0036	0.0063	0.0058	0.0052
Mg	0.7322	0.7883	0.7572	0.8854	0.8833	0.7432	0.8606	0.7295	0.8693
Cr	0.0077	0.0334	0.0115	0.0169	0.0235	0.0134	0.0110	0.0041	0.0148
Ni	0.0000	0.0010	0.0016	0.0012	0.0022	0.0016	0.0022	0.0006	0.0002
Ca	0.8738	0.8410	0.8697	0.8310	0.8072	0.8552	0.8028	0.8375	0.8386
Na	0.0253	0.0212	0.0190	0.0174	0.0182	0.0271	0.0155	0.0332	0.0177
K	0.0002	0.0024	0.0014	0.0009	0.0000	0.0004	0.0004	0.0022	0.0000
TOTAL	4.0000	3.9963	3.9991	3.9986	3.9966	3.9977	3.9927	3.9986	3.9951
Mg/(Fe^(t)+Mg)	0.7842	0.8111	0.8011	0.8323	0.8286	0.7917	0.8145	0.7585	0.8323

Sample No	AA-15a	AA-15a	AA-15a	AA-15a	AA-15a	AA-15a	AA-15a	AA-15a	AA-15a
Photo Area	F	F	F	F	F	F	H	H	H
Analysis No	67	68	69	70	76	77	85	87	88
SiO₂	49.73	48.92	47.62	49.35	50.40	52.74	50.57	49.96	48.69
TiO₂	1.66	2.56	2.80	2.01	1.44	0.90	1.22	1.74	2.31
Al₂O₃	5.30	6.92	6.85	5.55	4.70	2.90	4.56	5.90	6.65
Fe₂O₃	5.89	6.67	7.46	6.89	7.08	6.11	5.93	6.33	6.47
MnO	0.13	0.08	0.17	0.16	0.16	0.13	0.15	0.13	0.13
MgO	13.98	13.78	12.82	14.04	14.07	16.24	14.90	14.35	13.77
CaO	22.14	21.44	21.44	21.16	21.00	20.21	21.23	21.72	21.22
Na₂O	0.36	0.39	0.38	0.38	0.55	0.30	0.39	0.29	0.38
K₂O	0.01	0.00	0.00	0.00	0.00	0.01	0.01	0.01	0.03
Cr₂O₃	0.99	0.23	0.00	0.43	0.61	0.71	0.83	0.29	0.22
NiO	0.05	0.02	0.02	0.00	0.09	0.04	0.02	0.05	0.03
TOTAL	100.24	101.03	99.56	99.97	100.10	100.29	99.83	100.77	99.91
Si	1.8356	1.7923	1.7799	1.8281	1.8635	1.9270	1.8667	1.8311	1.8025
Al^[4]	0.1644	0.2069	0.2201	0.1719	0.1365	0.0665	0.1333	0.1689	0.1972
Al^[6]	0.0662	0.0920	0.0817	0.0704	0.0684	0.0588	0.0651	0.0860	0.0930
Ti	0.0461	0.0706	0.0787	0.0560	0.0401	0.0248	0.0339	0.0480	0.0643
Fe³⁺	0.0034	0.0000	0.0081	0.0042	0.0097	0.0000	0.0046	0.0000	0.0000
Fe²⁺	0.1785	0.2045	0.2251	0.2092	0.2093	0.1873	0.1785	0.1940	0.2003
Mn	0.0042	0.0025	0.0054	0.0050	0.0051	0.0040	0.0047	0.0041	0.0042
Mg	0.7693	0.7530	0.7143	0.7753	0.7756	0.8876	0.8199	0.7841	0.7601
Cr	0.0289	0.0068	0.0001	0.0126	0.0178	0.0205	0.0244	0.0083	0.0064
Ni	0.0016	0.0006	0.0006	0.0000	0.0025	0.0013	0.0007	0.0015	0.0010
Ca	0.8756	0.8420	0.8586	0.8398	0.8320	0.7938	0.8397	0.8530	0.8418
Na	0.0258	0.0281	0.0273	0.0273	0.0396	0.0211	0.0280	0.0206	0.0275
K	0.0005	0.0000	0.0000	0.0000	0.0000	0.0007	0.0006	0.0005	0.0013
TOTAL	4.0000	3.9992	4.0000	4.0000	4.0000	3.9935	4.0000	4.0000	3.9997
Mg/(Fe^(t)+Mg)	0.8088	0.7864	0.7539	0.7841	0.7799	0.8257	0.8175	0.8016	0.7914

APPENDIX F
MAJOR AND MINOR ELEMENT CHEMICAL ANALYSES FOR
FELDSPAR FROM METABASALTS

Sample No	AA-7-1	AA-7-1	AA-7-1	AA-7-1	AA-7-1	AA-7-1	AA-7-1	AA-7-1
Photo Area	A	C	C	C	C	D	D	D
Analysis No	11	12	13	14	15	28	29	30
SiO₂	66.21	67.61	66.85	66.10	67.71	67.98	66.56	67.33
Al₂O₃	18.49	18.88	18.63	18.87	18.69	18.82	18.78	18.68
CaO	0.05	0.03	0.12	0.20	0.05	0.01	0.03	0.13
FeO	0.26	0.24	0.22	0.45	0.18	0.15	0.61	0.31
BaO	0.13	0.03	0.00	0.18	0.02	0.00	0.05	0.00
Na₂O	10.86	11.57	11.30	9.48	11.22	11.21	9.36	11.39
K₂O	0.50	0.09	0.07	1.98	0.05	0.12	2.64	0.04
TOTAL	96.50	98.44	97.19	97.27	97.92	98.29	98.03	97.88
Si	3.0050	3.0030	3.0054	2.9931	3.0164	3.0162	2.9976	3.0067
Al	0.9890	0.9883	0.9871	1.0070	0.9812	0.9841	0.9968	0.9831
Ca	0.0024	0.0017	0.0060	0.0097	0.0023	0.0004	0.0016	0.0060
Fe	0.0097	0.0088	0.0082	0.0171	0.0068	0.0056	0.0228	0.0116
Ba	0.0024	0.0005	0.0000	0.0033	0.0003	0.0000	0.0009	0.0000
Na	0.9555	0.9963	0.9849	0.8322	0.9690	0.9642	0.8172	0.9861
K	0.0289	0.0048	0.0042	0.1144	0.0028	0.0069	0.1517	0.0023
TOTAL	4.9928	5.0034	4.9956	4.9767	4.9789	4.9774	4.9885	4.9959

APPENDIX G

MAJOR AND MINOR ELEMENT CHEMICAL ANALYSES FOR FELDSPAR FROM DYKES

Sample No	AA-10a	AA-10a	AA-10a	AA-10a	AA-10a
Photo Area	General	General	General	General	General
Analysis No	64	65	66	67	68
SiO₂	67.79	68.07	67.84	67.98	68.77
Al₂O₃	19.65	19.29	19.54	19.38	19.00
CaO	0.45	0.35	0.31	0.30	0.05
FeO	0.10	0.13	0.11	0.15	0.09
BaO	0.00	0.08	0.04	0.00	0.01
Na₂O	11.27	11.24	11.22	11.33	11.54
K₂O	0.17	0.02	0.07	0.03	0.04
TOTAL	99.43	99.19	99.12	99.17	99.50
Si	2.9811	2.9976	2.9890	2.9936	3.0150
Al	1.0184	1.0011	1.0146	1.0058	0.9817
Ca	0.0212	0.0165	0.0144	0.0142	0.0024
Fe	0.0036	0.0049	0.0039	0.0055	0.0032
Ba	0.0000	0.0014	0.0006	0.0000	0.0003
Na	0.9608	0.9596	0.9584	0.9673	0.9809
K	0.0098	0.0012	0.0038	0.0018	0.0023
TOTAL	4.9950	4.9823	4.9848	4.9881	4.9857

Sample No	AA-10a	AA-10a	AA-10a	AA-10a	AA-10a	AA-10a
Photo Area	General	General	General	General	General	General
Analysis No	69	70	71	72	73	74
SiO₂	66.63	68.33	67.61	67.54	68.12	67.21
Al₂O₃	19.57	19.28	19.57	19.39	19.43	19.51
CaO	1.35	0.13	0.45	0.22	0.37	0.55
FeO	0.40	0.15	0.06	0.06	0.15	0.10
BaO	0.04	0.02	0.07	0.05	0.08	0.08
Na₂O	10.90	11.49	11.21	11.03	11.20	10.97
K₂O	0.06	0.03	0.02	0.36	0.05	0.04
TOTAL	98.95	99.43	98.98	98.65	99.39	98.46
Si	2.9571	3.0006	2.9842	2.9920	2.9939	2.9826
Al	1.0236	0.9978	1.0180	1.0123	1.0064	1.0203
Ca	0.0641	0.0063	0.0211	0.0106	0.0172	0.0263
Fe	0.0150	0.0055	0.0022	0.0023	0.0053	0.0037
Ba	0.0007	0.0004	0.0011	0.0008	0.0014	0.0013
Na	0.9378	0.9782	0.9592	0.9473	0.9543	0.9438
K	0.0034	0.0015	0.0013	0.0203	0.0029	0.0022
TOTAL	5.0017	4.9904	4.9871	4.9857	4.9815	4.9803

Sample No	AA-10a	AA-10a	AA-10a	AA-10a	AA-10a	AA-10a
Photo Area	General	General	General	General	General	General
Analysis No	75	76	77	78	79	80
SiO₂	68.50	68.75	68.12	68.29	67.58	66.10
Al₂O₃	19.08	19.06	19.11	19.36	19.53	19.06
CaO	0.03	0.00	0.04	0.23	0.32	0.34
FeO	0.22	0.21	0.36	0.19	0.13	0.09
BaO	0.00	0.00	0.13	0.01	0.16	0.05
Na₂O	11.26	11.63	11.48	11.25	11.06	11.05
K₂O	0.09	0.03	0.06	0.05	0.09	0.04
TOTAL	99.18	99.68	99.31	99.37	98.87	96.73
Si	3.0124	3.0110	3.0011	2.9994	2.9873	2.9861
Al	0.9888	0.9838	0.9922	1.0021	1.0174	1.0147
Ca	0.0013	0.0000	0.0018	0.0106	0.0153	0.0162
Fe	0.0082	0.0077	0.0133	0.0069	0.0047	0.0034
Ba	0.0000	0.0000	0.0023	0.0001	0.0028	0.0009
Na	0.9600	0.9875	0.9805	0.9580	0.9478	0.9678
K	0.0049	0.0016	0.0034	0.0027	0.0050	0.0026
TOTAL	4.9756	4.9916	4.9947	4.9798	4.9804	4.9917

Sample No	AA-10a	AA-10a	AA-10a	AA-10a	AA-10a	AA-10a	AA-10a	AA-10a	AA-10a
Photo Area	A	A	A	A	A	A	A	B	B
Analysis No	21	22	23	24	25	26	27	28	29
SiO₂	68.72	69.42	69.47	69.16	69.27	69.68	69.13	68.24	69.33
Al₂O₃	19.53	19.32	19.35	19.37	19.53	19.16	19.53	19.52	18.75
CaO	0.33	0.30	0.15	0.21	0.34	0.04	0.29	1.11	0.92
FeO	0.13	0.05	0.08	0.07	0.11	0.13	0.11	0.37	0.12
BaO	0.13	0.04	0.00	0.01	0.07	0.02	0.18	0.14	0.00
Na₂O	11.65	11.53	11.70	11.77	11.62	11.92	11.13	10.90	11.52
K₂O	0.13	0.11	0.06	0.16	0.08	0.11	0.60	0.16	0.09
TOTAL	100.74	100.90	100.88	100.86	101.16	101.05	101.07	100.52	100.75
Si	2.9902	3.0081	3.0082	3.0012	2.9976	3.0129	2.9986	2.9797	3.0123
Al	1.0015	0.9866	0.9875	0.9906	0.9960	0.9764	0.9983	1.0045	0.9601
Ca	0.0153	0.0139	0.0069	0.0097	0.0160	0.0020	0.0135	0.0521	0.0430
Fe	0.0049	0.0020	0.0028	0.0024	0.0041	0.0047	0.0042	0.0134	0.0045
Ba	0.0021	0.0006	0.0000	0.0001	0.0012	0.0003	0.0031	0.0024	0.0000
Na	0.9828	0.9686	0.9822	0.9902	0.9748	0.9992	0.9360	0.9227	0.9704
K	0.0074	0.0062	0.0033	0.0088	0.0045	0.0060	0.0333	0.0092	0.0052
TOTAL	5.0041	4.9860	4.9908	5.0030	4.9941	5.0015	4.9868	4.9840	4.9954

Sample No	AA-10a	AA-10a	AA-10a	AA-10a	AA-10a	AA-10a	AA-10a	AA-10a
Photo Area	B	B	B	B	B	D	D	D
Analysis No	30	31	32	33	34	67	69	70
SiO₂	69.10	69.41	69.90	69.52	69.40	69.40	69.00	69.39
Al₂O₃	19.71	19.47	19.15	19.75	19.60	19.60	19.84	19.57
CaO	0.28	0.39	0.10	0.25	0.37	0.32	0.37	0.35
FeO	0.08	0.13	0.15	0.04	0.09	0.15	0.16	0.07
BaO	0.00	0.13	0.00	0.21	0.24	0.12	0.09	0.12
Na₂O	11.35	11.67	11.54	11.37	11.45	11.65	11.47	11.43
K₂O	0.71	0.08	0.04	0.27	0.15	0.06	0.41	0.15
TOTAL	101.31	101.36	100.91	101.50	101.49	101.41	101.51	101.31
Si	2.9903	2.9986	3.0210	2.9976	2.9978	2.9964	2.9835	3.0001
Al	1.0052	0.9913	0.9754	1.0036	0.9978	0.9973	1.0110	0.9971
Ca	0.0128	0.0180	0.0048	0.0117	0.0171	0.0149	0.0172	0.0163
Fe	0.0030	0.0049	0.0054	0.0016	0.0031	0.0053	0.0058	0.0025
Ba	0.0000	0.0022	0.0000	0.0035	0.0040	0.0021	0.0016	0.0021
Na	0.9522	0.9774	0.9669	0.9505	0.9589	0.9751	0.9615	0.9581
K	0.0392	0.0042	0.0023	0.0148	0.0084	0.0031	0.0226	0.0084
TOTAL	5.0028	4.9966	4.9759	4.9832	4.9870	4.9941	5.0031	4.9846

APPENDIX H
MAJOR AND MINOR ELEMENT CHEMICAL ANALYSES FOR
FELDSPAR FROM BASALTS

Sample No	AA-11c	AA-11c	AA-12a	AA-12a	AA-12a	AA-12a	AA-12a	AA-12a	AA-12a
Photo Area	A	A	A	A	A	A	B	B	B
Analysis No	12	13	10	17	18	20	23	24	34
SiO₂	67.49	67.76	69.21	68.96	69.63	69.12	69.29	69.05	70.12
Al₂O₃	19.15	18.89	19.39	19.56	19.40	19.65	19.38	19.33	19.17
CaO	0.36	0.07	0.42	0.48	0.30	0.23	0.40	0.30	0.01
FeO	0.20	0.16	0.13	0.11	0.11	0.28	0.19	0.08	0.03
BaO	0.07	0.03	0.10	0.06	0.00	0.11	0.04	0.00	0.00
Na₂O	11.21	11.39	11.99	11.85	11.83	11.03	11.75	11.69	11.65
K₂O	0.10	0.03	0.05	0.06	0.10	0.56	0.05	0.06	0.05
TOTAL	98.58	98.34	101.29	101.12	101.40	101.01	101.19	100.52	101.03
Si	2.9938	3.0082	2.9938	2.9877	3.0029	2.9962	2.9986	3.0017	3.0242
Al	1.0011	0.9883	0.9885	0.9987	0.9860	1.0038	0.9884	0.9903	0.9744
Ca	0.0173	0.0034	0.0193	0.0221	0.0139	0.0106	0.0183	0.0140	0.0006
Fe	0.0074	0.0061	0.0047	0.0041	0.0041	0.0102	0.0069	0.0030	0.0009
Ba	0.0012	0.0005	0.0016	0.0010	0.0000	0.0019	0.0007	0.0000	0.0000
Na	0.9641	0.9803	1.0055	0.9953	0.9891	0.9269	0.9858	0.9852	0.9741
K	0.0055	0.0019	0.0027	0.0031	0.0053	0.0312	0.0027	0.0031	0.0028
TOTAL	4.9904	4.9887	5.0161	5.0121	5.0013	4.9809	5.0015	4.9973	4.9771

Sample No	AA-12a	AA-12a	AA-12a	AA-12a	AA-12a	AA-12a	AA-12a	AA-12a	AA-12a
Photo Area	B	C	C	C	E	E	E	E	F
Analysis No	35	41	42	43	77	79	81	82	97
SiO₂	69.03	68.63	69.20	69.44	69.46	69.91	69.47	69.77	69.31
Al₂O₃	18.91	19.39	19.62	19.52	19.60	19.31	19.52	19.23	19.84
CaO	0.09	0.41	0.36	0.45	0.39	0.04	0.29	0.03	0.55
FeO	0.64	0.17	0.04	0.08	0.14	0.16	0.11	0.07	0.03
BaO	0.00	0.00	0.02	0.04	0.02	0.02	0.00	0.01	0.07
Na₂O	11.10	11.26	11.66	11.42	11.88	12.07	11.88	12.07	11.45
K₂O	0.59	0.34	0.10	0.06	0.06	0.04	0.07	0.03	0.13
TOTAL	100.38	100.20	101.05	101.10	101.58	101.55	101.39	101.20	101.47
Si	3.0136	2.9961	2.9944	3.0017	2.9929	3.0091	2.9975	3.0114	2.9889
Al	0.9729	0.9976	1.0005	0.9944	0.9953	0.9795	0.9926	0.9782	1.0083
Ca	0.0043	0.0191	0.0166	0.0210	0.0181	0.0017	0.0134	0.0013	0.0255
Fe	0.0232	0.0063	0.0014	0.0030	0.0051	0.0059	0.0040	0.0027	0.0011
Ba	0.0000	0.0000	0.0003	0.0007	0.0003	0.0003	0.0000	0.0001	0.0011
Na	0.9395	0.9530	0.9782	0.9571	0.9924	1.0072	0.9938	1.0100	0.9573
K	0.0326	0.0189	0.0057	0.0032	0.0031	0.0023	0.0038	0.0016	0.0070
TOTAL	4.9860	4.9910	4.9972	4.9812	5.0071	5.0059	5.0050	5.0053	4.9891

Sample No	AA-12a	AA-12a	AA-12a	AA-12a	AA-12a	AA-12a	AA-12a	AA-15a	AA-15a	AA-15a
Photo Area	F	F	G	G	H	I	I	A	B	B
Analysis No	98	99	122	123	137	146	147	1	14	15
SiO₂	69.75	69.56	69.62	69.29	69.92	69.59	69.46	69.88	69.67	69.19
Al₂O₃	19.59	19.39	19.44	19.03	19.39	19.43	19.24	19.30	19.30	18.97
CaO	0.32	0.34	0.21	0.80	0.14	0.41	0.22	0.07	0.15	0.29
FeO	0.04	0.01	0.10	0.67	0.12	0.03	0.05	0.07	0.13	0.27
BaO	0.00	0.00	0.05	0.01	0.08	0.04	0.00	0.04	0.04	0.12
Na₂O	11.74	11.63	11.68	11.38	11.72	11.80	11.54	12.01	11.90	11.87
K₂O	0.03	0.07	0.30	0.07	0.10	0.07	0.10	0.09	0.15	0.27
TOTAL	101.49	101.03	101.41	101.30	101.48	101.45	100.65	101.53	101.46	101.02
Si	3.0016	3.0065	3.0033	3.0010	3.0101	3.0014	3.0125	3.0100	3.0066	3.0053
Al	0.9935	0.9877	0.9883	0.9713	0.9837	0.9876	0.9834	0.9797	0.9816	0.9711
Ca	0.0147	0.0158	0.0098	0.0371	0.0067	0.0188	0.0102	0.0032	0.0071	0.0135
Fe	0.0013	0.0003	0.0035	0.0241	0.0043	0.0012	0.0017	0.0026	0.0046	0.0100
Ba	0.0000	0.0001	0.0008	0.0001	0.0014	0.0007	0.0000	0.0007	0.0007	0.0020
Na	0.9795	0.9745	0.9768	0.9555	0.9782	0.9867	0.9703	1.0029	0.9956	0.9996
K	0.0016	0.0040	0.0165	0.0039	0.0057	0.0037	0.0055	0.0050	0.0084	0.0150
TOTAL	4.9922	4.9889	4.9992	4.9931	4.9900	5.0000	4.9837	5.0041	5.0046	5.0164

Sample No	AA-15a	AA-15a	AA-15a	AA-15a	AA-15a	AA-15a	AA-15a	AA-15a	AA-15a
Photo Area	B	C	C	C	D	F	F	F	F
Analysis No	16	34	35	47	61	63	71	74	75
SiO₂	69.16	69.75	70.35	69.63	70.07	69.56	70.00	69.98	70.06
Al₂O₃	19.00	19.33	19.17	18.70	19.41	19.09	19.11	19.24	19.38
CaO	0.77	0.10	0.09	0.50	0.15	0.47	0.05	0.30	0.14
FeO	0.47	0.13	0.12	0.11	0.12	0.36	0.21	0.17	0.17
BaO	0.10	0.01	0.03	0.08	0.05	0.06	0.01	0.03	0.02
Na₂O	11.72	11.64	11.73	11.64	11.68	11.89	11.80	11.68	11.63
K₂O	0.04	0.09	0.06	0.05	0.06	0.07	0.03	0.06	0.13
TOTAL	101.26	101.07	101.59	100.70	101.56	101.49	101.23	101.46	101.54
Si	2.9981	3.0124	3.0224	3.0227	3.0121	3.0039	3.0194	3.0130	3.0127
Al	0.9707	0.9838	0.9706	0.9567	0.9833	0.9715	0.9714	0.9763	0.9821
Ca	0.0357	0.0048	0.0041	0.0233	0.0070	0.0215	0.0021	0.0137	0.0064
Fe	0.0169	0.0048	0.0044	0.0039	0.0044	0.0129	0.0074	0.0063	0.0062
Ba	0.0017	0.0001	0.0005	0.0013	0.0009	0.0010	0.0001	0.0005	0.0004
Na	0.9850	0.9746	0.9770	0.9796	0.9734	0.9954	0.9868	0.9749	0.9696
K	0.0020	0.0049	0.0036	0.0026	0.0035	0.0038	0.0018	0.0033	0.0072
TOTAL	5.0100	4.9854	4.9826	4.9901	4.9846	5.0100	4.9891	4.9880	4.9846

Sample No	AA-15a	AA-14	AA-14	AA-14	AA-14	AA-14	AA-14
Photo Area	H	B	B	D	E	E	H
Analysis No	80	22	23	48	57	59	92
SiO₂	69.89	69.52	69.14	69.97	69.79	68.60	69.50
Al₂O₃	19.27	19.30	18.51	19.34	19.15	17.50	18.67
CaO	0.05	0.08	0.43	0.13	0.17	1.16	0.53
FeO	0.28	0.08	0.49	0.17	0.23	1.33	0.59
BaO	0.06	0.00	0.06	0.00	0.03	0.00	0.06
Na₂O	11.92	11.75	11.41	11.75	11.93	10.82	11.40
K₂O	0.05	0.01	0.06	0.04	0.08	0.03	0.06
TOTAL	101.57	100.74	100.13	101.43	101.37	99.47	100.82
Si	3.0102	3.0109	3.0227	3.0123	3.0109	3.0320	3.0188
Al	0.9781	0.9851	0.9537	0.9812	0.9736	0.9115	0.9557
Ca	0.0023	0.0039	0.0201	0.0060	0.0081	0.0550	0.0248
Fe	0.0100	0.0029	0.0178	0.0062	0.0081	0.0492	0.0214
Ba	0.0010	0.0000	0.0010	0.0000	0.0005	0.0000	0.0009
Na	0.9953	0.9866	0.9671	0.9807	0.9978	0.9271	0.9600
K	0.0027	0.0008	0.0035	0.0021	0.0043	0.0017	0.0035
TOTAL	4.9998	4.9902	4.9858	4.9885	5.0034	4.9766	4.9851